

2014

# A Probabilistic Based Failure Model for Components Fabricated from Anisotropic Graphite

Chengfeng Xiao  
*Cleveland State University*

Follow this and additional works at: <https://engagedscholarship.csuohio.edu/etdarchive>

 Part of the [Civil and Environmental Engineering Commons](#)

**How does access to this work benefit you? Let us know!**

---

## Recommended Citation

Xiao, Chengfeng, "A Probabilistic Based Failure Model for Components Fabricated from Anisotropic Graphite" (2014). *ETD Archive*. 312.

<https://engagedscholarship.csuohio.edu/etdarchive/312>

This Dissertation is brought to you for free and open access by EngagedScholarship@CSU. It has been accepted for inclusion in ETD Archive by an authorized administrator of EngagedScholarship@CSU. For more information, please contact [library.es@csuohio.edu](mailto:library.es@csuohio.edu).

A PROBABILISTIC BASED FAILURE MODEL FOR  
COMPONENTS FABRICATED FROM ANISOTROPIC  
GRAPHITE

CHENGFENG XIAO

**Bachelor of Science**

Sun Yat-Seng University, Guangzhou, China, 2001

**Master of Mechanical Engineering**

Sun Yat-Seng University, Guangzhou, China. 2004

Submitted in partial fulfillment of the requirements for the degree

**DOCTOR OF ENGINEERING**

At the

**CLEVELAND STATE UNIVERSITY**

April 2014

We hereby approve the dissertation  
of  
Chengfeng Xiao

---

Candidate for the Doctor of Engineering degree.  
This dissertation has been approved for the Department of

CIVIL AND ENVIRONMENTAL ENGINEERING

and CLEVELAND STATE UNIVERSITY  
College of Graduate Studies by

---

Stephen F. Duffy PhD, PE, F.ASCE - Dissertation Committee Chairman    Date  
Department of Civil and Environmental Engineering

---

Lutful I. Khan PhD, PE - Dissertation Committee Member    Date  
Department of Civil and Environmental Engineering

---

Mehdi Jalalpour PhD - Dissertation Committee Member    Date  
Department of Civil and Environmental Engineering

---

Miron Kaufman PhD - Dissertation Committee Member    Date  
Department of Physics, College of Sciences and Health Professions

---

John P. Gyekenyesi PhD, PE, F.ACerS - Dissertation Committee Member    Date  
NASA Glenn Research Center (retired)

---

Paul A. Bosela PhD, PE, F.ASCE - Dissertation Committee Member    Date  
Department of Civil and Environmental Engineering (retired)

---

Student's Date of Defense

This student has fulfilled all requirements for the Doctor of Engineering degree.

---

Dan Simon PhD - Doctoral Program Director

## ACKNOWLEDGMENTS

This academic project used up many of weekend and vacations, which I would normally have spent with my family and it is indeed extremely difficult to acknowledge their sacrifice. I wish to acknowledge the love and support I received from my wife, Xiang Li, during the duration of this project. I wish to note a deep and special gratitude to my parents, Yougang Xiao and Meifen Liang, for their patience and understanding. In addition, I wish to thank my brothers, Chengjun and Chenghao, and sister, Chengxia for your gentle encouragement.

Next, I wish acknowledge how indebted I am to my dissertation committee chairman and graduate advisor Dr. Stephen Duffy. He provided the seed ideas for the efforts outlined in this dissertation. He was patient and provided encouragement as well as advice when I needed it. I am grateful and proud to be one Dr. Duffy's students.

I also want to recognize the generous support received from the United States Department of Energy (DoE), and I especially wish to thank the technical point of contact (POC) Dr. Rob Bratton at the Idaho National Laboratory (INL). My efforts were supported under DoE Contract Number 00088589, Project #09-347 entitled "*Modeling Stress Strain Relationships and Predicting Failure Probabilities For Graphite Core*

*Components.*” Many thanks to Dr. Timothy Burchell at ORNL for the use of his graphite data. It was an honor to be associated with the great minds and wonderful talent at both INL and the Oak Ridge National Laboratory (ORNL).

# A PROBABILISTIC BASED FAILURE MODEL FOR COMPONENTS FABRICATED FROM ANISOTROPIC GRAPHITE

CHENGFENG XIAO

## ABSTRACT

The nuclear moderator for high temperature nuclear reactors are fabricated from graphite. During reactor operations graphite components are subjected to complex stress states arising from structural loads, thermal gradients, neutron irradiation damage, and seismic events. Graphite is a quasi-brittle material. Two aspects of nuclear grade graphite, i.e., material anisotropy and different behavior in tension and compression, are explicitly accounted for in this effort. Fracture mechanic methods are useful for metal alloys, but they are problematic for anisotropic materials with a microstructure that makes it difficult to identify a “critical” flaw. In fact cracking in a graphite core component does not necessarily result in the loss of integrity of a nuclear graphite core assembly. A phenomenological failure criterion that does not rely on flaw detection has been derived that accounts for the material behaviors mentioned. The probability of failure of components fabricated from graphite is governed by the scatter in strength. The design protocols being proposed by international code agencies recognize that design

and analysis of reactor core components must be based upon probabilistic principles. The reliability models proposed herein for isotropic graphite and graphite that can be characterized as being transversely isotropic are another set of design tools for the next generation very high temperature reactors (VHTR) as well as molten salt reactors.

The work begins with a review of phenomenologically based deterministic failure criteria. A number of this genre of failure models are compared with recent multiaxial nuclear grade failure data. Aspects in each are shown to be lacking. The basic behavior of different failure strengths in tension and compression is exhibited by failure models derived for concrete, but attempts to extend these concrete models to anisotropy were unsuccessful. The phenomenological models are directly dependent on stress invariants. A set of invariants, known as an integrity basis, was developed for a non-linear elastic constitutive model. This integrity basis allowed the non-linear constitutive model to exhibit different behavior in tension and compression and moreover, the integrity basis was amenable to being augmented and extended to anisotropic behavior. This integrity basis served as the starting point in developing both an isotropic reliability model and a reliability model for transversely isotropic materials.

At the heart of the reliability models is a failure function very similar in nature to the yield functions found in classic plasticity theory. The failure function is derived and presented in the context of a multiaxial stress space. States of stress inside the failure



envelope denote safe operating states. States of stress on or outside the failure envelope denote failure. The phenomenological strength parameters associated with the failure function are treated as random variables. There is a wealth of failure data in the literature that supports this notion. The mathematical integration of a joint probability density function that is dependent on the random strength variables over the safe operating domain defined by the failure function provides a way to compute the reliability of a state of stress in a graphite core component fabricated from graphite. The evaluation of the integral providing the reliability associated with an operational stress state can only be carried out using a numerical method. Monte Carlo simulation with importance sampling was selected to make these calculations.

The derivation of the isotropic reliability model and the extension of the reliability model to anisotropy are provided in full detail. Model parameters are cast in terms of strength parameters that can (and have been) characterized by multiaxial failure tests. Comparisons of model predictions with failure data is made and a brief comparison is made to reliability predictions called for in the ASME Boiler and Pressure Vessel Code.. Future work is identified that would provide further verification and augmentation of the numerical methods used to evaluate model predictions.

# TABLE OF CONTENTS

ACKNOWLEDGMENTS .....	IV
ABSTRACT.....	VI
LIST OF NOMENCLATURE.....	XII
CHAPTER I GRAPHITE COMPONENTS IN NUCLEAR REACTORS .....	1
1.1 Research Objectives.....	5
CHAPTER II STRENGTH BASED FAILURE DATA.....	9
2.1 Integrity Basis .....	10
2.2 Useful Invariants of the Cauchy and Deviatoric Stress Tensors.....	13
2.3 Graphical Representation of Stress.....	15
2.4 Graphite Failure Data.....	18
2.5 The von Mises Failure Criterion (One Parameter) .....	21
CHAPTER III TWO AND THREE PARAMETER FAILURE CRITERIA .....	28
3.1 The Drucker-Prager Failure Criterion (Two Parameter) .....	28
3.2 Willam-Warnke Failure Criterion (Three Parameter).....	45

CHAPTER IV	ISOTROPIC FAILURE CRITERION FOR GRAPHITE.....	59
4.2	Integrity Basis and Functional Dependence .....	60
4.3	Functional Forms and Associated Gradients by Stress Region .....	61
4.4	Relationships Between Functional Constants.....	69
4.5	Functional Constants in Terms of Strength Parameters.....	77
CHAPTER V	ANISOTROPIC FAILURE CRITERION.....	87
5.1	Integrity Base for Anisotropy .....	88
5.2	Functional Forms and Associated Gradients by Stress Region .....	89
5.3	Relationships Between Functional Constants.....	96
5.4	Functional Constants in Terms of Strength Parameters.....	120
CHAPTER VI	MATERIAL STRENGTH AS A RANDOM VARIABLE.....	149
6.1	Integration by Monte Carlo Simulation .....	156
6.2	The Concept of Importance Sampling Simulation.....	164
6.3	Isotropic Limit State Function – Importance Sampling.....	175
6.4	Anisotropic Limit State Functions – Importance Sampling .....	184

CHAPTER VII SUMMARY AND CONCLUSIONS .....	192
7.1 Comparison With the ASME Simplified Assessment Method.....	193
7.2 Theoretical Development - Summary .....	208
7.3 Conclusions and Future Efforts .....	211
REFERENCES .....	214

## NOMENCLATURE

$a_i$	unit vector aligned with principal stress direction
$d_i$	unit vector aligned with preferred material direction
$\bar{e}$	unit vector aligned with the hydrostatic stress line
$f_{Y_\alpha}$	probability density function of a random strength variable characterized by a two parameter Weibull distribution
$F_{Y_\alpha}$	cumulative probability density function of a random strength variable characterized by a two parameter Weibull distribution
$g$	general failure criterion function
$g_i$	failure function associated with principal stress region “ $i$ ”
$I$	indicator function
$\hat{I}$	transformed indicator function
$I_1$	first invariant of the Cauchy stress tensor
$I_2$	second invariant of the Cauchy stress tensor
$I_3$	third invariant of the Cauchy stress tensor
$J_1$	first invariant of the deviatoric stress tensor
$J_2$	second invariant of the deviatoric stress tensor
$J_3$	third invariant of the deviatoric stress tensor

$k_{y_\alpha}$	importance sampling density function
$K_{y_\alpha}$	cumulative importance sampling density function
$m$	Weibull modulus
$P_f$	probability of failure
$r$	deviatoric component of a stress state
$R$	reliability
$R_{tc}$	the ratio of the mean compressive strength to the mean tensile strength
$S$	deviatoric principal stress
$S_{ij}$	deviatoric stress tensor
$y_\alpha$	realization of a random strength parameter
$Y_\alpha$	random strength parameters
$Z_\alpha$	standard normal random strength variables
$\delta_{ij}$	Kronecker delta tensor
$\theta$	Lode angle in the deviatoric stress plane
$\delta_{y_\alpha}$	standard deviation of a random strength parameter
$\delta_{f_{y_\alpha}}$	standard deviation of the Weibull distribution
$\delta_{k_{y_\alpha}}$	standard deviation of the importance sampling function
$\mu_{y_\alpha}$	mean of a random strength variable
$\mu_{f_{y_\alpha}}$	the mean of the Weibull distribution

$\mu_{k_{\gamma\alpha}}$	mean of the importance sampling function
$\sigma_{ij}$	Cauchy stress tensor
$\sigma_i$	principal stress
$\sigma_\theta$	Weibull characteristic strength
$\sigma_T$	tensile strength parameter
$\sigma_C$	compressive strength parameter
$\sigma_{BC}$	equal biaxial compressive strength parameter in the plane of isotropy
$\sigma_{TT}$	tensile strength parameter in the plane of isotropy
$\sigma_{TC}$	compressive strength parameter in the plane of isotropy
$\sigma_{YT}$	tensile strength parameter in the preferred material direction
$\sigma_{YC}$	compressive strength parameter in the preferred material direction
$\sigma_{MBC}$	equal biaxial compressive strength parameter with one stress component in the plane of isotropy
$\sigma_v$	equivalent stress as defined by ASME
$\xi$	hydrostatic component of a stress state
$\nu$	Poisson's ratio
$\Omega$	joint probability density function of material strength parameters

## **CHAPTER I**

### **GRAPHITE COMPONENTS IN NUCLEAR REACTORS**

As discussed by Saito (2010) nuclear energy plays an important role as a means to secure a consistent and reliable source of electricity that can easily help utilities meet system demand for the nation's power grid and do so in a way that positively impacts global warming issues. Proposed system designs for nuclear power plants, e.g., the Generation IV Very High Temperature Reactors (VHTR) (2002) among others, will generate sustainable, safe and reliable energy. The nuclear moderator and major structural components for VHTRs are fabricated from graphite. During operations the graphite components are subjected to complex stress states arising from structural loads, thermal gradients, neutron irradiation damage, and seismic events, any and/or all of which can lead to failure. As discussed by Burchell et al. (2007) failure theories that predict reliability of graphite components for a given stress state are important.

Graphite is often described as a brittle or quasi-brittle material. An excellent overview of advanced technology applications involving the use of graphite material as



well as the unique behavior of this carbon based material can be found in Burchell (1999). Tabeddor (1979) and Vijayakumar, et al. (1987, 1990) emphasize the anisotropic effect the elongated grain graphite structure has on the stress-strain relationship for graphite. These authors also discuss the aspect that the material behaves differently in tension and in compression. These two properties, i.e., material anisotropy and different behavior in tension and compression, make formulating a failure model challenging.

Classical brittle material failure criteria can include modeling failure by treating a material as a collection of anharmonic springs at an atomistic level, fracture mechanics based failure models at a constituent level, as well as phenomenological failure criteria posed at a continuum level. For example Kaufman and Ferrante (1996) developed a statistical model for mechanical failure based on computing failure thresholds that are dependent on the energy of a pair of neighboring atoms. The approach taken in linear elastic fracture mechanics involves estimating the amount of energy needed to grow a pre-existing crack. The earliest fracture mechanics approach for unstable crack growth was proposed by Griffiths (1921). Li (2001) points out that the strain energy release rate approach has proven to be quite useful for metal alloys. Romanoski and Burchell (1999) tailored fracture mechanics to the typical microstructure encountered in graphite. However, linear elastic fracture mechanics is difficult to apply to anisotropic materials with a microstructure that makes it difficult to identify a “critical” flaw. An alternative approach can be found in the numerous phenomenological failure criteria identified in the engineering literature.

Popular phenomenological failure criteria for brittle materials tend to build on the one parameter Tresca model (1864), and the two parameters Mohr-Coulomb failure criterion (1776) that has been utilized for cohesive-frictional solids. Included with these fundamental model is the von Mises criterion (1913) (a one-parameter model) and the two parameter Drucker-Prager failure criterion (1952) for pressure-dependent solids. Boresi and Schmidt (2003) provide a very lucid overview of these models. In the past these models have been used to capture failure due to ductile yielding. Paul (1968) developed a generalized pyramidal criterion model which he proposed for use with brittle material. In Paul's (1968) work, an assumption that the yield criterion surface is piecewise linear is utilized which is similar to Tresca's (1864) model. The Willam and Warnke (1974) model is a three-parameter model that captures different behavior in tension and compression exhibited by concrete. Willam and Warnke's (1974) model is composed of piecewise continuous functions that maintain smooth transitions across the boundaries of the functions. The proposed work here will focus extensively on models similar to Willam and Warnke's (1974) efforts.

With regards to phenomenological models that account for anisotropic behavior the classic Tsai and Wu (1971) failure criterion is a seminal effort. Presented in the context of invariant based stress tensors for fiber-reinforced composites, the Tsai-Wu (1971) criterion is widely used in engineering for different types of anisotropic materials. In addition, Boehler and Sawczuk (1977) as well as Boehler (1987, 1994) developed yield criterion utilizing the framework of anisotropic invariant theory. Yield functions can

easily serve as the framework for failure models. Subsequent work by Nova and Zaninetti (1990) developed an anisotropic failure criterion for materials with failure behavior different in tension and compression. Theocaris (1991) proposed an elliptic paraboloid failure criterion that accounts for different behavior in tension and compression. An invariant formulation of a failure criterion for transversely isotropic solids was proposed by Cazacu et al. (1998, 1999). Cazacu's criterion reduces to the Mises-Schleicher criterion (1926), which captured different behavior in tension and compression for isotropic conditions. Green and Mkrtychian (1977) also proposed functional forms account for different behavior in tension and compression. Their work will be focused on later in this effort.

In addition to anisotropy and different behavior in tension and compression, failure of components fabricated from graphite is also governed by the scatter in strength. When material strength varies, it is desirable to be able to predict the probability of failure for a component given a stress state. Weibull (1939) first introduced a method for quantifying variability in failure strength and the size effect in brittle material. His approach was based on the weakest link theory. The work by Batdorf and Crose (1974) represented the first attempt at extending fracture mechanics to reliability analysis in a consistent and rational manner. Work by Gyekenyesi (1986), Cooper et al. (1986), Cooper (1988) and Lamon (1990) are representative of the reliability design philosophy used in analyzing structural components fabricated from monolithic ceramic. Duffy et al. (1987, 1989, 1990, 1991, 1993, 1994, 2012) presented an array of failure models to predict reliability of

ceramic components that have isotropic, transversely isotropic, or orthotropic material symmetries. All of these models were based on developing an appropriate integrity basis for each type of anisotropy.

## 1.1 Research Objectives

Given the discussion above the primary objective of this research is establishing a single form invariant probabilistic based failure model for the analysis of components fabricated from graphite. Achieving this objective begins with the adoption of an appropriate integrity basis that can reflect the failure characteristics of isotropic graphite. Through the application of invariant theory and the Cayley-Hamilton theorem as outlined in Spencer (1971, 1984), an integrity basis with a finite number of stress invariants can be formulated that reflects the failure behavior of graphite. An integrity basis, when posed properly, spans the functional space for the failure model under construction.

An isotropic model formulated as a linear combination of stress invariants that are components of an appropriate isotropic integrity basis was formulated first. The intent was to create a failure criterion based on interpretations of the literature surveyed in the previous section. Accordingly, this effort begins by proposing a deterministic failure criterion based on the work of Green and Mkrtychian (1977). Their work includes an integrity basis that reflects material behavior relevant to isotropic graphite – primarily the different failure characteristics of graphite in tension and compression. Moreover, their

integrity basis was amenable to being augmented and extended to anisotropic behaviors. Thus the Green and Mkrtychian (1977) integrity basis serves as the starting point in developing both an isotropic reliability model and a reliability model for materials that exhibit transversely isotropic failure behavior. Developing a transversely isotropic reliability model is the primary goal of this research endeavor and represents a contribution to the body of knowledge made by this research project. This was also one of the two primary objectives of the grant that supported this effort.

It must be noted that this effort is a proof of concept endeavor. An anisotropic reliability model is needed for design purposes for the grades of nuclear graphite that exhibit anisotropic failure behavior. Currently a unified reliability model does not exist that captures anisotropy and that also captures different failure characteristics in tension and compression. Developing an integrity basis for transversely isotropic failure behavior, formulating a deterministic failure criterion from that integrity basis, and finally transforming that anisotropic failure criterion into a reliability model that can predict the probability of failure given the state of stress at a point is the overarching goal of this work.

This goal is obviously achieved in steps. A failure criterion is developed first for isotropic graphite. The deterministic isotropic failure criterion is then transformed into a reliability model using well accepted stochastic principles associated with interactive reliability models. The isotropic failure criterion and the reliability model derived from this criterion is exercised to insure that both the criterion and the model bring forth

relevant behavior in a multiaxial stress setting. Throughout the dissertation classical failure models and the failure criterion proposed here will be characterized and compared with the experiment results obtained from Burchell et al. (2007). Exercising the classical failure criterion with this data systematically demonstrates the deficiencies associated with each one. The final versions of the isotropic and anisotropic reliability models developed here are examined in a similar manner, i.e., the models derived here are examined for aberrant and/or inconsistent characteristics.

Thus at the heart of an interactive reliability model is a failure function very similar in nature to the yield functions found in classic plasticity theory. States of stress inside the failure envelope denote safe operating states. States of stress on or outside the failure envelope denote failure. When sufficient scatter is present in the phenomenological strength parameters associated with the failure function then these strength parameters must be treated as random variables. There is a wealth of publications in the open literature that supports this notion. The mathematical integration of a joint probability density function that is dependent on the random strength variables over the safe operating domain defined by the failure function provides a way to compute the reliability of a state of stress in a graphite core component. The evaluation of the integral that provides the reliability associated with an operational stress state can only be carried out using a numerical method. Monte Carlo simulation with importance sampling was selected to make these calculations.

The derivation of the isotropic reliability model and the extension of the reliability model to anisotropy are provided in full detail. Model parameters are cast in terms of strength parameters that can be characterized with data from multiaxial failure tests. Conducting these strength tests are not a part of this effort. Comparison of model predictions with failure data is made and a brief comparison to reliability predictions called for in the ASME Boiler and Pressure Vessel Code is outlined. Future work is identified that would provide further verification and augmentation of the numerical methods used to evaluate model predictions.

## CHAPTER II

### STRENGTH BASED FAILURE DATA

A function associated with a phenomenological failure criterion based on multi-axial stress for isotropic materials will have the basic form

$$g = g(\sigma_{ij}) \quad (2.1)$$

This function is dependent on the Cauchy stress tensor,  $\sigma_{ij}$ , which is a second order tensor, and parameters associated with material strength. Given a change in reference coordinates, e.g., a rotation of coordinate axes, the components of the stress tensor change. The intent here is to formulate a scalar valued failure function such that it is not affected when components of the stress tensors change under a simple orthogonal transformation of coordinate axes. A convenient way of formulating a failure function to accomplish this is utilizing the invariants of stress. The development below follows the method outlined by Duffy (1987) and serves as a brief discussion on the invariants that comprise an integrity basis.



## 2.1 Integrity Basis

Assume a scalar valued function exists that is dependent upon several second order tensors, i.e.,

$$g = g(A, B, C) \quad (2.1.1)$$

Here the uppercase letters  $A$ ,  $B$  and  $C$  are matrices representing second order tensor quantities. One way of constructing an invariant formulation for this function is to express  $g$  as a polynomial in all possible traces of the  $A$ ,  $B$  and  $C$ , i.e.,

$$tr(A), tr(A^2), tr(A^3), \dots \quad (2.1.2)$$

$$tr(AB), tr(AC), tr(BC), tr(A^2B) \dots \quad (2.1.3)$$

$$tr(ABC), tr(A^2BC), tr(A^3BC), \dots \quad (2.1.4)$$

$$tr(AB^2C), tr(AB^3C), \dots \quad (2.1.5)$$

$$tr(ABC^2), tr(ABC^3), \dots \quad (2.1.6)$$

$$tr(A^2B^2C), tr(A^3B^2C), \dots \quad (2.1.7)$$

where using index notation allows

$$\begin{aligned} tr(A) &= A_{ii} \\ &\vdots \end{aligned} \quad (2.1.8)$$

$$\begin{aligned} tr(AB) &= A_{ij} B_{ji} \\ &\vdots \end{aligned} \quad (2.1.9)$$

$$\begin{aligned} tr(ABC) &= A_{ij} B_{jk} C_{ki} \\ &\vdots \end{aligned} \quad (2.1.10)$$

These are all scalar invariants of the second order tensors represented by the matrices  $A$ ,  $B$  and  $C$ . Construction of a polynomial in terms of all possible traces of the three second order tensors is analogous to expanding the function in terms of an infinite Fourier series.

However a polynomial with an infinite number of terms is clearly intractable. On the other hand if it is possible to express a number of the above traces in terms of any of the remaining traces, then the former can be eliminated. Systematically culling the list of all possible traces to an irreducible set leaves a finite number of scalar quantities (invariants) that form what is known as an integrity basis. This set is conceptually similar to the set of unit vectors that span Cartesian three spaces.

The approach to systematically eliminate members from the infinite list can best be illustrated with a simple example. Consider

$$g = g(A) \quad (2.1.11)$$

By the Cayley-Hamilton theorem, the second order tensor  $A$  will satisfy its own characteristic polynomial, i.e.,

$$A^3 + k_1 A^2 + k_2 A + k_3 [I] = [0] \quad (2.1.12)$$

where

$$k_1 = -tr(A) \quad (2.1.13)$$

$$k_2 = \frac{(tr(A))^2 - tr(A^2)}{2} \quad (2.1.14)$$

$$k_3 = \frac{-(tr(A))^3 - (3)tr(A) tr(A^2) + (2)tr(A^3)}{6} \quad (2.1.15)$$

$$[0] = \text{null tensor} \quad (2.1.16)$$

and

$$[I] = \text{identity tensor} \quad (2.1.17)$$

Multiplying the characteristic polynomial equation by  $A$  gives

$$A^4 + k_1 A^3 + k_2 A^2 + k_3 A = [0] \quad (2.1.18)$$

Taking the trace of this last expression yields

$$\text{tr}(A^4) = -[k_1 \text{tr}(A^3) + k_2 \text{tr}(A^2) + k_3 \text{tr}(A)] \quad (2.1.19)$$

and this shows that since  $k_1$ ,  $k_2$  and  $k_3$  are functions of  $\text{tr}(A)$ ,  $\text{tr}(A^2)$ , and  $\text{tr}(A^3)$ , then

$$\text{tr}(A^4) = h[\text{tr}(A^3), \text{tr}(A^2), \text{tr}(A)] \quad (2.1.20)$$

Is a function of only these three invariants as well. Indeed repeated applications of the preceding argument would demonstrate that  $\text{tr}(A^5)$ ,  $\text{tr}(A^6)$ , ... , can be written in terms of a linear combination of the first three traces of  $A$ . Therefore, by induction

$$\text{tr}(A^p) = h^*[\text{tr}(A), \text{tr}(A^2), \text{tr}(A^3)] \quad (2.1.21)$$

for any

$$p > 3$$

Furthermore, any scalar function that is dependent on  $A$  can be formulated as a linear combination of these three traces. That is if

$$g = g(A) \quad (2.1.22)$$

then the following polynomial form is possible

$$g = (k_1) \text{tr}(A^3) + (k_2) \text{tr}(A^2) + (k_3) \text{tr}(A) \quad (2.1.23)$$

and the expression for  $g$  is form invariant. The invariants  $tr(A^3)$ ,  $tr(A^2)$ ,  $tr(A)$  constitute the integrity basis for the function  $g$ . In general the results hold for the dependence on any number of tensors. If the second order tensor represented by  $A$  is the Cauchy stress tensor, then this infers the first three invariants of the Cauchy stress tensor span the functional space for scalar functions dependent on  $\sigma_{ij}$ .

## 2.2 Useful Invariants of the Cauchy and Deviatoric Stress Tensors

If one accepts the premise from the previous section for a single second order tensor, and if this tensor is the Cauchy stress tensor  $\sigma_{ij}$ , then

$$g(\sigma_{ij}) = g(I_1, I_2, I_3) \quad (2.2.1)$$

where

$$I_1 = \sigma_{ii} \quad (2.2.2)$$

$$I_2 = \left(\frac{1}{2}\right) \left( (\sigma_{ii})^2 - \sigma_{jk} \sigma_{kj} \right) \quad (2.2.3)$$

and

$$I_3 = \left(\frac{1}{6}\right) \left[ (2)(\sigma_{ij} \sigma_{jk} \sigma_{ki}) - (3)(\sigma_{ii})(\sigma_{jk} \sigma_{kj}) + (\sigma_{ii})^3 \right] \quad (2.2.4)$$

are the first three invariants of the Cauchy stress. Since the invariants are functions of principal stresses

$$I_1 = \sigma_1 + \sigma_2 + \sigma_3 \quad (2.2.5)$$

$$I_2 = \sigma_1 \sigma_2 + \sigma_2 \sigma_3 + \sigma_1 \sigma_3 \quad (2.2.6)$$

and

$$I_3 = \sigma_1 \sigma_2 \sigma_3 \quad (2.2.7)$$

then

$$\begin{aligned} g(\sigma_{ij}) &= g(I_1, I_2, I_3) \\ &= g(\sigma_1, \sigma_2, \sigma_3) \end{aligned} \quad (2.2.8)$$

Furthermore, the stress tensor  $\sigma_{ij}$  can be decomposed into a hydrostatic stress component and a deviatoric component in the following manner. Take

$$S_{ij} = \sigma_{ij} - \left(\frac{1}{3}\right)\sigma_{kk} \delta_{ij} \quad (2.2.9)$$

If we look for the eigenvalues for the second order deviatoric stress tensor ( $S_{ij}$ ) using the following determinant

$$|S_{ij} - S\delta_{ij}| = 0 \quad (2.2.10)$$

then the resultant characteristic polynomial is

$$S^3 - J_1 S^2 - J_2 S - J_3 = 0 \quad (2.2.11)$$

The coefficients  $J_1$ ,  $J_2$  and  $J_3$  are the invariants of  $S_{ij}$  and are defined as

$$J_1 = S_{ii} = 0 \quad (2.2.12)$$

$$\begin{aligned} J_2 &= \left(\frac{1}{2}\right)S_{ij} S_{ji} \\ &= I_2 - \left(\frac{1}{3}\right)I_1^2 \end{aligned} \quad (2.2.13)$$

and

$$\begin{aligned}
J_3 &= \left(\frac{1}{3}\right) S_{ij} S_{jk} S_{ki} \\
&= \left(\frac{2}{27}\right) I_1^3 - \left(\frac{1}{3}\right) I_1 I_2 + I_3
\end{aligned}
\tag{2.2.14}$$

These deviatoric invariants will be utilized as needed in the discussions that follow.

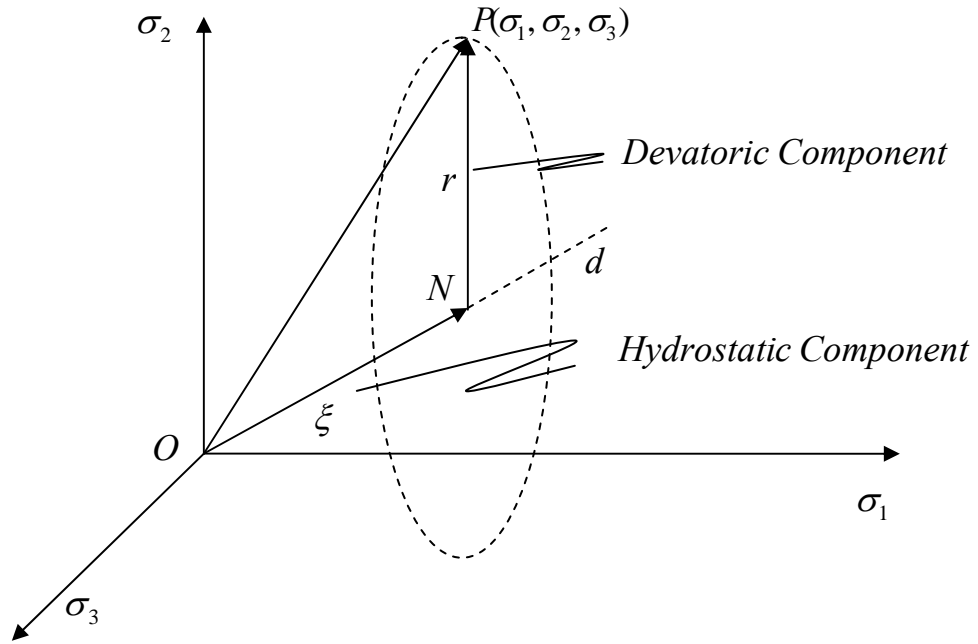


Figure 2.3.1 Decomposition of Stress in the Haigh-Westergaard (Principal) Stress Space

### 2.3 Graphical Representation of Stress

The reader is directed to Boresi and Schmidt (2003) for a comprehensive discussion on the graphical representation of models in various stress spaces. In the Haigh-Westergaard stress space a given stress state  $(\sigma_1, \sigma_2, \sigma_3)$  can be graphically decomposed into hydrostatic and deviatoric components. This decomposition is depicted graphically in Figure 2.3.1. Line  $d$  in figure 2.3.1 represents the hydrostatic

axis where  $\sigma_1 = \sigma_2 = \sigma_3$  such that the line makes equal angles to the coordinate axes. We define the planes normal to the hydrostatic stress line as deviatoric planes. As a special case the deviatoric plane passing through the origin is called the  $\Pi$ -plane, or the principal deviatoric plane. Point P ( $\sigma_1, \sigma_2, \sigma_3$ ) in this stress space represents an arbitrary state of stress. The vector NP represents the deviatoric component of the arbitrary stress state, and the vector ON represents the hydrostatic component. The unit vector  $\bar{e}$  in the direction of the hydrostatic stress line  $d$  is

$$e = \frac{1}{\sqrt{3}} [1 \ 1 \ 1] \quad (2.2.15)$$

The length of ON, which is identified as  $\xi$ , is

$$\begin{aligned} \xi &= (OP)e \\ &= [\sigma_1 \ \sigma_2 \ \sigma_3] \frac{1}{\sqrt{3}} \begin{bmatrix} 1 \\ 1 \\ 1 \end{bmatrix} \\ &= \left( \frac{1}{\sqrt{3}} \right) I_1 \end{aligned} \quad (2.2.16)$$

The length of NP, which is identified as a radial distance ( $r$ ) in a deviatoric plane, is

$$\begin{aligned} \bar{r} &= \overline{OP} - \overline{ON} \\ &= [\sigma_1 \ \sigma_2 \ \sigma_3] - \left( \frac{I_1}{\sqrt{3}} \right) [1 \ 1 \ 1] \\ &= [S_1 \ S_2 \ S_3] \end{aligned} \quad (2.2.17)$$

From this we obtain

$$\begin{aligned} |\bar{r}| &= r^2 \\ &= S_1^2 + S_2^2 + S_3^2 \\ &= 2J_2 \end{aligned} \quad (2.2.18)$$

such that

$$r = \sqrt{2J_2} \quad (2.2.19)$$

One more relationship between invariants is presented. An angle, identified in the literature as Lode's angle, can be defined on the deviatoric plane. This angle is formed from the projection of the  $\sigma_1 - \sigma_2$  axis onto a deviatoric plane and the radius vector in the deviatoric plane,  $\bar{r}$ . The magnitude of the angle is computed from the expression

$$\theta = \left(\frac{1}{3}\right) \cos^{-1} \left[ \left(\frac{3\sqrt{3}}{2}\right) \frac{J_3}{(J_2)^{3/2}} \right] \quad (0^\circ \leq \theta \leq 60^\circ) \quad (2.2.20)$$

As the reader will see this relationship will be used to develop failure criterion. It is also used here to plot failure data.

We now have several graphical schemes to present functions that are defined by various failure criteria. They are

- a principal stress plane (e.g., the  $\sigma_1 - \sigma_2$  plane);
- the use of a deviatoric plane presented in the Haigh-Westergaard stress space; or
- meridians along failure surfaces presented in the Haigh-Westergaard stress space that are projected onto a plane defined by the coordinate axes  $(\xi - r)$ .



Each presentation method will be utilized in turn to highlight aspects of the failure criteria discussed herein. We begin with one parameter phenomenological models and then discuss progressively more complex models in later chapters.

## 2.4 Graphite Failure Data

In the following section a common failure criterion is introduced and the constants for the model are characterized using uniaxial and biaxial failure data generated by Burchell et al. (2007). For the simpler models the data from Burchell et al. (2007) has more information than is necessary. For some models all the constants cannot be approximated because there is not enough appropriate data for that particular model. These issues are identified for each of the failure model presented in this chapter and for the failure models presented in the later chapters. The specimens from Burchell et al. (2007) were fabricated from grade H-451 graphite. There were nine load cases presented, including two uniaxial tensile load paths along two different material directions (data suggests that the material is anisotropic), one uniaxial compression load path, and six biaxial stress load paths. The test data is summarized in Table 2.1. The mean values of the normal stress components for each load path in the data from Burchell et al. (2007) are presented in Table 2.2. In addition, corresponding invariants are calculated and presented in Table 2.2 along with Lode's angle. All the load paths (#B-1 through #B-9) are identified in Figure 2.4.1.

**Table 2.1 Grade H-451 Graphite: Load Paths and Corresponding Failure Data**

Data Set	Ratio $\sigma_1 : \sigma_2$	Failure Stresses (MPa)		Data Set	Ratio $\sigma_1 : \sigma_2$	Failure Stresses (MPa)		Data Set	Ratio $\sigma_1 : \sigma_2$	Failure Stresses (MPa)	
		$\sigma_1$	$\sigma_2$			$\sigma_1$	$\sigma_2$			$\sigma_1$	$\sigma_2$
# B-1	1 : 0	10.97	0	# B-5	2 : 1	7.81	3.57	# B-8	1 : 1.5	6.69	10.03
		9.90	0			8.54	3.89			6.51	9.78
		9.08	0			11.2	5.6			8.07	12.11
		9.22	0			13.00	6.42			9.13	13.74
		12.19	0			11.54	5.76			6.11	9.19
		11.51	0			12.12	6.03			9.24	13.91
# B-2	0 : 1	0	15.87	# B-6	1 : 2	6.36	12.67	# B-9	1 : - 5	6.35	-31.61
		0	12.83			6.42	12.86			8.69	-43.44
		0	18.06			6.74	13.42			7.40	-36.86
		0	20.29			7.69	15.36			7.09	-35.30
		0	14.32			6.46	12.95			5.94	-29.50
		0	14.22			7.17	14.36			6.83	-32.83
# B-3	0 : - 1	0	-47.55	# B-7	1 : - 2	7.98	-15.99	# B-9	1 : - 5	8.06	-40.21
		0	-50.63			5.50	-10.96			7.75	-38.58
		0	-59.72			6.69	-13.37				
		0	-56.22			10.49	-21.01				
		0	-48.19			9.18	-18.30				
		0	-51.54			11.31	-22.61				
# B-4	1 : - 1	9.01	-8.94								
		7.68	-7.68								
		14.34	-14.16								
		8.93	-8.78								
		13.23	-13.14								
		9.21	-9.11								

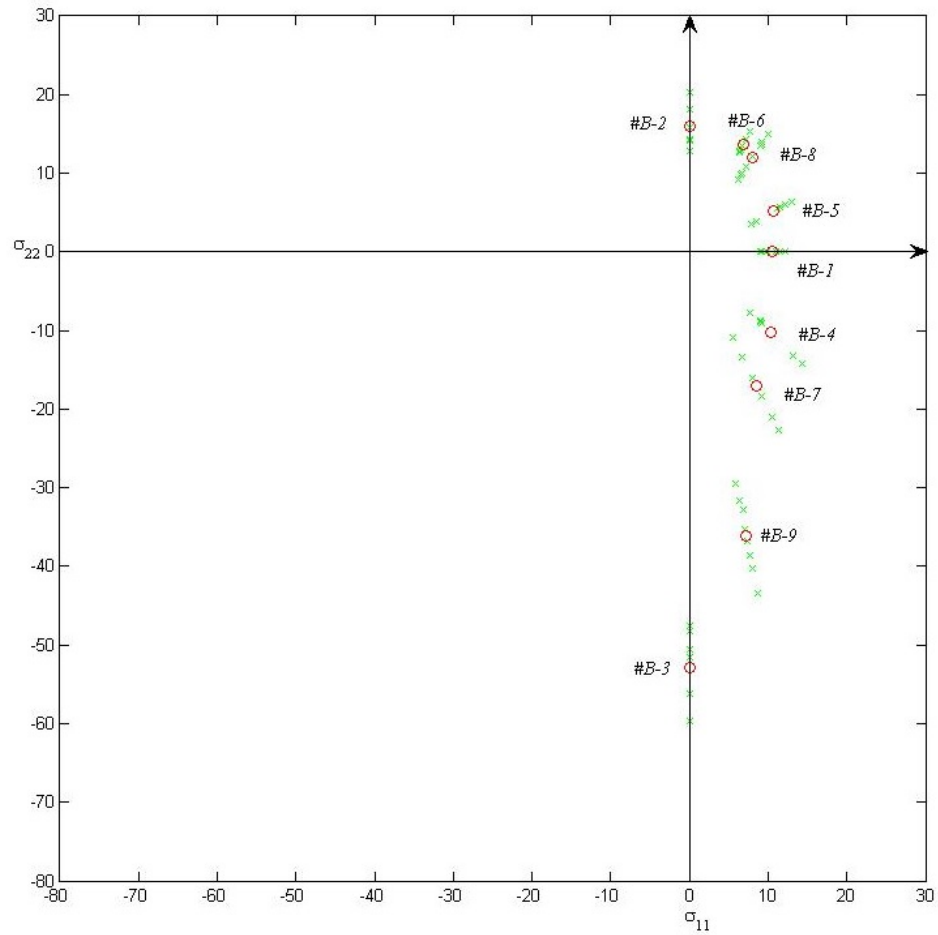


Figure 2.4.1 Load Paths from Burchell et al. (2007) Plotted in a  $\sigma_1 - \sigma_2$  Stress Space

Table 2.2 Invariants of the Average Failure Strengths for All 9 Load Paths

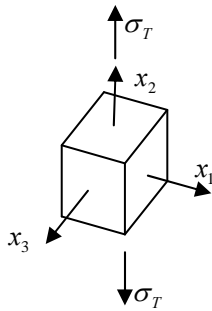
Data Set	$(\sigma_1)_{ave}$ (MPa)	$(\sigma_2)_{ave}$ (MPa)	$\xi$ (MPa)	$r$ (MPa)	$\theta$
# B-1	10.48	0	6.05	8.56	0.00°
# B-2	0	15.93	9.20	13.01	0.00°
# B-3	0	-52.93	-30.56	43.22	60.00°
# B-4	10.4	-10.3	0.06	14.64	29.84°
# B-5	10.7	5.21	9.19	7.57	29.13°
# B-6	6.81	13.6	11.78	9.62	30.05°
# B-7	8.53	-17.04	-4.91	18.41	40.88°
# B-8	7.98	11.99	11.53	8.63	40.82°
# B-9	7.26	-36.04	-16.62	32.79	50.99°

## 2.5 The von Mises Failure Criterion (One Parameter)

The von Mises criterion (1913) is based on failure defined by the octahedral shearing stress reaching a critical value. Failure occurs along octahedral planes and the basic formulation for the criterion is

$$\begin{aligned} g(\sigma_{ij}) &= g(J_2) \\ &= AJ_2 - 1 \\ &= 0 \end{aligned} \quad (2.5.1)$$

To determine the constant  $A$  consider the following stress state at failure



$$\sigma_{ij} = \begin{bmatrix} 0 & 0 & 0 \\ 0 & \sigma_T & 0 \\ 0 & 0 & 0 \end{bmatrix} \quad (2.5.2)$$

here  $\sigma_T$  is the tensile strength of the material, and for this uniaxial load case

$$J_2 = \left(\frac{1}{3}\right)\sigma_T^2 \quad (2.5.3)$$

Substitution of the value of the invariant  $J_2$  into the failure function expressed in (2.5.1)

yields

$$A = \frac{3}{\sigma_T^2} \quad (2.5.4)$$

So the failure function for von Mises (1913) criterion takes the form

$$g(\sigma_{ij}) = \left(\frac{3}{\sigma_T^2}\right)J_2 - 1 \quad (2.5.5)$$

As mentioned previously we have several means to graphically present the von Mises (1913) criterion. The von Mises (1913) failure function is a right circular cylinder in the Haigh-Westergaard stress space shown as Figure 2.5.1. The axis of the cylinder is coincident with the hydrostatic stress line. The right circular cylinder is open along the hydrostatic stress line (i.e., no end caps) in either the tensile or compressive direction. Thus a hydrostatic state of stress cannot lead to failure.

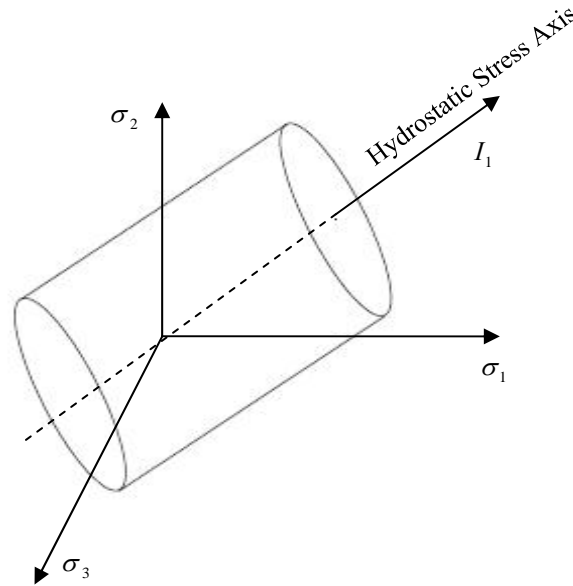


Figure 2.5.1 Von Mises (1913) Failure in Haigh-Westergaard Stress Space

Data set #B-2, which is tabulated in Table 2.3, represents a uniaxial tensile load case. One can easily determine from this data that the mean strength is  $\sigma_T = 15.93$  MPa and that

$$A = \frac{3}{\sigma_T^2} = \frac{3}{(15.93)^2} = 0.0118 \quad (2.5.6)$$

For a uniaxial load path where the stress is equal to the mean strength value for  $\sigma_T$ , the components of this stress state in the Haigh-Westergaard stress space are

$$\begin{aligned} r &= 13.01 \text{ MPa} \\ \xi &= 9.20 \text{ MPa} \end{aligned} \tag{2.5.7}$$

*Table 2.3 Invariants of the Failure Stresses for Load Path #B-2*

$\sigma_{11}$	$\sigma_{22}$	$\xi$ (MPa)	$r$ (MPa)	$\theta$
15.87	0	9.16	12.96	0°
12.83	0	7.41	10.48	0°
18.06	0	10.43	14.75	0°
20.29	0	11.71	16.57	0°
14.32	0	8.27	11.69	0°
14.22	0	8.21	11.61	0°

The von Mises (1913) failure criterion is projected onto a deviatoric plane in Figure 2.5.2 utilizing these parameter values. The result of this projection is a circle. Figure 2.5.2 also depicts the data from load path #B-2 projected onto the deviatoric plane.

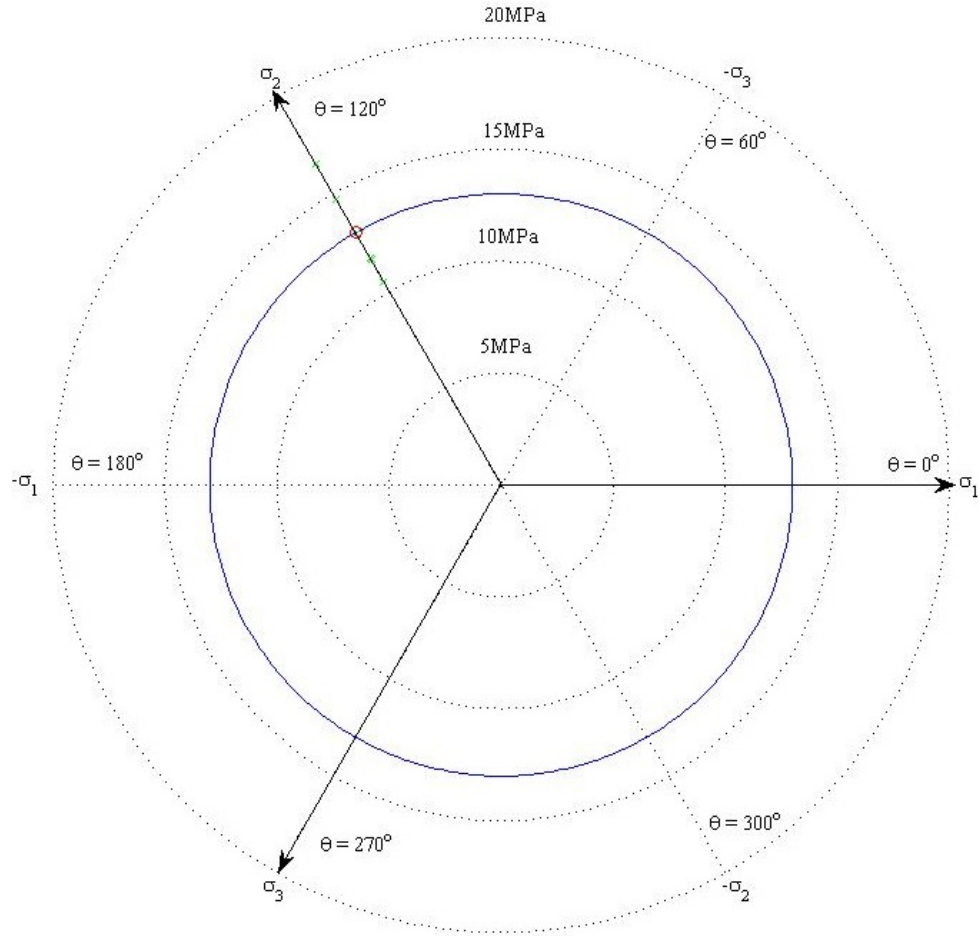


*Figure 2.5.2 The Von Mises (1913) Criterion Is Projected onto a Deviatoric Plane ( $\xi = 9.20\text{MPa}$ ) Parallel to the Deviatoric Plan with  $\sigma_T = 15.93\text{MPa}$*

The von Mises (1913) failure criterion is also projected onto a  $\sigma_1 - \sigma_2$  stress plane in Figure 2.5.3. A right circular cylinder projected onto this plane presents as an ellipse. An aspect of the von Mises (1913) failure model is that tensile and compressive failure strengths are equal which is clearly evident in Figure 2.5.3. Obviously the data from Burchell et al. (2007), which is also depicted in Figure 2.5.3, strongly suggests that tensile strength is not equal to the compressive strength for this graphite material.

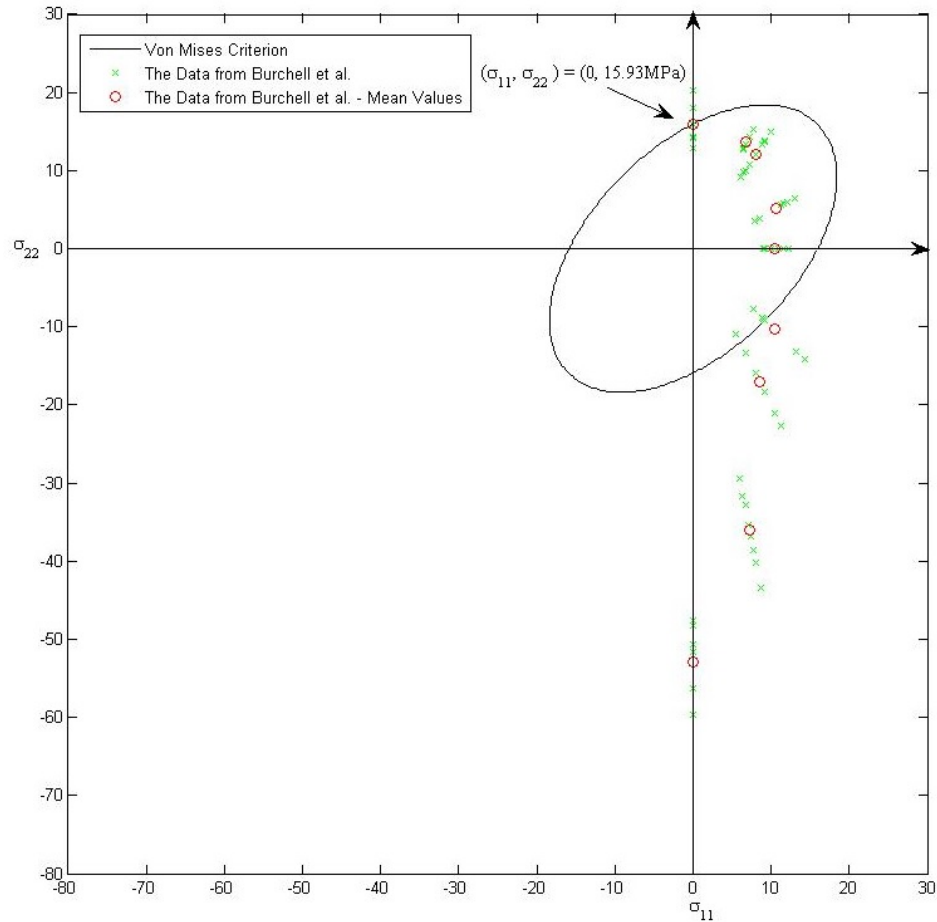


*Figure 2.5.3 The Von Mises (1913) Criterion Characterized with  $(\sigma_T = 15.93 \text{ MPa})$  Projected onto the  $\sigma_1 - \sigma_2$  Principal Stress Plane Depicting Failure Stress Values for All Load Paths*

The third type of graphic presentation is a projection of the von Mises (1913) failure criterion onto the coordinate plane identified by the axes  $(\xi - r)$ . As noted above the von Mises (1913) criterion is a right circular cylinder in the principal stress space. The function depicted in Figure 2.5.4 results from a cutting plane that contains the hydrostatic line coinciding with the axis of the right circular cylinder. The axis of the cylinder is coincident with the  $\xi$  – axis and all meridians will be parallel to the  $\xi$  – axis. Thus all meridians along the surface of the right circular cylinder representing the von



Mises (1913) failure criterion are identical, i.e., the slope of all meridians is zero and the intercepts along the r-axis are the same value. This is not the case for subsequent failure criterion presented below.

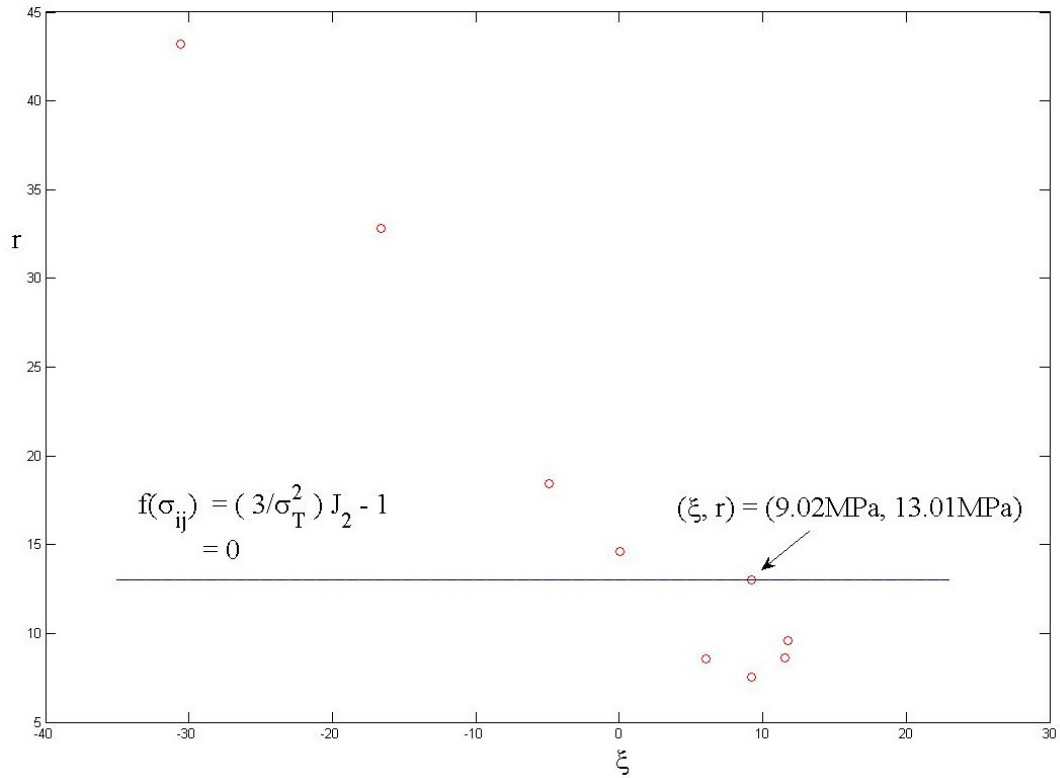


Figure 2.5.4 The Von Mises (1913) Criterion Projected onto a Meridian Plane ( $\sigma_T = 15.93$  MPa)

Using the average normal strength values from the nine load paths in Burchell et al. (2007) one can generate nine  $\xi - r$  pairs, and these pairs appear in Table 2.2. This information is depicted in Figure 2.5.4. As can be seen in the figure the averaged data from Burchell et al (2007) does not match well with the von Mises (1913) criterion characterized with  $\sigma_T = 15.93$  MPa. The depiction in Figure 2.5.4 strongly suggests that

$\xi$ , or  $I_1$ , should be considered in developing the failure function, i.e., something more than the  $J_2$  should be used to construct the model. Since nuclear graphite is not fully dense, we will assume that the hydrostatic component of the stress state contributes to failure. In addition, the von Mises (1913) criterion does not allow different strength in tension and compression. When other formulations are considered in the next chapter their dependence will have a well-defined dependence on  $I_1$ . This invariant will permit different strengths in tension and compression, e.g., the classic the Drucker–Prager (1952) failure criterion outlined in the next section.

As a final note on the one parameter models, the Tresca criterion (1864) could have been considered here. Although based on the concept that failure occurs when a maximum shear strength of a material is attained, this model is a piecewise continuous failure criterion. Although later criterion considered here are similarly piecewise continuous, the Tresca (1864) failure criterion does not mandate continuous slopes at the boundaries of various regions of the stress space. This condition will be imposed on the failure criterion considered later.

## CHAPTER III

### TWO AND THREE PARAMETER FAILURE CRITERIA

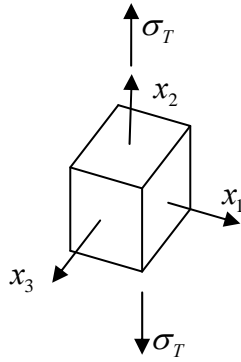
In the previous chapter failure data from Burchell et al. (2007) was presented in terms of a familiar one parameter failure criterion, i.e., the von Mises (1913) criterion. The von Mises (1913) failure criterion can be characterized through a single strength parameter – the shear strength on the octahedral stress plane. In this chapter the view is expanded and details of two and three parameter failure criterion are presented in terms of how well the criterion perform relative to the mean strength of various load paths from Burchell et al. (2007).

#### 3.1 The Drucker-Prager Failure Criterion (Two Parameter)

In this section we consider an extension of the Von Mises (1913) criterion, i.e., a failure model that includes the  $I_1$  invariant. This extension is the Drucker – Prager (1952) criterion and is defined by the failure function

$$\begin{aligned} g(I_1, J_2) &= AI_1 + B\sqrt{J_2} - 1 \\ &= 0 \end{aligned} \tag{3.1.1}$$

To determine the constants  $A$  and  $B$  first consider the following stress state at failure, i.e.,  
a uniaxial tensile load



$$\sigma_{ij} = \begin{bmatrix} 0 & 0 & 0 \\ 0 & \sigma_T & 0 \\ 0 & 0 & 0 \end{bmatrix} \quad (3.1.2)$$

here

$$I_1 = \sigma_T \quad (3.1.3)$$

and

$$\sqrt{J_2} = \left( \frac{1}{\sqrt{3}} \right) \sigma_T \quad (3.1.4)$$

Here the positive root is used to obtain a nontrivial solution for the constants  $A$  and  $B$ .

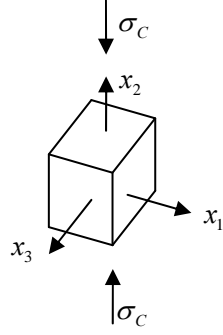
Substitution of these invariants into the failure function (3.1.1) yields

$$A \sigma_T + \left( \frac{1}{\sqrt{3}} \right) B \sigma_T - 1 = 0 \quad (3.1.5)$$

or

$$A + \left( \frac{1}{\sqrt{3}} \right) B = \frac{1}{\sigma_T} \quad (3.1.6)$$

Next, consider the following stress state at failure under a uniaxial compression  
load



$$\sigma_{ij} = \begin{bmatrix} 0 & 0 & 0 \\ 0 & \sigma_c & 0 \\ 0 & 0 & 0 \end{bmatrix} \quad (3.1.7)$$

where

$$I_1 = \sigma_c \quad (3.1.8)$$

and

$$\sqrt{J_2} = -\left(\frac{1}{\sqrt{3}}\right)\sigma_c \quad (3.1.9)$$

where the negative root is used here to obtain a nontrivial solution for the constants A and

B. Substitution of these invariants into the failure function (3.1.1) yields

$$A\sigma_c - \left(\frac{1}{\sqrt{3}}\right)B\sigma_c - 1 = 0 \quad (3.1.10)$$

or

$$A - \left(\frac{1}{\sqrt{3}}\right)B = \frac{1}{\sigma_c} \quad (3.1.11)$$

Simultaneous solution of equations (3.1.6) and (3.1.11) yields

$$A = \left(\frac{1}{2}\right)\left(\frac{1}{\sigma_T} - \frac{1}{\sigma_c}\right) \quad (3.1.12)$$

$$B = \left(\frac{\sqrt{3}}{2}\right)\left(\frac{1}{\sigma_T} + \frac{1}{\sigma_c}\right) \quad (3.1.13)$$

Using the data from load path #B-2 in Burchell et al. (2007) the average tensile strength is

$$\sigma_T = 15.93 \text{ MPa} \quad (3.1.14)$$

In a similar manner, using the load path #B-3, the average compressive strength is

$$\sigma_C = -52.93 \text{ MPa} \quad (3.1.15)$$

With these values of  $\sigma_T$  and  $\sigma_C$  the parameters  $A$  and  $B$  are

$$\begin{aligned} A &= \left(\frac{1}{2}\right) \left(\frac{1}{15.93} - \frac{1}{52.93}\right) \\ &= 0.02194 \text{ MPa}^{-1} \end{aligned} \quad (3.1.16)$$

and

$$\begin{aligned} B &= \left(\frac{\sqrt{3}}{2}\right) \left(\frac{1}{15.93} + \frac{1}{52.93}\right) \\ &= 0.07073 \text{ MPa}^{-1} \end{aligned} \quad (3.1.17)$$

The Drucker-Prager (1952) failure criterion is first projected onto the deviatoric plane defined by

$$\xi = 9.20 \text{ MPa} \quad (3.1.18)$$

in Figure 3.1.1. There are an infinite number of deviatoric planes parallel to the  $II$ -plane. For the Drucker-Prager (1952) failure criterion each projection will represent a circle with a different diameter on a different deviatoric plane. In addition, the graphical depiction of the Drucker-Prager (1952) failure criterion projected onto the deviatoric plane defined by

$$\xi = -30.2 \text{ MPa} \quad (3.1.19)$$

is depicted in Figure 3.1.2. This value of  $\xi$  is obtained from averaging the compressive strength data along load path #B-3. The invariants associated with a strength averaged from all the load data along path #B-3 are listed in Table 2.2. The invariants for individual failure strengths along load path #B-3 are presented in Table 3.1 and the failure data along load path #B-3 are also depicted in Figure 3.1.2. The Drucker-Prager (1952) failure criterion can be thought of as a right circular cone with the tip of the cone located along the positive  $\xi$  - axis. The cone opens up along the  $\xi$  - axis as  $\xi$  becomes more and more negative. The negative value of  $\xi$  from equation 3.1.19 denotes a deviatoric plane beyond the  $II$  - plane where  $\xi = 0$ . The failure criterion depicted in Figure 3.1.2 has a larger diameter than the failure criterion depicted in Figure 3.1.1.

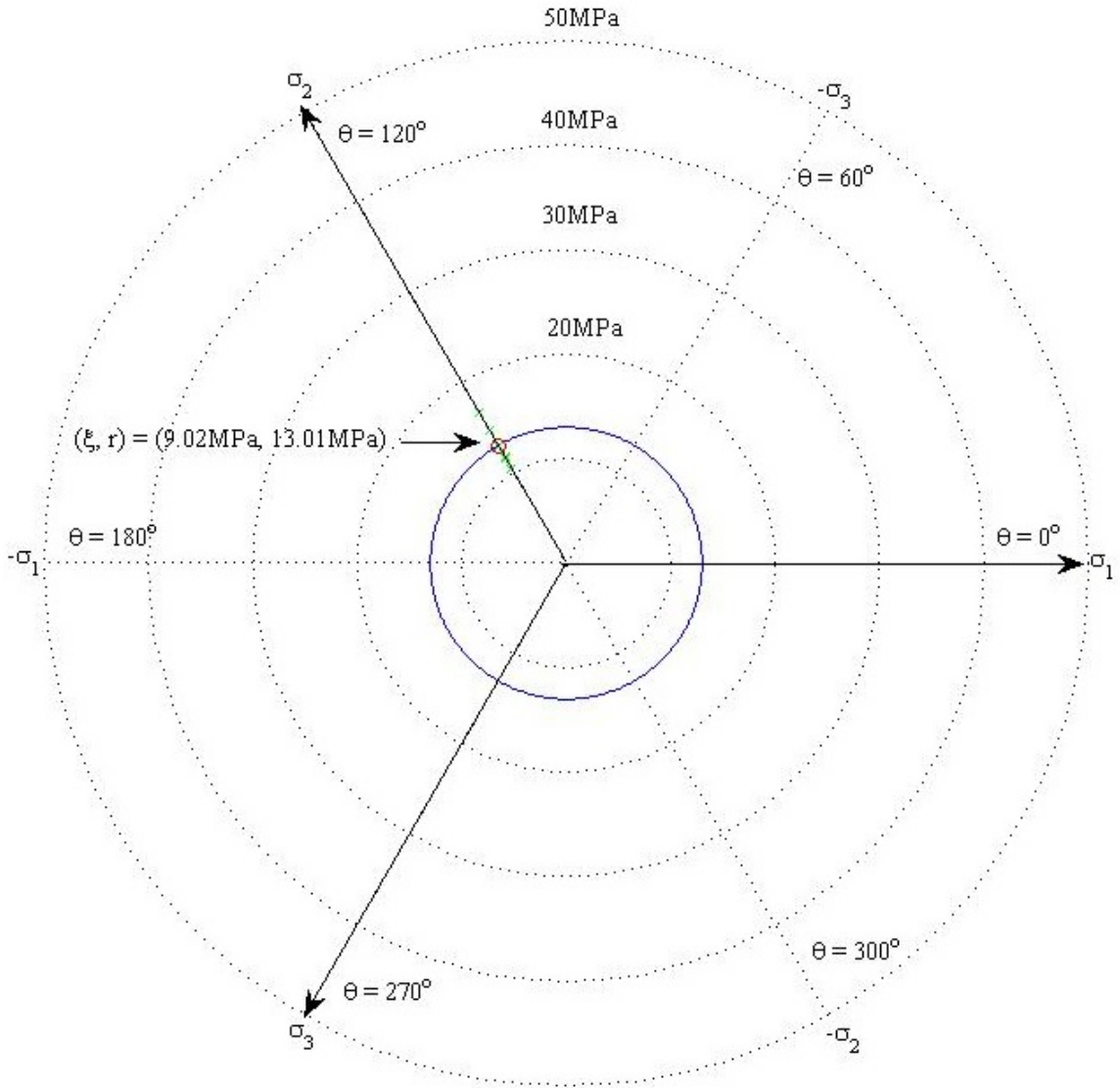


Figure 3.1.1 The Drucker-Prager (1952) Criterion Projected onto a Deviatoric Plane ( $\xi = 9.20\text{Mpa}$ ) Parallel to the  $\Pi$ -plane with  $\sigma_r = 15.93\text{MPa}$ ,  $\sigma_c = -52.93\text{MPa}$



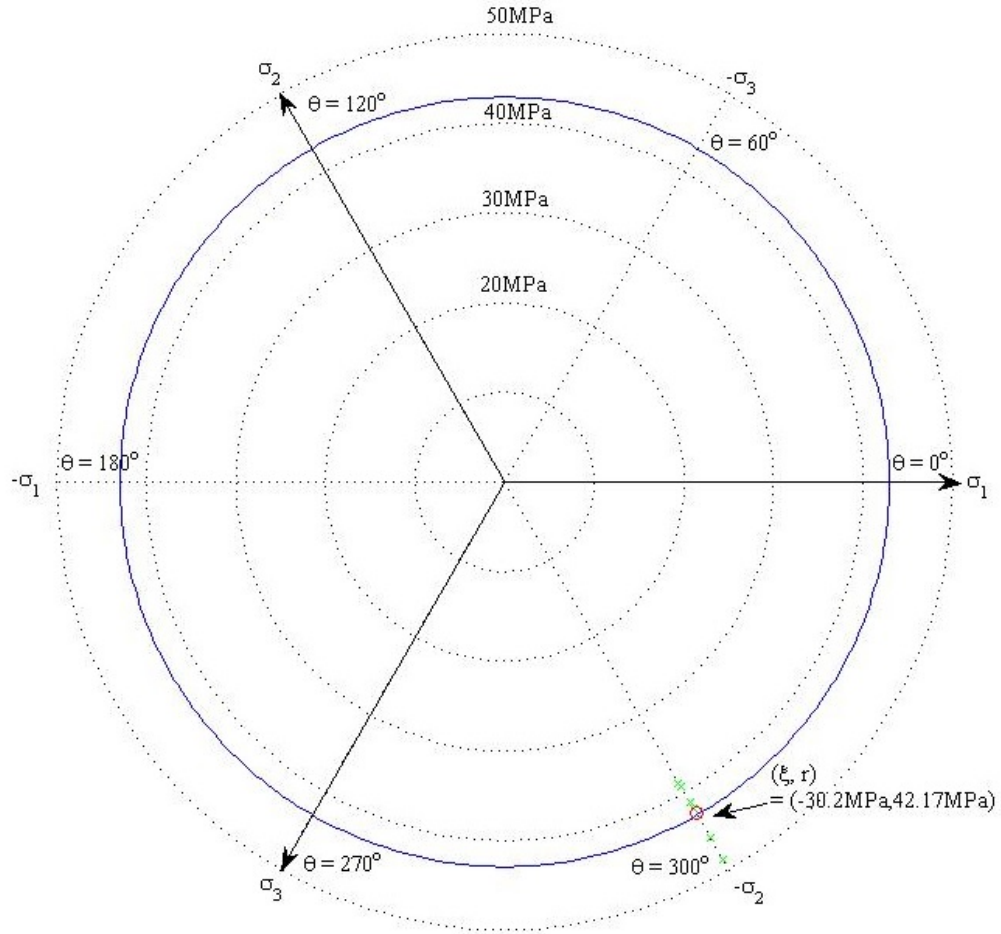


Figure 3.1.2 The Drucker-Prager (1952) Criterion Projected onto a Deviatoric Plane ( $\xi = -30.2\text{MPa}$ ) Parallel to the  $\Pi$ -plane with  $\sigma_T = 15.93\text{MPa}$ ,  $\sigma_C = -52.93\text{MPa}$

Table 3.1 Invariants of the Failure Stresses for Load Path #B-3

$\sigma_{11}(\text{MPa})$	$\sigma_{22}(\text{MPa})$	$\xi (\text{MPa})$	$r (\text{MPa})$	$\theta$
0	-47.55	-27.45	38.82	$0^\circ$
0	-50.63	-29.23	41.34	$0^\circ$
0	-59.72	-34.48	48.76	$0^\circ$
0	-56.22	-32.46	45.90	$0^\circ$
0	-48.19	-27.82	39.35	$0^\circ$
0	-51.54	-29.76	42.08	$0^\circ$

In Figure 3.1.3 the failure criterion is projected onto the  $\sigma_1 - \sigma_2$  stress plane along and is compared with all the data from Burchell et al. (2007). The right circular cone typically projects as an elongated ellipse in this stress space. The Drucker-Prager (1952) failure criterion matches the mean failure stress along the  $\sigma_1$  - tensile load path (load path #B-2) and the  $\sigma_1$  - compressive load path (load path #B-3), as it should since the criterion was characterized with the data along these two load paths. However the criterion does not match the data along the  $\sigma_2$  tensile load path (load path #B-1). The H-451 graphite that Burchell et al. (2007) tested is slightly anisotropic. Moreover, the failure data from the biaxial stress load paths, #B-4 through #B-8 do not match well with the criterion characterized using tensile and compressive strength data. The exception to this is along load path #B-9. This indicates a need for more flexibility from the failure model in order to phenomenologically capture the biaxial failure data.

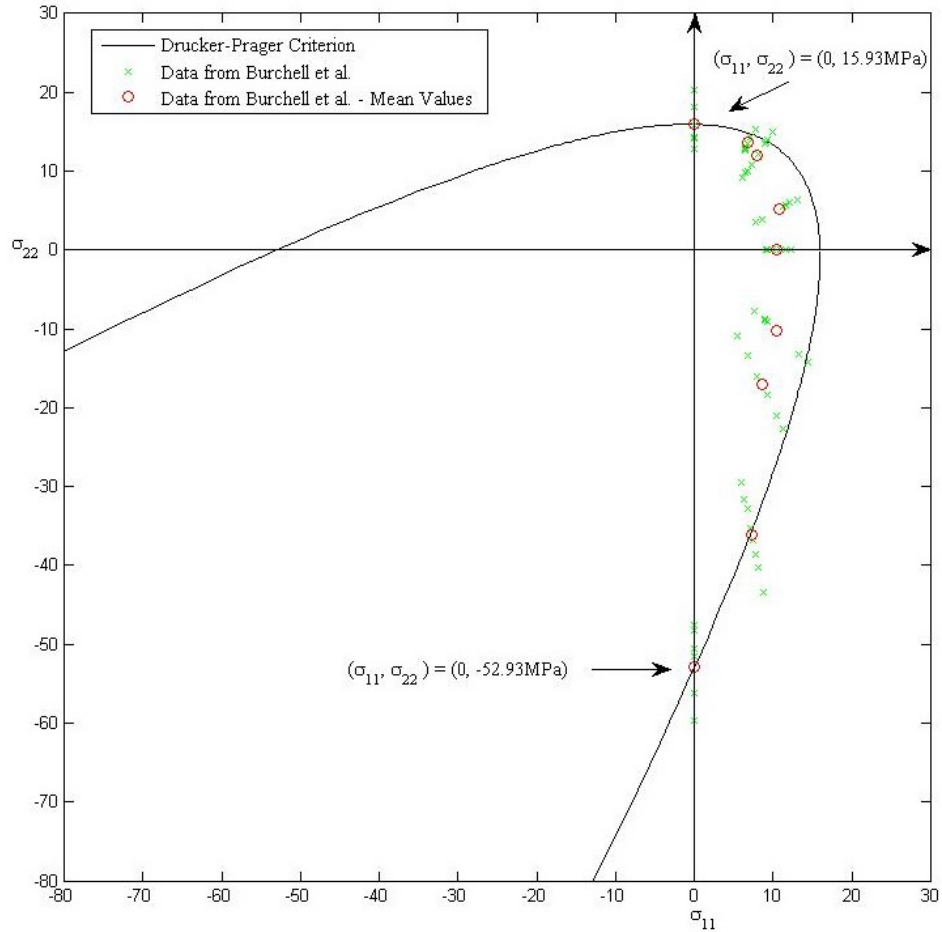


Figure 3.1.3 The Drucker-Prager (1952) Criterion Projected onto the  $\sigma_1$  -  $\sigma_2$  Principal Stress Plane ( $\sigma_T = 15.93$  MPa,  $\sigma_C = -52.93$  MPa)

The need for more flexibility is also evident when the Drucker-Prager (1952) failure criterion is projected onto the stress space defined by the  $\xi$  -  $r$  coordinate axes. This projection is shown in Fig. 3.1.4 along with projections of the average strength values from all nine load paths. As in the von Mises (1913) failure criterion, there is a single meridian. The meridian for the Drucker-Prager (1952) failure criterion has a slope, where the meridian for the von Mises (1913) failure criterion was parallel to the  $\xi$  - axis. As can be seen in Figure 3.1.4 three out of the nine average strength values align well with the failure meridian projected into this figure based on the parameter values  $\sigma_T$

= 15.93 MPa, and  $\sigma_C = -52.93$  MPa. These two parameters define the slope of the meridian, and the meridian passes through the corresponding  $\xi$ - $r$  values, as it should. The other six average strength values do not map closely to this single meridian for the Drucker-Prager (1952) criterion. Keep in mind that the projection in Figure 3.1.4 is a result of a cutting plane through the right circular cone and contains the hydrostatic stress line. The data indicates that the failure function meridians should exhibit a dependence on  $\theta$  - defined by equation 2.2.20 and depicted in Figure 2.4.2. This can be accomplished by including a dependence on the  $J_3$  invariant, and this is discussed in the next section.

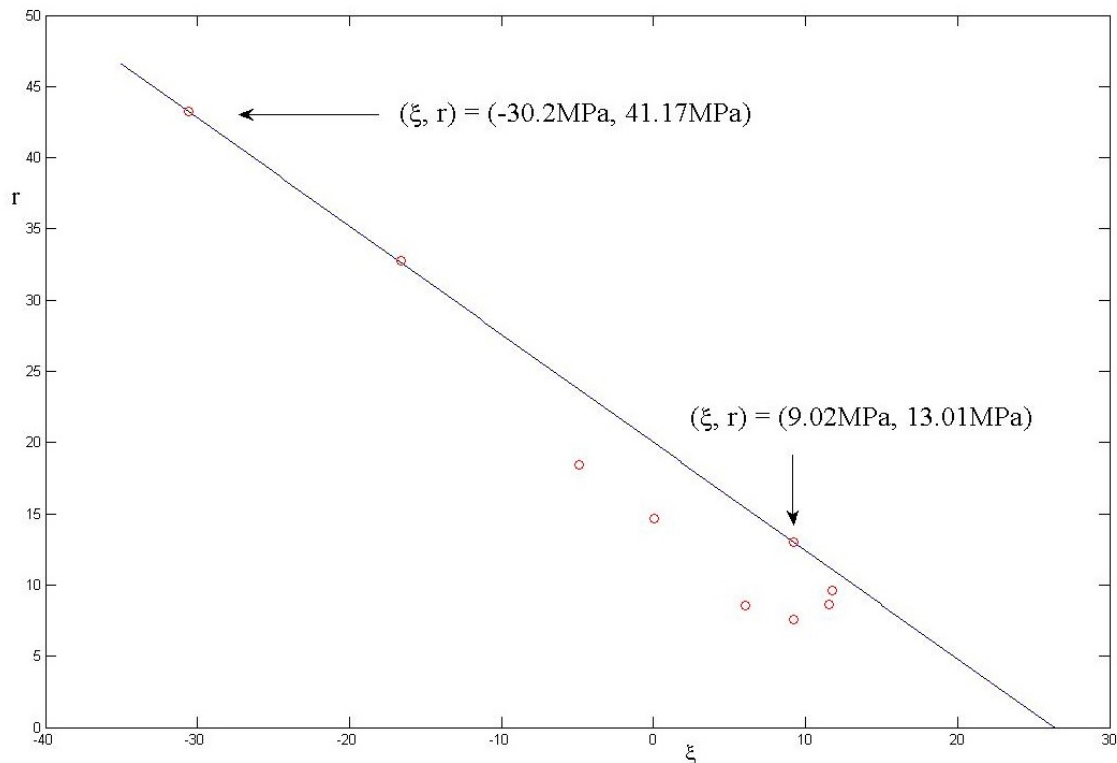


Figure 3.1.4 The Drucker-Prager Criterion Projected onto the Meridian Plane  
 $(\sigma_T = 15.93$  MPa,  $\sigma_C = -52.93$  MPa)

As noted above and depicted in Figure 3.1.3 the Drucker-Prager failure curve is open along the equal biaxial compression load path. The following derivation will demonstrate the transition from a parabolic (open) curve to an elliptic (closed) curve is based on the strength ratio  $\sigma_C / \sigma_T$ . Consider the equal biaxial compression stress state with  $\sigma_{BC} < 0$

$$\sigma_{ij} = \begin{bmatrix} \sigma_{BC} & 0 & 0 \\ 0 & \sigma_{BC} & 0 \\ 0 & 0 & 0 \end{bmatrix} \quad (3.1.20)$$

The corresponding deviatoric stress tensor is

$$S_{ij} = \begin{bmatrix} \frac{\sigma_{BC}}{3} & 0 & 0 \\ 0 & \frac{\sigma_{BC}}{3} & 0 \\ 0 & 0 & -\frac{2\sigma_{BC}}{3} \end{bmatrix} \quad (3.1.21)$$

The stress invariants of this state of stress are

$$I_1 = 2\sigma_{BC} \quad (3.1.22)$$

and

$$\sqrt{J_2} = \left( -\frac{1}{\sqrt{3}} \right) \sigma_{BC} \quad (3.1.23)$$

Substitution of these invariants into the failure function (3.1.1) yields

$$A(2\sigma_{BC}) + B \left( -\frac{1}{\sqrt{3}} \right) \sigma_{BC} - 1 = 0 \quad (3.1.24)$$

or

$$\sigma_{BC} = \frac{1}{2A - \left(\frac{1}{\sqrt{3}}\right)B} \quad (3.1.25)$$

Since  $\sigma_{BC} < 0$ , then

$$\sigma_{BC} = \frac{1}{2A - \left(\frac{1}{\sqrt{3}}\right)B} < 0 \quad (3.1.26)$$

which infers

$$2A < \left(\frac{1}{\sqrt{3}}\right)B \quad (3.1.27)$$

This leads to

$$2\left(\frac{1}{2}\right)\left(\frac{1}{\sigma_T} - \frac{1}{\sigma_C}\right) < \left(\frac{1}{\sqrt{3}}\right)\left(\frac{\sqrt{3}}{2}\right)\left(\frac{1}{\sigma_T} + \frac{1}{\sigma_C}\right) \quad (3.1.28)$$

or

$$\frac{1}{\sigma_T} < \frac{3}{\sigma_C} \quad (3.1.29)$$

Thus

$$\frac{\sigma_C}{\sigma_T} < 3 \quad (3.1.30)$$

When the ratio of compressive strength and tensile strength  $(\sigma_C / \sigma_T) < 3$ , the Drucker-Prager failure criterion projects an elliptical (closed) curve in the  $\sigma_1 - \sigma_2$  stress plane.

Consider the following biaxial state of stress

$$\sigma_{ij} = \begin{bmatrix} \sigma_x & 0 & 0 \\ 0 & \sigma_y & 0 \\ 0 & 0 & 0 \end{bmatrix} \quad (3.1.31)$$

The corresponding deviatoric stress tensor is

$$S_{ij} = \begin{bmatrix} \frac{2\sigma_x - \sigma_y}{3} & 0 & 0 \\ 0 & \frac{2\sigma_y - \sigma_x}{3} & 0 \\ 0 & 0 & -\frac{\sigma_x + \sigma_y}{3} \end{bmatrix} \quad (3.1.33)$$

The stress invariants for this state of stress are

$$I_1 = \sigma_x + \sigma_y \quad (3.1.32)$$

and

$$\sqrt{J_2} = \sqrt{\left(\frac{1}{3}\right)(\sigma_x^2 - \sigma_x\sigma_y + \sigma_y^2)} \quad (3.1.34)$$

Substitution of these invariants into equation (3.1.1) yields

$$\begin{aligned} f(I_1, J_2) &= A(\sigma_x + \sigma_y) \\ &+ B\sqrt{\left(\frac{1}{3}\right)(\sigma_x^2 - \sigma_x\sigma_y + \sigma_y^2)} - 1 \\ &= 0 \end{aligned} \quad (3.1.35)$$

or

$$\sqrt{\left(\frac{1}{3}\right)(\sigma_x^2 - \sigma_x\sigma_y + \sigma_y^2)} = \frac{1 - A(\sigma_x + \sigma_y)}{B} \quad (3.1.36)$$

Squaring both sides yields

$$\begin{aligned} (B^2 - 3A)\sigma_x^2 + (B^2 - 3A)\sigma_y + (6A - B^2)\sigma_x\sigma_y^2 \\ + 6A\sigma_x + 6A\sigma_y - 3 = 0 \end{aligned} \quad (3.1.37)$$

The shape of the failure criterion defined by equation (3.1.37) is determined by the values of the two parameters  $A$  and  $B$ . Using tensile data from Burchell et al. (2007) where  $\sigma_T = 15.93 \text{ MPa}$  and a ratio of compressive strength to tensile strength of  $(\sigma_C / \sigma_T) = 2$ , then  $\sigma_C = -31.86 \text{ MPa}$  and the parameters  $A$  and  $B$  are

$$\begin{aligned} A &= \left(\frac{1}{2}\right)\left(\frac{1}{15.93} - \frac{1}{31.86}\right) \\ &= 0.01569 \text{ MPa}^{-1} \end{aligned} \quad (3.1.38)$$

and

$$\begin{aligned} B &= \left(\frac{\sqrt{3}}{2}\right)\left(\frac{1}{15.93} + \frac{1}{31.86}\right) \\ &= 0.08155 \text{ MPa}^{-1} \end{aligned} \quad (3.1.39)$$

Equation (3.1.37) becomes

$$\begin{aligned} (0.0059)\sigma_x^2 + (0.0059)\sigma_y^2 - (0.0081)\sigma_x\sigma_y \\ + (0.0942)\sigma_x + (0.0942)\sigma_y = 3 \end{aligned} \quad (3.1.40)$$

This expression is plotted in the  $\sigma_{11} - \sigma_{22}$  stress plane depicted in Figure 3.1.5



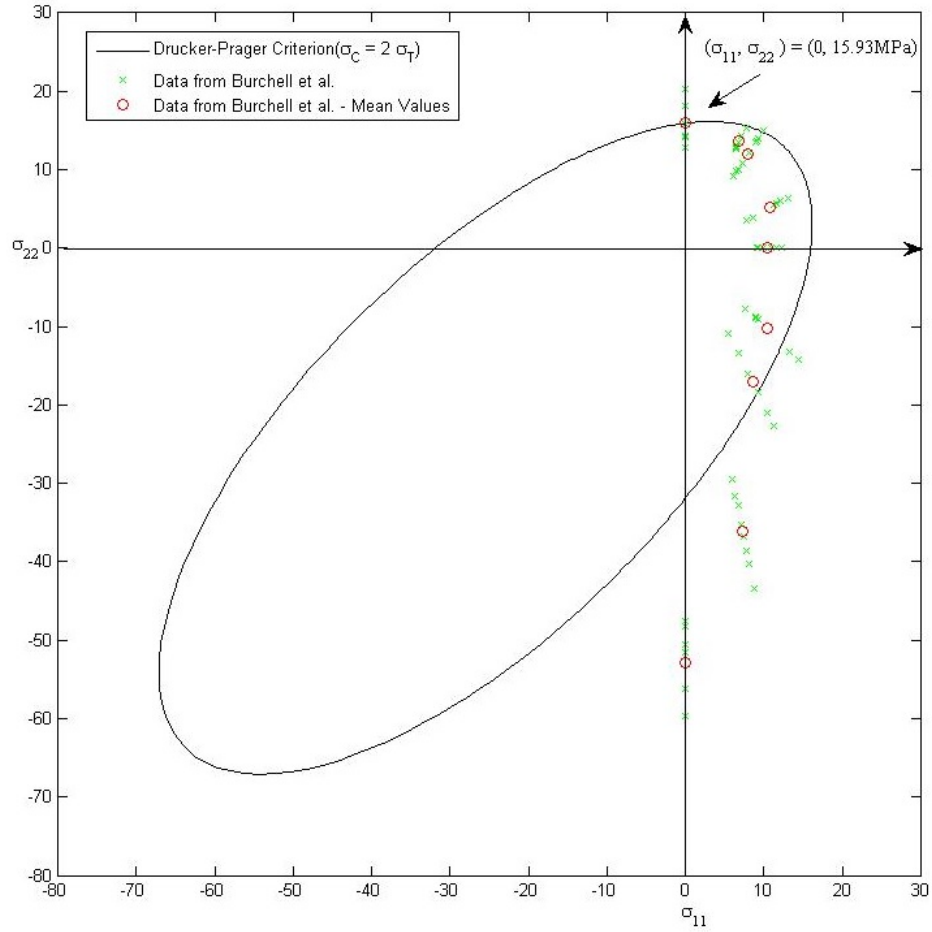


Figure 3.1.5 The Drucker-Prager (1952) Criterion Projected onto the  $\sigma_1 - \sigma_2$  Principal Stress Plane ( $\sigma_T = 15.93 \text{ MPa}$ ,  $\sigma_C = -31.86 \text{ MPa}$ ) and Compared with the Data from Burchell et al. (2007)

This combination of strength parameters leads to a biaxial strength of well over  $60 \text{ MPa}$ .

If compressive strength of  $\sigma_C = -52.93 \text{ MPa}$  from Burchell et al. (2007) is utilized from along with a stress ratio ( $\sigma_C / \sigma_T = 2$ ), then the tensile strength is  $\sigma_T = 26.465 \text{ MPa}$ .

The parameters  $A$  and  $B$  are

$$\begin{aligned}
 A &= \left(\frac{1}{2}\right) \left( \frac{1}{26.465} - \frac{1}{52.93} \right) \\
 &= 0.009446 \text{ MPa}^{-1}
 \end{aligned}
 \tag{3.1.41}$$

and

$$\begin{aligned}
 B &= \left( \frac{\sqrt{3}}{2} \right) \left( \frac{1}{26.465} + \frac{1}{52.93} \right) \\
 &= 0.0490855 \text{ MPa}^{-1}
 \end{aligned}
 \tag{3.1.42}$$

Now

$$\begin{aligned}
 (0.0021)\sigma_x^2 + (0.0021)\sigma_y^2 - (0.0029)\sigma_x\sigma_y \\
 + (0.0567)\sigma_x + (0.0567)\sigma_y = 3
 \end{aligned}
 \tag{3.1.44}$$

This expression is plotted in the  $\sigma_{11} - \sigma_{22}$  stress plane depicted in Figure 3.1.6

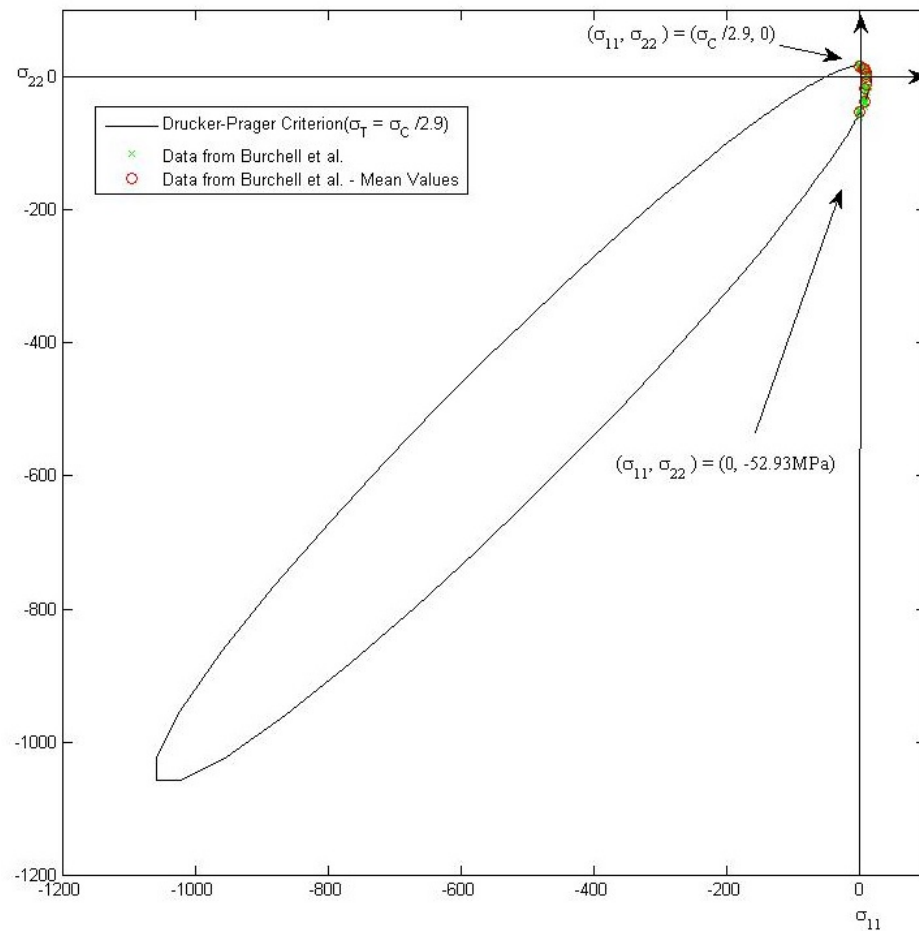


*Figure 3.1.6 The Drucker-Prager (1952) Criterion Projected onto the  $\sigma_1 - \sigma_2$  Principal Stress Plane ( $\sigma_T = 18.25 \text{ MPa}$ ,  $\sigma_C = -52.93 \text{ MPa}$ ) and Compared with the Data from Burchell et al. (2007)*

Here the biaxial compressive strength is somewhat less than  $1,100 \text{ MPa}$ . In both figures, i.e., Figure 3.1.5 and 3.1.6, closed ellipses are obtained which are important since all load paths in this stress space eventually lead to failure. In Figure 3.1.3 the equal biaxial compression load path was not bounded by the failure criterion given the strength parameters extracted from the data from Burchell et al. (2007). For all failure criteria considered, only those with closed failure surfaces are relevant for consideration.

In order to see the full effect of the ratio of compression to tension strengths, this ratio is varied from a value of 1.0 to 2.75 in increments of 0.25 in Figure 3.1.7. The ratio was computed by holding  $\sigma_T$  fixed at the mean value of the data from Burchell et al. (2007) for load path B-2, i.e., 15.93 MPa, and increasing the strength parameter  $\sigma_C$  from 15.93 MPa to 2.75 times this value, i.e., 43.81 MPa.

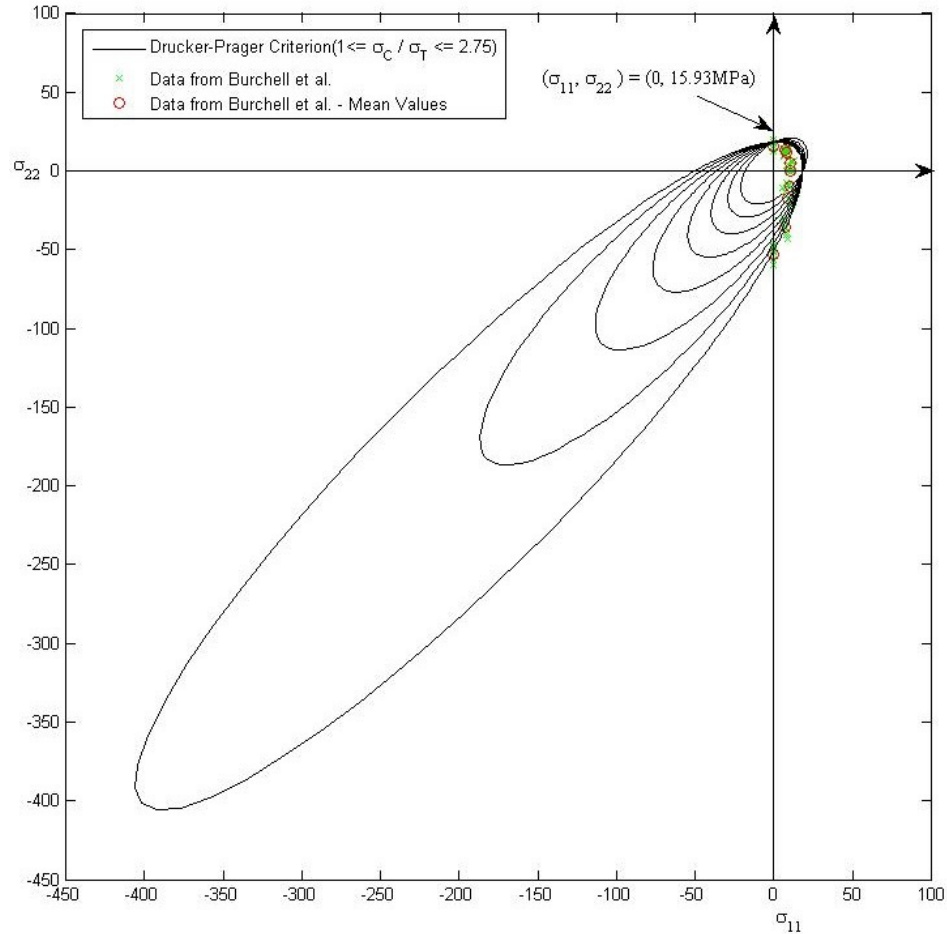


*Figure 3.1.7 The Drucker-Prager (1952) Criterion Projected onto the  $\sigma_1$  -  $\sigma_2$  Principal Stress Plane. Tensile Strength  $\sigma_T$  Fixed at 15.93MPa, and Compressive Strength  $\sigma_C$  Varies from 15.93 MPa to 43.18 MPa.*

### 3.2 Willam-Warnke Failure Criterion (Three Parameter)

Willam and Warnke (1974) proposed a three-parameter failure criterion that takes the shape of a pyramid with a triangular base in the Haigh-Westergaard ( $\sigma_1$  -  $\sigma_2$  -  $\sigma_3$ ) stress space. In a manner similar to the Drucker-Prager (1952) failure criterion, linear meridians are assumed. However, the slopes of the meridians vary around the pyramidal failure surface. The model is linear in stress through the use of  $I_1$  and  $\sqrt{J_2}$ , which is evident in the following expression

$$\begin{aligned}
 g(I_1, J_2, J_3) &= AI_1 + [B(J_2, J_3)]\sqrt{J_2} - 1 \\
 &= 0
 \end{aligned}
 \tag{3.2.1}$$

Given the formulation above, in the Haigh-Westergaard stress space the Willam-Warnke (1974) failure criterion is piecewise continuous with a threefold symmetry. This symmetry is depicted in Figure 3.2.1 where the criterion is projected onto an arbitrary deviatoric plane. The segment associated with  $0^\circ \leq \theta \leq 60^\circ$  is presented. The failure function is symmetric with respect to each tensile and compressive principal stress axis projected onto the plane.

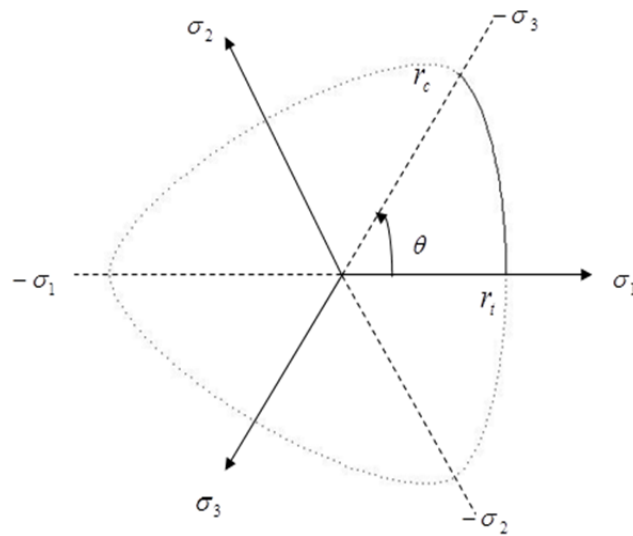


*Figure 3.2.1 The Willam-Warnke (1974) Criterion Projected onto the Deviatoric Plane ( $0^\circ \leq \theta \leq 60^\circ$ )*

As the deviatoric plane of the projection moves up the hydrostatic stress line in the positive direction, the projection of the failure criterion shrinks. As the deviatoric plane of projection moves down the hydrostatic line in the negative direction, the projection of the failure criterion increases in size.

Willam and Warnke (1974) defined the parameter  $B$  from equation 3.2.1 in the following manner

$$B = \frac{1}{r(\theta)} \quad (3.2.2)$$

where  $r$  is a radial vector located in a plane parallel to the  $\Pi$ -plane. Willam and Warnke (1974) assumed that when the failure surface was projected onto a deviatoric plane that a segment of this projection could be defined as a segment of an elliptic curve with the following formulation

$$r(\theta) = \frac{2r_c(r_c^2 - r_t^2)\cos\theta + r_c(2r_t - r_c)[4((r_c^2 - r_t^2)\cos^2\theta + 5r_t^2 - 4r_t r_c)]^{1/2}}{4((r_c^2 - r_t^2)\cos^2\theta + (r_c - 2r_t)^2)} \quad (3.2.3)$$

Here  $\theta$  is Lode's angle, where once again

$$\theta = \left(\frac{1}{3}\right) \cos^{-1}\left[\left(\frac{3\sqrt{3}}{2}\right)\frac{(J_3)^3}{(J_2)^3}\right] \quad (0^\circ \leq \theta \leq 60^\circ) \quad (3.2.4)$$

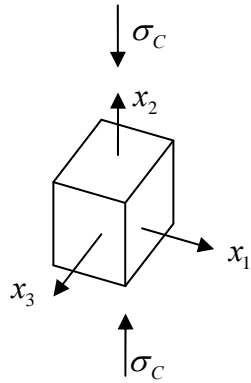
When  $\theta = 0^\circ$ ,  $B = B_T$ ,  $r = r_T$  and

$$r_T = \frac{1}{B_T} \quad (3.2.5)$$

Similarly, with  $\theta = 60^\circ$ ,  $B = B_C$ ,  $r = r_C$  and

$$r_C = \frac{1}{B_C} \quad (3.2.6)$$

In order to determine the constants  $B_T$  and  $B_C$  consider the following stress state



A 3D coordinate system with axes  $x_1$ ,  $x_2$ , and  $x_3$ . A cube is centered at the origin. A vertical arrow pointing downwards from the top face and an arrow pointing upwards from the bottom face are both labeled  $\sigma_C$ , representing compressive stress.

$$\sigma_{ij} = \begin{bmatrix} 0 & 0 & 0 \\ 0 & \sigma_T & 0 \\ 0 & 0 & 0 \end{bmatrix} \quad (3.2.7)$$

The deviatoric stress tensor is

$$S_{ij} = \begin{bmatrix} -\frac{1}{3} & 0 & 0 \\ 0 & \frac{2}{3} & 0 \\ 0 & 0 & -\frac{1}{3} \end{bmatrix} \sigma_T \quad (3.2.8)$$

and Lode's angle as well as the three invariants obtained are expressed as

$$(I_1, \sqrt{J_2}, \sqrt[3]{J_3}) = \left( \sigma_T, \frac{\sqrt{3}}{3} \sigma_T, \frac{\sqrt[3]{2}}{3} \sigma_T \right) \quad (3.2.9)$$

$$\theta = 0^\circ \quad (0^\circ \leq \theta \leq 60^\circ) \quad (3.2.10)$$

Substitution of the values of invariants into failure function given by equation (3.2.1)

yields

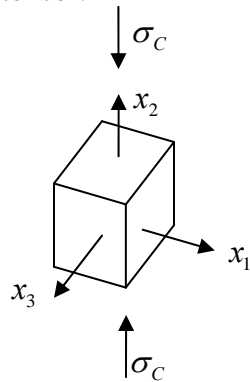
$$A(\sigma_T) + \left( \frac{\sqrt{3}}{3} B_T \right) (\sigma_T) - 1 = 0 \quad (3.2.11)$$

or

$$A + \left( \frac{\sqrt{3}}{3} \right) B_T = \frac{1}{\sigma_T} \quad (3.2.12)$$

Next consider a uniaxial compressive stress state characterized by the following

stress tensor.



$$\sigma_{ij} = \begin{bmatrix} 0 & 0 & 0 \\ 0 & \sigma_c & 0 \\ 0 & 0 & 0 \end{bmatrix} \quad (3.2.13)$$

then

$$S_{ij} = \begin{bmatrix} -\frac{1}{3} & 0 & 0 \\ 0 & \frac{2}{3} & 0 \\ 0 & 0 & -\frac{1}{3} \end{bmatrix} \sigma_c \quad (3.2.14)$$

and

$$(I_1, \sqrt{J_2}, \sqrt[3]{J_3}) = \left( \sigma_c, -\frac{\sqrt{3}}{3}\sigma_c, -\frac{\sqrt[3]{2}}{3}\sigma_c \right) \quad (3.2.15)$$

$$\theta = 60^\circ \quad (3.2.16)$$

Substitution of these the values for the invariants into the Willam-Warke (1974) failure

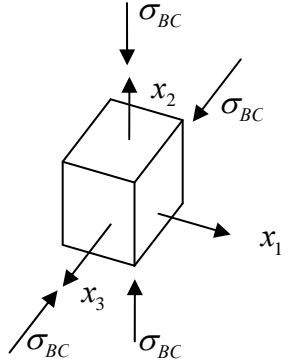
function yields

$$A\sigma_c - \left( \frac{\sqrt{3}}{3} B_c \right) (\sigma_c) - 1 = 0 \quad (3.2.17)$$

$$-A + \left( \frac{\sqrt{3}}{3} \right) B_c = \frac{1}{\sigma_c} \quad (3.2.18)$$



At this point we have two equations (3.2.12 and 3.2.18) and three unknowns ( $A$ ,  $B_T$ , and  $B_C$ ). In order to obtain a third equation consider an equal biaxial compressive stress state characterized as



$$\sigma_{ij} = \begin{bmatrix} 0 & 0 & 0 \\ 0 & \sigma_{BC} & 0 \\ 0 & 0 & \sigma_{BC} \end{bmatrix} \quad (3.2.19)$$

Now the deviatoric stress tensor becomes

$$S_{ij} = \begin{bmatrix} -\frac{2}{3} & 0 & 0 \\ 0 & \frac{1}{3} & 0 \\ 0 & 0 & \frac{1}{3} \end{bmatrix} \sigma_{BC} \quad (3.2.20)$$

and

$$(I_1, \sqrt{J_2}, \sqrt[3]{J_3}) = \left( 2\sigma_{BC}, -\frac{\sqrt{3}}{3}\sigma_{BC}, \frac{\sqrt[3]{2}}{3}\sigma_{BC} \right) \quad (3.2.21)$$

$$\theta = 0^\circ \quad (3.2.22)$$

Substitution of these invariants into failure function defined by equation (3.2.1) yields

$$(2A)\sigma_{BC} + \left( -\frac{\sqrt{3}}{3}B_T \right)(\sigma_{BC}) - 1 = 0 \quad (3.2.23)$$

or

$$-2A + \left(\frac{\sqrt{3}}{3}\right)B_T = \frac{1}{\sigma_{BC}} \quad (3.2.24)$$

We now have three equations, i.e., (3.2.12), (3.2.18) and (3.2.24), in three unknowns  $A$ ,  $B_t$  and  $B_c$ . Solution of this system of equations leads to the following three expressions for the unknown model parameters

$$A = \left(\frac{1}{3}\right)\left(\frac{1}{\sigma_T} - \frac{1}{\sigma_C}\right) \quad (3.2.25)$$

and

$$B_T = \left(\frac{\sqrt{3}}{3}\right)\left(\frac{2}{\sigma_T} + \frac{1}{\sigma_{BC}}\right) \quad (3.2.26)$$

and

$$B_C = (\sqrt{3})\left[\frac{1}{\sigma_C} + \left(\frac{1}{3}\right)\left(\frac{1}{\sigma_T} - \frac{1}{\sigma_{BC}}\right)\right] \quad (3.2.27)$$

In order to characterize to characterize the Willam and Warnke (1974) model in a straight forward manner one would need failure data from a uniaxial load path, a uniaxial compressive load path, and an equal biaxial compression load path. Unfortunately, Burchell et al. (2007) did not conduct biaxial compression stress tests. It must be pointed out that these tests are extremely difficult to perform. Here we arbitrarily assume the magnitude of the biaxial compression stress at failure is 1.16 times the uniaxial compression stress at failure. Thus the three sets of strength parameters obtained from the data found in Burchell et al. (2007) are

$$\sigma_T = 15.93 \text{ MPa} \quad (3.2.28)$$

for tension,

$$\sigma_C = -52.93 \text{ MPa} \quad (3.2.29)$$

for compression and

$$\sigma_{BC} = -61.40 \text{ MPa} \quad (3.2.30)$$

for the biaxial compression material strength. The important thing is that with the three parameter Willam-Warnke (1974) criterion the biaxial compression strength is a direct model input. Biaxial compression strength could be controlled indirectly in the Drucker-Prager model (1952). The additional strength parameter in the Willam-Warnke (1974) model brings additional flexibility and the criterion represents an increased flexibility in modeling material behavior relative to the Drucker-Prager (1952) criterion in a manner similar to a comparison of the Drucker-Prager (1952) model to the von Mises (1913) model. However, the additional flexibility is not enough to capture the anisotropic behavior exhibited by the graphite data from Burchell et al. (2007).

This is evident in Figure 3.2.2 where the Willam-Warnke (1974) criterion and all of test data from Burchell et al. (2007) are projected onto the principal stress plane defined by the  $\sigma_1$  -  $\sigma_2$  coordinate axes. The criterion seems to capture the biaxial failure data along load path #B-8. However, there is an increasing loss of fidelity with load paths #B-7 and #B-6. Load path #B-5 represents anisotropic strength behavior and the Willam and Warnke (1974) model was constructed based on the assumption of an isotropic material. The same behavior can be seen in biaxial load paths #B-4, #B-3 and

#B-2. As we move away from the load paths used to characterize the model parameters we encounter the loss in fidelity and here we attribute the loss to material anisotropy.

This anisotropic phenomena will drive the research proposed for this effort.

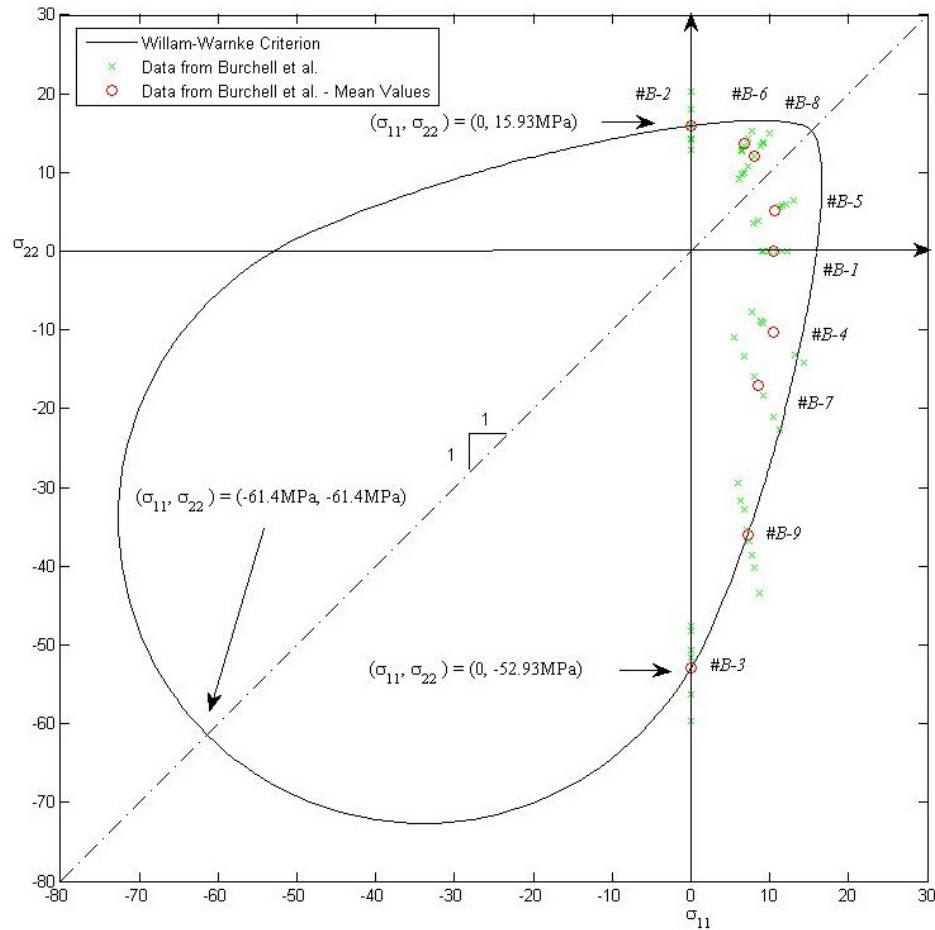


Figure 3.2.2 The Willam-Warnke (1974) Criterion Projected onto the  $\sigma_1 - \sigma_2$  Principal Stress Plane ( $\sigma_T = 15.93$  MPa,  $\sigma_C = -52.93$  MPa,  $\sigma_{BC} = -61.40$  MPa)

Varying the biaxial compressive strength of the material does not help in matching the criterion with the data from biaxial load paths #B-2 through #B-4 and load paths #B-6 as well as #B-7. This is evident in Figure 3.2.3 where the biaxial strength is varied from 0.96 of the uniaxial compression strength to 1.16 times the uniaxial

compressive strength. The various projections based on differing values of  $\sigma_{BC}$  did not improve the criterion's ability to match the data from the load paths just mentioned.

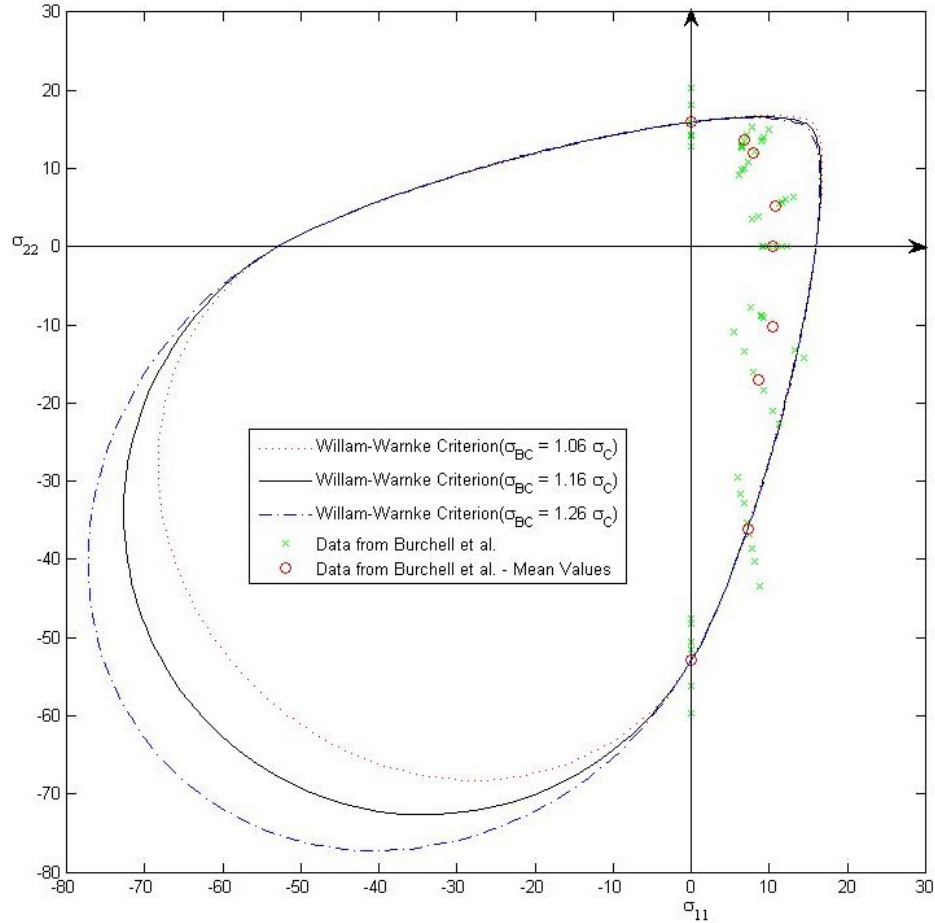


Figure 3.2.3 The Willam-Warnke (1974) Criterion Projected onto the  $\sigma_1 - \sigma_2$  Principal Stress Plane for Multiple  $\sigma_T = 15.93 \text{ MPa}$ ,  $\sigma_C = -52.93 \text{ MPa}$ , and  $\sigma_{BC} = -56.11 \text{ MPa}$ ,  $-61.40 \text{ MPa}$ ,  $-66.69 \text{ MPa}$

In Figures 3.2.4 and 3.2.5 the Willam-Warnke (1974) model is projected onto deviatoric planes. In Figure 3.2.4

$$\xi = 9.20 \text{ MPa} \quad (3.2.31)$$

and in Figure 3.2.5

$$\xi = -30.2 \text{ MPa} \quad (3.2.32)$$

In these figures the Willam-Warnke (1974) criterion presents as slices through a right triangular pyramid.

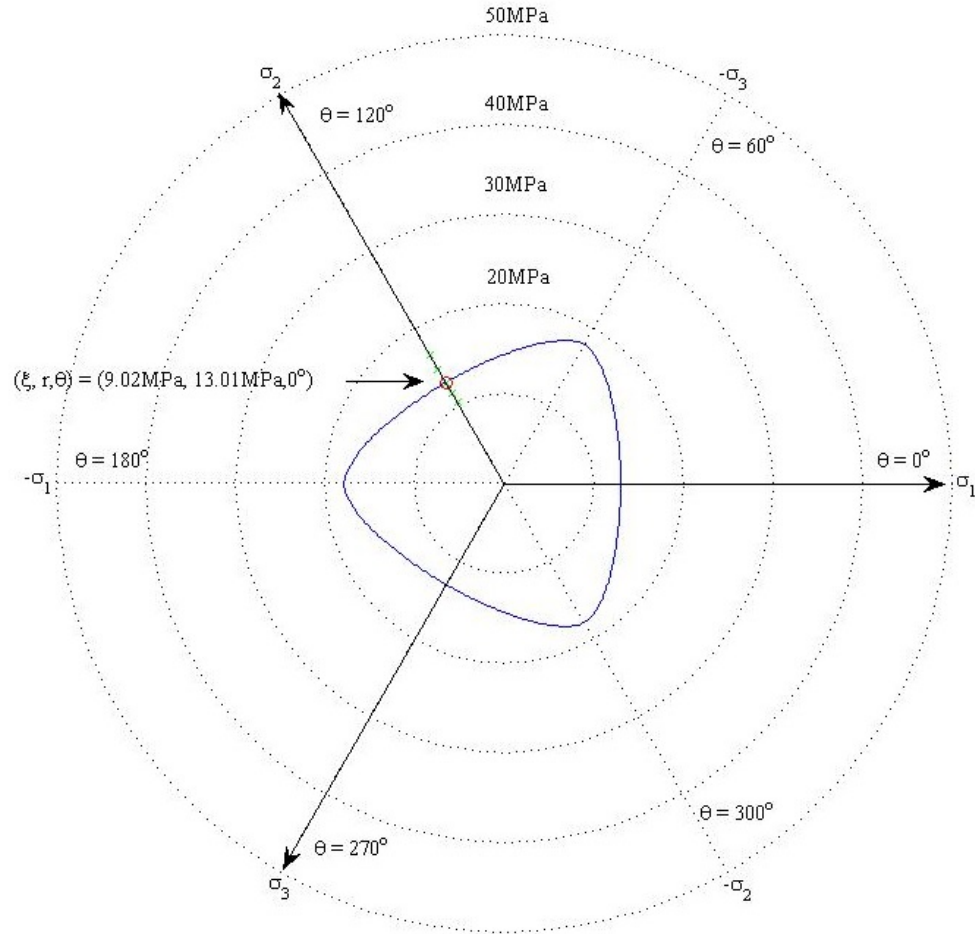


Figure 3.2.4 The Willam-Warnke (1974) Criterion Projected onto a Deviatoric Plane  
 $(\xi = 6.05 \text{ MPa})$  Parallel to the  $\Pi$ -plane with  $\sigma_T = 15.93 \text{ MPa}$ ,  $\sigma_C = -52.93 \text{ MPa}$ ,  
 $\sigma_{BC} = -61.40 \text{ MPa}$

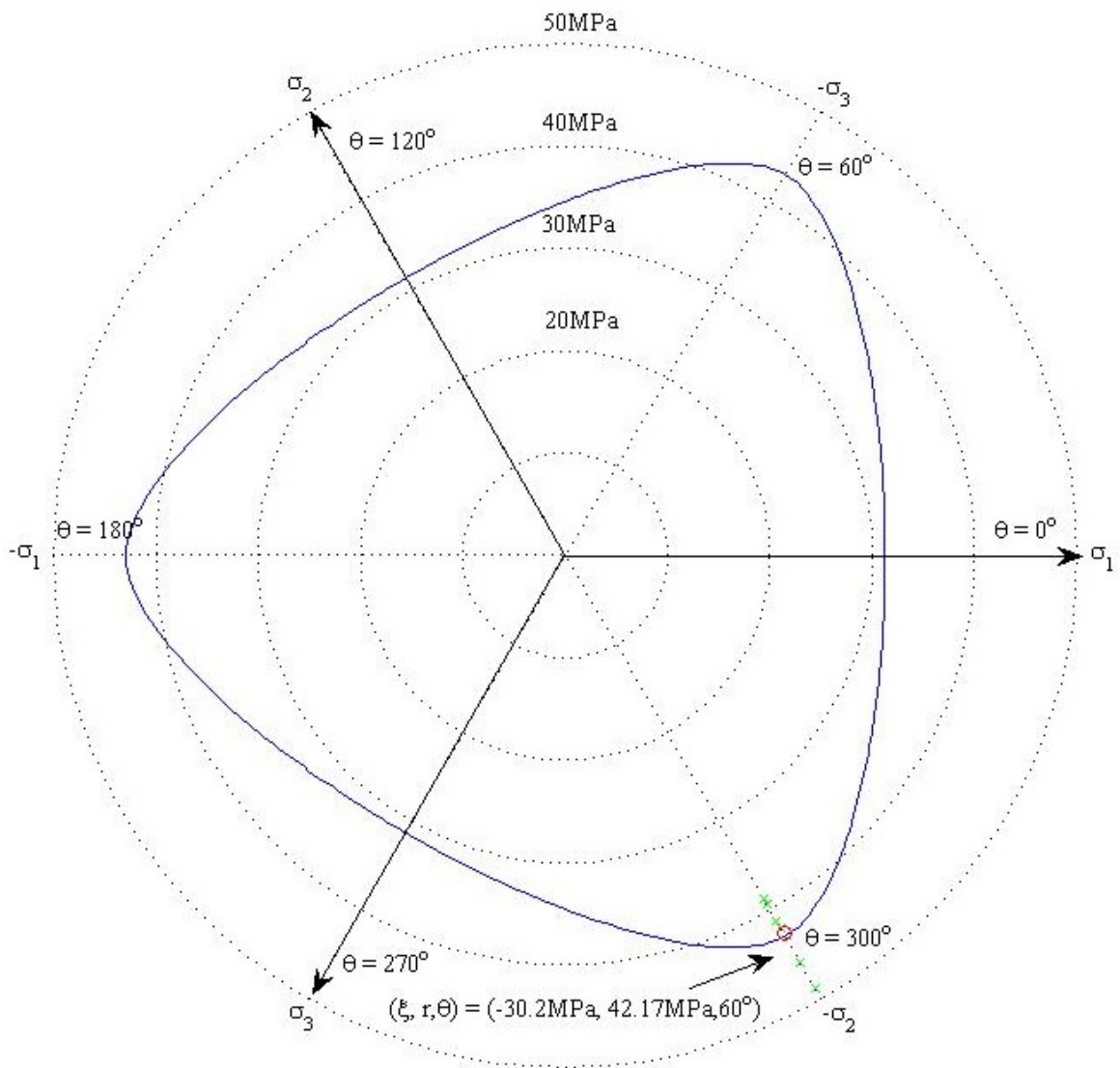


Figure 3.2.5 The Willam-Warnke (1974) Criterion Projected onto a Deviatoric Plane ( $\xi_1 = -30.2\text{MPa}$ ) Parallel to the  $\Pi$ -plane with  $\sigma_T = 15.93\text{MPa}$ ,  $\sigma_C = -52.93\text{MPa}$ ,  $\sigma_{BC} = -61.40\text{MPa}$

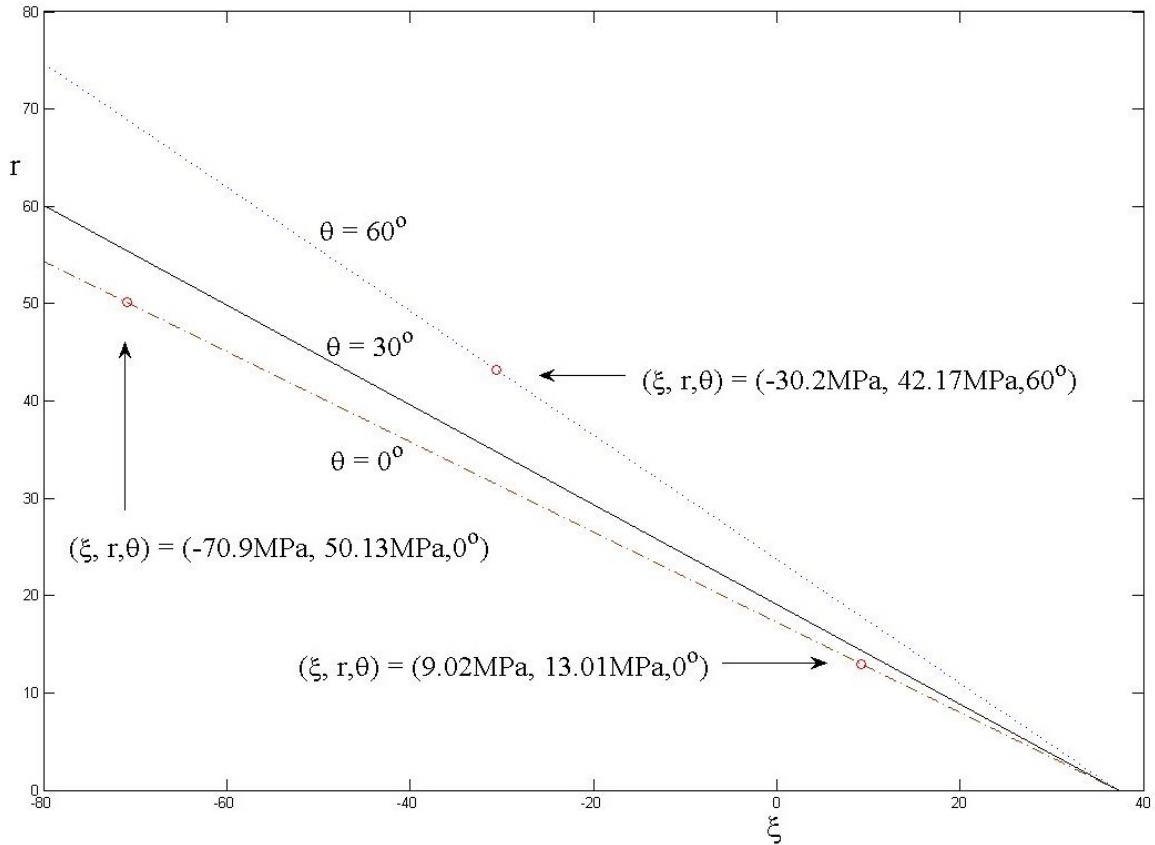


Figure 3.2.6 The Willam-Warnke (1974) Criterion Projected onto the Meridian Plane for a Material Strength Parameter of  $\sigma_T = 15.93 \text{ MPa}$ ,  $\sigma_C = -52.93 \text{ MPa}$ ,  $\sigma_{BC} = -61.40 \text{ MPa}$

The meridian lines associated with the Willam-Warnke (1974) failure criterion for Lode angle values of  $\theta = 0^\circ$  and  $\theta = 60^\circ$  are depicted on Figure 3.2.6. The meridians for each Lode angle are distinct from one another since one is a tensile meridian and passes through the tensile strength parameter along a principal stress axis. The other is a compressive meridian and intercepts a principal stress axis at the value of the compressive strength parameter. The  $\theta = 0^\circ$  meridian line goes through point ( $r = 9.02 \text{ MPa}$ ,  $\xi = 13.01 \text{ MPa}$ ) and the  $\theta = 60^\circ$  meridian line goes through point ( $r = 30.56 \text{ MPa}$ ,  $\xi = 43.22 \text{ MPa}$ ) as they should since these data values were used to characterize the



model. The point ( $r = 6.05$  MPa,  $\xi = 8.56$  MPa) represents the average strength for load path #B-5, a uniaxial load path that was not used to characterize the model. The data from load path #B-5 represents anisotropic strength behavior and one should not expect this data to match well with the isotropic Willam-Warnke (1974) model.

Up to this point it has been noted several times that the data from Burchell et al. (2007) exhibits anisotropic behavior. As part of this effort many attempts were made to extend the Willam-Warnke (1974) model in order to capture anisotropic behavior through the use of tensor based stress invariants. The primary difficulty with extending the Willam-Warnke (1974) failure criterion to anisotropy is the fact that the function is linear in stress and based on a trial and error approach, the belief here is that at least a quadratic dependence is needed in order to capture anisotropic behavior through stress invariants. The next section presents a failure criterion analogous to the Willam-Warnke (1974) failure model that is quadratic in stress.

## CHAPTER IV

### AN ISOTROPIC FAILURE CRITERION FOR GRAPHITE

The next phenomenological failure criterion considered in this effort was constructed from the integrity basis proposed by Green and Mkrtychian (1977). This isotropic failure criterion has the basic form

$$g = g(\sigma_{ij}, a_i) \quad (4.1)$$

Green and Mkrtychian (1977) tracked the principal stress direction using the vector  $a_i$ . Utilizing the eigenvectors of the principal stresses enables the identification of tensile and compressive principal stress directions. The authors of this model consider different behavior in tension and compression as a type of material anisotropy in construction a nonlinear elasticity model. Utilizing first order tensors (the eigenvectors) to construct second order directional tensors is an accepted approach in modeling anisotropy through the use of invariants. Spencer (1984) pointed out the mathematics that underlies the concept. This model produces results very similar to the Willam-Warnke (1974) failure criterion. The utility of deriving an isotropic form based on the integrity basis from

Green and Mkrtychian (1977) work is that this failure criterion is quadratic in stress whereas the Willam-Warnke (1974) failure criterion was linear in stress. Being quadratic in stress makes the isotropic model more amenable to including anisotropic behavior, which is discussed in the next chapter. This chapter outlines fundamental aspects of the isotropic failure criterion in preparation for the extension to anisotropy.

## 4.2 Integrity Basis and Functional Dependence

The integrity basis for the a function with a dependence specified in equation (4.1) is

$$I_1 = \sigma_{ii} \quad (4.2.1)$$

$$I_2 = \sigma_{ij} \sigma_{ji} \quad (4.2.2)$$

$$I_3 = \sigma_{ij} \sigma_{jk} \sigma_{ki} \quad (4.2.3)$$

$$I_4 = a_i a_j \sigma_{ij} \quad (4.2.4)$$

and

$$I_5 = a_i a_j \sigma_{jk} \sigma_{ki} \quad (4.2.5)$$

These invariants from the work of Green and Mkrtychian (1977) (with the exception of  $I_3$ , which can be derived from  $I_1$  and  $I_2$ ) constitute an integrity basis and span the space of possible stress invariants that can be utilized to compose scalar valued functions that are dependent on stress. Thus the dependence of the isotropic failure criterion can be characterized in general as

$$g(\sigma_{ij}) = g(I_1, I_2, I_4, I_5) \quad (4.2.6)$$

One possible polynomial formulation for  $g$  in terms of the integrity basis is

$$g(\sigma_{ij}) = A (I_1)^2 + B I_2 + C I_1 I_4 + D I_5 - 1 \quad (4.2.7)$$

This functional form is quadratic in stress which, as is seen in the next section, is convenient when extending this formulation to include anisotropy. The invariants  $I_4$  and  $I_5$  are associated with the directional tensor  $a_i$ , and we note that Green and Mkrichian (1977) utilized these invariants in their functional dependence very judiciously. They partitioned the Haigh-Westergaard stress space and offered four forms for their functions. The same approach is adopted here.

### 4.3 Functional Forms and Associated Gradients by Stress Region

By definition the principal stresses are identified such that

$$\sigma_1 \geq \sigma_2 \geq \sigma_3 \quad (4.3.1)$$

The four function approach proposed by Green and Mkrichian (1977) spans the stress space which is partitioned as follows:

Region #1:  $\sigma_1 \geq \sigma_2 \geq \sigma_3 \geq 0$  – all principal stresses are tensile

Region #2:  $\sigma_1 \geq \sigma_2 \geq 0 \geq \sigma_3$  – one principal stress is compressive, the others are tensile

Region #3:  $\sigma_1 \geq 0 \geq \sigma_2 \geq \sigma_3$  – one principal stress is tensile, the others are compressive

Region #4:  $0 \geq \sigma_1 \geq \sigma_2 \geq \sigma_3$  – all principal stresses are compressive.

Thus the isotropic criterion has a specific formulation for the case of all tensile principal stresses, and a different formulation for all compressive principal stresses (see derivation below). For these two formulations there is no need to track principal stress orientations and thus for Regions #1 and #4 the isotropic failure criterion did not include the terms associated with  $I_4$  and  $I_5$ , both of which contain information regarding the directional tensor. A third and fourth formulation exists for Regions #3 and #4 where two principal stresses are tensile and when two principal stresses are compressive, respectively and the failure behavior depends on the direction of the principal tensile and compressive stresses. For these regions of the stress space for the failure criterion includes the invariants  $I_4$  and  $I_5$ .

The functional values of the four formulations  $g_1$ ,  $g_2$ ,  $g_3$  and  $g_4$  must match along their common boundaries. In addition, the tangents associated with the failure surfaces along the common boundaries must be single valued. This will provide a smooth transition from one region to the next. To insure this, the gradients to the failure surfaces along each boundary are equated. The specifics of equating the formulations and equating the gradients at common boundaries are presented below. Relationships are developed for the constants associated with each term of the failure function for the four different regions.

**Region #1:** ( $\sigma_1 \geq \sigma_2 \geq \sigma_3 \geq 0$ ) assume the failure function for this region of the stress space is

$$g_1 = 1 - \left[ \left( \frac{1}{2} \right) A_1 I_1^2 + B_1 I_2 \right] \quad (4.3.2)$$

From equation (4.3.10) it is evident that there will be a group of constants for each region of the stress space. Hence the subscripts for the constants associated with each invariant as well as the failure function will run from one to four. Also note the absence of invariants  $I_4$  and  $I_5$ . The corresponding normal to the failure surface is

$$\frac{\partial g_1}{\partial \sigma_{ij}} = \frac{\partial g_1}{\partial I_1} \frac{\partial I_1}{\partial \sigma_{ij}} + \frac{\partial g_1}{\partial I_2} \frac{\partial I_2}{\partial \sigma_{ij}} \quad (4.3.3)$$

where

$$\frac{\partial g_1}{\partial I_1} = -A_1 I_1 \quad (4.3.4)$$

$$\frac{\partial g_1}{\partial I_2} = -B_1 \quad (4.3.5)$$

$$\frac{\partial I_1}{\partial \sigma_{ij}} = \delta_{ij} \quad (4.3.6)$$

and

$$\frac{\partial I_2}{\partial \sigma_{ij}} = 2\sigma_{ij} \quad (4.3.7)$$

Here  $\delta_{ij}$  is the Kronecker delta tensor. Substitution of equations (4.3.4) through (4.3.7) into (4.3.3) leads to the following tensor expression

$$\frac{\partial g_1}{\partial \sigma_{ij}} = -(A_1 I_1 \delta_{ij} + 2B_1 \sigma_{ij}) \quad (4.3.8)$$

or in a matrix format

$$\begin{aligned} \frac{\partial g_1}{\partial \sigma_{ij}} = & \begin{bmatrix} \sigma_1 + \sigma_2 + \sigma_3 & 0 & 0 \\ 0 & \sigma_1 + \sigma_2 + \sigma_3 & 0 \\ 0 & 0 & \sigma_1 + \sigma_2 + \sigma_3 \end{bmatrix} (-A_1) \\ & + \begin{bmatrix} 2\sigma_1 & 0 & 0 \\ 0 & 2\sigma_2 & 0 \\ 0 & 0 & 2\sigma_3 \end{bmatrix} (-B_1) \end{aligned} \quad (4.3.9)$$

The matrix formulation allows easy identification of relationships between the various constants.

**Region #2:** ( $\sigma_1 \geq \sigma_2 \geq 0 \geq \sigma_3$ ) The failure function for region #2 is

$$g_2 = 1 - \left[ \left( \frac{1}{2} \right) A_2 I_1^2 + B_2 I_2 + C_2 I_1 I_4 + D_2 I_5 \right] \quad (4.3.10)$$

Note the subscripts on the constants and the failure function. The normal to the surface is

$$\frac{\partial g_2}{\partial \sigma_{ij}} = \frac{\partial g_2}{\partial I_1} \frac{\partial I_1}{\partial \sigma_{ij}} + \frac{\partial g_2}{\partial I_2} \frac{\partial I_2}{\partial \sigma_{ij}} + \frac{\partial g_2}{\partial I_4} \frac{\partial I_4}{\partial \sigma_{ij}} + \frac{\partial g_2}{\partial I_5} \frac{\partial I_5}{\partial \sigma_{ij}} \quad (4.3.11)$$

Here

$$\frac{\partial g_2}{\partial I_1} = -(A_2 I_1 + C_2 I_4) \quad (4.3.12)$$

$$\frac{\partial g_2}{\partial I_2} = -B_2 \quad (4.3.13)$$

$$\frac{\partial g_2}{\partial I_4} = -C_2 I_1 \quad (4.3.14)$$

$$\frac{\partial g_2}{\partial I_5} = -D_2 \quad (4.3.15)$$

$$\frac{\partial I_4}{\partial \sigma_{ij}} = a_i a_j \quad (4.3.16)$$

and

$$\frac{\partial I_5}{\partial \sigma_{ij}} = a_k a_i \sigma_{jk} + a_j a_k \sigma_{ki} \quad (4.3.17)$$

The principal stress direction of interest in this region of the stress space is the one associated with the third principal stress. Assuming the Cartesian coordinate system is aligned with the principal stress directions then the eigenvector associated with the third principal stress is

$$a_i = (0, 0, 1) \quad (4.3.18)$$

Thus for equation (4.3.16) and (4.3.17)

$$\begin{aligned} a_k a_i &= a_j a_k = a_i a_j = \begin{bmatrix} 0 \\ 0 \\ 1 \end{bmatrix} [0 \ 0 \ 1] \\ &= \begin{bmatrix} 0 & 0 & 0 \\ 0 & 0 & 0 \\ 0 & 0 & 1 \end{bmatrix} \end{aligned} \quad (4.3.19)$$

Given the principal stress direction of interest the fourth and fifth invariants are

$$I_4 = \sigma_3 \quad (4.3.20)$$

and

$$I_5 = \sigma_3^2 \quad (4.3.21)$$



for this region of the stress space. Substitution of equations (4.3.12) through (4.3.21)

into (4.3.11) yields the following tensor expression for the normal to the failure surface

$$\frac{\partial g_2}{\partial \sigma_{ij}} = - \left[ A_2 I_1 \delta_{ij} + 2B_2 \sigma_{ij} + C_2 (\sigma_3 \delta_{ij} + I_1 a_i a_j) + D_2 (a_k a_i \sigma_{jk} + a_j a_k \sigma_{ki}) \right] \quad (4.3.22)$$

The matrix form of equation (4.3.22) is

$$\begin{aligned} \frac{\partial g_2}{\partial \sigma_{ij}} = & \begin{bmatrix} \sigma_1 + \sigma_2 + \sigma_3 & 0 & 0 \\ 0 & \sigma_1 + \sigma_2 + \sigma_3 & 0 \\ 0 & 0 & \sigma_1 + \sigma_2 + \sigma_3 \end{bmatrix} (-A_2) + \begin{bmatrix} 2\sigma_1 & 0 & 0 \\ 0 & 2\sigma_2 & 0 \\ 0 & 0 & 2\sigma_3 \end{bmatrix} (-B_2) \\ & + \begin{bmatrix} \sigma_3 & 0 & 0 \\ 0 & \sigma_3 & 0 \\ 0 & 0 & \sigma_1 + \sigma_2 + 2\sigma_3 \end{bmatrix} (-C_2) + \begin{bmatrix} 0 & 0 & 0 \\ 0 & 0 & 0 \\ 0 & 0 & 2\sigma_3 \end{bmatrix} (-D_2) \end{aligned} \quad (4.3.23)$$

**Region #3:** ( $\sigma_1 \geq 0 \geq \sigma_2 \geq \sigma_3$ ) The failure function for this region of the stress space is

$$g_3 = 1 - \left[ \left( \frac{1}{2} \right) A_3 I_1^2 + B_3 I_2 + C_3 I_1 I_4 + D_3 I_5 \right] \quad (4.3.24)$$

The normal to the surface is

$$\frac{\partial g_3}{\partial \sigma_{ij}} = \frac{\partial g_3}{\partial I_1} \frac{\partial I_1}{\partial \sigma_{ij}} + \frac{\partial g_3}{\partial I_2} \frac{\partial I_2}{\partial \sigma_{ij}} + \frac{\partial g_3}{\partial I_4} \frac{\partial I_4}{\partial \sigma_{ij}} + \frac{\partial g_3}{\partial I_5} \frac{\partial I_5}{\partial \sigma_{ij}} \quad (4.3.25)$$

Here

$$\frac{\partial g_3}{\partial I_1} = -(A_3 I_1 + C_3 I_4) \quad (4.3.26)$$

$$\frac{\partial g_3}{\partial I_2} = -B_3 \quad (4.3.27)$$

$$\frac{\partial g_3}{\partial I_4} = -C_3 I_1 \quad (4.3.28)$$

and

$$\frac{\partial g_3}{\partial I_5} = -D_3 \quad (4.3.29)$$

The principal stress direction of interest for this stress state is the one associated with the first principal stress, i.e.,

$$a_i = (1, 0, 0) \quad (4.3.30)$$

Now

$$\begin{aligned} a_k a_i &= a_j a_k = a_i a_j = \begin{bmatrix} 1 \\ 0 \\ 0 \end{bmatrix} [1 \ 0 \ 0] \\ &= \begin{bmatrix} 1 & 0 & 0 \\ 0 & 0 & 0 \\ 0 & 0 & 0 \end{bmatrix} \end{aligned} \quad (4.3.31)$$

The fourth and fifth invariants for this region of the stress space are

$$I_4 = \sigma_1 \quad (4.3.32)$$

and

$$I_5 = \sigma_1^2 \quad (4.3.33)$$

Substitution of the quantities specified above into (4.3.25) yields the following tensor expression

$$\begin{aligned} \frac{\partial g_3}{\partial \sigma_{ij}} &= -[A_3 I_1 \delta_{ij} + 2B_3 \sigma_{ij} + C_3 (\sigma_1 \delta_{ij} + I_1 a_i a_j) \\ &\quad + D_3 (a_k a_i \sigma_{jk} + a_j a_k \sigma_{ki})] \end{aligned} \quad (4.3.34)$$

The matrix form of this equation is as follows

$$\begin{aligned} \frac{\partial g_3}{\partial \sigma_{ij}} = & \begin{bmatrix} \sigma_1 + \sigma_2 + \sigma_3 & 0 & 0 \\ 0 & \sigma_1 + \sigma_2 + \sigma_3 & 0 \\ 0 & 0 & \sigma_1 + \sigma_2 + \sigma_3 \end{bmatrix} (-A_3) + \begin{bmatrix} 2\sigma_1 & 0 & 0 \\ 0 & 2\sigma_2 & 0 \\ 0 & 0 & 2\sigma_3 \end{bmatrix} (-B_3) \\ & + \begin{bmatrix} 2\sigma_1 + \sigma_2 + \sigma_3 & 0 & 0 \\ 0 & \sigma_1 & 0 \\ 0 & 0 & \sigma_1 \end{bmatrix} (-C_3) + \begin{bmatrix} 2\sigma_1 & 0 & 0 \\ 0 & 0 & 0 \\ 0 & 0 & 0 \end{bmatrix} (-D_3) \end{aligned} \quad (4.3.35)$$

**Region #4:**  $0 \geq \sigma_1 \geq \sigma_2 \geq \sigma_3$  The failure function for this region of the stress space is

$$g_4 = 1 - \left[ \left( \frac{1}{2} \right) A_4 I_1^2 + B_4 I_2 \right] \quad (4.3.36)$$

The corresponding normal to the failure surface is

$$\frac{\partial g_4}{\partial \sigma_{ij}} = \frac{\partial g_4}{\partial I_1} \frac{\partial I_1}{\partial \sigma_{ij}} + \frac{\partial g_4}{\partial I_2} \frac{\partial I_2}{\partial \sigma_{ij}} \quad (4.3.37)$$

Here

$$\frac{\partial g_4}{\partial I_1} = A_4 I_1 \quad (4.3.38)$$

and

$$\frac{\partial g_4}{\partial I_2} = B_4 \quad (4.3.39)$$

Substitution of the equations above into (4.3.37) yields the following tensor expression

$$\frac{\partial g_4}{\partial \sigma_{ij}} = 1 - \left( A_4 I_1 \delta_{ij} + 2B_4 \sigma_{ij} \right) \quad (4.3.40)$$

The matrix format of this expression is

$$\frac{\partial g_4}{\partial \sigma_{ij}} = \begin{bmatrix} \sigma_1 + \sigma_2 + \sigma_3 & 0 & 0 \\ 0 & \sigma_1 + \sigma_2 + \sigma_3 & 0 \\ 0 & 0 & \sigma_1 + \sigma_2 + \sigma_3 \end{bmatrix} (-A_4) + \begin{bmatrix} 2\sigma_1 & 0 & 0 \\ 0 & 2\sigma_2 & 0 \\ 0 & 0 & 2\sigma_3 \end{bmatrix} (-B_4) \quad (4.3.41)$$

#### 4.4 Relationships Between Functional Constants

With the failure functions and the normals to those functions defined for each region, attention is now turned to defining the constants. Consider the region of the Haigh-Westergaard stress space where with  $\sigma_1 > 0$ ,  $\sigma_2 > 0$  and  $\sigma_3 = 0$ . The stress state in a matrix format is

$$\sigma_{ij} = \begin{bmatrix} \sigma_1 & 0 & 0 \\ 0 & \sigma_2 & 0 \\ 0 & 0 & 0 \end{bmatrix} \quad (4.4.1)$$

and this stress state lies along the boundary shared by region #1 and region #2. At this boundary we impose

$$g_1 = g_2 \quad (4.4.2)$$

and

$$\frac{\partial g_1}{\partial \sigma_{ij}} = \frac{\partial g_2}{\partial \sigma_{ij}} \quad (4.4.3)$$

For this stress state the invariants  $I_1$  and  $I_2$  are

$$I_1 = \sigma_1 + \sigma_2 \quad (4.4.4)$$

and

$$I_2 = \sigma_1^2 + \sigma_2^2 \quad (4.4.5)$$

for both  $g_1$  and  $g_2$ . The invariants  $I_4$  and  $I_5$  for  $g_2$  are

$$I_4 = \sigma_3 = 0 \quad (4.4.6)$$

and

$$I_5 = (\sigma_3)^2 = 0 \quad (4.4.7)$$

Substitution of equations (4.4.4) through (4.4.7) into equation (4.4.2) yields the following

matrix expression

$$\begin{aligned} & \begin{bmatrix} \sigma_1 + \sigma_2 + \sigma_3 & 0 & 0 \\ 0 & \sigma_1 + \sigma_2 + \sigma_3 & 0 \\ 0 & 0 & \sigma_1 + \sigma_2 + \sigma_3 \end{bmatrix} A_1 + \begin{bmatrix} 2\sigma_1 & 0 & 0 \\ 0 & 2\sigma_2 & 0 \\ 0 & 0 & 2\sigma_3 \end{bmatrix} B_1 \\ &= \begin{bmatrix} \sigma_1 + \sigma_2 + \sigma_3 & 0 & 0 \\ 0 & \sigma_1 + \sigma_2 + \sigma_3 & 0 \\ 0 & 0 & \sigma_1 + \sigma_2 + \sigma_3 \end{bmatrix} A_2 + \begin{bmatrix} 2\sigma_1 & 0 & 0 \\ 0 & 2\sigma_2 & 0 \\ 0 & 0 & 2\sigma_3 \end{bmatrix} B_2 \\ &+ \begin{bmatrix} \sigma_3 & 0 & 0 \\ 0 & \sigma_3 & 0 \\ 0 & 0 & \sigma_1 + \sigma_2 + \sigma_3 \end{bmatrix} C_2 + \begin{bmatrix} 0 & 0 & 0 \\ 0 & 0 & 0 \\ 0 & 0 & 2\sigma_3 \end{bmatrix} D_2 \end{aligned} \quad (4.4.8)$$

with

$$\sigma_3 = 0 \quad (4.4.9)$$

then

$$\begin{aligned}
& \begin{bmatrix} \sigma_1 + \sigma_2 & 0 & 0 \\ 0 & \sigma_1 + \sigma_2 & 0 \\ 0 & 0 & \sigma_1 + \sigma_2 \end{bmatrix} A_1 + \begin{bmatrix} 2\sigma_1 & 0 & 0 \\ 0 & 2\sigma_2 & 0 \\ 0 & 0 & 0 \end{bmatrix} B_1 \\
&= \begin{bmatrix} \sigma_1 + \sigma_2 & 0 & 0 \\ 0 & \sigma_1 + \sigma_2 & 0 \\ 0 & 0 & \sigma_1 + \sigma_2 \end{bmatrix} A_2 + \begin{bmatrix} 2\sigma_1 & 0 & 0 \\ 0 & 2\sigma_2 & 0 \\ 0 & 0 & 0 \end{bmatrix} B_2 \\
&+ \begin{bmatrix} 0 & 0 & 0 \\ 0 & 0 & 0 \\ 0 & 0 & \sigma_1 + \sigma_2 \end{bmatrix} C_2 + \begin{bmatrix} 0 & 0 & 0 \\ 0 & 0 & 0 \\ 0 & 0 & 0 \end{bmatrix} D_2
\end{aligned} \tag{4.4.10}$$

The following three expressions can be extracted from equation (4.4.10)

$$(\sigma_1 + \sigma_2)A_1 + (2\sigma_1)B_1 = (\sigma_1 + \sigma_2)A_2 + (2\sigma_1)B_2 \tag{4.4.11}$$

$$(\sigma_1 + \sigma_2)A_1 + (2\sigma_2)B_1 = (\sigma_1 + \sigma_2)A_2 + (2\sigma_2)B_2 \tag{4.4.12}$$

$$(\sigma_1 + \sigma_2)A_1 = (\sigma_1 + \sigma_2)A_2 + (\sigma_1 + \sigma_2)C_2 \tag{4.4.13}$$

The constant  $D_2$  does not appear due to its multiplication with the null matrix.

However,  $C_2$  does appear in the third expression but in the first two immediately above.

Focusing on equation (4.4.11) and equation (4.4.12) which represents two equations in two unknowns then

$$B_1 = B_2 \tag{4.4.14}$$

and

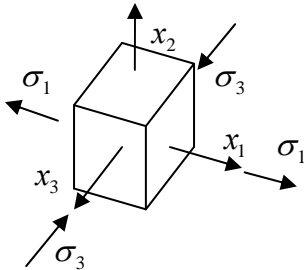
$$A_1 = A_2 \tag{4.4.15}$$

Substitution of equation (4.4.15) into equation (4.4.13) yields

$$C_2 = 0 \tag{4.4.16}$$

and at this point  $D_2$  is indeterminate

Now consider the region of the Haigh-Westergaard stress space where  $\sigma_1 > 0$ ,  $\sigma_2 = 0$  and  $\sigma_3 < 0$ . The stress state in a matrix format is



$$\sigma_{ij} = \begin{bmatrix} \sigma_1 & 0 & 0 \\ 0 & 0 & 0 \\ 0 & 0 & \sigma_3 \end{bmatrix} \quad (4.4.17)$$

and this stress state lies at the boundary shared by region #2 and region #4. At this boundary we impose

$$g_2 = g_3 \quad (4.4.18)$$

and

$$\frac{\partial g_2}{\partial \sigma_{ij}} = \frac{\partial g_3}{\partial \sigma_{ij}} \quad (4.4.19)$$

Under these conditions the invariants  $I_1$  and  $I_2$  are

$$I_1 = \sigma_1 + \sigma_3 \quad (4.4.20)$$

and

$$I_2 = \sigma_1^2 + \sigma_3^2 \quad (4.4.21)$$

Substitution of equation (4.4.20) and (4.4.21) into equation (4.4.19) yields

$$\begin{aligned}
& \begin{bmatrix} \sigma_1 + \sigma_2 + \sigma_3 & 0 & 0 \\ 0 & \sigma_1 + \sigma_2 + \sigma_3 & 0 \\ 0 & 0 & \sigma_1 + \sigma_2 + \sigma_3 \end{bmatrix} A_2 + \begin{bmatrix} 2\sigma_1 & 0 & 0 \\ 0 & 2\sigma_2 & 0 \\ 0 & 0 & 2\sigma_3 \end{bmatrix} B_2 \\
& + \begin{bmatrix} \sigma_3 & 0 & 0 \\ 0 & \sigma_3 & 0 \\ 0 & 0 & \sigma_1 + \sigma_2 + 2\sigma_3 \end{bmatrix} C_2 + \begin{bmatrix} 0 & 0 & 0 \\ 0 & 0 & 0 \\ 0 & 0 & 2\sigma_3 \end{bmatrix} D_2 \\
= & \begin{bmatrix} \sigma_1 + \sigma_2 + \sigma_3 & 0 & 0 \\ 0 & \sigma_1 + \sigma_2 + \sigma_3 & 0 \\ 0 & 0 & \sigma_1 + \sigma_2 + \sigma_3 \end{bmatrix} A_3 + \begin{bmatrix} 2\sigma_1 & 0 & 0 \\ 0 & 2\sigma_2 & 0 \\ 0 & 0 & 2\sigma_3 \end{bmatrix} B_3 \\
& + \begin{bmatrix} 2\sigma_1 + \sigma_2 + \sigma_3 & 0 & 0 \\ 0 & \sigma_1 & 0 \\ 0 & 0 & \sigma_1 \end{bmatrix} C_3 + \begin{bmatrix} 2\sigma_1 & 0 & 0 \\ 0 & 0 & 0 \\ 0 & 0 & 0 \end{bmatrix} D_3
\end{aligned} \tag{4.4.22}$$

with

$$\sigma_2 = 0 \tag{4.4.23}$$

then

$$\begin{aligned}
& \begin{bmatrix} \sigma_1 + \sigma_3 & 0 & 0 \\ 0 & \sigma_1 + \sigma_3 & 0 \\ 0 & 0 & \sigma_1 + \sigma_3 \end{bmatrix} A_2 + \begin{bmatrix} 2\sigma_1 & 0 & 0 \\ 0 & 0 & 0 \\ 0 & 0 & 2\sigma_3 \end{bmatrix} B_2 \\
& + \begin{bmatrix} \sigma_3 & 0 & 0 \\ 0 & \sigma_3 & 0 \\ 0 & 0 & \sigma_1 + 2\sigma_3 \end{bmatrix} C_2 + \begin{bmatrix} 0 & 0 & 0 \\ 0 & 0 & 0 \\ 0 & 0 & 2\sigma_3 \end{bmatrix} D_2 \\
= & \begin{bmatrix} \sigma_1 + \sigma_3 & 0 & 0 \\ 0 & \sigma_1 + \sigma_3 & 0 \\ 0 & 0 & \sigma_1 + \sigma_3 \end{bmatrix} A_3 + \begin{bmatrix} 2\sigma_1 & 0 & 0 \\ 0 & 0 & 0 \\ 0 & 0 & 2\sigma_3 \end{bmatrix} B_3 \\
& + \begin{bmatrix} 2\sigma_1 + \sigma_3 & 0 & 0 \\ 0 & \sigma_1 & 0 \\ 0 & 0 & \sigma_1 \end{bmatrix} C_3 + \begin{bmatrix} 2\sigma_1 & 0 & 0 \\ 0 & 0 & 0 \\ 0 & 0 & 0 \end{bmatrix} D_3
\end{aligned} \tag{4.4.24}$$

The following three expressions can be extracted from equation (4.4.24)

$$\begin{aligned}
& (\sigma_1 + \sigma_3)A_2 + (2\sigma_1)B_2 + (\sigma_3)C_2 \\
= & (\sigma_1 + \sigma_3)A_3 + (2\sigma_1)B_3 + (2\sigma_1 + \sigma_3)C_3 + (2\sigma_1)D_3
\end{aligned} \tag{4.4.25}$$



$$(\sigma_1 + \sigma_3)A_2 + (\sigma_3)C_2 = (\sigma_1 + \sigma_3)A_3 + (\sigma_1)C_3 \quad (4.4.26)$$

and

$$\begin{aligned} (\sigma_1 + \sigma_3)A_2 + (2\sigma_3)B_2 + (\sigma_1 + 2\sigma_3)C_2 + (2\sigma_3)D_2 \\ = (\sigma_1 + \sigma_3)A_3 + (2\sigma_3)B_3 + (\sigma_1)C_3 \end{aligned} \quad (4.4.27)$$

Earlier it was determined that  $C_2 = 0$ , so from equation (4.4.26) we obtain

$$A_2 = A_3 + \frac{\sigma_3}{(\sigma_1 + \sigma_3)}C_3 \quad (4.4.28)$$

From equation (4.4.74) and equation (4.4.75) we obtain

$$B_2 = B_3 + \frac{(\sigma_1 + \sigma_3)}{2\sigma_1}C_3 + D_3 \quad (4.4.29)$$

In addition, from equation (4.4.27) and equation (4.4.26) we obtain

$$D_2 = -\frac{(\sigma_1 + \sigma_3)}{2\sigma_1}C_3 - D_3 \quad (4.4.30)$$

Consider the Region of the Haigh-Westergaard stress space where  $\sigma_1 = 0$ ,  $\sigma_2 < 0$  and  $\sigma_3 < 0$ . The stress state in a matrix format is

$$\sigma_{ij} = \begin{bmatrix} 0 & 0 & 0 \\ 0 & \sigma_2 & 0 \\ 0 & 0 & \sigma_3 \end{bmatrix} \quad (4.4.31)$$

and this stress state lies along the boundary shared by region #3 and region #4. At this boundary we impose

$$g_3 = g_4 \quad (4.4.32)$$

and

$$\frac{\partial g_3}{\partial \sigma_{ij}} = \frac{\partial g_4}{\partial \sigma_{ij}} \quad (4.4.33)$$

Under these conditions the invariants  $I_1$  and  $I_2$  are

$$I_1 = \sigma_2 + \sigma_3 \quad (4.4.34)$$

and

$$I_2 = \sigma_2^2 + \sigma_3^2 \quad (4.4.35)$$

Substitution of equations (4.4.34) and (4.4.35) into equation (4.4.32) yields

$$\begin{aligned} & \begin{bmatrix} \sigma_1 + \sigma_2 + \sigma_3 & 0 & 0 \\ 0 & \sigma_1 + \sigma_2 + \sigma_3 & 0 \\ 0 & 0 & \sigma_1 + \sigma_2 + \sigma_3 \end{bmatrix} A_3 + \begin{bmatrix} 2\sigma_1 & 0 & 0 \\ 0 & 2\sigma_2 & 0 \\ 0 & 0 & 2\sigma_3 \end{bmatrix} B_3 \\ & + \begin{bmatrix} 2\sigma_1 + \sigma_2 + \sigma_3 & 0 & 0 \\ 0 & 0 & 0 \\ 0 & 0 & 0 \end{bmatrix} C_3 + \begin{bmatrix} 2\sigma_1 & 0 & 0 \\ 0 & 0 & 0 \\ 0 & 0 & 0 \end{bmatrix} D_3 \\ & = \begin{bmatrix} \sigma_1 + \sigma_2 + \sigma_3 & 0 & 0 \\ 0 & \sigma_1 + \sigma_2 + \sigma_3 & 0 \\ 0 & 0 & \sigma_1 + \sigma_2 + \sigma_3 \end{bmatrix} A_4 \\ & + \begin{bmatrix} 2\sigma_1 & 0 & 0 \\ 0 & 2\sigma_2 & 0 \\ 0 & 0 & 2\sigma_3 \end{bmatrix} B_4 \end{aligned} \quad (4.4.36)$$

with

$$\sigma_1 = 0 \quad (4.4.37)$$

then

$$\begin{aligned}
& \begin{bmatrix} \sigma_2 + \sigma_3 & 0 & 0 \\ 0 & \sigma_2 + \sigma_3 & 0 \\ 0 & 0 & \sigma_2 + \sigma_3 \end{bmatrix} A_3 + \begin{bmatrix} 0 & 0 & 0 \\ 0 & 2\sigma_2 & 0 \\ 0 & 0 & 2\sigma_3 \end{bmatrix} B_3 \\
& + \begin{bmatrix} \sigma_2 + \sigma_3 & 0 & 0 \\ 0 & 0 & 0 \\ 0 & 0 & 0 \end{bmatrix} C_3 + \begin{bmatrix} 0 & 0 & 0 \\ 0 & 0 & 0 \\ 0 & 0 & 0 \end{bmatrix} D_3 \\
& = \begin{bmatrix} \sigma_2 + \sigma_3 & 0 & 0 \\ 0 & \sigma_2 + \sigma_3 & 0 \\ 0 & 0 & \sigma_2 + \sigma_3 \end{bmatrix} A_4 + \begin{bmatrix} 0 & 0 & 0 \\ 0 & 2\sigma_2 & 0 \\ 0 & 0 & 2\sigma_3 \end{bmatrix} B_4
\end{aligned} \tag{4.4.38}$$

The following three expressions can be extracted from equation (4.4.38)

$$(\sigma_2 + \sigma_3)A_3 + (\sigma_2 + \sigma_3)C_3 = (\sigma_2 + \sigma_3)A_4 \tag{4.4.39}$$

$$(\sigma_2 + \sigma_3)A_3 + (2\sigma_2)B_3 = (\sigma_2 + \sigma_3)A_4 + (2\sigma_2)B_4 \tag{4.4.40}$$

and

$$(\sigma_2 + \sigma_3)A_3 + (2\sigma_3)B_3 = (\sigma_2 + \sigma_3)A_4 + (2\sigma_3)B_4 \tag{4.4.41}$$

From equation (4.4.39) we discern that

$$A_3 + C_3 = A_4 \tag{4.4.42}$$

From equation (4.4.40) and equation (4.4.41) we obtain

$$(2\sigma_2 - 2\sigma_3)B_3 = (2\sigma_2 - 2\sigma_3)B_4 \tag{4.4.43}$$

or that

$$B_3 = B_4 \tag{4.4.44}$$

Substitution of equations (4.4.34) and (4.4.35) into equation (4.4.41) leads to

$$A_3 = A_4 \tag{4.4.45}$$

and

$$C_3 = 0 \quad (4.4.46)$$

Substitution of equation (4.4.46) into equations (4.4.28), (4.4.29) and (4.4.30) yields

$$A_2 = A_3 \quad (4.4.47)$$

$$B_2 = B_3 + D_3 \quad (4.4.48)$$

and

$$D_2 = -D_3 \quad (4.4.49)$$

So the relationships between the functional constants is as follows

$$A_1 = A_2 = A_3 = A_4 \quad (4.4.50)$$

$$B_1 = B_2 = B_3 - D_2 = B_4 - D_2 \quad (4.4.51)$$

$$C_2 = C_3 = 0 \quad (4.4.52)$$

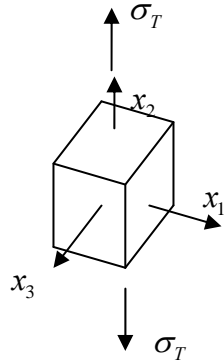
and

$$D_2 + D_3 = 0 \quad (4.4.53)$$

These relationships insure that the four functional forms for the failure function are smooth and continuous along the boundaries of the four regions.

#### 4.5 Functional Constants in Terms of Strength Parameters

Next we utilize specific load paths in order to define the constants defined above in terms of stress values obtained at failure. Consider the following stress state at failure under a uniaxial tensile load



$$\sigma_{ij} = \begin{bmatrix} 0 & 0 & 0 \\ 0 & \sigma_T & 0 \\ 0 & 0 & 0 \end{bmatrix} \quad (4.5.1)$$

This stress state lies on the boundary of region #1. The invariants for this stress state are

$$I_1 = \sigma_T \quad (4.5.2)$$

and

$$I_2 = \sigma_T^2 \quad (4.5.3)$$

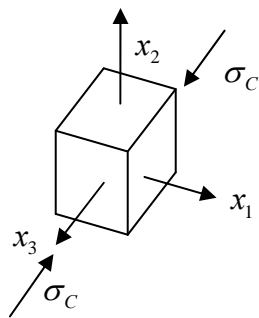
The failure function takes the form

$$\begin{aligned} g_1 &= 1 - \left[ \frac{1}{2} A_1 \sigma_T^2 + B_1 \sigma_T^2 \right] \\ &= 0 \end{aligned} \quad (4.5.4)$$

from which the following relationship is obtained

$$\frac{1}{2} A_1 + B_1 = \frac{1}{\sigma_T^2} \quad (4.5.5)$$

Next a uniaxial compressive stress state is considered where



$$\sigma_{ij} = \begin{bmatrix} 0 & 0 & 0 \\ 0 & 0 & 0 \\ 0 & 0 & \sigma_C \end{bmatrix} \quad (4.5.6)$$

The principal stress direction for this stress state is

$$a_i = (0, 0, 1) \quad (4.5.7)$$

thus

$$a_i a_j = \begin{bmatrix} 0 & 0 & 0 \\ 0 & 0 & 0 \\ 0 & 0 & 1 \end{bmatrix} \quad (4.5.8)$$

The invariants are as follows

$$I_1 = \sigma_C \quad (4.5.9)$$

$$I_2 = \sigma_C^2 \quad (4.5.10)$$

$$I_4 = \sigma_C \quad (4.5.11)$$

and

$$I_5 = \sigma_C^2 \quad (4.5.12)$$

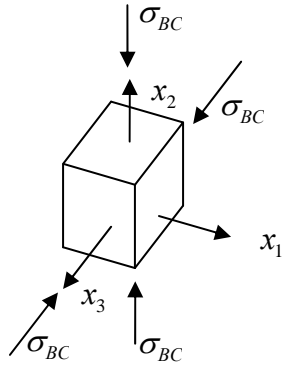
Thus

$$\begin{aligned} g_2 &= \frac{1}{2}A_2\sigma_C^2 + B_2\sigma_C^2 + D_2\sigma_C^2 - 1 \\ &= 0 \end{aligned} \quad (4.5.13)$$

which leads to

$$\frac{1}{2}A_2 + B_2 + D_2 = \frac{1}{\sigma_C^2} \quad (4.5.14)$$

Next consider an equal biaxial compressive stress state where



$$\sigma_{ij} = \begin{bmatrix} 0 & 0 & 0 \\ 0 & \sigma_{BC} & 0 \\ 0 & 0 & \sigma_{BC} \end{bmatrix} \quad (4.5.15)$$

This stress state lies within region #4 and the invariants are as follows

$$I_1 = 2\sigma_{BC} \quad (4.5.16)$$

and

$$I_2 = \sigma_{BC}^2 \quad (4.5.17)$$

The failure function for this particular stress state is

$$\begin{aligned} f_4 &= \frac{1}{2}A_4(2\sigma_{BC})^2 + B_4(2\sigma_{BC}^2) - 1 \\ &= 0 \end{aligned} \quad (4.5.18)$$

which leads to

$$A_1 + B_1 + D_2 = \frac{1}{2\sigma_{BC}^2} \quad (4.5.19)$$

Solving equations (4.5.5), (4.5.4) and (4.5.19) using equations (4.3.50) through (4.3.53)

leads to

$$A_1 = A_2 = A_3 = A_4 = \frac{1}{\sigma_{BC}^2} - \frac{2}{\sigma_C^2} \quad (4.5.20)$$

$$B_1 = B_2 = \frac{1}{\sigma_T^2} - \frac{1}{2\sigma_{BC}^2} + \frac{1}{\sigma_C^2} \quad (4.5.21)$$

$$B_3 = B_4 = \frac{2}{\sigma_C^2} - \frac{1}{2\sigma_{BC}^2} \quad (4.5.22)$$

and

$$D_2 = -D_3 = \frac{1}{\sigma_C^2} - \frac{1}{\sigma_T^2} \quad (4.5.23)$$

In order to visualize the isotropic failure criterion relative to failure data from Burchell et al. (2007), values were computed for the strength parameters identified immediately above, i.e.,  $\sigma_T = 15.93 \text{ MPa}$  for tension,  $\sigma_C = -52.93 \text{ MPa}$  for compression and  $\sigma_{BC} = -61.40 \text{ MPa}$  for the biaxial compression. The values for  $\sigma_T$  and  $\sigma_C$  and were obtained directly from Burchell et al. (2007). The value for  $\sigma_{BC}$  was determined by a best fit approximation of the failure curve to the data in Figure 4.5.1. Various projections of the isotropic failure criterion are presented in the next several figures along with the data from Burchell et al. (2007). The first is a projection onto the  $\sigma_{11} - \sigma_{22}$  stress space which is depicted in Figure 4.5.1. As can be seen in this figure the isotropic failure model captures the different behavior in tension and compression exhibited by the data from Burchell et al. (2007) along the  $\sigma_{22}$  axis. However, the isotropic failure criterion does not capture material anisotropy which is clearly exhibited by the failure data from Burchell et al. (2007) along the tensile segments of the  $\sigma_{11}$  axis relative to the  $\sigma_{22}$  axis.



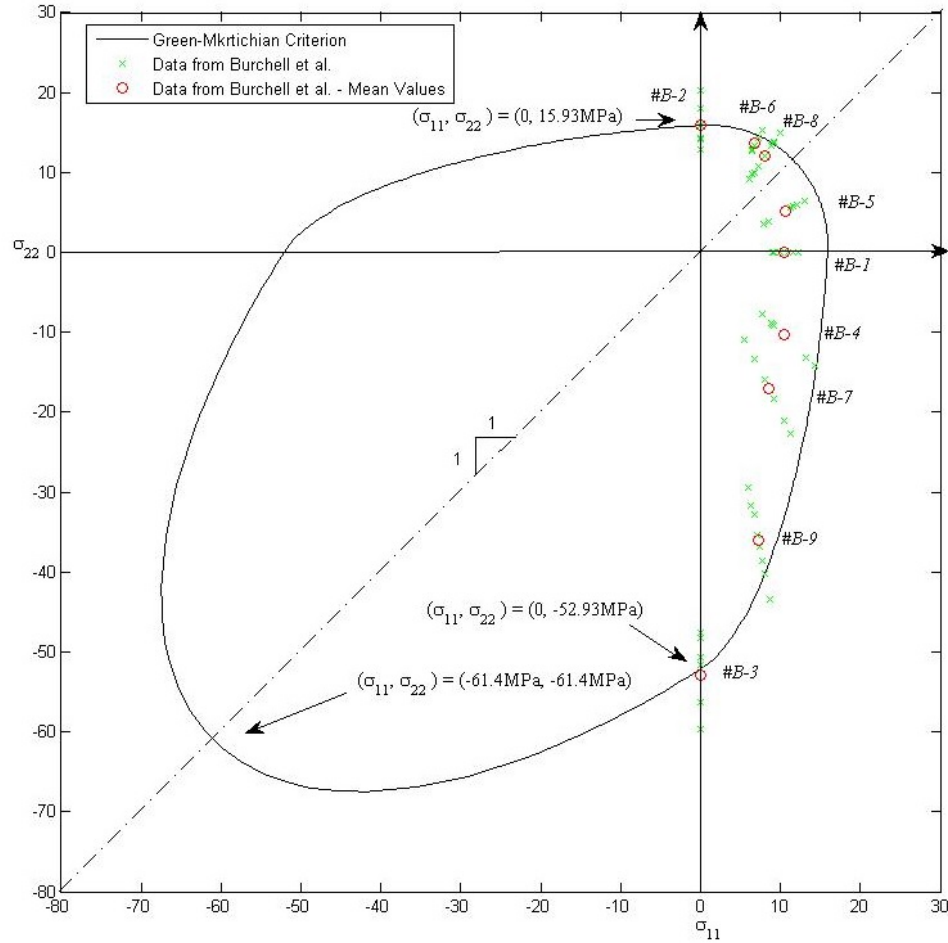


Figure 4.5.1 The Isotropic Failure Criterion Projected onto the  $\sigma_1$ - $\sigma_2$  Principal Stress Plane ( $\sigma_T = 15.93$  MPa,  $\sigma_C = -52.93$  MPa,  $\sigma_{BC} = -61.40$  MPa)

The isotropic failure criterion is projected onto the deviatoric planes in Figures 4.5.2 and 4.5.3. Note that a cross section through the failure function perpendicular to the hydrostatic axis transitions from a pyramidal shape (Figure 4.5.3) to a circular shape (Figure 4.5.2) with an increasing value of the stress invariant  $I_1$ . This suggests that the apex of the failure function presented in a full Haigh-Westergaard stress space is blunt, i.e., quite rounded for the particular criterion.

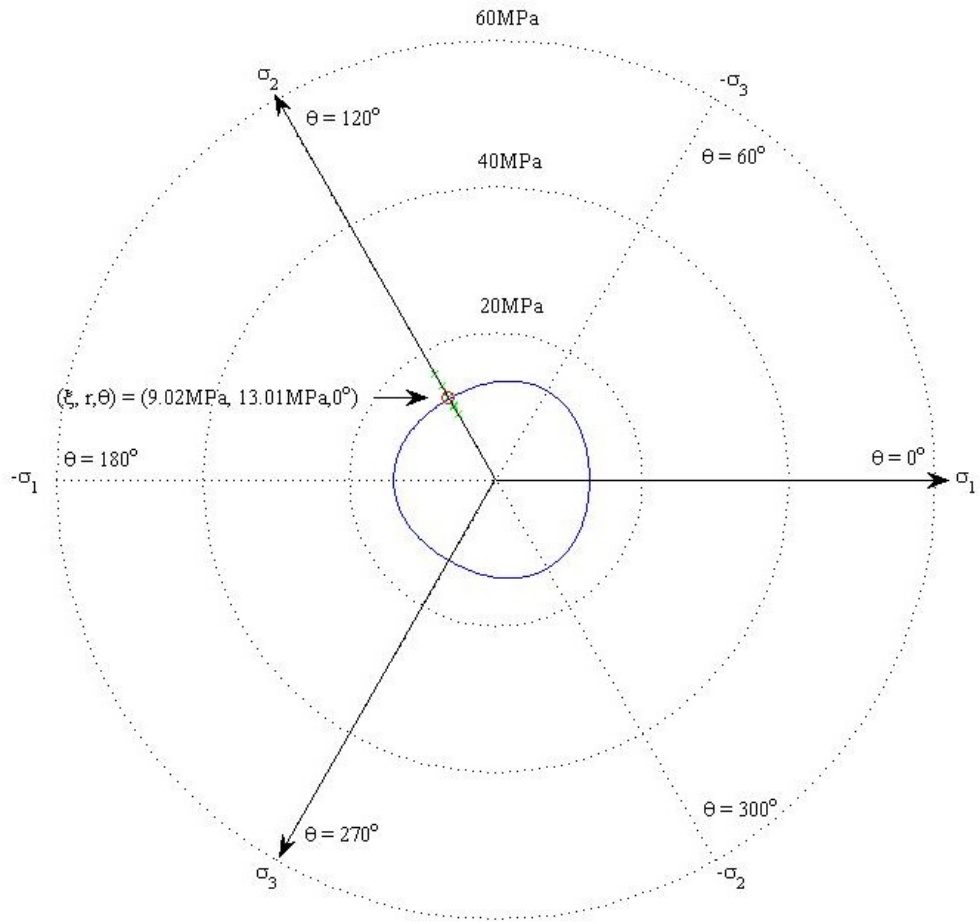


Figure 4.5.2 The Isotropic Failure Criterion Projected onto a Deviatoric Plane ( $\xi = 9.20\text{MPa}$ ) Parallel to the  $\Pi$ -plane with  $\sigma_T = 15.93\text{MPa}$ ,  $\sigma_C = -52.93\text{MPa}$ ,  $\sigma_{BC} = -61.40\text{MPa}$

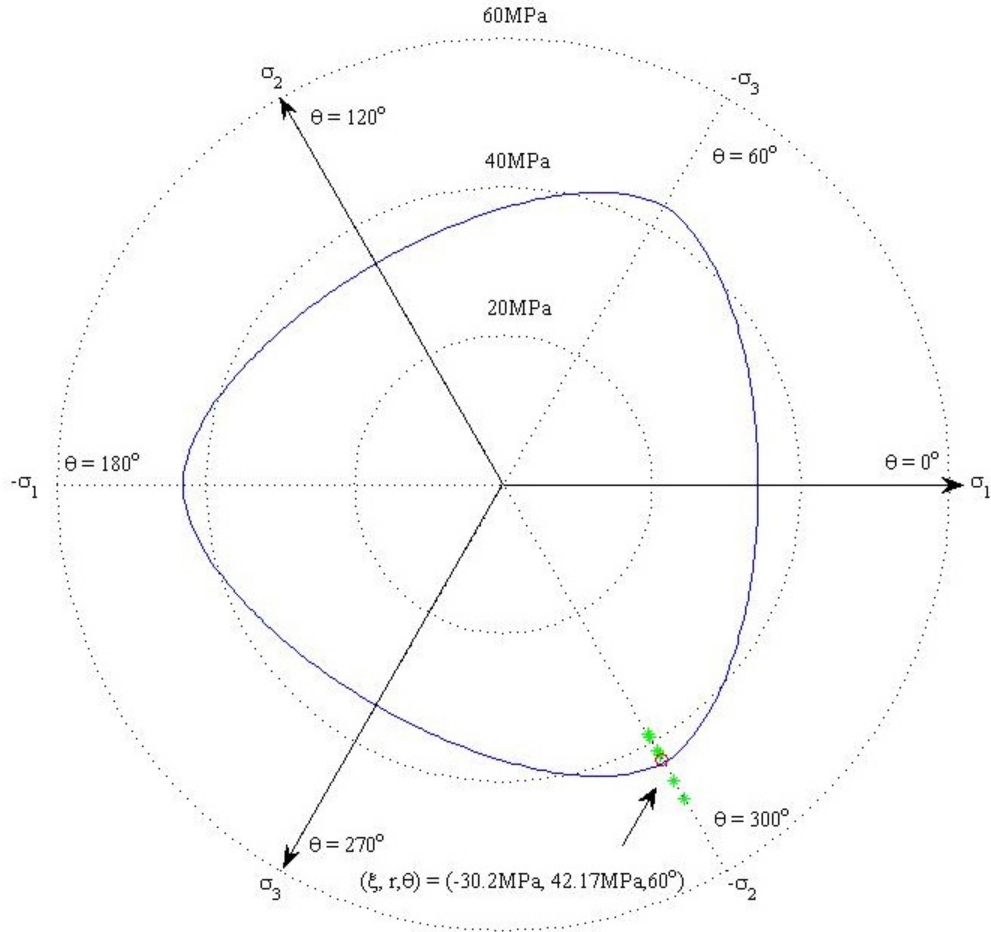
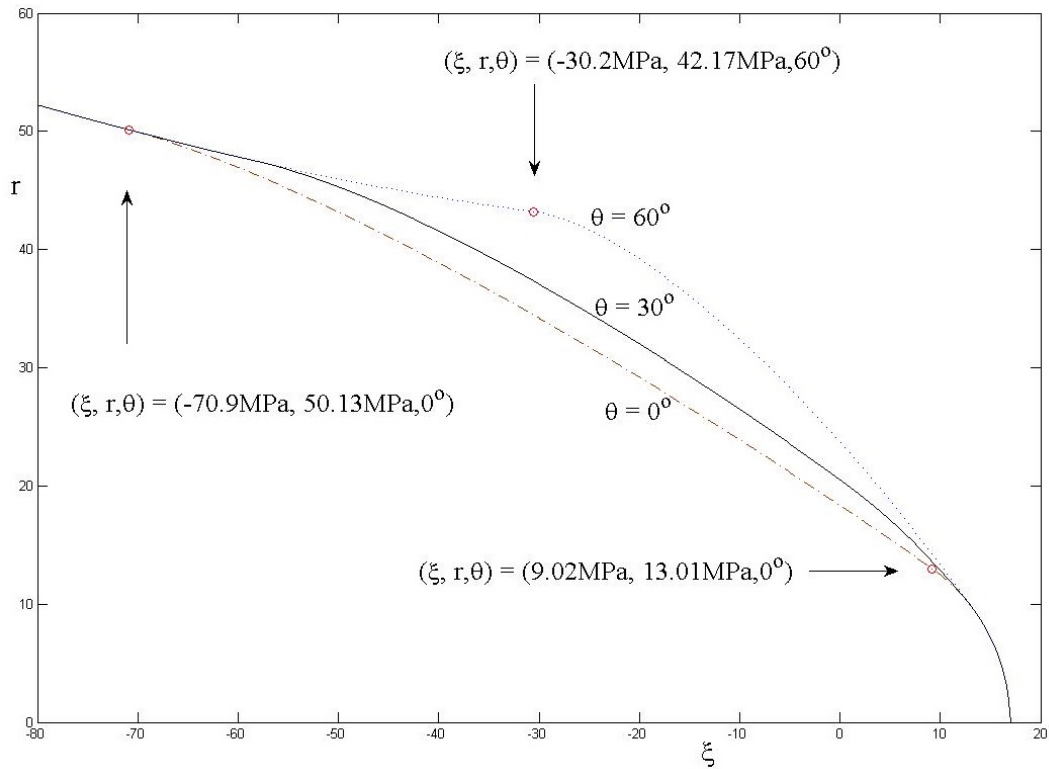


Figure 4.5.3 The Isotropic Failure Criterion Projected onto a Deviatoric Plane ( $\xi = -30.2\text{MPa}$ ) Parallel to the  $\Pi$ -plane with  $\sigma_T = 15.93\text{MPa}$ ,  $\sigma_C = -52.93\text{MPa}$ ,  $\sigma_{BC} = -61.40\text{MPa}$

The meridian lines of the isotropic failure surface corresponding to  $\theta = 0^\circ$  and  $\theta = 60^\circ$  are depicted on Figure 4.5.4. Obviously the meridian lines are not linear. The  $\theta = 0^\circ$  meridian line goes through point defined by  $\xi = 9.02\text{MPa}$  and  $r = 13.01\text{MPa}$ . The  $\theta = 60^\circ$  meridian line goes through the point defined by  $\xi = 30.56\text{MPa}$  and  $r = 43.22\text{MPa}$ .



*Figure 4.5.4 The Isotropic Failure Criterion Projected onto the Meridian Plane for a Material Strength Parameter of  $\sigma_T = 15.93 \text{ MPa}$ ,  $\sigma_C = -52.93 \text{ MPa}$ ,  $\sigma_{BC} = -61.40 \text{ MPa}$*

As the value of the  $I_1$  stress invariant associated with the hydrostatic stress increases in the negative direction, failure surfaces perpendicular to the hydrostatic stress line become circular again. The model suggests that as hydrostatic compression stress increases the difference between tensile strength and compressive strength diminishes and approach each other asymptotically. This is a material behavior that should be verified experimentally in a manner similar to Bridgman's (1953) bend bar experiments conducted in hyperbaric chambers on cast metal alloys. Balzer (1998) provides an excellent overview of Bridgman's (1953) experimental efforts, as well as others and their accomplishments in the field of high pressure testing.

However, as indicated in Figure 4.5.1, the isotropic formulation of the failure criterion does not capture the anisotropic behavior of the data from Burchell et al. (2007). The isotropic formulation is extended to transverse isotropy in the next chapter. Orthotropic behavior and other types of anisotropic behavior can be captured through similar use of tensorial invariants.

## CHAPTER V

### ANISOTROPIC FAILURE CRITERION

As discussed in earlier sections the multiaxial failure data from Burchell et al. (2007) strongly suggests that the graphite tested was anisotropic. Thus there is a need to extend the isotropic failure model discussed in the previous section so that anisotropic failure behavior is captured. This can be done again by utilizing stress based invariants where the material anisotropy is captured through the use of a direction vector associated with primary material directions. The concept is identical to the extension of the isotropic inelastic constitutive model. The extension of a phenomenological failure criterion will be made for a transversely isotropic material. Other material symmetries, e.g., an orthotropic material symmetry, can be included as well. Duffy and Manderscheid (1990b) as well as others have suggested an appropriate integrity basis for the orthotropic material symmetry. Transversely isotropic materials have the same properties in one plane and different properties in a direction normal to this plane. Orthotropic materials have different properties in three mutually perpendicular directions.

## 5.1 Integrity Base for Anisotropy

The preferred material direction is designated through a second direction vector,  $d_i$ . The dependence of the failure function is extended such that

$$g(\sigma_{ij}, d_i d_j, a_i a_j) = 0 \quad (5.1.1)$$

The definition of the unit vector  $a_i$  is the same as in earlier sections. Rivlin and Smith (1969) as well as Spencer (1971) show that for a scalar valued function with dependence stipulated by equation (5.1.1) the integrity basis is

$$I_1 = \sigma_{kk} \quad (5.1.2)$$

$$I_2 = \sigma_{ij} \sigma_{ji} \quad (5.1.3)$$

$$I_3 = \sigma_{ij} \sigma_{jk} \sigma_{ki} \quad (5.1.4)$$

$$I_4 = a_i a_j \sigma_{ij} \quad (5.1.5)$$

$$I_5 = a_i a_j \sigma_{jk} \sigma_{ki} \quad (5.1.6)$$

$$I_6 = d_i d_j \sigma_{ji} \quad (5.1.7)$$

$$I_7 = d_i d_j \sigma_{jk} \sigma_{ki} \quad (5.1.8)$$

$$I_8 = a_i a_j d_j d_k \sigma_{kj} \quad (5.1.9)$$

and

$$I_9 = a_i a_j d_j d_k \sigma_{km} \sigma_{mi} \quad (5.1.10)$$

The invariant  $I_3$  is omitted again since this invariant is cubic in stress. As before those invariants linear in stress enter the functional dependence as squared terms or as products

with another invariant linear in stress. Therefore the anisotropic failure function has the following dependence

$$\begin{aligned}
 g(\sigma_{ij}, d_i d_j, a_i a_j) &= g(I_1, I_2, I_4, I_5, I_6, I_7, I_8, I_9) \\
 &= 1 - \left[ \left( \frac{1}{2} \right) A I_1^2 + B I_2 + C I_1 I_4 + D I_5 \right. \\
 &\quad \left. + E I_1 I_6 + F I_7 + G I_1 I_8 + H I_9 \right] \quad (5.1.11)
 \end{aligned}$$

The form of the failure function was constructed as a polynomial in the invariants listed above. The constants in this formulation ( $A, B, C, D, E, F, G,$  and  $H$ ) are characterized by adopting simple strength tests. The proposed failure function was incorporated into a reliability model through the use of Monte Carlo simulation and importance sampling techniques. This feature is discussed in a subsequent section.

## 5.2 Functional Forms and Associated Gradients by Stress Region

Similar to the approach adopted for anisotropic constitutive models, the underlying concept is that the response of the material depends on the stress state, a preferred material direction and whether the principal stresses are tensile or compressive. The principal stress space is divided again into four regions. The regions and associated failure functions are listed below. In the first region all of the principal stresses are tensile, i.e.,

**Region #1:**  $(\sigma_1 \geq \sigma_2 \geq \sigma_3 \geq 0)$

$$g_1 = 1 - \left[ \left( \frac{1}{2} \right) A_1 I_1^2 + B_1 I_2 + E_1 I_1 I_6 + F_1 I_7 \right] \quad (5.2.1)$$



In Region #1 a direction vector associated with the principal stresses is unnecessary since all principal stresses are tensile. The corresponding normal to the failure surface is

$$\frac{\partial g_1}{\partial \sigma_{ij}} = \frac{\partial g_1}{\partial I_1} \frac{\partial I_1}{\partial \sigma_{ij}} + \frac{\partial g_1}{\partial I_2} \frac{\partial I_2}{\partial \sigma_{ij}} + \frac{\partial g_1}{\partial I_6} \frac{\partial I_6}{\partial \sigma_{ij}} + \frac{\partial g_1}{\partial I_7} \frac{\partial I_7}{\partial \sigma_{ij}} \quad (5.2.2)$$

where

$$\frac{\partial g_1}{\partial I_1} = -A_1 I_1 - E_1 I_6 \quad (5.2.3)$$

$$\frac{\partial g_1}{\partial I_2} = -B_1 \quad (5.2.4)$$

$$\frac{\partial g_1}{\partial I_6} = -E_1 I_1 \quad (5.2.5)$$

$$\frac{\partial g_1}{\partial I_7} = -F_1 \quad (5.2.6)$$

$$\frac{\partial I_1}{\partial \sigma_{ij}} = \delta_{ij} \quad (5.2.7)$$

$$\frac{\partial I_2}{\partial \sigma_{ij}} = 2\sigma_{ij} \quad (5.2.8)$$

$$\frac{\partial I_6}{\partial \sigma_{ij}} = d_i d_j \quad (5.2.9)$$

and

$$\frac{\partial I_7}{\partial \sigma_{ij}} = d_k d_j \sigma_{ki} + d_i d_k \sigma_{jk} \quad (5.2.10)$$

Substitution of equations (5.2.3) through (5.2.10) into (5.2.2) leads to the following tensor expression

$$\frac{\partial g_1}{\partial \sigma_{ij}} = -\left[ (A_1 I_1 + E_1 I_6) \delta_{ij} + 2B_1 \sigma_{ij} + E_1 I_1 d_i d_j + F_1 (d_k d_i \sigma_{jk} + d_j d_k \sigma_{ki}) \right] \quad (5.2.11)$$

or

$$\frac{\partial g_1}{\partial \sigma_{ij}} = -\left[ A_1 I_1 \delta_{ij} + 2B_1 \sigma_{ij} + E_1 (I_1 d_i d_j + I_6 \delta_{ij}) + F_1 (d_k d_i \sigma_{jk} + d_j d_k \sigma_{ki}) \right] \quad (5.2.12)$$

**Region #2:**  $(\sigma_1 \geq \sigma_2 \geq 0 \geq \sigma_3)$

$$g_2 = 1 - \left[ \left( \frac{1}{2} \right) A_2 I_1^2 + B_2 I_2 + C_2 I_1 I_4 + D_2 I_5 + E_2 I_1 I_6 + F_2 I_7 + G_2 I_1 I_8 + H_2 I_9 \right] \quad (5.2.13)$$

In Region #2 the direction vector  $a_i$  is associated with the compressive principal stress  $\sigma_3$ .

Thus for this region

$$a_i = (0, 0, 1) \quad (5.2.14)$$

.The corresponding normal to the failure surface is

$$\begin{aligned} \frac{\partial g_2}{\partial \sigma_{ij}} = & \frac{\partial g_2}{\partial I_1} \frac{\partial I_1}{\partial \sigma_{ij}} + \frac{\partial g_2}{\partial I_2} \frac{\partial I_2}{\partial \sigma_{ij}} + \frac{\partial g_2}{\partial I_4} \frac{\partial I_4}{\partial \sigma_{ij}} + \frac{\partial g_2}{\partial I_5} \frac{\partial I_5}{\partial \sigma_{ij}} \\ & + \frac{\partial g_2}{\partial I_6} \frac{\partial I_6}{\partial \sigma_{ij}} + \frac{\partial g_2}{\partial I_7} \frac{\partial I_7}{\partial \sigma_{ij}} + \frac{\partial g_2}{\partial I_8} \frac{\partial I_8}{\partial \sigma_{ij}} + \frac{\partial g_2}{\partial I_9} \frac{\partial I_9}{\partial \sigma_{ij}} \end{aligned} \quad (5.2.15)$$

where

$$\frac{\partial g_2}{\partial I_1} = -(A_2 I_1 + C_2 I_4 + E_2 I_6 + G_2 I_8) \quad (5.2.16)$$

$$\frac{\partial g_2}{\partial I_2} = -B_2 \quad (5.2.17)$$

$$\frac{\partial g_2}{\partial I_4} = -C_2 I_1 \quad (5.2.18)$$

$$\frac{\partial g_2}{\partial I_5} = -D_2 \quad (5.2.19)$$

$$\frac{\partial g_2}{\partial I_6} = -E_2 I_1 \quad (5.2.20)$$

$$\frac{\partial g_2}{\partial I_7} = -F_2 \quad (5.2.21)$$

$$\frac{\partial g_2}{\partial I_8} = -G_2 I_1 \quad (5.2.22)$$

$$\frac{\partial g_2}{\partial I_9} = -H_2 \quad (5.2.23)$$

$$\frac{\partial I_4}{\partial \sigma_{ij}} = a_i a_j \quad (5.2.24)$$

$$\frac{\partial I_5}{\partial \sigma_{ij}} = a_k a_i \sigma_{jk} + a_j a_k \sigma_{ki} \quad (5.2.25)$$

$$\frac{\partial I_8}{\partial \sigma_{ij}} = a_i a_k d_k d_j \quad (5.2.26)$$

and

$$\frac{\partial I_9}{\partial \sigma_{ij}} = a_k a_l d_l d_j \sigma_{ki} + a_i a_l d_l d_k \sigma_{jk} \quad (5.2.27)$$

Substitution of equations (5.2.7) through (5.2.10) and (5.2.16) through (5.2.27) into (5.2.15) leads to the following tensor expression

$$\begin{aligned} \frac{\partial g_2}{\partial \sigma_{ij}} = & -\left[ (A_2 I_1 + C_2 I_4 + E_2 I_6 + G_2 I_8) \delta_{ij} + 2 B_2 \sigma_{ij} \right. \\ & + (C_2 I_1) a_i a_j + D_2 (a_k a_i \sigma_{jk} + a_j a_k \sigma_{ki}) \\ & + (E_2 I_1) d_i d_j + F_2 (d_k d_j \sigma_{ki} + d_i d_k \sigma_{jk}) \\ & \left. + (G_2 I_1) a_i a_k d_k d_j + H_2 (a_k a_l d_l d_j \sigma_{ki} + a_i a_l d_l d_k \sigma_{jk}) \right] \end{aligned} \quad (5.2.28)$$

then

$$\begin{aligned} \frac{\partial g_2}{\partial \sigma_{ij}} = & -\left[ A_2 I_1 \delta_{ij} + 2 B_2 \sigma_{ij} + C_2 (I_1 a_i a_j + I_4 \delta_{ij}) \right. \\ & + D_2 (a_k a_i \sigma_{jk} + a_j a_k \sigma_{ki}) + E_2 (I_1 d_i d_j + I_6 \delta_{ij}) \\ & + F_2 (d_k d_j \sigma_{ki} + d_i d_k \sigma_{jk}) + G_2 (I_1 a_i a_k d_k d_j + I_8 \delta_{ij}) \\ & \left. + H_2 (a_k a_l d_l d_j \sigma_{ki} + a_i a_l d_l d_k \sigma_{jk}) \right] \end{aligned} \quad (5.2.29)$$

**Region #3:**  $(\sigma_1 \geq 0 \geq \sigma_2 \geq \sigma_3)$

The failure function for this region of the stress space is

$$\begin{aligned} g_3 = 1 - & \left[ \left( \frac{1}{2} \right) A_3 I_1^2 + B_3 I_2 + C_3 I_1 I_4 + D_3 I_5 I_7 \right. \\ & \left. + E_3 I_1 I_6 + F_3 + G_3 I_1 I_8 + H_3 I_9 \right] \end{aligned} \quad (5.2.30)$$

In Region #3 the direction vector  $a_i$  is associated with the tensile principal stress direction

$\sigma_1$ . For this region

$$a_i = (1, 0, 0) \quad (5.2.31)$$

The corresponding normal to the failure surface is

$$\begin{aligned} \frac{\partial g_3}{\partial \sigma_{ij}} = & \frac{\partial g_3}{\partial I_1} \frac{\partial I_1}{\partial \sigma_{ij}} + \frac{\partial g_3}{\partial I_2} \frac{\partial I_2}{\partial \sigma_{ij}} + \frac{\partial g_3}{\partial I_4} \frac{\partial I_4}{\partial \sigma_{ij}} + \frac{\partial g_3}{\partial I_5} \frac{\partial I_5}{\partial \sigma_{ij}} \\ & + \frac{\partial g_3}{\partial I_6} \frac{\partial I_6}{\partial \sigma_{ij}} + \frac{\partial g_3}{\partial I_7} \frac{\partial I_7}{\partial \sigma_{ij}} + \frac{\partial g_3}{\partial I_8} \frac{\partial I_8}{\partial \sigma_{ij}} + \frac{\partial g_3}{\partial I_9} \frac{\partial I_9}{\partial \sigma_{ij}} \end{aligned} \quad (5.2.32)$$

where

$$\frac{\partial g_3}{\partial I_1} = -(A_3 I_1 + C_3 I_4 + E_3 I_6 + G_3 I_8) \quad (5.2.33)$$

$$\frac{\partial g_3}{\partial I_2} = -B_3 \quad (5.2.34)$$

$$\frac{\partial g_3}{\partial I_4} = -C_3 I_1 \quad (5.2.35)$$

$$\frac{\partial g_3}{\partial I_5} = -D_3 \quad (5.2.36)$$

$$\frac{\partial g_3}{\partial I_6} = -E_3 I_1 \quad (5.2.37)$$

$$\frac{\partial g_3}{\partial I_7} = -F_3 \quad (5.2.38)$$

$$\frac{\partial g_3}{\partial I_8} = -G_3 I_1 \quad (5.2.39)$$

and

$$\frac{\partial g_3}{\partial I_9} = -H_3 \quad (5.2.40)$$

Substitution of equations (5.2.7) through (5.2.10), (5.2.24) through (5.2.27) and (5.2.33)

through (5.2.40) into (5.2.32) leads to the following tensor expression

$$\begin{aligned} \frac{\partial g_3}{\partial \sigma_{ij}} = & -[(A_3 I_1 + C_3 I_4 + E_3 I_6 + G_3 I_8) \delta_{ij} + 2B_3 \sigma_{ij} \\ & + (C_3 I_1) a_i a_j + D_3 (a_k a_i \sigma_{jk} + a_j a_k \sigma_{ki}) \\ & + (E_3 I_1) d_i d_j + F_3 (d_k d_j \sigma_{ki} + d_i d_k \sigma_{jk}) \\ & + (G_3 I_1) a_i a_k d_k d_j + H_3 (a_k a_l d_l d_j \sigma_{ki} + a_i a_l d_l d_k \sigma_{jk})] \end{aligned} \quad (5.2.41)$$

or

$$\begin{aligned}
\frac{\partial g_3}{\partial \sigma_{ij}} = & -[A_3 I_1 \delta_{ij} + 2B_3 \sigma_{ij} + C_3 (I_1 a_i a_j + I_4 \delta_{ij}) \\
& + D_3 (a_k a_i \sigma_{jk} + a_j a_k \sigma_{ki}) + E_3 (I_1 d_i d_j + I_6 \delta_{ij}) \\
& + F_3 (d_k d_j \sigma_{ki} + d_i d_k \sigma_{jk}) + G_3 (I_1 a_i a_k d_k d_j + I_8 \delta_{ij}) \\
& + H_3 (a_k a_i d_l d_j \sigma_{ki} + a_i a_l d_l d_k \sigma_{jk})]
\end{aligned} \quad (5.2.42)$$

**Region #4:**  $0 \geq \sigma_1 \geq \sigma_2 \geq \sigma_3$

The failure function for this region of the stress space is

$$g_4 = 1 - \left[ \left( \frac{1}{2} \right) A_4 I_1^2 + B_4 I_2 + E_4 I_1 I_6 + F_4 I_7 \right] \quad (5.2.43)$$

and since all principal stresses are compressive a direction vector associated with the principal stress direction is unnecessary. The corresponding normal to the failure surface is

$$\frac{\partial g_4}{\partial \sigma_{ij}} = \frac{\partial g_4}{\partial I_1} \frac{\partial I_1}{\partial \sigma_{ij}} + \frac{\partial g_4}{\partial I_2} \frac{\partial I_2}{\partial \sigma_{ij}} + \frac{\partial g_4}{\partial I_6} \frac{\partial I_6}{\partial \sigma_{ij}} + \frac{\partial g_4}{\partial I_7} \frac{\partial I_7}{\partial \sigma_{ij}} \quad (5.2.44)$$

where

$$\frac{\partial g_4}{\partial I_1} = -A_4 I_1 + E_4 I_6 \quad (5.2.45)$$

$$\frac{\partial g_4}{\partial I_2} = -B_4 \quad (5.2.46)$$

$$\frac{\partial g_4}{\partial I_6} = -E_4 I_1 \quad (5.2.47)$$

$$\frac{\partial g_4}{\partial I_7} = -F_4 \quad (5.2.48)$$

and

$$\frac{\partial g_4}{\partial I_7} = -F_4 \quad (5.2.49)$$

Substitution of equations (5.2.7) through (5.2.10) and (5.2.45) through (5.2.49) into (5.2.44) leads to the following tensor expression

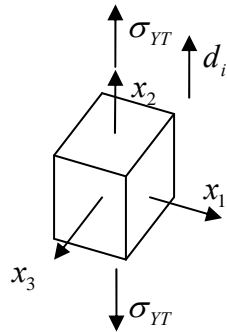
$$\begin{aligned} \frac{\partial g_4}{\partial \sigma_{ij}} = & - \left[ (A_1 I_1 + E_1 I_6) \delta_{ij} + 2B_1 \sigma_{ij} + E_1 I_1 d_i d_j \right. \\ & \left. + F_1 (d_k d_i \sigma_{jk} + d_j d_k \sigma_{ki}) \right] \end{aligned} \quad (5.2.50)$$

or

$$\begin{aligned} \frac{\partial g_4}{\partial \sigma_{ij}} = & - \left[ A_1 I_1 \delta_{ij} + 2B_1 \sigma_{ij} + E_1 (I_1 d_i d_j + I_6 \delta_{ij}) \right. \\ & \left. + F_1 (d_k d_i \sigma_{jk} + d_j d_k \sigma_{ki}) \right] \end{aligned} \quad (5.2.51)$$

### 5.3 Relationships Between Functional Constants

With the failure functions and the normals to those functions defined in general terms for each region, attention is now turned to establishing functional relationships between the constants. Consider the following stress state at failure under a tensile load in the preferred material direction with material direction  $d_i = (0, 1, 0)$ , i.e.,



$$\sigma_{ij} = \begin{bmatrix} 0 & 0 & 0 \\ 0 & \sigma_{YT} & 0 \\ 0 & 0 & 0 \end{bmatrix} \quad (5.3.1)$$

The first stress subscript  $Y$  denotes a strength parameter associated with the strong direction, and second subscript  $T$  denotes this quantity is a tensile strength parameter. The principal stresses for this stress state are

$$(\sigma_1, \sigma_2, \sigma_3) = (\sigma_{YT}, 0, 0) \quad (5.3.2)$$

and this stress state lies along the boundary shared by region #1 and region #2, as well as the shared boundary along region #2 and region #3. At both boundaries we impose the requirements that the gradients match, i.e.,

$$\frac{\partial g_1}{\partial \sigma_{ij}} = \frac{\partial g_2}{\partial \sigma_{ij}} \quad (5.3.3)$$

$$\frac{\partial g_2}{\partial \sigma_{ij}} = \frac{\partial g_3}{\partial \sigma_{ij}} \quad (5.3.4)$$

providing a smooth transition from one principal stress region to another. For this stress state the first, second, sixth and seventh invariants of stress are

$$I_1 = \sigma_{YT} \quad (5.3.5)$$

$$I_2 = \sigma_{YT}^2 \quad (5.3.6)$$

$$I_6 = \sigma_{YT} \quad (5.3.7)$$

and

$$I_7 = \sigma_{YT}^2 \quad (5.3.8)$$

These stress invariants are common for stress region #1, #2 and #3. With these invariants



$$\frac{\partial g_1}{\partial \sigma_{ij}} = - \begin{bmatrix} \sigma_{YT} & 0 & 0 \\ 0 & \sigma_{YT} & 0 \\ 0 & 0 & \sigma_{YT} \end{bmatrix} A_1 - \begin{bmatrix} 0 & 0 & 0 \\ 0 & 2\sigma_{YT} & 0 \\ 0 & 0 & 0 \end{bmatrix} B_1$$

$$- \begin{bmatrix} \sigma_{YT} & 0 & 0 \\ 0 & 2\sigma_{YT} & 0 \\ 0 & 0 & \sigma_{YT} \end{bmatrix} E_1 - \begin{bmatrix} 0 & 0 & 0 \\ 0 & 2\sigma_{YT} & 0 \\ 0 & 0 & 0 \end{bmatrix} F_1 \quad (5.3.9)$$

For the stress state in region #2 given above the unit principal stress vector is

$${}^2a_i = (0, 0, 1) \quad (5.3.10)$$

The left superscript “2” denotes a vector associated with principal stress region #2. Thus

$$({}^2a_i)({}^2a_j) = \begin{bmatrix} 0 & 0 & 0 \\ 0 & 0 & 0 \\ 0 & 0 & 1 \end{bmatrix} \quad (5.3.11)$$

The stress invariants associated with this vector and the stress state given above are

$${}^2I_4 = 0 \quad (5.3.12)$$

$${}^2I_5 = 0 \quad (5.3.13)$$

$${}^2I_8 = 0 \quad (5.3.14)$$

and

$${}^2I_9 = 0 \quad (5.3.15)$$

With these stress invariants and stress state the gradient along the boundary for stress

region #2 is

$$\begin{aligned} \frac{\partial g_2}{\partial \sigma_{ij}} = & - \begin{bmatrix} \sigma_{YT} & 0 & 0 \\ 0 & \sigma_{YT} & 0 \\ 0 & 0 & \sigma_{YT} \end{bmatrix} A_2 - \begin{bmatrix} 0 & 0 & 0 \\ 0 & 2\sigma_{YT} & 0 \\ 0 & 0 & 0 \end{bmatrix} B_2 - \begin{bmatrix} 0 & 0 & 0 \\ 0 & 0 & 0 \\ 0 & 0 & \sigma_{YT} \end{bmatrix} C_2 \\ & - \begin{bmatrix} \sigma_{YT} & 0 & 0 \\ 0 & 2\sigma_{YT} & 0 \\ 0 & 0 & \sigma_{YT} \end{bmatrix} E_2 - \begin{bmatrix} 0 & 0 & 0 \\ 0 & 2\sigma_{YT} & 0 \\ 0 & 0 & 0 \end{bmatrix} F_2 \end{aligned} \quad (5.3.16)$$

Utilizing equations (5.3.9) and (5.3.16) in equation (5.3.3) then at the boundary between stress region #1 and stress region #2

$$\begin{aligned} & \begin{bmatrix} \sigma_{YT} & 0 & 0 \\ 0 & \sigma_{YT} & 0 \\ 0 & 0 & \sigma_{YT} \end{bmatrix} A_1 + \begin{bmatrix} 0 & 0 & 0 \\ 0 & 2\sigma_{YT} & 0 \\ 0 & 0 & 0 \end{bmatrix} B_1 \\ & + \begin{bmatrix} \sigma_{YT} & 0 & 0 \\ 0 & 2\sigma_{YT} & 0 \\ 0 & 0 & \sigma_{YT} \end{bmatrix} E_1 + \begin{bmatrix} 0 & 0 & 0 \\ 0 & 2\sigma_{YT} & 0 \\ 0 & 0 & 0 \end{bmatrix} F_1 \\ = & \begin{bmatrix} \sigma_{YT} & 0 & 0 \\ 0 & \sigma_{YT} & 0 \\ 0 & 0 & \sigma_{YT} \end{bmatrix} A_2 + \begin{bmatrix} 0 & 0 & 0 \\ 0 & 2\sigma_{YT} & 0 \\ 0 & 0 & 0 \end{bmatrix} B_2 \\ & + \begin{bmatrix} 0 & 0 & 0 \\ 0 & 0 & 0 \\ 0 & 0 & \sigma_{YT} \end{bmatrix} C_2 + \begin{bmatrix} \sigma_{YT} & 0 & 0 \\ 0 & 2\sigma_{YT} & 0 \\ 0 & 0 & \sigma_{YT} \end{bmatrix} E_2 + \begin{bmatrix} 0 & 0 & 0 \\ 0 & 2\sigma_{YT} & 0 \\ 0 & 0 & 0 \end{bmatrix} F_2 \end{aligned} \quad (5.3.17)$$

The following three expressions can be extracted from equation (5.3.17), i.e.,

$$A_1 + E_1 = A_2 + E_2 \quad (5.3.18)$$

$$A_1 + 2B_1 + 2E_1 + 2F_1 = A_2 + 2B_2 + 2E_2 + 2F_2 \quad (5.3.19)$$

and

$$A_1 + E_1 = A_2 + C_2 + E_2 \quad (5.3.20)$$

For the stress state in region #3 given above the unit principal stress vector is

$${}^3a_i = (0, 1, 0) \quad (5.3.21)$$

Thus

$$\begin{pmatrix} a_i \\ a_j \end{pmatrix} = \begin{bmatrix} 0 & 0 & 0 \\ 0 & 1 & 0 \\ 0 & 0 & 0 \end{bmatrix} \quad (5.3.22)$$

The stress invariants associated with this unit vector and stress state are

$${}^3I_4 = \sigma_{YT} \quad (5.3.23)$$

$${}^3I_5 = \sigma_{YT}^2 \quad (5.3.24)$$

$${}^3I_8 = \sigma_{YT} \quad (5.3.25)$$

and

$${}^3I_9 = \sigma_{YT}^2 \quad (5.3.26)$$

With these stress invariants and stress state the gradient along the boundary for stress

region #3 is

$$\begin{aligned} \frac{\partial g_3}{\partial \sigma_{ij}} = & - \begin{bmatrix} \sigma_{YT} & 0 & 0 \\ 0 & \sigma_{YT} & 0 \\ 0 & 0 & \sigma_{YT} \end{bmatrix} A_3 - \begin{bmatrix} 0 & 0 & 0 \\ 0 & 2\sigma_{YT} & 0 \\ 0 & 0 & 0 \end{bmatrix} B_3 \\ & - \begin{bmatrix} \sigma_{YT} & 0 & 0 \\ 0 & 2\sigma_{YT} & 0 \\ 0 & 0 & \sigma_{YT} \end{bmatrix} C_3 - \begin{bmatrix} \sigma_{YT} & 0 & 0 \\ 0 & 2\sigma_{YT} & 0 \\ 0 & 0 & \sigma_{YT} \end{bmatrix} E_3 \\ & - \begin{bmatrix} 0 & 0 & 0 \\ 0 & 2\sigma_{YT} & 0 \\ 0 & 0 & 0 \end{bmatrix} F_3 - \begin{bmatrix} \sigma_{YT} & 0 & 0 \\ 0 & 2\sigma_{YT} & 0 \\ 0 & 0 & \sigma_{YT} \end{bmatrix} G_3 \\ & - \begin{bmatrix} 0 & 0 & 0 \\ 0 & 2\sigma_{YT} & 0 \\ 0 & 0 & 0 \end{bmatrix} H_3 \end{aligned} \quad (5.3.27)$$

Utilizing equations (5.3.16) and (5.3.27) in equation (5.3.4) then at the boundary between

stress region #2 and stress region #3

$$\begin{aligned}
& \begin{bmatrix} \sigma_{YT} & 0 & 0 \\ 0 & \sigma_{YT} & 0 \\ 0 & 0 & \sigma_{YT} \end{bmatrix} A_2 + \begin{bmatrix} 0 & 0 & 0 \\ 0 & 2\sigma_{YT} & 0 \\ 0 & 0 & 0 \end{bmatrix} B_2 \\
& + \begin{bmatrix} 0 & 0 & 0 \\ 0 & 0 & 0 \\ 0 & 0 & \sigma_{YT} \end{bmatrix} C_2 + \begin{bmatrix} \sigma_{YT} & 0 & 0 \\ 0 & 2\sigma_{YT} & 0 \\ 0 & 0 & \sigma_{YT} \end{bmatrix} E_2 + \begin{bmatrix} 0 & 0 & 0 \\ 0 & 2\sigma_{YT} & 0 \\ 0 & 0 & 0 \end{bmatrix} F_2 \\
= & \begin{bmatrix} \sigma_{YT} & 0 & 0 \\ 0 & \sigma_{YT} & 0 \\ 0 & 0 & \sigma_{YT} \end{bmatrix} A_3 + \begin{bmatrix} 0 & 0 & 0 \\ 0 & 2\sigma_{YT} & 0 \\ 0 & 0 & 0 \end{bmatrix} B_3 \\
& + \begin{bmatrix} \sigma_{YT} & 0 & 0 \\ 0 & 2\sigma_{YT} & 0 \\ 0 & 0 & \sigma_{YT} \end{bmatrix} C_3 + \begin{bmatrix} 0 & 0 & 0 \\ 0 & 2\sigma_{YT} & 0 \\ 0 & 0 & 0 \end{bmatrix} D_3 + \begin{bmatrix} \sigma_{YT} & 0 & 0 \\ 0 & 2\sigma_{YT} & 0 \\ 0 & 0 & \sigma_{YT} \end{bmatrix} E_3 \\
& + \begin{bmatrix} 0 & 0 & 0 \\ 0 & 2\sigma_{YT} & 0 \\ 0 & 0 & 0 \end{bmatrix} F_3 + \begin{bmatrix} \sigma_{YT} & 0 & 0 \\ 0 & 2\sigma_{YT} & 0 \\ 0 & 0 & \sigma_{YT} \end{bmatrix} G_3 + \begin{bmatrix} 0 & 0 & 0 \\ 0 & 2\sigma_{YT} & 0 \\ 0 & 0 & 0 \end{bmatrix} H_3 \quad (5.3.28)
\end{aligned}$$

The following three expressions can be extracted from equation (5.3.28), i.e.,

$$A_2 + E_2 = A_3 + C_3 + E_3 + G_3 \quad (5.3.29)$$

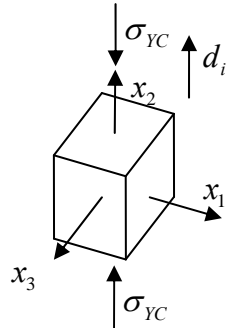
$$\begin{aligned}
& A_2 + 2B_2 + 2E_2 + 2F_2 \\
= & A_3 + 2B_3 + 2C_3 + 2D_3 \\
& + 2E_3 + 2F_3 + 2G_3 + 2H_3 \quad (5.3.30)
\end{aligned}$$

and

$$A_2 + C_2 + E_2 = A_3 + C_3 + E_3 + G_3 \quad (5.3.31)$$

Next consider the following stress state at failure under a compression load with

the same material direction  $d_i = (0, 1, 0)$  as above, i.e.,



$$\sigma_{ij} = \begin{bmatrix} 0 & 0 & 0 \\ 0 & \sigma_{YC} & 0 \\ 0 & 0 & 0 \end{bmatrix} \quad (5.3.32)$$

The subscript  $C$  denotes a compressive failure strength compression stress and it is noted that this strength is algebraically less than zero. The principal stresses are obviously

$$(\sigma_1, \sigma_2, \sigma_3) = (0, 0, \sigma_{YC}) \quad (5.3.33)$$

At the boundary of region #2 and region #3 the second principal stress is zero, i.e.,  $\sigma_2 = 0$ . Similarly, at the boundary of region #3 and region #4 the first principal stress is zero, i.e.,  $\sigma_1 = 0$ . At both boundaries we impose the requirements that the gradients match, i.e.,

$$\frac{\partial g_2}{\partial \sigma_{ij}} = \frac{\partial g_3}{\partial \sigma_{ij}} \quad (5.3.34)$$

$$\frac{\partial g_3}{\partial \sigma_{ij}} = \frac{\partial g_4}{\partial \sigma_{ij}} \quad (5.3.35)$$

providing a smooth transition from one principal stress region to another. Here the first, second, sixth and seventh invariants of stress are

$$I_1 = \sigma_{YC} \quad (5.3.36)$$

$$I_2 = \sigma_{YC}^2 \quad (5.3.37)$$

$$I_6 = \sigma_{YC} \quad (5.3.38)$$

and

$$I_7 = \sigma_{YC}^2 \quad (5.3.39)$$

These stress invariants are common for stress regions #2, #3, and #4 given this state of stress.

For the stress state in region # 2 the unit principal vector is

$${}^2a_i = (0, 1, 0) \quad (5.3.40)$$

thus

$$({}^2a_i)({}^2a_j) = \begin{bmatrix} 0 & 0 & 0 \\ 0 & 1 & 0 \\ 0 & 0 & 0 \end{bmatrix} \quad (5.3.41)$$

The stress invariants associated with this unit vector and stress state are

$${}^2I_4 = \sigma_{YC} \quad (5.3.42)$$

$${}^2I_5 = \sigma_{YC}^2 \quad (5.3.43)$$

$${}^2I_8 = \sigma_{YC} \quad (5.3.44)$$

and

$${}^2I_9 = \sigma_{YC}^2 \quad (5.3.45)$$

With these stress invariants and stress state, the gradient along the boundary for stress

region #2 is

$$\begin{aligned} \frac{\partial g_2}{\partial \sigma_{ij}} = & - \begin{bmatrix} \sigma_{YC} & 0 & 0 \\ 0 & \sigma_{YC} & 0 \\ 0 & 0 & \sigma_{YC} \end{bmatrix} A_2 - \begin{bmatrix} 0 & 0 & 0 \\ 0 & 2\sigma_{YC} & 0 \\ 0 & 0 & 0 \end{bmatrix} B_2 \\ & - \begin{bmatrix} \sigma_{YC} & 0 & 0 \\ 0 & 2\sigma_{YC} & 0 \\ 0 & 0 & \sigma_{YC} \end{bmatrix} C_2 - \begin{bmatrix} 0 & 0 & 0 \\ 0 & 2\sigma_{YC} & 0 \\ 0 & 0 & 0 \end{bmatrix} D_2 \\ & - \begin{bmatrix} \sigma_{YC} & 0 & 0 \\ 0 & 2\sigma_{YC} & 0 \\ 0 & 0 & \sigma_{YC} \end{bmatrix} E_2 - \begin{bmatrix} 0 & 0 & 0 \\ 0 & 2\sigma_{YC} & 0 \\ 0 & 0 & 0 \end{bmatrix} F_2 \\ & - \begin{bmatrix} \sigma_{YC} & 0 & 0 \\ 0 & 2\sigma_{YC} & 0 \\ 0 & 0 & \sigma_{YC} \end{bmatrix} G_2 - \begin{bmatrix} 0 & 0 & 0 \\ 0 & 2\sigma_{YC} & 0 \\ 0 & 0 & 0 \end{bmatrix} H_2 \end{aligned} \quad (5.3.46)$$

As noted earlier the unit vector associated with region #3 is

$${}^3a_i = (1, 0, 0) \quad (5.3.47)$$

thus

$$({}^3a_i)({}^3a_j) = \begin{bmatrix} 1 & 0 & 0 \\ 0 & 0 & 0 \\ 0 & 0 & 0 \end{bmatrix} \quad (5.3.48)$$

The stress invariants associated with this unit vector and stress state are

$${}^3I_4 = 0 \quad (5.3.49)$$

$${}^3I_5 = 0 \quad (5.3.50)$$

$${}^3I_8 = 0 \quad (5.3.51)$$

and

$${}^3I_9 = 0 \quad (5.3.52)$$

With these stress invariants and stress state, the gradient along the boundary for stress

region #3 is

$$\begin{aligned} \frac{\partial g_3}{\partial \sigma_{ij}} = & - \begin{bmatrix} \sigma_{YC} & 0 & 0 \\ 0 & \sigma_{YC} & 0 \\ 0 & 0 & \sigma_{YC} \end{bmatrix} A_3 - \begin{bmatrix} 0 & 0 & 0 \\ 0 & 2\sigma_{YC} & 0 \\ 0 & 0 & 0 \end{bmatrix} B_3 - \begin{bmatrix} \sigma_{YC} & 0 & 0 \\ 0 & 0 & 0 \\ 0 & 0 & 0 \end{bmatrix} C_3 \\ & - \begin{bmatrix} \sigma_{YC} & 0 & 0 \\ 0 & 2\sigma_{YC} & 0 \\ 0 & 0 & \sigma_{YC} \end{bmatrix} E_3 - \begin{bmatrix} 0 & 0 & 0 \\ 0 & 2\sigma_{YC} & 0 \\ 0 & 0 & 0 \end{bmatrix} F_3 \end{aligned} \quad (5.3.53)$$

Utilizing equations (5.3.46) and (5.3.53) in equation (5.3.34) then at the boundary

between stress region #2 and stress region #3

$$\begin{aligned}
& \begin{bmatrix} \sigma_{YC} & 0 & 0 \\ 0 & \sigma_{YC} & 0 \\ 0 & 0 & \sigma_{YC} \end{bmatrix} A_2 + \begin{bmatrix} 0 & 0 & 0 \\ 0 & 2\sigma_{YC} & 0 \\ 0 & 0 & 0 \end{bmatrix} B_2 + \begin{bmatrix} \sigma_{YC} & 0 & 0 \\ 0 & 2\sigma_{YC} & 0 \\ 0 & 0 & \sigma_{YC} \end{bmatrix} C_2 \\
& + \begin{bmatrix} 0 & 0 & 0 \\ 0 & 2\sigma_{YC} & 0 \\ 0 & 0 & 0 \end{bmatrix} D_2 + \begin{bmatrix} \sigma_{YC} & 0 & 0 \\ 0 & 2\sigma_{YC} & 0 \\ 0 & 0 & \sigma_{YC} \end{bmatrix} E_2 + \begin{bmatrix} 0 & 0 & 0 \\ 0 & 2\sigma_{YC} & 0 \\ 0 & 0 & 0 \end{bmatrix} F_2 \\
& + \begin{bmatrix} \sigma_{YC} & 0 & 0 \\ 0 & 2\sigma_{YC} & 0 \\ 0 & 0 & \sigma_{YC} \end{bmatrix} G_2 + \begin{bmatrix} 0 & 0 & 0 \\ 0 & 2\sigma_{YC} & 0 \\ 0 & 0 & 0 \end{bmatrix} H_2 \\
= & \begin{bmatrix} \sigma_{YC} & 0 & 0 \\ 0 & \sigma_{YC} & 0 \\ 0 & 0 & \sigma_{YC} \end{bmatrix} A_3 + \begin{bmatrix} 0 & 0 & 0 \\ 0 & 2\sigma_{YC} & 0 \\ 0 & 0 & 0 \end{bmatrix} B_3 + \begin{bmatrix} \sigma_{YC} & 0 & 0 \\ 0 & 0 & 0 \\ 0 & 0 & 0 \end{bmatrix} C_3 \\
& + \begin{bmatrix} \sigma_{YC} & 0 & 0 \\ 0 & 2\sigma_{YC} & 0 \\ 0 & 0 & \sigma_{YC} \end{bmatrix} E_3 + \begin{bmatrix} 0 & 0 & 0 \\ 0 & 2\sigma_{YC} & 0 \\ 0 & 0 & 0 \end{bmatrix} F_3 \tag{5.3.54}
\end{aligned}$$

The following three expressions can be extracted from equation (5.3.54), i.e.,

$$A_2 + C_2 + E_2 + G_2 = A_3 + C_3 + E_3 \tag{5.3.55}$$

$$\begin{aligned}
& A_2 + 2B_2 + 2C_2 + 2D_2 \\
& + 2E_2 + 2F_2 + 2G_2 + 2H_2 \\
= & A_3 + 2B_3 + 2E_3 + 2F_3 \tag{5.3.56}
\end{aligned}$$

and

$$A_2 + C_2 + E_2 + G_2 = A_3 + E_3 \tag{5.3.57}$$

With the invariants established in equations (5.3.36) through (5.3.39), the following gradient for region #3 takes the following form



$$\begin{aligned} \frac{\partial g_4}{\partial \sigma_{ij}} = & \begin{bmatrix} \sigma_{YC} & 0 & 0 \\ 0 & \sigma_{YC} & 0 \\ 0 & 0 & \sigma_{YC} \end{bmatrix} A_4 + \begin{bmatrix} 0 & 0 & 0 \\ 0 & 2\sigma_{YC} & 0 \\ 0 & 0 & 0 \end{bmatrix} B_4 \\ & + \begin{bmatrix} \sigma_{YC} & 0 & 0 \\ 0 & 2\sigma_{YC} & 0 \\ 0 & 0 & \sigma_{YC} \end{bmatrix} E_4 + \begin{bmatrix} 0 & 0 & 0 \\ 0 & 2\sigma_{YC} & 0 \\ 0 & 0 & 0 \end{bmatrix} F_4 \end{aligned} \quad (5.3.58)$$

Utilizing equations (5.3.53) and (5.3.58) in equation (5.3.35) then at the boundary

between principal stress region #3 and principal stress region #4

$$\begin{aligned} & \begin{bmatrix} \sigma_{YC} & 0 & 0 \\ 0 & \sigma_{YC} & 0 \\ 0 & 0 & \sigma_{YC} \end{bmatrix} A_3 + \begin{bmatrix} 0 & 0 & 0 \\ 0 & 2\sigma_{YC} & 0 \\ 0 & 0 & 0 \end{bmatrix} B_3 \\ & + \begin{bmatrix} \sigma_{YC} & 0 & 0 \\ 0 & 0 & 0 \\ 0 & 0 & 0 \end{bmatrix} C_3 + \begin{bmatrix} \sigma_{YC} & 0 & 0 \\ 0 & 2\sigma_{YC} & 0 \\ 0 & 0 & \sigma_{YC} \end{bmatrix} E_3 + \begin{bmatrix} 0 & 0 & 0 \\ 0 & 2\sigma_{YC} & 0 \\ 0 & 0 & 0 \end{bmatrix} F_3 \\ = & \begin{bmatrix} \sigma_{YC} & 0 & 0 \\ 0 & \sigma_{YC} & 0 \\ 0 & 0 & \sigma_{YC} \end{bmatrix} A_4 + \begin{bmatrix} 0 & 0 & 0 \\ 0 & 2\sigma_{YC} & 0 \\ 0 & 0 & 0 \end{bmatrix} B_4 \\ & + \begin{bmatrix} \sigma_{YC} & 0 & 0 \\ 0 & 2\sigma_{YC} & 0 \\ 0 & 0 & \sigma_{YC} \end{bmatrix} E_4 + \begin{bmatrix} 0 & 0 & 0 \\ 0 & 2\sigma_{YC} & 0 \\ 0 & 0 & 0 \end{bmatrix} F_4 \end{aligned} \quad (5.3.59)$$

The following three expressions can be extracted from equation (5.3.59), i.e.,

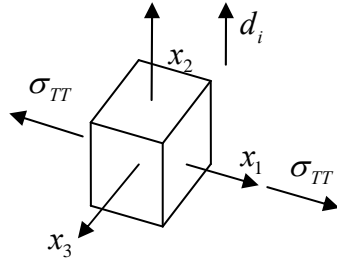
$$A_3 + C_3 + E_3 = A_4 + E_4 \quad (5.3.60)$$

$$A_3 + 2B_3 + 2E_3 + 2F_3 = A_4 + 2B_4 + 2E_4 + 2F_4 \quad (5.3.61)$$

and

$$A_3 + E_3 = A_4 + E_4 \quad (5.3.62)$$

Next consider the following stress state at failure under a tensile load with the same preferred material direction  $d_i = (0, 1, 0)$ , i.e.,



$$\sigma_{ij} = \begin{bmatrix} \sigma_{TT} & 0 & 0 \\ 0 & 0 & 0 \\ 0 & 0 & 0 \end{bmatrix} \quad (5.3.63)$$

The first subscript  $T$  denotes as stress in the direction transverse to the strong direction of the material and the second subscript  $T$  means tension ( $\sigma_{TT} > 0$ ). The principal stresses are

$$(\sigma_1, \sigma_2, \sigma_3) = (\sigma_{TT}, 0, 0) \quad (5.3.64)$$

In order to satisfy the definitions given earlier for the principal stress regions at the shared boundary of region #2 and region #3 the second principal stress must be zero, i.e.,  $\sigma_2 = 0$ . At the shared boundary between region #1 and region #2 the third principal stress must be zero, i.e.,  $\sigma_3 = 0$ . The stress state given above satisfies these stress conditions, i.e., both  $\sigma_2 = 0$  and  $\sigma_3 = 0$ . At both boundaries we impose the requirements that the gradients match, i.e.,

$$\frac{\partial g_1}{\partial \sigma_{ij}} = \frac{\partial g_2}{\partial \sigma_{ij}} \quad (5.3.65)$$

$$\frac{\partial g_2}{\partial \sigma_{ij}} = \frac{\partial g_3}{\partial \sigma_{ij}} \quad (5.3.66)$$

providing a smooth transition from one principal stress region to another. Using the stress state given above the first, second, sixth and seventh invariants are

$$I_1 = \sigma_{TT} \quad (5.3.67)$$

$$I_2 = \sigma_{TT}^2 \quad (5.3.68)$$

$$I_6 = 0 \quad (5.3.69)$$

and

$$I_7 = 0 \quad (5.3.70)$$

These four invariants are common to stress regions #1, #2 and #3 for the stress state given above. With these stress invariants the following gradient can be formulated for this stress state

$$\begin{aligned} \frac{\partial g_1}{\partial \sigma_{ij}} = & - \begin{bmatrix} \sigma_{TT} & 0 & 0 \\ 0 & \sigma_{TT} & 0 \\ 0 & 0 & \sigma_{TT} \end{bmatrix} A_1 \\ & - \begin{bmatrix} 2\sigma_{TT} & 0 & 0 \\ 0 & 0 & 0 \\ 0 & 0 & 0 \end{bmatrix} B_1 - \begin{bmatrix} 0 & 0 & 0 \\ 0 & \sigma_{TT} & 0 \\ 0 & 0 & 0 \end{bmatrix} E_1 \end{aligned} \quad (5.3.71)$$

For the stress state in region # 2 the unit principal vector is

$${}^2a_i = (0, 0, 1) \quad (5.3.72)$$

Thus

$$({}^2a_i)({}^2a_j) = \begin{bmatrix} 0 & 0 & 0 \\ 0 & 0 & 0 \\ 0 & 0 & 1 \end{bmatrix} \quad (5.3.73)$$

The invariants associated with this principal stress vector and stress state are

$${}^2I_4 = 0 \quad (5.3.74)$$

$${}^2I_5 = 0 \quad (5.3.75)$$

$${}^2I_8 = 0 \quad (5.3.76)$$

and

$${}^2I_9 = 0 \quad (5.3.77)$$

With these invariants and stress state the gradient along the boundary for stress region #2

is

$$\begin{aligned} \frac{\partial g_2}{\partial \sigma_{ij}} = & - \begin{bmatrix} \sigma_{TT} & 0 & 0 \\ 0 & \sigma_{TT} & 0 \\ 0 & 0 & \sigma_{TT} \end{bmatrix} A_2 - \begin{bmatrix} 2\sigma_{TT} & 0 & 0 \\ 0 & 0 & 0 \\ 0 & 0 & 0 \end{bmatrix} B_2 \\ & - \begin{bmatrix} 0 & 0 & 0 \\ 0 & 0 & 0 \\ 0 & 0 & \sigma_{TT} \end{bmatrix} C_2 - \begin{bmatrix} 0 & 0 & 0 \\ 0 & \sigma_{TT} & 0 \\ 0 & 0 & 0 \end{bmatrix} E_2 \end{aligned} \quad (5.3.78)$$

Utilizing equations (5.71) and (5.3.78) in equation (5.3.65) then at the boundary between principal stress region #1 and principal stress region #2

$$\begin{aligned} & \begin{bmatrix} \sigma_{TT} & 0 & 0 \\ 0 & \sigma_{TT} & 0 \\ 0 & 0 & \sigma_{TT} \end{bmatrix} A_1 + \begin{bmatrix} 2\sigma_{TT} & 0 & 0 \\ 0 & 0 & 0 \\ 0 & 0 & 0 \end{bmatrix} B_1 + \begin{bmatrix} 0 & 0 & 0 \\ 0 & \sigma_{TT} & 0 \\ 0 & 0 & 0 \end{bmatrix} E_1 \\ = & \begin{bmatrix} \sigma_{TT} & 0 & 0 \\ 0 & \sigma_{TT} & 0 \\ 0 & 0 & \sigma_{TT} \end{bmatrix} A_2 + \begin{bmatrix} 2\sigma_{TT} & 0 & 0 \\ 0 & 0 & 0 \\ 0 & 0 & 0 \end{bmatrix} B_2 + \begin{bmatrix} 0 & 0 & 0 \\ 0 & 0 & 0 \\ 0 & 0 & \sigma_{TT} \end{bmatrix} C_2 \\ & + \begin{bmatrix} 0 & 0 & 0 \\ 0 & \sigma_{TT} & 0 \\ 0 & 0 & 0 \end{bmatrix} E_2 \end{aligned} \quad (5.3.79)$$

The following three relationships between functional constants can be extracted from equation (5.3.79)

$$A_1 + 2B_1 = A_2 + 2B_2 + 2C_2 \quad (5.3.80)$$

$$A_1 + E_1 = A_2 + E_2 \quad (5.3.81)$$

and

$$A_1 = A_2 + C_2 \quad (5.3.82)$$

For the stress state stipulated above the unit principal vector in region # 3 is

$${}^3a_i = (1, 0, 0) \quad (5.3.83)$$

thus

$$({}^3a_i)({}^3a_j) = \begin{bmatrix} 1 & 0 & 0 \\ 0 & 0 & 0 \\ 0 & 0 & 0 \end{bmatrix} \quad (5.3.84)$$

And the stress invariants for this principal stress vector and stress state are

$${}^3I_4 = \sigma_{TT} \quad (5.3.85)$$

$${}^3I_5 = \sigma_{TT}^2 \quad (5.3.86)$$

$${}^3I_8 = 0 \quad (5.3.87)$$

and

$${}^3I_9 = 0 \quad (5.3.88)$$

With these invariants and stress state the gradient along the boundary for stress region #3

is

$$\begin{aligned} \frac{\partial g_3}{\partial \sigma_{ij}} = & - \begin{bmatrix} \sigma_{TT} & 0 & 0 \\ 0 & \sigma_{TT} & 0 \\ 0 & 0 & \sigma_{TT} \end{bmatrix} A_3 - \begin{bmatrix} 2\sigma_{TT} & 0 & 0 \\ 0 & 0 & 0 \\ 0 & 0 & 0 \end{bmatrix} B_3 \\ & - \begin{bmatrix} 2\sigma_{TT} & 0 & 0 \\ 0 & \sigma_{TT} & 0 \\ 0 & 0 & \sigma_{TT} \end{bmatrix} C_3 - \begin{bmatrix} 2\sigma_{TT} & 0 & 0 \\ 0 & 0 & 0 \\ 0 & 0 & 0 \end{bmatrix} D_3 - \begin{bmatrix} 0 & 0 & 0 \\ 0 & \sigma_{TT} & 0 \\ 0 & 0 & 0 \end{bmatrix} E_3 \end{aligned} \quad (5.3.89)$$

Utilizing equations (5.78) and (5.3.89) in equation (5.3.66) then at the boundary between principal stress region #2 and principal stress region #3

$$\begin{aligned}
& \begin{bmatrix} \sigma_{TT} & 0 & 0 \\ 0 & \sigma_{TT} & 0 \\ 0 & 0 & \sigma_{TT} \end{bmatrix} A_2 + \begin{bmatrix} 2\sigma_{TT} & 0 & 0 \\ 0 & 0 & 0 \\ 0 & 0 & 0 \end{bmatrix} B_2 \\
& + \begin{bmatrix} 0 & 0 & 0 \\ 0 & 0 & 0 \\ 0 & 0 & \sigma_{TT} \end{bmatrix} C_2 + \begin{bmatrix} 0 & 0 & 0 \\ 0 & \sigma_{TT} & 0 \\ 0 & 0 & 0 \end{bmatrix} E_2 \\
& = \begin{bmatrix} \sigma_{TT} & 0 & 0 \\ 0 & \sigma_{TT} & 0 \\ 0 & 0 & \sigma_{TT} \end{bmatrix} A_3 + \begin{bmatrix} 2\sigma_{TT} & 0 & 0 \\ 0 & 0 & 0 \\ 0 & 0 & 0 \end{bmatrix} B_3 \\
& + \begin{bmatrix} 2\sigma_{TT} & 0 & 0 \\ 0 & \sigma_{TT} & 0 \\ 0 & 0 & \sigma_{TT} \end{bmatrix} C_3 + \begin{bmatrix} 2\sigma_{TT} & 0 & 0 \\ 0 & 0 & 0 \\ 0 & 0 & 0 \end{bmatrix} D_3 + \begin{bmatrix} 0 & 0 & 0 \\ 0 & \sigma_{TT} & 0 \\ 0 & 0 & 0 \end{bmatrix} E_3
\end{aligned} \tag{5.3.90}$$

The following three expressions can be extracted from equation (5.3.90)

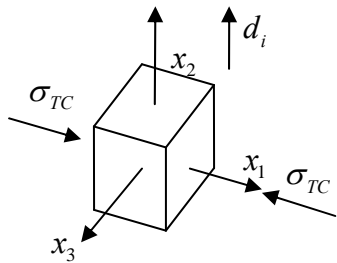
$$A_2 + 2B_2 = A_3 + 2B_3 + 2C_3 + 2D_3 \tag{5.3.91}$$

$$A_2 + E_2 = A_3 + C_3 + E_3 \tag{5.3.92}$$

and

$$A_2 + C_2 = A_3 + C_3 \tag{5.3.93}$$

Next consider the following stress state at failure under a compressive load with the preferred material direction  $d_i = (0, 1, 0)$ , i.e.,



$$\sigma_{ij} = \begin{bmatrix} \sigma_{TC} & 0 & 0 \\ 0 & 0 & 0 \\ 0 & 0 & 0 \end{bmatrix} \tag{5.3.94}$$

The first subscript  $T$  denotes a stress in the direction transverse to the strong direction of the material, and the second subscript  $C$  denotes compression ( $\sigma_{TC} < 0$ ). The principal stresses are

$$(\sigma_1, \sigma_2, \sigma_3) = (0, 0, \sigma_{TC}) \quad (5.3.95)$$

In order to satisfy the definitions given earlier for the principal stress regions at the shared boundary of region #3 and region #4 the first principal stress must be zero, i.e.,  $\sigma_1 = 0$ . At the shared boundary between region #2 and region #3 the second principal stress must be zero, i.e.,  $\sigma_2 = 0$ . The stress state given above satisfies these stress conditions, i.e., both  $\sigma_2 = 0$  and  $\sigma_3 = 0$ . At both boundaries we impose the requirements that the gradients match, i.e.,

$$\frac{\partial g_2}{\partial \sigma_{ij}} = \frac{\partial g_3}{\partial \sigma_{ij}} \quad (5.3.96)$$

$$\frac{\partial g_3}{\partial \sigma_{ij}} = \frac{\partial g_4}{\partial \sigma_{ij}} \quad (5.3.97)$$

providing a smooth transition from one principal stress region to another. Using the stress state given above the first, second, sixth and seventh invariants are

$$I_1 = \sigma_{TC} \quad (5.3.98)$$

$$I_2 = \sigma_{TC}^2 \quad (5.3.99)$$

$$I_6 = 0 \quad (5.3.100)$$

and

$$I_7 = 0 \quad (5.3.101)$$

These four invariants are common to stress regions #2, #3 and #4 for the stress state given above. With these stress invariants the following gradient can be formulated for this stress state

$$\begin{aligned} \frac{\partial g_4}{\partial \sigma_{ij}} = & - \begin{bmatrix} \sigma_{TC} & 0 & 0 \\ 0 & \sigma_{TC} & 0 \\ 0 & 0 & \sigma_{TC} \end{bmatrix} A_4 \\ & - \begin{bmatrix} 2\sigma_{TC} & 0 & 0 \\ 0 & 0 & 0 \\ 0 & 0 & 0 \end{bmatrix} B_4 - \begin{bmatrix} 0 & 0 & 0 \\ 0 & \sigma_{TC} & 0 \\ 0 & 0 & 0 \end{bmatrix} E_4 \end{aligned} \quad (5.3.102)$$

For the stress state in region # 2 the unit principal vector is

$${}^2a_i = (1, 0, 0) \quad (5.3.103)$$

Thus

$$({}^2a_i)({}^2a_j) = \begin{bmatrix} 1 & 0 & 0 \\ 0 & 0 & 0 \\ 0 & 0 & 0 \end{bmatrix} \quad (5.3.104)$$

The stress invariants for this principal stress vector are

$${}^2I_4 = \sigma_{TC} \quad (5.3.105)$$

$${}^2I_5 = \sigma_{TC}^2 \quad (5.3.106)$$

$${}^2I_8 = 0 \quad (5.3.107)$$

and

$${}^2I_9 = 0 \quad (5.3.108)$$

With these stress invariants the following gradient can be formulated for this stress state



$$\begin{aligned} \frac{\partial g_2}{\partial \sigma_{ij}} = & - \begin{bmatrix} \sigma_{TC} & 0 & 0 \\ 0 & \sigma_{TC} & 0 \\ 0 & 0 & \sigma_{TC} \end{bmatrix} A_2 - \begin{bmatrix} 2\sigma_{TC} & 0 & 0 \\ 0 & 0 & 0 \\ 0 & 0 & 0 \end{bmatrix} B_2 \\ & - \begin{bmatrix} 2\sigma_{TC} & 0 & 0 \\ 0 & \sigma_{TC} & 0 \\ 0 & 0 & \sigma_{TC} \end{bmatrix} C_2 - \begin{bmatrix} 2\sigma_{TC} & 0 & 0 \\ 0 & 0 & 0 \\ 0 & 0 & 0 \end{bmatrix} D_2 - \begin{bmatrix} 0 & 0 & 0 \\ 0 & \sigma_{TC} & 0 \\ 0 & 0 & 0 \end{bmatrix} E_2 \end{aligned} \quad (5.3.109)$$

For the stress state in region #3 the unit principal vector is

$${}^3a_i = (0, 1, 0) \quad (5.3.110)$$

Thus

$$({}^3a_i)({}^3a_j) = \begin{bmatrix} 0 & 0 & 0 \\ 0 & 1 & 0 \\ 0 & 0 & 0 \end{bmatrix} \quad (5.3.111)$$

And the stress invariants for this principal stress vector are

$${}^3I_4 = 0 \quad (5.3.112)$$

$${}^3I_5 = 0 \quad (5.3.113)$$

$${}^3I_8 = 0 \quad (5.3.114)$$

and

$${}^3I_9 = 0 \quad (5.3.115)$$

With these stress invariants the following gradient can be formulated for this stress state

$$\begin{aligned} \frac{\partial g_3}{\partial \sigma_{ij}} = & - \begin{bmatrix} \sigma_{TC} & 0 & 0 \\ 0 & \sigma_{TC} & 0 \\ 0 & 0 & \sigma_{TC} \end{bmatrix} A_3 - \begin{bmatrix} 2\sigma_{TC} & 0 & 0 \\ 0 & 0 & 0 \\ 0 & 0 & 0 \end{bmatrix} B_3 \\ & - \begin{bmatrix} 0 & 0 & 0 \\ 0 & \sigma_{TC} & 0 \\ 0 & 0 & 0 \end{bmatrix} C_3 - \begin{bmatrix} 0 & 0 & 0 \\ 0 & \sigma_{TC} & 0 \\ 0 & 0 & 0 \end{bmatrix} E_3 \end{aligned} \quad (5.3.116)$$

Utilizing equations (5.116) and (5.3.109) in equation (5.3.96) then at the boundary

between principal stress region #2 and principal stress region #3

$$\begin{aligned}
& \begin{bmatrix} \sigma_{TC} & 0 & 0 \\ 0 & \sigma_{TC} & 0 \\ 0 & 0 & \sigma_{TC} \end{bmatrix} A_2 + \begin{bmatrix} 2\sigma_{TC} & 0 & 0 \\ 0 & 0 & 0 \\ 0 & 0 & 0 \end{bmatrix} B_2 \\
& + \begin{bmatrix} 2\sigma_{TC} & 0 & 0 \\ 0 & \sigma_{TC} & 0 \\ 0 & 0 & \sigma_{TC} \end{bmatrix} C_2 + \begin{bmatrix} 2\sigma_{TC} & 0 & 0 \\ 0 & 0 & 0 \\ 0 & 0 & 0 \end{bmatrix} D_2 + \begin{bmatrix} 0 & 0 & 0 \\ 0 & \sigma_{TC} & 0 \\ 0 & 0 & 0 \end{bmatrix} E_2 \\
& = \begin{bmatrix} \sigma_{TC} & 0 & 0 \\ 0 & \sigma_{TC} & 0 \\ 0 & 0 & \sigma_{TC} \end{bmatrix} A_3 + \begin{bmatrix} 2\sigma_{TC} & 0 & 0 \\ 0 & 0 & 0 \\ 0 & 0 & 0 \end{bmatrix} B_3 \\
& + \begin{bmatrix} 0 & 0 & 0 \\ 0 & \sigma_{TC} & 0 \\ 0 & 0 & 0 \end{bmatrix} C_3 + \begin{bmatrix} 0 & 0 & 0 \\ 0 & \sigma_{TC} & 0 \\ 0 & 0 & 0 \end{bmatrix} E_3
\end{aligned} \tag{5.3.117}$$

The following three expressions can be extracted from equation (5.3.117), i.e.,

$$A_2 + 2B_2 + 2C_2 + 2D_2 = A_3 + 2B_3 \tag{5.3.118}$$

$$A_2 + C_2 + E_2 = A_3 + C_3 + E_3 \tag{5.3.119}$$

and

$$A_2 + C_2 = A_3 \tag{5.3.120}$$

Utilizing equations (5.102) and (5.3.116) in equation (5.3.97) then at the boundary

between principal stress region #3 and principal stress region #4

$$\begin{aligned}
& \begin{bmatrix} \sigma_{TC} & 0 & 0 \\ 0 & \sigma_{TC} & 0 \\ 0 & 0 & \sigma_{TC} \end{bmatrix} A_3 + \begin{bmatrix} 2\sigma_{TC} & 0 & 0 \\ 0 & 0 & 0 \\ 0 & 0 & 0 \end{bmatrix} B_3 \\
& + \begin{bmatrix} 0 & 0 & 0 \\ 0 & \sigma_{TC} & 0 \\ 0 & 0 & 0 \end{bmatrix} C_3 + \begin{bmatrix} 0 & 0 & 0 \\ 0 & \sigma_{TC} & 0 \\ 0 & 0 & 0 \end{bmatrix} E_3 \\
& = \begin{bmatrix} \sigma_{TC} & 0 & 0 \\ 0 & \sigma_{TC} & 0 \\ 0 & 0 & \sigma_{TC} \end{bmatrix} A_4 \\
& + \begin{bmatrix} 2\sigma_{TC} & 0 & 0 \\ 0 & 0 & 0 \\ 0 & 0 & 0 \end{bmatrix} B_4 + \begin{bmatrix} 0 & 0 & 0 \\ 0 & \sigma_{TC} & 0 \\ 0 & 0 & 0 \end{bmatrix} E_4
\end{aligned} \tag{5.3.121}$$

The following three expressions can be extracted from equation (5.3.121)

$$A_3 + 2B_3 = A_4 + 2B_4 \tag{5.3.122}$$

$$A_3 + C_3 + E_3 = A_4 + E_4 \tag{5.3.123}$$

and

$$A_3 = A_4 \tag{5.3.124}$$

Equations (5.3.18) through (5.3.20), (5.3.29) through (5.3.31), (5.3.55) through (5.3.57), (5.3.60) through (5.3.62), (5.3.80) through (5.3.82), (5.3.91) through (5.3.93), (5.3.118) through (5.3.120), as well as (5.3.122) through (5.3.124) represent twenty four equations in terms of twenty four unknowns, i.e.,  $A_1, A_2, A_3, A_4, B_1, B_2, B_3, B_4, C_2, C_3, D_2, D_3, E_1, E_2, E_3, E_4, F_1, F_2, F_3, F_4, G_2, G_3, H_2$  and  $H_3$ .

Although in the current formulation there appears to be twenty-four constants, not all of the constants are independent. From equations (5.3.18) and (5.3.20) it is apparent that

$$C_2 = 0 \quad (5.3.125)$$

Substitution of equation (5.3.125) into equations (5.3.82) yields

$$A_1 = A_2 \quad (5.3.126)$$

Substitution of equation (5.3.125) into equation (5.3.120) yields

$$A_2 = A_3 \quad (5.3.127)$$

With equation (5.3.124) then

$$A_1 = A_2 = A_3 = A_4 \quad (5.3.128)$$

Thus none of the “ $A$ ” constants are independent.

Substitution of equation (5.3.125) and (5.3.127) into equation (5.3.93) leads to

$$C_3 = 0 \quad (5.3.129)$$

Using equation (5.3.129) along with equation (5.3.128) in equation (5.3.60) results in

$$E_3 = E_4 \quad (5.3.130)$$

Substitution of equation (5.3.126) into equation (5.3.18) yields

$$E_1 = E_2 \quad (5.3.131)$$

Substituting equations (5.3.125), (5.3.125) and (5.3.125) into equation (5.3.119) results in

$$E_2 = E_3 \quad (5.3.132)$$

With equations (5.3.130), (5.3.131) and (5.3.132) then

$$E_1 = E_2 = E_3 = E_4 \quad (5.3.133)$$

Therefore none of the “ $E$ ” constants are independent.

Substitution of equations (5.3.125), (5.3.127) and (5.3.133) into equations (5.3.57)

leads to

$$G_2 = 0 \quad (5.3.134)$$

Similarly substituting equations (5.3.127), (5.3.129) and (5.3.133) into equation (5.3.29)

leads to

$$G_3 = 0 \quad (5.3.135)$$

and the “ $G$ ” constants are both zero.

With equations (5.3.125) and (5.3.126) then from equation (5.3.80) takes the form

$$B_1 = B_2 \quad (5.3.136)$$

Utilizing equation (5.3.128) in equation (5.3.122) then

$$B_3 = B_4 \quad (5.3.137)$$

With equations (5.3.127) and (5.3.129) then equation (5.3.91) takes the form

$$B_2 = B_3 + D_3 \quad (5.3.138)$$

Similarly, with equations (5.3.125) and (5.3.127) then equation (5.3.118) takes the form

$$B_2 + D_2 = B_3 \quad (5.3.139)$$

Subtracting equation (5.3.138) from equation (5.3.139) leads to

$$D_2 = -D_3 \quad (5.3.140)$$

and the “ $D$ ” constants are not independent of one another.

With equations (5.3.126), (5.3.136) and (5.3.131) then equation (5.3.19) takes the form

$$F_1 = F_2 \quad (5.3.141)$$

With equations (5.3.128), (5.3.137) and (5.3.130) then from equation (5.3.61)

$$F_3 = F_4 \quad (5.3.142)$$

In a like manner, with equations (5.3.127), (5.3.132), (5.3.129) and (5.3.135) then equation (5.3.30) takes the form

$$F_2 = F_3 + H_3 \quad (5.3.143)$$

With equations (5.3.127), (5.3.132), (5.3.125) and (5.3.134) then equation (5.3.56) takes the form

$$F_2 + H_2 = F_3 \quad (5.3.144)$$

Subtracting equation (5.3.143) from equation (5.3.144) leads to

$$H_2 = -H_3 \quad (5.3.145)$$

From equations (5.3.125) and (5.3.129) the identity

$$C_2 = C_3 = 0 \quad (5.3.148)$$

can be established. From equations (5.3.134) and (5.3.155) it is easily shown that

$$G_2 = G_3 = 0 \quad (5.3.152)$$

In addition, the following relationships between the remaining coefficients are established from equations (5.3.125) through (5.3.145)

$$A_1 = A_2 = A_3 = A_4 = \mathcal{A} \quad (5.3.146)$$

$$B_1 = B_2 = B_3 + D_3 = B_4 + D_3 = \mathcal{B} \quad (5.3.147)$$

$$D_2 = -D_3 = \mathcal{D} \quad (5.3.148)$$

$$E_1 = E_2 = E_3 = E_4 = \mathcal{E} \quad (5.3.149)$$

$$F_1 = F_2 = F_3 + H_3 = F_4 + H_3 = \mathcal{F} \quad (5.3.150)$$

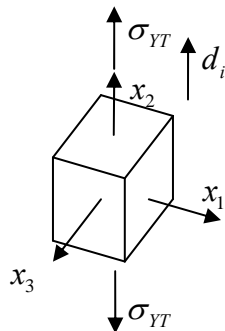
and

$$H_2 = -H_3 = \mathcal{H} \quad (5.3.151)$$

These relationships represent requirements that insure the four functional forms for the failure function are smooth and continuous along the boundaries of the four stress regions. Moreover, the last group of constants identified as  $\mathcal{A}$ ,  $\mathcal{B}$ ,  $\mathcal{D}$ ,  $\mathcal{E}$ ,  $\mathcal{F}$  and  $\mathcal{H}$  represent the independent constants for the failure function. Since there are six independent constants, then one is required to conduct six mechanical tests to characterize the model. These tests are outlined in the next section.

#### 5.4 Functional Constants in Terms of Strength Parameters

Next specific load paths are utilized in order to define the constants defined above in terms of strength values obtained in mechanical failure tests. Consider the following stress state at failure under a uniaxial tensile load in the preferred material direction  $d_i = (0, 1, 0)$



$$\sigma_{ij} = \begin{bmatrix} 0 & 0 & 0 \\ 0 & \sigma_{YT} & 0 \\ 0 & 0 & 0 \end{bmatrix} \quad (5.4.1)$$

The principal stresses for this state of stress are

$$(\sigma_1, \sigma_2, \sigma_3) = (\sigma_{YT}, 0, 0) \quad (5.4.2)$$

Note that one principal stress is tensile and the others are zero. This state of stress lies along the border of region #1, region #2 and region #3. For region #1 the first, second, sixth and seventh invariants are

$$I_1 = \sigma_{YT} \quad (5.4.3)$$

$$I_2 = \sigma_{YT}^2 \quad (5.4.4)$$

$$I_6 = \sigma_{YT} \quad (5.4.5)$$

and

$$I_7 = \sigma_{YT}^2 \quad (5.4.6)$$

With the failure function defined as

$$\begin{aligned} g_1 &= 1 - \left[ \left( \frac{1}{2} \right) A_1 I_1^2 + B_1 I_2 + E_1 I_1 I_6 + F_1 I_7 \right] \\ &= 0 \end{aligned} \quad (5.4.7)$$

in region #1 of the principal stress space, then substitution of equations (5.4.3) through

(5.4.6) into the (5.4.7) yields

$$0 = 1 - \left[ \left( \frac{1}{2} \right) A_1 (\sigma_{YT})^2 + B_1 \sigma_{YT}^2 + E_1 \sigma_{YT} \sigma_{YT} + F_1 \sigma_{YT}^2 \right] \quad (5.4.8)$$

or

$$\left( \frac{1}{2} \right) A_1 + B_1 + E_1 + F_1 = \frac{1}{\sigma_{YT}^2} \quad (5.4.9)$$

The unit principal stress vector associated with this state of stress in the region # 2 is



$${}^2a_i = (0, 0, 1) \quad (5.4.10)$$

thus

$$({}^2a_i)({}^2a_j) = \begin{bmatrix} 0 & 0 & 0 \\ 0 & 0 & 0 \\ 0 & 0 & 1 \end{bmatrix} \quad (5.4.11)$$

The stress invariants associated with this principal stress vector and state of stress are

$${}^2I_4 = 0 \quad (5.4.12)$$

$${}^2I_5 = 0 \quad (5.4.13)$$

$${}^2I_8 = 0 \quad (5.4.14)$$

and

$${}^2I_9 = 0 \quad (5.4.15)$$

The failure function for stress region #2 has the form

$$\begin{aligned} g_2 = 1 - & \left[ \left( \frac{1}{2} \right) A_2 I_1^2 + B_2 I_2 + C_2 I_1 I_4 + D_2 I_5 \right. \\ & \left. + E_2 I_1 I_6 + F_2 I_7 + G_2 I_1 I_8 + H_2 I_9 \right] \\ = 0 \end{aligned} \quad (5.4.16)$$

With equations (5.4.3) through (5.4.6) as well as equations (5.4.12) through (5.4.15) then

$$0 = 1 - \left[ \left( \frac{1}{2} \right) A_2 (\sigma_{YT})^2 + B_2 \sigma_{YT}^2 + E_2 (\sigma_{YT})(\sigma_{YT}) + F_2 \sigma_{YT}^2 \right] \quad (5.4.17)$$

or

$$\left( \frac{1}{2} \right) A_2 + B_2 + E_2 + F_2 = \frac{1}{\sigma_{YT}^2} \quad (5.4.18)$$

The unit principal stress vector associated with this state of stress in the region # 3

is

$${}^3a_i = (0, 1, 0) \quad (5.4.19)$$

thus

$$({}^3a_i)({}^3a_j) = \begin{bmatrix} 0 & 0 & 0 \\ 0 & 1 & 0 \\ 0 & 0 & 0 \end{bmatrix} \quad (5.4.20)$$

The stress invariants associated with this principal stress vector and state of stress are

$${}^3I_4 = \sigma_{YT} \quad (5.4.21)$$

$${}^3I_5 = \sigma_{YT}^2 \quad (5.4.22)$$

$${}^3I_8 = \sigma_{YT} \quad (5.4.23)$$

and

$${}^3I_9 = \sigma_{YT}^2 \quad (5.4.24)$$

The failure function for stress region #3 has the form

$$\begin{aligned} g_3 &= 1 - \left[ \left( \frac{1}{2} \right) A_3 I_1^2 + B_3 I_2 + C_3 I_1 I_4 + D_3 I_5 I_7 \right. \\ &\quad \left. + E_3 I_1 I_6 + F_3 + G_3 I_1 I_8 + H_3 I_9 \right] \\ &= 0 \end{aligned} \quad (5.4.25)$$

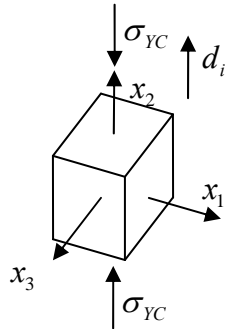
With equations (5.4.3) through (5.4.6) as well as equations (5.4.21) through (5.4.24) then

$$\begin{aligned} 0 &= 1 - \left[ \left( \frac{1}{2} \right) A_3 (\sigma_{YT})^2 + B_3 \sigma_{YT}^2 + D_3 \sigma_{YT}^2 \right. \\ &\quad \left. + E_3 (\sigma_{YT})(\sigma_{YT}) + F_3 \sigma_{YT}^2 + H_3 \sigma_{YT}^2 \right] \end{aligned} \quad (5.4.26)$$

and

$$\left(\frac{1}{2}\right)A_3 + B_3 + D_3 + E_3 + F_3 + H_3 = \frac{1}{\sigma_{YT}^2} \quad (5.4.27)$$

Next consider the following stress state at failure due to a compressive stress aligned with the material direction  $d_i = (0, 1, 0)$ , i.e.,



$$\sigma_{ij} = \begin{bmatrix} 0 & 0 & 0 \\ 0 & \sigma_{YC} & 0 \\ 0 & 0 & 0 \end{bmatrix} \quad (5.4.28)$$

The principal stresses are

$$(\sigma_1, \sigma_2, \sigma_3) = (0, 0, \sigma_{YC}) \quad (5.4.29)$$

Note that one principal stress is compressive and the others are zero. This state of stress lies along the border of region #2, region #3 and region #4. For region #4 the first, second, sixth and seventh invariants for this stress state are

$$I_1 = \sigma_{YC} \quad (5.4.30)$$

$$I_2 = \sigma_{YC}^2 \quad (5.4.31)$$

$$I_6 = \sigma_{YC} \quad (5.4.32)$$

and

$$I_7 = \sigma_{YC}^2 \quad (5.4.33)$$

With the failure function defined as

$$\begin{aligned}
g_4 &= 1 - \left[ \left( \frac{1}{2} \right) A_4 I_1^2 + B_4 I_2 + E_4 I_1 I_6 + F_4 I_7 \right] \\
&= 0
\end{aligned} \tag{5.4.34}$$

in region #4 of the principal stress space, then substitution of equations (5.4.30) through (5.4.33) into the (5.4.34) yields

$$0 = 1 - \left[ \left( \frac{1}{2} \right) A_4 (\sigma_{YC})^2 + B_4 \sigma_{YC}^2 + E_4 (\sigma_{YC})(\sigma_{YC}) + F_4 \sigma_{YC}^2 \right] \tag{5.4.35}$$

or

$$\left( \frac{1}{2} \right) A_4 + B_4 + E_4 + F_4 = \frac{1}{\sigma_{YC}^2} \tag{5.4.36}$$

The unit principal stress vector associated with this state of stress in region #2 is

$${}^2a_i = (0, 1, 0) \tag{5.4.37}$$

thus

$$({}^2a_i)({}^2a_j) = \begin{bmatrix} 0 & 0 & 0 \\ 0 & 1 & 0 \\ 0 & 0 & 0 \end{bmatrix} \tag{5.4.38}$$

The stress invariants associated with this principal stress vector and state of stress are

$${}^2I_4 = \sigma_{YC} \tag{5.4.39}$$

$${}^2I_5 = \sigma_{YC}^2 \tag{5.4.40}$$

$${}^2I_8 = \sigma_{YC} \tag{5.4.41}$$

and

$${}^2I_9 = \sigma_{YC}^2 \tag{5.4.42}$$

Again, the failure function for stress region #2 has the form

$$\begin{aligned}
g_2 &= 1 - \left[ \left( \frac{1}{2} \right) A_2 I_1^2 + B_2 I_2 + C_2 I_1 I_4 + D_2 I_5 \right. \\
&\quad \left. + E_2 I_1 I_6 + F_2 I_7 + G_2 I_1 I_8 + H_2 I_9 \right] \quad (5.4.43) \\
&= 0
\end{aligned}$$

With equations (5.4.30) through (5.4.33) as well as equations (5.4.39) through (5.4.42)

then

$$\begin{aligned}
0 &= 1 - \left[ \left( \frac{1}{2} \right) A_2 (\sigma_{YC})^2 + B_2 \sigma_{YC}^2 + D_2 \sigma_{YC}^2 \right. \\
&\quad \left. + E_2 (\sigma_{YC})(\sigma_{YC}) + F_2 \sigma_{YC}^2 + H_2 \sigma_{YC}^2 \right] \quad (5.4.44)
\end{aligned}$$

or

$$\left( \frac{1}{2} \right) A_2 + B_2 + D_2 + E_2 + F_2 + H_2 = \frac{1}{\sigma_{YC}^2} \quad (5.4.45)$$

The unit principal stress vector associated with this state of stress in region #3 is

$${}^3a_i = (1, 0, 0) \quad (5.4.46)$$

thus

$$({}^3a_i)({}^3a_j) = \begin{bmatrix} 1 & 0 & 0 \\ 0 & 0 & 0 \\ 0 & 0 & 0 \end{bmatrix} \quad (5.4.47)$$

The stress invariants associated with this principal stress vector and state of stress are

$${}^3I_4 = 0 \quad (5.4.48)$$

$${}^3I_5 = 0 \quad (5.4.49)$$

$${}^3I_8 = 0 \quad (5.4.50)$$

and

$${}^3I_9 = 0 \quad (5.4.51)$$

Again, the failure function for stress region #3 has the form

$$g_3 = 1 - \left[ \left( \frac{1}{2} \right) A_3 I_1^2 + B_3 I_2 + C_3 I_1 I_4 + D_3 I_5 I_7 + E_3 I_1 I_6 + F_3 + G_3 I_1 I_8 + H_3 I_9 \right] \quad (5.4.52)$$

$$= 0$$

With equations (5.4.30) through (5.4.33) as well as equations (5.4.48) through (5.4.51)

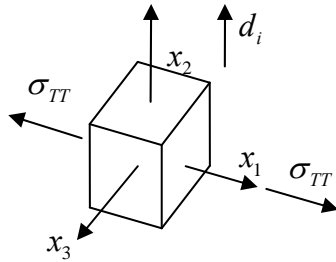
then

$$0 = 1 - \left[ \left( \frac{1}{2} \right) A_3 (\sigma_{YC})^2 + B_3 \sigma_{YC}^2 + E_3 (\sigma_{YC})(\sigma_{YC}) + F_3 \sigma_{YC}^2 \right] \quad (5.4.53)$$

or

$$\left( \frac{1}{2} \right) A_3 + B_3 + E_3 + F_3 = \frac{1}{\sigma_{YC}^2} \quad (5.4.54)$$

Next consider the following stress state at failure due to a tensile stress perpendicular to the material direction  $d_i = (0, 1, 0)$ , i.e.,



$$\sigma_{ij} = \begin{bmatrix} \sigma_{TT} & 0 & 0 \\ 0 & 0 & 0 \\ 0 & 0 & 0 \end{bmatrix} \quad (5.4.55)$$

The principal stresses are

$$(\sigma_1, \sigma_2, \sigma_3) = (\sigma_{TT}, 0, 0) \quad (5.4.56)$$

Note that principal stress aligned transverse to the preferred direction of the material is tensile and the others are zero. This state of stress lies along the border of region #1,

region #2 and region #3. For region #1 the first, second, sixth and seventh invariants are obtained

$$I_1 = \sigma_{TT} \quad (5.4.57)$$

$$I_2 = \sigma_{TT}^2 \quad (5.4.58)$$

$$I_6 = 0 \quad (5.4.59)$$

and

$$I_7 = 0 \quad (5.4.60)$$

Again, with the failure function defined as

$$g_1 = 1 - \left[ \left( \frac{1}{2} \right) A_1 I_1^2 + B_1 I_2 + E_1 I_1 I_6 + F_1 I_7 \right] \quad (5.4.61)$$

$$= 0$$

in region #1 of the principal stress space, then substitution of equations (5.4.57) through (5.4.60) into the (5.4.61) leads to

$$0 = 1 - \left[ \left( \frac{1}{2} \right) A_1 (\sigma_{TT})^2 + B_1 \sigma_{TT}^2 \right] \quad (5.4.62)$$

or

$$\left( \frac{1}{2} \right) A_1 + B_1 = \frac{1}{\sigma_{TT}^2} \quad (5.4.63)$$

The unit principal stress vector associated with this state of stress in region #2 is

$${}^2a_i = (0, 0, 1) \quad (5.4.64)$$

thus

$$({}^2a_i)({}^2a_j) = \begin{bmatrix} 0 & 0 & 0 \\ 0 & 0 & 0 \\ 0 & 0 & 1 \end{bmatrix} \quad (5.4.65)$$

The stress invariants associated with this principal stress vector and state of stress are

$${}^2I_4 = 0 \quad (5.4.66)$$

$${}^2I_5 = 0 \quad (5.4.67)$$

$${}^2I_8 = 0 \quad (5.4.68)$$

and

$${}^2I_9 = 0 \quad (5.4.69)$$

Again, the failure function for stress region #2 has the form

$$\begin{aligned} g_2 &= 1 - \left[ \left( \frac{1}{2} \right) A_2 I_1^2 + B_2 I_2 + C_2 I_1 I_4 + D_2 I_5 \right. \\ &\quad \left. + E_2 I_1 I_6 + F_2 I_7 + G_2 I_1 I_8 + H_2 I_9 \right] \\ &= 0 \end{aligned} \quad (5.4.70)$$

With equations (5.4.57) through (5.4.60) as well as equations (5.4.66) through (5.4.69)

then

$$0 = 1 - \left[ \left( \frac{1}{2} \right) A_2 (\sigma_{TT})^2 + B_2 \sigma_{TT}^2 \right] \quad (5.4.71)$$

or

$$\left( \frac{1}{2} \right) A_2 + B_2 = \frac{1}{\sigma_{TT}^2} \quad (5.4.72)$$

The unit principal stress vector associated with this state of stress in region #3 is

$${}^3a_i = (1, 0, 0) \quad (5.4.73)$$



thus

$$\begin{pmatrix} a_i \end{pmatrix} \begin{pmatrix} a_j \end{pmatrix} = \begin{bmatrix} 1 & 0 & 0 \\ 0 & 0 & 0 \\ 0 & 0 & 0 \end{bmatrix} \quad (5.4.74)$$

The stress invariants associated with this principal stress vector and state of stress are

$${}^3I_4 = \sigma_{TT} \quad (5.4.75)$$

$${}^3I_5 = \sigma_{TT}^2 \quad (5.4.76)$$

$${}^3I_8 = 0 \quad (5.4.77)$$

and

$${}^3I_9 = 0 \quad (5.4.78)$$

Again, the failure function for stress region #3 has the form

$$\begin{aligned} g_3 &= 1 - \left[ \left( \frac{1}{2} \right) A_3 I_1^2 + B_3 I_2 + C_3 I_1 I_4 + D_3 I_5 I_7 \right. \\ &\quad \left. + E_3 I_1 I_6 + F_3 + G_3 I_1 I_8 + H_3 I_9 \right] \\ &= 0 \end{aligned} \quad (5.4.79)$$

With equations (5.4.57) through (5.4.60) as well as equations (5.4.75) through (5.4.78)

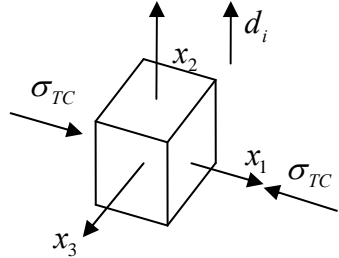
then

$$0 = 1 - \left[ \left( \frac{1}{2} \right) A_3 (\sigma_{TT})^2 + B_3 \sigma_{TT}^2 + D_3 \sigma_{TT}^2 \right] \quad (5.4.80)$$

or

$$\left( \frac{1}{2} \right) A_3 + B_3 + D_3 = \frac{1}{\sigma_{TT}^2} \quad (5.4.81)$$

Next consider the following stress state at failure due to a compressive stress perpendicular to the material direction  $d_i = (0, 1, 0)$ , i.e.,



$$\sigma_{ij} = \begin{bmatrix} \sigma_{TC} & 0 & 0 \\ 0 & 0 & 0 \\ 0 & 0 & 0 \end{bmatrix} \quad (5.4.82)$$

The principal stresses are

$$(\sigma_1, \sigma_2, \sigma_3) = (0, 0, \sigma_{TC}) \quad (5.4.83)$$

Note that one principal stress is compressive and the others are zero. This state of stress lies along the border of region #2, region #3 and region #4. For region #4 the first, second, sixth and seventh invariants are

$$I_1 = \sigma_{TC} \quad (5.4.84)$$

$$I_2 = \sigma_{TC}^2 \quad (5.4.85)$$

$$I_6 = 0 \quad (5.4.86)$$

and

$$I_7 = 0 \quad (5.4.87)$$

Again, with the failure function defined as

$$\begin{aligned} g_4 &= 1 - \left[ \left( \frac{1}{2} \right) A_4 I_1^2 + B_4 I_2 + E_4 I_1 I_6 + F_4 I_7 \right] \\ &= 0 \end{aligned} \quad (5.4.88)$$

in region #4 of the principal stress space, then substitution of equations (5.4.84) through

(5.4.87) into the (5.4.88) leads to

$$0 = 1 - \left[ \left( \frac{1}{2} \right) A_4 \sigma_{TC}^2 + B_4 \sigma_{TC}^2 \right] \quad (5.4.89)$$

or

$$\left( \frac{1}{2} \right) A_4 + B_4 = \frac{1}{\sigma_{TC}^2} \quad (5.4.90)$$

The unit principal stress vector associated with this state of stress in region #2 is

$${}^2a_i = (1, 0, 0) \quad (5.4.91)$$

thus

$$({}^2a_i)({}^2a_j) = \begin{bmatrix} 1 & 0 & 0 \\ 0 & 0 & 0 \\ 0 & 0 & 0 \end{bmatrix} \quad (5.4.92)$$

The stress invariants associated with this principal stress vector and state of stress are

$${}^2I_4 = \sigma_{TC} \quad (5.4.93)$$

$${}^2I_5 = \sigma_{TC}^2 \quad (5.4.94)$$

$${}^2I_8 = 0 \quad (5.4.95)$$

and

$${}^2I_9 = 0 \quad (5.4.96)$$

Again, the failure function for stress region #2 has the form

$$\begin{aligned} g_2 &= 1 - \left[ \left( \frac{1}{2} \right) A_2 I_1^2 + B_2 I_2 + C_2 I_1 I_4 + D_2 I_5 \right. \\ &\quad \left. + E_2 I_1 I_6 + F_2 I_7 + G_2 I_1 I_8 + H_2 I_9 \right] \\ &= 0 \end{aligned} \quad (5.4.97)$$

With equations (5.4.84) through (5.4.87) as well as equations (5.4.93) through (5.4.96)

then

$$g_2 = 1 - \left[ \left( \frac{1}{2} \right) A_2 \sigma_{TC}^2 + B_2 \sigma_{TC}^2 + D_2 \sigma_{TC}^2 \right] \quad (5.4.98)$$

or

$$\left( \frac{1}{2} \right) A_2 + B_2 + D_2 = \frac{1}{\sigma_{TC}^2} \quad (5.4.99)$$

The unit principal stress vector associated with this state of stress in region #3 is

$${}^3a_i = (0, 1, 0) \quad (5.4.100)$$

thus

$$({}^3a_i)({}^3a_j) = \begin{bmatrix} 0 & 0 & 0 \\ 0 & 1 & 0 \\ 0 & 0 & 0 \end{bmatrix} \quad (5.4.101)$$

The stress invariants associated with this principal stress vector and state of stress are

$${}^3I_4 = 0 \quad (5.4.102)$$

$${}^3I_5 = 0 \quad (5.4.103)$$

$${}^3I_8 = 0 \quad (5.4.104)$$

and

$${}^3I_9 = 0 \quad (5.4.105)$$

Again, the failure function for stress region #3 has the form

$$\begin{aligned}
g_3 &= 1 - \left[ \left( \frac{1}{2} \right) A_3 I_1^2 + B_3 I_2 + C_3 I_1 I_4 + D_3 I_5 I_7 \right. \\
&\quad \left. + E_3 I_1 I_6 + F_3 + G_3 I_1 I_8 + H_3 I_9 \right] \quad (5.4.106) \\
&= 0
\end{aligned}$$

With equations (5.4.84) through (5.4.87) as well as equations (5.4.102) through (5.4.105)

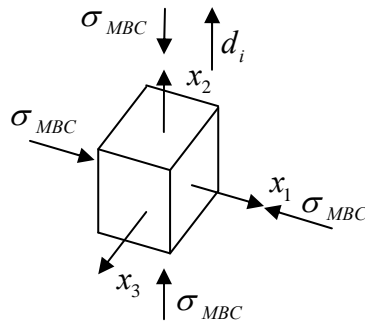
then

$$0 = 1 - \left[ \left( \frac{1}{2} \right) A_3 \sigma_{TT}^2 + B_3 \sigma_{TT}^2 + D_3 \sigma_{TT}^2 \right] \quad (5.4.107)$$

or

$$\left( \frac{1}{2} \right) A_3 + B_3 = \frac{1}{\sigma_{TC}^2} \quad (5.4.108)$$

Next consider the following stress state at failure due to an equal biaxial compressive stress where one component of the applied stress is directed along the material direction  $d_i = (0, 1, 0)$ , i.e.,



$$\sigma_{ij} = \begin{bmatrix} \sigma_{MBC} & 0 & 0 \\ 0 & \sigma_{MBC} & 0 \\ 0 & 0 & 0 \end{bmatrix} \quad (5.4.109)$$

The subscript “MBC” denotes “mixed equal-biaxial-compression” and because the applied stress is compressive, then algebraically  $\sigma_{MBC} < 0$ . The principal stresses are

$$(\sigma_1, \sigma_2, \sigma_3) = (0, \sigma_{MBC}, \sigma_{MBC}) \quad (5.4.110)$$

Note that two principal stresses are compressive and the other is zero. This state of stress lies along the border region #3 and region #4. For stress region #4 the first, second, sixth and seventh invariants are

$$I_1 = 2\sigma_{MBC} \quad (5.4.111)$$

$$I_2 = 2\sigma_{MBC}^2 \quad (5.4.112)$$

$$I_6 = \sigma_{MBC} \quad (5.4.113)$$

and

$$I_7 = \sigma_{MBC}^2 \quad (5.4.114)$$

Again, with the failure function defined as

$$g_4 = 1 - \left[ \left( \frac{1}{2} \right) A_4 I_1^2 + B_4 I_2 + E_4 I_1 I_6 + F_4 I_7 \right] \quad (5.4.115)$$

$$= 0$$

in region #4 of the principal stress space, then substitution of equations (5.4.111) through (5.4.114) into the (5.4.115) leads to

$$0 = 1 - \left[ \left( \frac{1}{2} \right) A_4 (2\sigma_{MBC})^2 + B_4 (2\sigma_{MBC}^2) \right. \quad (5.4.116)$$

$$\left. + E_4 (2\sigma_{MBC})(\sigma_{MBC}) + F_4 \sigma_{MBC}^2 \right]$$

or

$$2A_4 + 2B_4 + 2E_4 + F_4 = \frac{1}{\sigma_{MBC}^2} \quad (5.4.117)$$

The unit principal stress vector associated with this state of stress in region #3 is

$${}^3a_i = (0, 0, 1) \quad (5.4.118)$$

thus

$$({}^3a_i)({}^3a_j) = \begin{bmatrix} 0 & 0 & 0 \\ 0 & 0 & 0 \\ 0 & 0 & 1 \end{bmatrix} \quad (5.4.119)$$

The stress invariants associated with this principal stress vector and state of stress are

$${}^3I_4 = 0 \quad (5.4.120)$$

$${}^3I_5 = 0 \quad (5.4.121)$$

$${}^3I_8 = 0 \quad (5.4.122)$$

and

$${}^3I_9 = 0 \quad (5.4.123)$$

The failure function for stress region #3 now has the form

$$\begin{aligned} g_3 &= 1 - \left[ \left( \frac{1}{2} \right) A_3 I_1^2 + B_3 I_2 + C_3 I_1 I_4 + D_3 I_5 I_7 \right. \\ &\quad \left. + E_3 I_1 I_6 + F_3 + G_3 I_1 I_8 + H_3 I_9 \right] \quad (5.4.124) \\ &= 0 \end{aligned}$$

With equations (5.4.111) through (5.4.114) as well as equations (5.4.120) through

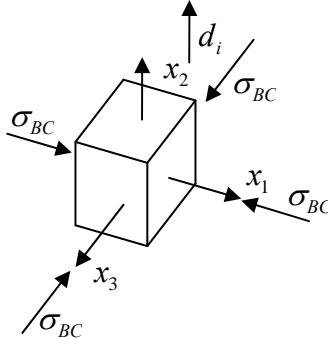
(5.4.123) then

$$\begin{aligned} 0 &= 1 - \left[ \left( \frac{1}{2} \right) A_3 (2\sigma_{MBC})^2 + B_3 (2\sigma_{MBC})^2 \right. \\ &\quad \left. + E_3 (2\sigma_{MBC})(\sigma_{MBC}) + F_3 \sigma_{MBC}^2 \right] \quad (5.4.125) \end{aligned}$$

or

$$2A_3 + 2B_3 + 2E_3 + F_3 = \frac{1}{\sigma_{MBC}^2} \quad (5.4.126)$$

Next consider the following stress state at failure under a biaxial equal compression load



$$\sigma_{ij} = \begin{bmatrix} \sigma_{BC} & 0 & 0 \\ 0 & 0 & 0 \\ 0 & 0 & \sigma_{BC} \end{bmatrix} \quad (5.4.127)$$

The subscript “BC” denotes “biaxial-compression” and because the stress is compressive then algebraically  $\sigma_{BC} < 0$ . Also note that the stresses are applied in the plane of isotropy. The principal stresses are

$$(\sigma_1, \sigma_2, \sigma_3) = (0, \sigma_{BC}, \sigma_{BC}) \quad (5.4.128)$$

This state of stress lies along the border between principal stress region #3 and region #4.

For this state of stress the first, second, sixth and seventh invariants are

$$I_1 = 2\sigma_{BC} \quad (5.4.129)$$

$$I_2 = 2\sigma_{BC}^2 \quad (5.4.130)$$

$$I_6 = 0 \quad (5.4.131)$$

and

$$I_7 = 0 \quad (5.4.132)$$

Again, with the failure function defined as



$$\begin{aligned}
g_4 &= 1 - \left[ \left( \frac{1}{2} \right) A_4 I_1^2 + B_4 I_2 + E_4 I_1 I_6 + F_4 I_7 \right] \\
&= 0
\end{aligned} \tag{5.4.133}$$

in region #4 of the principal stress space, then substitution of equations (5.4.129) through (5.4.132) into the (5.4.133) leads to

$$0 = \left( \frac{1}{2} \right) A_4 (2\sigma_{BC})^2 + B_4 (2\sigma_{BC}^2) - 1 \tag{5.4.134}$$

or

$$2A_4 + 2B_4 = \frac{1}{\sigma_{BC}^2} \tag{5.4.135}$$

The unit principal stress vector associated with this state of stress in region #3 is

$${}^3a_i = (0, 1, 0) \tag{5.4.136}$$

thus

$$({}^3a_i)({}^3a_j) = \begin{bmatrix} 0 & 0 & 0 \\ 0 & 1 & 0 \\ 0 & 0 & 0 \end{bmatrix} \tag{5.4.137}$$

The stress invariants associated with this principal stress vector and state of stress are

$${}^3I_4 = 0 \tag{5.4.138}$$

$${}^3I_5 = 0 \tag{5.4.139}$$

$${}^3I_8 = 0 \tag{5.4.140}$$

and

$${}^3I_9 = 0 \tag{5.4.141}$$

The failure function for stress region #3 now has the form

$$\begin{aligned}
g_3 &= 1 - \left[ \left( \frac{1}{2} \right) A_3 I_1^2 + B_3 I_2 + C_3 I_1 I_4 + D_3 I_5 I_7 \right. \\
&\quad \left. + E_3 I_1 I_6 + F_3 + G_3 I_1 I_8 + H_3 I_9 \right] \quad (5.4.142) \\
&= 0
\end{aligned}$$

With equations (5.4.129) through (5.4.132) as well as equations (5.4.138) through (5.4.141) then

$$0 = 1 - \left[ \left( \frac{1}{2} \right) A_3 (2\sigma_{BC})^2 + B_3 (2\sigma_{BC}^2) \right] \quad (5.4.143)$$

or

$$2A_3 + 2B_3 = \frac{1}{\sigma_{BC}^2} \quad (5.4.144)$$

With equations (5.4.9), (5.4.18), (5.4.27), (5.4.36), (5.4.45), (5.4.54), (5.4.63), (5.4.72), (5.4.81), (5.4.90), (5.4.99), (5.4.108), (5.4.117), (5.4.126), (5.4.135), and (5.4.144) there are sixteen equations in terms of six strength parameters, i.e.,

$\sigma_{YT}$  – tensile strength in the preferred material direction

$\sigma_{YC}$  – compressive strength in the preferred material direction

$\sigma_{TT}$  – tensile strength in the plane of isotropy

$\sigma_{TC}$  – compressive strength in the plane of isotropy

$\sigma_{BC}$  – equal biaxial compressive strength in the plane of isotropy

$\sigma_{MBC}$  – equal biaxial compressive strength with only one stress component in the plane of isotropy

These equations can be used to extract relationships between the functional constants ( $A_1$  through  $F_4$ ) and the mechanical strength parameters listed above. For example, subtracting equation (5.4.63) from equation (5.4.90) yields

$$B_4 - B_1 = \frac{1}{\sigma_{TC}^2} - \frac{1}{\sigma_{TT}^2} \quad (5.4.145)$$

and utilizing equations (5.3.147) and (5.3.148) leads to

$$\begin{aligned} B_4 - B_1 &= \frac{1}{\sigma_{TC}^2} - \frac{1}{\sigma_{TT}^2} \\ &= D_2 \end{aligned} \quad (5.4.146)$$

In addition, subtracting equation (5.4.9) from equation (5.4.36) yields

$$(B_4 - B_1) + (F_4 - F_1) = \frac{1}{\sigma_{YC}^2} - \frac{1}{\sigma_{YT}^2} \quad (5.4.147)$$

Furthermore, subtraction equation (5.4.145) from equation (5.4.147) results in

$$(F_4 - F_1) = \left( \frac{1}{\sigma_{YC}^2} - \frac{1}{\sigma_{YT}^2} \right) - \left( \frac{1}{\sigma_{TC}^2} - \frac{1}{\sigma_{TT}^2} \right) \quad (5.4.148)$$

and utilizing equations (5.3.150) and (5.3.151) leads to

$$\begin{aligned} (F_4 - F_1) &= \left( \frac{1}{\sigma_{YC}^2} - \frac{1}{\sigma_{YT}^2} \right) - \left( \frac{1}{\sigma_{TC}^2} - \frac{1}{\sigma_{TT}^2} \right) \\ &= H_2 \end{aligned} \quad (5.4.149)$$

In addition, subtracting equation (5.4.99) from equation (5.4.135) yields

$$(2A_4 - A_2) + (2B_4 - 2D_2 - 2B_2) = \frac{1}{\sigma_{BC}^2} - \frac{2}{\sigma_{TC}^2} \quad (5.4.150)$$

Utilizing equations (5.3.146) through (5.3.148) this expression simplifies to

$$A_4 = \frac{1}{\sigma_{BC}^2} - \frac{2}{\sigma_{TC}^2} \quad (5.4.151)$$

Subtraction of equation (5.4.135) from (5.4.108)

$$(A_3 - A_4) + (2B_3 - B_4) = \frac{2}{\sigma_{TC}^2} - \frac{1}{2\sigma_{BC}^2} \quad (5.4.152)$$

and utilizing equations (5.3.146) and (5.3.137) leads to

$$B_3 = B_4 = \frac{2}{\sigma_{TC}^2} - \frac{1}{2\sigma_{BC}^2} \quad (5.4.153)$$

Utilizing equation (5.3.146) and subtracting equation (5.4.151) from equation (5.4.63)

yields

$$B_1 = \frac{1}{\sigma_{TT}^2} - \frac{1}{2\sigma_{BC}^2} + \frac{1}{\sigma_{TC}^2} \quad (5.4.154)$$

With equations (5.3.124), (5.3.130), (5.3.137), and (5.3.142), then subtracting equation

(5.4.54) from equation (5.4.117) leads to

$$\frac{3}{2}A_4 + B_4 + E_4 = \frac{1}{\sigma_{MBC}^2} - \frac{1}{\sigma_{YC}^2} \quad (5.4.155)$$

Substitution of equations (5.4.151) and (5.4.153) into (5.4.155) yields the following

relationship

$$E_4 = \frac{1}{\sigma_{MBC}^2} - \frac{1}{\sigma_{YC}^2} - \frac{1}{\sigma_{BC}^2} + \frac{1}{\sigma_{TC}^2} \quad (5.4.156)$$

With equations (5.3.149) and (5.4.150), then subtraction equation (5.4.135) from

equation (5.4.126) results in

$$2E_4 + F_4 = \frac{1}{\sigma_{MBC}^2} - \frac{1}{\sigma_{BC}^2} \quad (5.4.157)$$

Substitution of equation (5.4.156) into (5.4.157) yields

$$F_4 = -\frac{1}{\sigma_{MBC}^2} + \frac{1}{\sigma_{BC}^2} + \frac{2}{\sigma_{YC}^2} - \frac{2}{\sigma_{TC}^2} \quad (5.4.158)$$

Substitution of equation (5.4.158) into (5.4.148) leads to the following

$$F_1 = -\frac{1}{\sigma_{MBC}^2} + \frac{1}{\sigma_{BC}^2} + \frac{1}{\sigma_{YC}^2} - \frac{1}{\sigma_{TC}^2} + \frac{1}{\sigma_{YT}^2} - \frac{1}{\sigma_{TT}^2} \quad (5.4.159)$$

In summary,

$$g_1 = 1 - \left[ \left( \frac{1}{2} \right) A_1 I_1^2 + B_1 I_2 + E_1 I_1 I_6 + F_1 I_7 \right] \quad (5.2.1)$$

$$g_2 = 1 - \left[ \left( \frac{1}{2} \right) A_2 I_1^2 + B_2 I_2 + D_2 I_5 + E_2 I_1 I_6 + F_2 I_7 + H_2 I_9 \right] \quad (5.4.160)$$

$$g_3 = 1 - \left[ \left( \frac{1}{2} \right) A_3 I_1^2 + B_3 I_2 + D_3 I_5 I_7 + E_3 I_1 I_6 + F_3 + H_3 I_9 \right] \quad (5.4.161)$$

and

$$g_4 = 1 - \left[ \left( \frac{1}{2} \right) A_4 I_1^2 + B_4 I_2 + E_4 I_1 I_6 + F_4 I_7 \right] \quad (5.2.43)$$

where

$$A_1 = A_2 = A_3 = A_4 = -\frac{2}{\sigma_{TC}^2} + \frac{1}{\sigma_{BC}^2} \quad (5.4.162)$$

$$B_1 = B_2 = \frac{1}{\sigma_{TT}^2} + \frac{1}{\sigma_{TC}^2} - \frac{1}{2\sigma_{BC}^2} \quad (5.4.163)$$

$$B_3 = B_4 = \frac{2}{\sigma_{TC}^2} - \frac{1}{2\sigma_{BC}^2} \quad (5.4.164)$$

$$D_2 = -D_3 = -\frac{1}{\sigma_{TT}^2} + \frac{1}{\sigma_{TC}^2} \quad (5.4.165)$$

$$\begin{aligned} E_1 &= E_2 = E_3 = E_4 \\ &= \frac{1}{\sigma_{TC}^2} - \frac{1}{\sigma_{BC}^2} - \frac{1}{\sigma_{YC}^2} + \frac{1}{\sigma_{MBC}^2} \end{aligned} \quad (5.4.166)$$

$$\begin{aligned} F_1 = F_2 &= -\frac{1}{\sigma_{TT}^2} - \frac{1}{\sigma_{TC}^2} + \frac{1}{\sigma_{BC}^2} \\ &+ \frac{1}{\sigma_{YT}^2} + \frac{1}{\sigma_{YC}^2} - \frac{1}{\sigma_{MBC}^2} \end{aligned} \quad (5.4.167)$$

$$F_3 = F_4 = -\frac{2}{\sigma_{TC}^2} + \frac{1}{\sigma_{BC}^2} + \frac{2}{\sigma_{YC}^2} - \frac{1}{\sigma_{MBC}^2} \quad (5.4.168)$$

and

$$H_2 = -H_3 = \frac{1}{\sigma_{TT}^2} - \frac{1}{\sigma_{TC}^2} - \frac{1}{\sigma_{YT}^2} + \frac{1}{\sigma_{YC}^2} \quad (5.4.169)$$

Equations (5.4.160) and (5.4.169) along with equations (5.2.1) and (5.2.43) is a complete statement of the anisotropic failure functions in a regions of the stress space.

The anisotropic failure criterion is projection onto the  $\sigma_{11} - \sigma_{22}$  stress space in Figure 5.4.1. The strength parameters were for the most part extracted from the data found in Burchell et al. (2007), i.e.,  $\sigma_{TT}$  = 10.48 MPa,  $\sigma_{YT}$  = 15.93 MPa and  $\sigma_{YC}$  = 52.93 MPa (see Table 2.2). These are average or mean strength values. The other three strength parameters  $\sigma_{YT}$ ,  $\sigma_{YC}$ ,  $\sigma_{BC}$  and  $\sigma_{MBC}$  were estimated. Values for the strength parameters listed above are given in the figure caption. Note the agreement with the

data along the two tensile axes, as well as along the failure curve for each load path.

These average strength values for each load path are depicted as open red circles in

Figure 5.4.1.

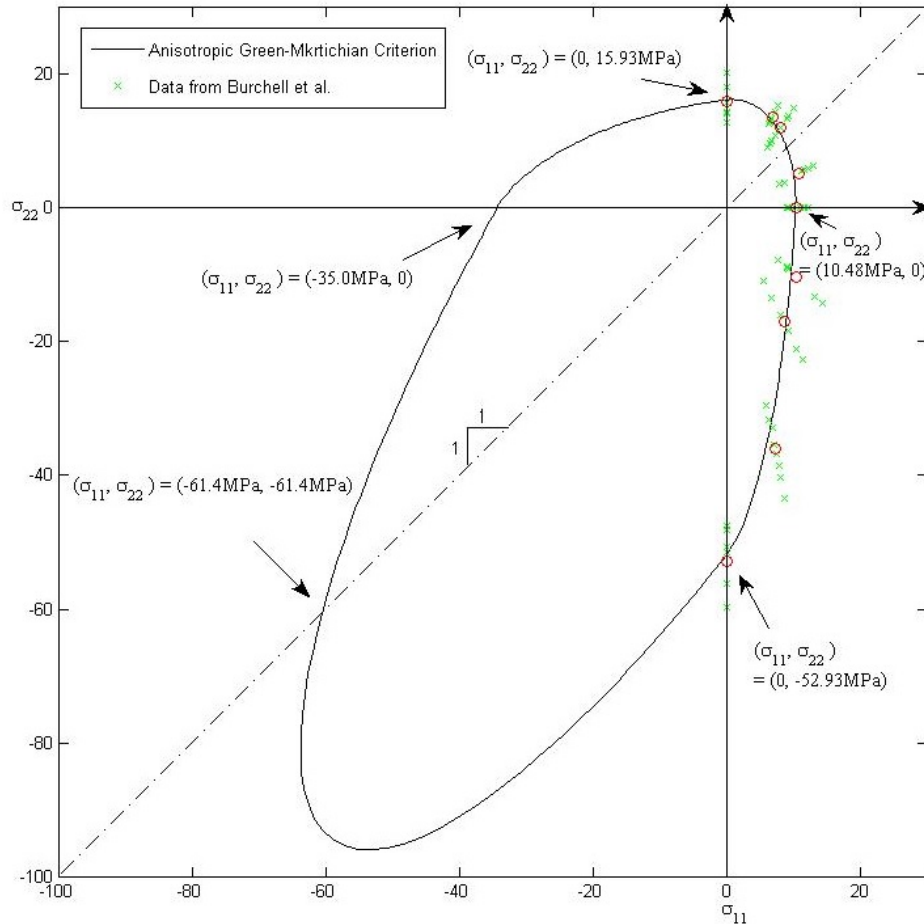


Figure 5.4.1 Anisotropic Failure Criterion with Failure Data from Burchell et al. (2007) Projected onto the  $\sigma_{11} - \sigma_{22}$  Principal Stress Plane ( $\sigma_{TT} = 10.48 \text{ MPa}$ ,  $\sigma_{TC} = -35 \text{ MPa}$ ,  $\sigma_{BC} = -40 \text{ MPa}$ ,  $\sigma_{YT} = 15.93 \text{ MPa}$ ,  $\sigma_{YC} = -52.93 \text{ MPa}$  and  $\sigma_{MBC} = -61.40 \text{ MPa}$ )

The anisotropic failure criterion is projected onto the deviatoric planes in Figures 5.4.2, 5.4.3 and 5.4.4. Note that a cross section through the failure function perpendicular to the hydrostatic axis transitions from a pyramidal shape (Figure 5.4.1) to

a circular shape (Figure 5.4.2) with an increasing value of the stress invariant  $I_I$ . This suggests that the apex of the failure function presented in a full Haigh-Westergaard stress space is blunt, i.e., quite rounded for this particular criterion.

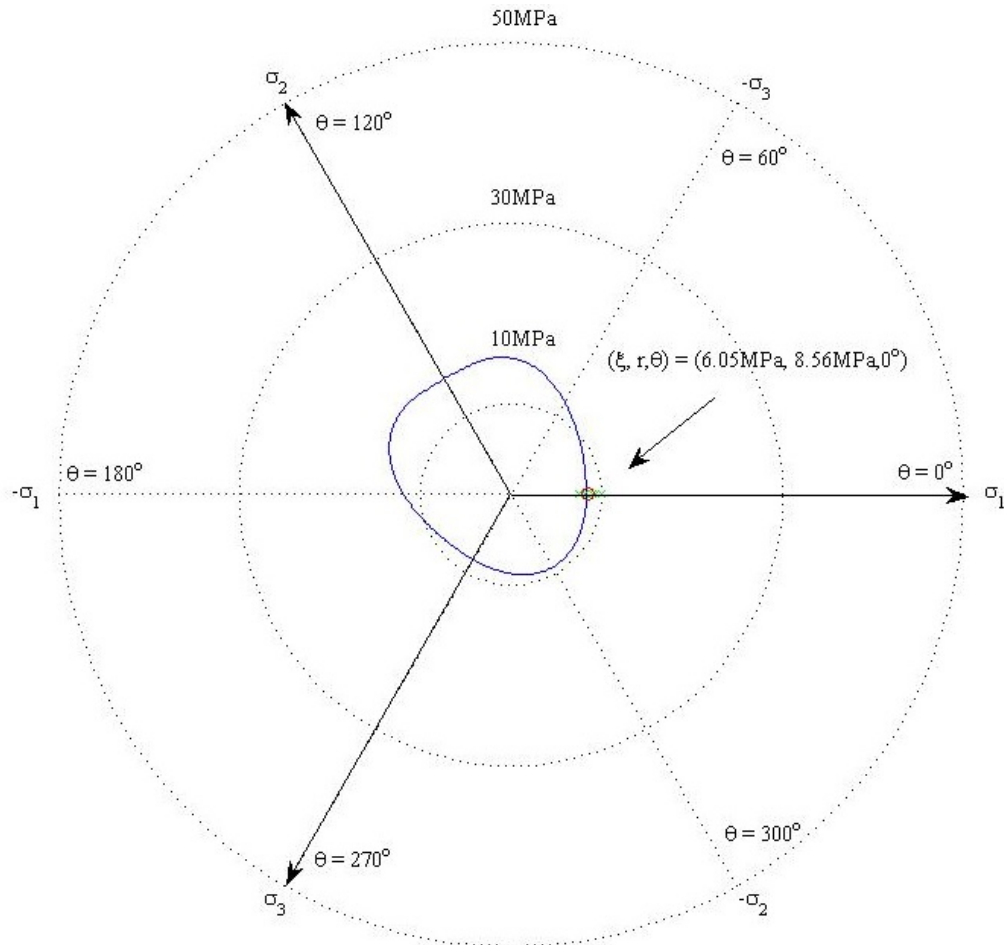


Figure 5.4.2 Anisotropic Failure Criterion with Failure Data from Burchell et al. (2007)  
 Projected onto ( $\xi = 6.05$  MPa) Parallel to the  $\Pi$ -plane ( $\sigma_{TT} = 10.48$  MPa,  $\sigma_{TC} = -35$  MPa,  
 $\sigma_{BC} = -40$  MPa  $\sigma_{YT} = 15.93$  MPa,  $\sigma_{YC} = -52.93$  MPa,  
 $\sigma_{MBC} = -61.40$  MPa)



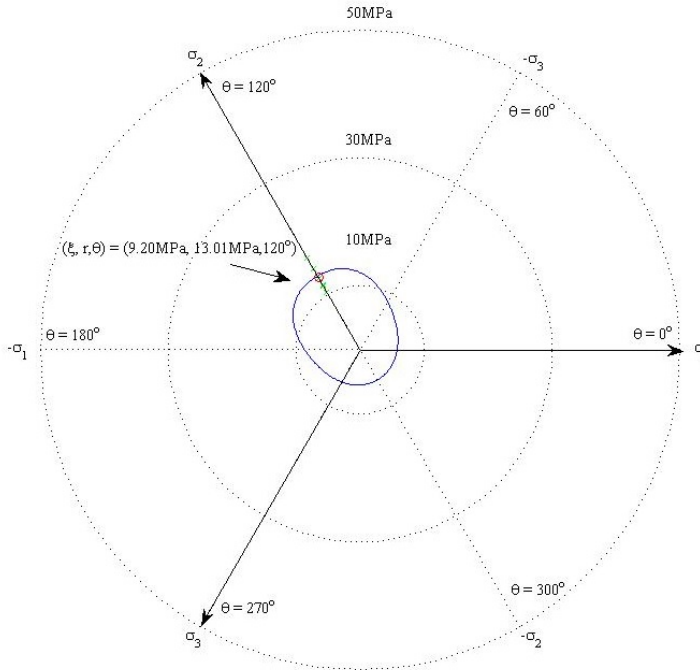


Figure 5.4.3 Anisotropic Failure Criterion with Failure Data from Burchell et al. (2007) Projected onto  $(\xi = 9.02 \text{ MPa})$  Parallel to the  $\Pi$ -plane ( $\sigma_{TT} = 10.48 \text{ MPa}$ ,  $\sigma_{TC} = -35 \text{ MPa}$ ,  $\sigma_{BC} = -40 \text{ MPa}$ ,  $\sigma_{YT} = 15.93 \text{ MPa}$ ,  $\sigma_{YC} = -52.93 \text{ MPa}$ ,  $\sigma_{MBC} = -61.40 \text{ MPa}$ )

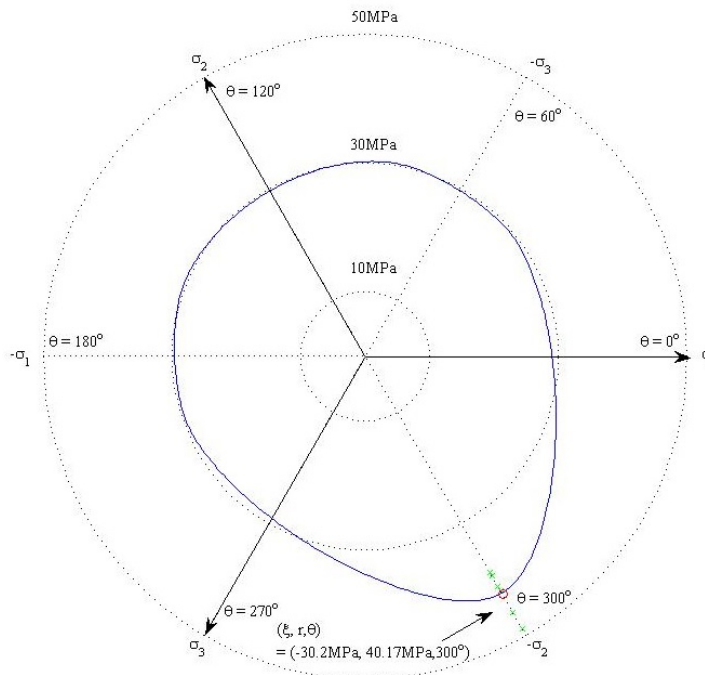


Figure 5.4.4 Anisotropic Failure Criterion with Burchell's (2007) Failure Data Projected onto  $(\xi = -30.20)$  Parallel to the  $\Pi$ -plane ( $\sigma_{TT} = 10.48 \text{ MPa}$ ,  $\sigma_{TC} = -35 \text{ MPa}$ ,  $\sigma_{BC} = -40 \text{ MPa}$ ,  $\sigma_{YT} = 15.93 \text{ MPa}$ ,  $\sigma_{YC} = -52.93 \text{ MPa}$ ,  $\sigma_{MBC} = -61.40 \text{ MPa}$ )

The meridian lines of the anisotropic failure surface corresponding to  $\theta=0^\circ$ ,  $\theta=120^\circ$  and  $\theta=300^\circ$  are depicted on Figure 5.4.5. Obviously the meridian lines are not linear. The  $\theta=0^\circ$  meridian line goes through point defined by  $\xi = 6.05 \text{ MPa}$  and  $r = 8.56 \text{ MPa}$ .  $\theta=120^\circ$  meridian line goes through point defined by  $\xi = 9.02 \text{ MPa}$  and  $r = 13.01 \text{ MPa}$ . The  $\theta=300^\circ$  meridian line goes through the point defined by  $\xi = 30.2 \text{ MPa}$  and  $r = 42.17 \text{ MPa}$ .

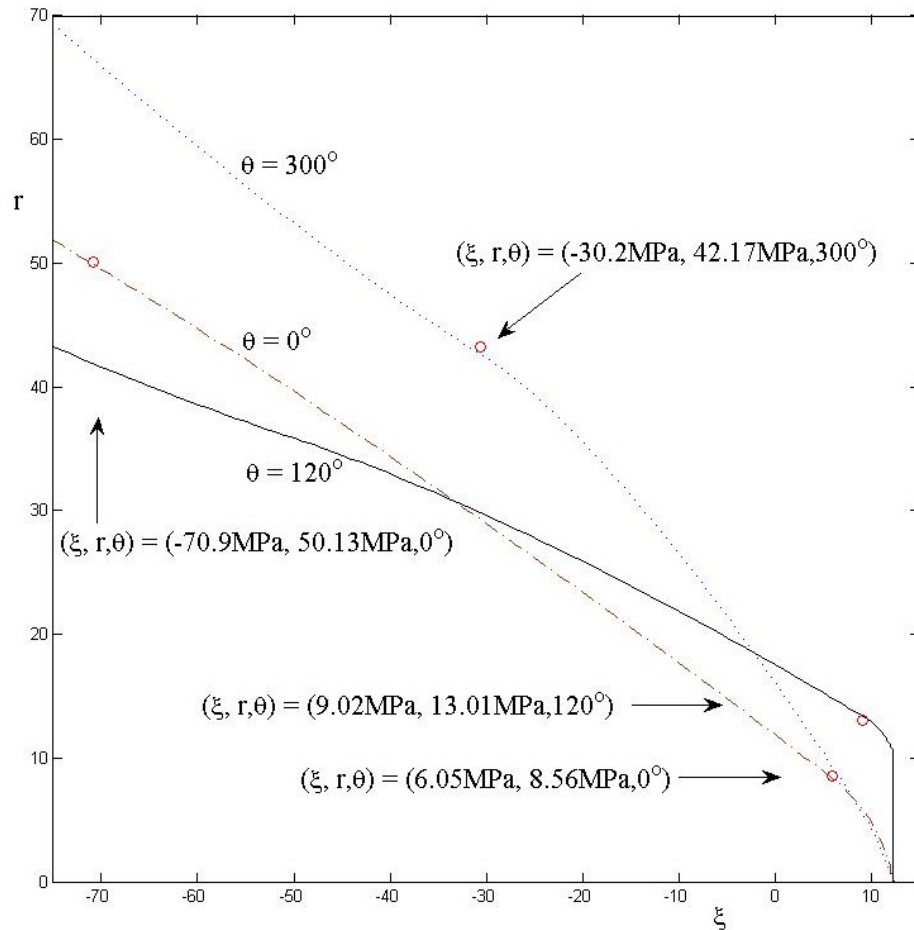


Figure 5.4.5 Anisotropic Failure Criterion with Failure Data from Burchell et al. (2007)  
 Projected onto Meridian-Plane ( $\sigma_{TT} = 10.48 \text{ MPa}$ ,  $\sigma_{TC} = -35 \text{ MPa}$ ,  $\sigma_{BC} = -40 \text{ MPa}$   
 $\sigma_{YT} = 15.93 \text{ MPa}$ ,  $\sigma_{YC} = -52.93 \text{ MPa}$ ,  $\sigma_{MBC} = -61.40 \text{ MPa}$ )

As the value of the  $I_1$  stress invariant associated with the hydrostatic stress increases in the negative direction, failure surfaces perpendicular to the hydrostatic stress line become circular again. The model suggests that as hydrostatic compression stress increases the difference between tensile strength and compressive strength diminishes and approach each other asymptotically. This is a material behavior that should be verified experimentally in a manner similar to Bridgman's (1953) bend bar experiments conducted in hyperbaric chambers on cast metal alloys. Balzer (1998) provides an excellent overview of Bridgman's (1953) experimental efforts, as well as others and their accomplishments in the field of high pressure testing.

## **CHAPTER VI**

### **MATERIAL STRENGTH AS A RANDOM VARIABLE**

All parameters in an engineering design can be treated as random variables. For example material strength, loads applied to the component, geometric dimensions, as well as the stiffness of the material utilized can all exhibit significant levels of variability. However, the assumption is made for graphite that the variability in material strength far exceeds the variability one would see in the other design parameters. This seems reasonable since the strength of graphite material can vary by 50% or more. Earthquake loads can be the exception to this exclusion of all other design parameters, although including load design parameters as well as resistance design parameters other than material strength as random variables is easily accomplished.

A failure function characterizes a limit state through its formulation and the design parameters that the function is dependent on. Although one can easily pose limit states for fracture (e.g., failure assessment diagrams), fatigue life or service issues relating to structural deformations in this effort all design parameters here are related to strength.

In the previous chapters a number of failure criteria, i.e., limit state functions, were highlighted and discussed. The goal in examining the various failure criteria is the development of a phenomenological, stress based function that captures the fundamental strength behavior of nuclear graphite exhibited through the data from Burchell et al. (2007). This behavior includes different failure behavior in tension and compression, as well as the anisotropy exhibited along different load paths. In the last chapter the isotropic failure criterion was extended to transversely anisotropic behavior through the use of tensorial invariants that include material direction tensors. Other types of anisotropies can be considered using this approach, e.g., orthotropic strength behavior. The phenomenological failure criteria outlined in the previous chapters were all posed as deterministic limit states. The last aspect of material behavior that is explored in this chapter requires consideration is how to account for the variability in the strength parameters.

The multiaxial graphite data from Burchell et al. (2007) has been cited throughout this work and one cannot help but see that the strength of graphite material is essentially stochastic along various load paths depicted in Figure 2.4.1. With the amount of variation exhibited by the graphite data in that figure and based on graphite failure data available throughout the literature, it is not difficult to identify graphite strength as a random variable. The strength parameters identified in the last chapter for the anisotropic failure criterion, i.e.,  $\sigma_{YT}$  (tensile strength in the preferred material direction),

$\sigma_{YC}$  (compressive strength in the preferred material direction),  $\sigma_{TT}$  (tensile strength in the plane of isotropy),  $\sigma_{TC}$  (compressive strength in the plane of isotropy),  $\sigma_{BC}$  (equal biaxial compressive strength in the plane of isotropy), and  $\sigma_{MBC}$  (equal biaxial compressive strength with only one stress component in the plane of isotropy) are all treated as random variables based on evidence found within the data from Burchell et al. (2007). The assumption is made that these strength parameters are statistically independent random variables. The veracity of this assumption will be left for future efforts. Methods available to interrogate this issue will be outlined in the summary chapter. Another assumption is made relative to the particular probability density function used to represent the strength random variables. Here the two parameter Weibull distribution is adopted for all random strength parameters. Again there are methods to test the validity of that assumption. But since this is a proof of concept effort, those sort of goodness of fit tests are left to others to pursue.

In general, the strength parameters associated with the load paths from the data found in Burchell et al. (2007) can be assembled into an  $k$ -dimensional vector, i.e.,

$$Y_\alpha = (Y_1, Y_2, \dots, Y_k) \quad (6.1)$$

and a limit state function can be defined in general terms as

$$g(y_\alpha, \sigma_{ij}) = 0 \quad (6.2)$$

Here  $y_\alpha$  represents a vector of realizations of the random variables identified by the strength parameters in the previous chapter and  $\sigma_{ij}$  is the applied Cauchy stress tensor.

This last expression defines a surface in an  $k$ -dimensional stress space. The limit state function for the anisotropic failure criterion is adopted for graphite and this criterion would have the following multipart formulation in the principal (Haigh-Westergaard) stress space

*Region #1:*  $(\sigma_1 \geq \sigma_2 \geq \sigma_3 \geq 0)$

$$\begin{aligned} g_1 &= 1 - \left[ \left( \frac{1}{2} \right) A_1 I_1^2 + B_1 I_2 + E_1 I_1 I_6 + F_1 I_7 \right] \\ &= 0 \end{aligned} \quad (6.3)$$

*Region #2:*  $(\sigma_1 \geq \sigma_2 \geq 0 \geq \sigma_3)$

$$\begin{aligned} g_2 &= 1 - \left[ \left( \frac{1}{2} \right) A_2 I_1^2 + B_2 I_2 + C_2 I_1 I_4 + D_2 I_5 \right. \\ &\quad \left. + E_2 I_1 I_6 + F_2 I_7 + G_2 I_1 I_8 + H_2 I_9 \right] \\ &= 0 \end{aligned} \quad (6.4)$$

*Region #3:*  $(\sigma_1 \geq 0 \geq \sigma_2 \geq \sigma_3)$

$$\begin{aligned} g_3 &= 1 - \left[ \left( \frac{1}{2} \right) A_3 I_1^2 + B_3 I_2 + C_3 I_1 I_4 + D_3 I_5 I_7 \right. \\ &\quad \left. + E_3 I_1 I_6 + F_3 + G_3 I_1 I_8 + H_3 I_9 \right] \\ &= 0 \end{aligned} \quad (6.5)$$

*Region #4:*  $0 \geq \sigma_1 \geq \sigma_2 \geq \sigma_3$

$$\begin{aligned} g_4 &= 1 - \left[ \left( \frac{1}{2} \right) A_4 I_1^2 + B_4 I_2 + E_4 I_1 I_6 + F_4 I_7 \right] \\ &= 0 \end{aligned} \quad (6.6)$$

The various constants defined in the previous chapter (identified above as  $A$  through  $F$  with subscripts) are no longer constants since they are functions of strength parameters.

Hence these parameters are now considered composite random variables. In essence they are functions of random variables

The fundamental issue of no longer treating material strength as a deterministic, single valued parameter complicates the issue of how to interpret failure at a point through the state of stress at that point. If strength is treated as a random variable, how does that affect the approach the design engineer takes in assessing whether a component performs its intended function properly or not? A different design philosophy must be adopted in this situation where a simple fail/no fail interpretation is replaced with an equivalent stochastic decision process that predicts the probability of component failure.

In general, the reliability (probability of failure) is computed based on the expression

$$\mathcal{R} = \text{Probability } [g(y_\alpha, \sigma_{ij}) > 0] \quad (6.7)$$

This calculation is made for a unit volume of a point of material with a homogenous state of stress. To calculate the reliability of an element the joint density function must be integrated over the “safe” region of the design space which is defined by the limit state function. This integration takes the form

$$\mathcal{R} = \iiint_{g(y_\alpha, \sigma_{ij}) > 0} \Omega(y_T, y_C, y_{BC}) dy_T dy_C dy_{BC} \quad (6.8)$$

for the isotropic formulation of the limit state function for graphite. Here the three random strength parameters  $Y_T$ ,  $Y_C$  and  $Y_{BC}$  are associated with the deterministic strength



parameters  $\sigma_T$ ,  $\sigma_C$  and  $\sigma_{BC}$ . Again, the lower case letters associated with the random strength parameters are realizations of the random strengths. In addition

$$\mathcal{R} = \int_{g(y_\alpha, \sigma_{ij}) > 0} \Omega(y_{TT}, y_{TC}, y_{BC}, y_{YT}, y_{YC}, y_{MBC}) dy_{TT} dy_{TC} dy_{BC} dy_{YT} dy_{YC} dy_{MBC} \quad (6.9)$$

serves as the generic integration for the anisotropic limit state function. Here  $\Omega$  is the joint density function of material strength parameters. Sun and Yamada (1978) as well as Wetherhold (1983) point out that the integration defined by either equations (6.8) and (6.9) yields the reliability of a unit volume based on the state of stress at a point. However, closed form solutions for these types of reliability expressions are not available. Palko (1992) and Hu (1994) illustrate how the integration in these expressions can be executed using techniques based on Monte Carlo simulation. These techniques are deployed here.

Having identified graphite strength as a random variable the next step is selecting an appropriate probability density function to characterize each strength random variable. In general material strength should be characterized by an extreme value distribution. In structural design one is always interested in the extreme minimum values in a random variable representing strength, i.e., a resistance random variable. If load is similarly characterized as a random variable the design engineer would be cognizant of the extreme maximum values representing of this variable. Weibull (1939) formulated a probability density function with two parameters to characterize a type III extreme value

distribution. If a single strength parameter is considered then  $\alpha$  is equal to one and the following notation can be adopted

$$\begin{aligned} Y_\alpha &= Y_1 \\ &= Y \end{aligned} \quad (6.10)$$

The cumulative probability density function for a two parameter Weibull distribution is given by the expression

$$\begin{aligned} F_{Y_\alpha} &= F_Y \\ &= 1 - \exp\left[-\left(\frac{y}{\sigma_\theta}\right)^m\right] \end{aligned} \quad (6.11)$$

where  $y$  is the realization of the strength random variable (usually an applied uniaxial stress,  $\sigma$ )  $m$  is the Weibull modulus and  $\sigma_\theta$  is known as the scale parameter. This equation can be linearized by taking the natural logarithm of both sides of the expression twice, i.e.,

$$\ln\left[\ln\left(\frac{1}{1-F_Y}\right)\right] = \ln(C) + m\ln(\sigma) \quad (6.12)$$

where

$$\ln(C) = \left(\frac{1}{\sigma_\theta}\right)^m \quad (6.13)$$

The format of equation (6.12) lends itself to an easy graphical format, an example of which is given in Figure 6.1. Here values for the Weibull parameters were arbitrarily assumed (see the figure caption). These linearized probability plots are used extensively in this chapter to explain the fundamentals of the numerical integration techniques used

to evaluate aspects of equation (6.9) and too compare the numerical approach to simple closed form solutions.

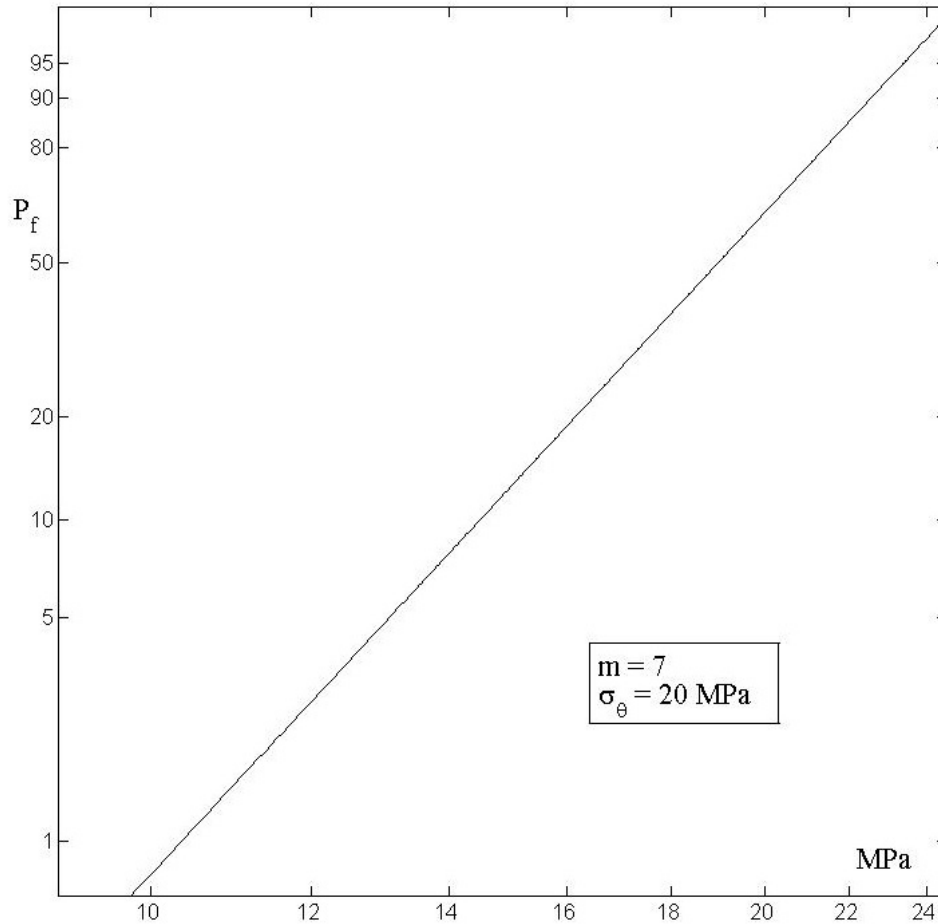


*Figure 6.1 Probability of Failure as a Function of Uniaxial Strength Using a Weibull Distribution with  $m = 7$  and  $\sigma_\theta = 20$  MPa*

### 6.1 Integration by Monte Carlo Simulation

In general the probability of failure at a point in a structural component can be expressed as

$$P_f = \int_{\delta_f} f_{y_\alpha}(y_\alpha) dy \quad \alpha = 1, \dots, k \quad (6.1.1)$$

As noted earlier  $Y_\alpha$  represents a vector of random strength variables,  $f_{Y_\alpha}$  is a vector of probability density functions associated with each component of the vector of random strength variables and  $\delta_f$  is the failure domain that satisfies the expression

$$g(y_\alpha, \sigma_{ij}) \leq 0 \quad \alpha = 1, \dots, k \quad (6.1.2)$$

Here  $g(y_\alpha, \sigma_{ij})$  is the functional representation of the failure criterion, e.g., equations (6.3) through (6.6). Although the evaluation of the integral appears straight forward, closed form solutions are unavailable except for simple failure criterion. Conventional Monte Carlo simulation can be used to numerically evaluate the probability of failure. However, conventional Monte Carlo simulation has its drawbacks that are discussed near the end of this section.

Monte Carlo simulation is relatively easy to implement. An indicator function  $I$  is defined such that

$$I = \begin{cases} 1 & g(y_\alpha) \leq 0 \\ 0 & g(y_\alpha) > 0 \end{cases} \quad \alpha = 1, \dots, k \quad (6.1.3)$$

This indicator function can be included in the integral above if the integration range is expanded to include the entire design variable space. Now

$$P_f = \int_{\delta_s + \delta_f} I f(y_\alpha) dy_\alpha \quad \alpha = 1, \dots, k \quad (6.1.4)$$

where  $\delta_s$  is defined as the *safe* domain of the design variable space. The integral on the right side of this expression defines the expectation of the indicator function, i.e.,

$$E[I] = \int_{\delta_s + \delta_f} I f(y_\alpha) dy_\alpha \quad (6.1.5)$$

The definition of the mean ( $\mu$ ) of a random variable is the expectation of the variable, i.e.,

$$\mu_x = \int_{-\infty}^{+\infty} x f(x) dx \quad (6.1.6)$$

The mean associated with a random variable can be estimated from a sample taken from the population that is being characterized by the distribution function  $f(x)$ . The estimated value of the mean is given by the simple expression

$$\mu_x = \frac{1}{n} \sum_{j=1}^n x_j \quad (6.1.7)$$

where  $x_j$  is the  $j^{\text{th}}$  observation in a random sample taken from the population. In a similar fashion the probability of failure ( $P_f$ ) represents the mean (or expected value) of the indicator function. Thus equation (6.1.4) can be expressed as

$$\begin{aligned} P_f &= E(I) \\ &= \lim_{n \rightarrow \infty} \left\{ \frac{1}{n} \sum_{j=1}^n I_j \right\} \end{aligned} \quad (6.1.8)$$

Here it is implied that a random sample of *successes* ( $I = 1$ ) or *failures* ( $I = 0$ ) has been generated. Thus  $I_j$  is the  $j^{\text{th}}$  evaluation of the limit state function where the random observations have been generated from the cumulative distribution function  $F_X$ .

The next four figures (6.1.1 through 6.1.4) depict the utility of Monte Carlo simulation. The probability of failure is estimated using Monte Carlo simulation at three uniaxial stress levels, i.e.,  $\sigma = 13.1 \text{ MPa}$ ,  $\sigma = 19.0 \text{ MPa}$ , and  $\sigma = 23.4 \text{ MPa}$ . These three stress levels correspond to probabilities of failures equal to 5%, 50% and

95% for a uniaxial strength random variable characterized by a two parameter Weibull distribution with  $m = 7$  and  $\sigma_\theta = 20$  MPa.

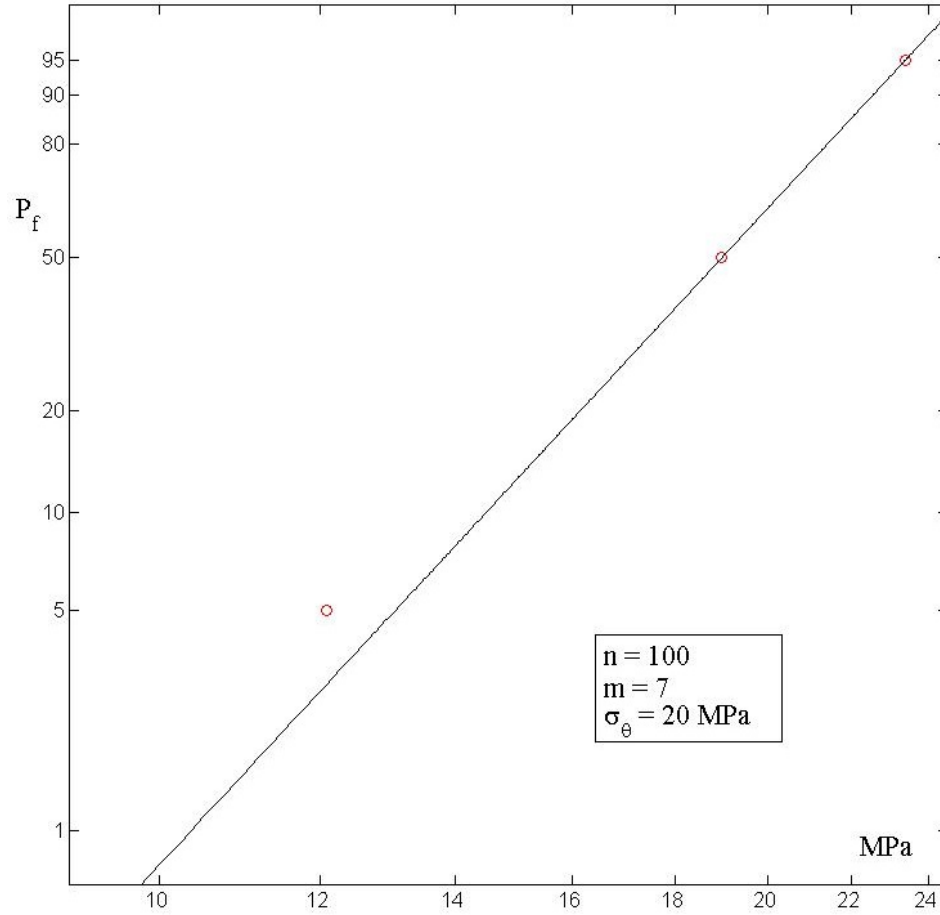


*Figure 6.1.1 Estimates from Monte Carlo Simulations ( $n=100$ ) at Low (5%), Medium (50%) and High (95%) Levels of Probability of Failure Compared to the Underlying Weibull Population Distribution ( $m = 7$  and  $\sigma_\theta = 20$  MPa)*

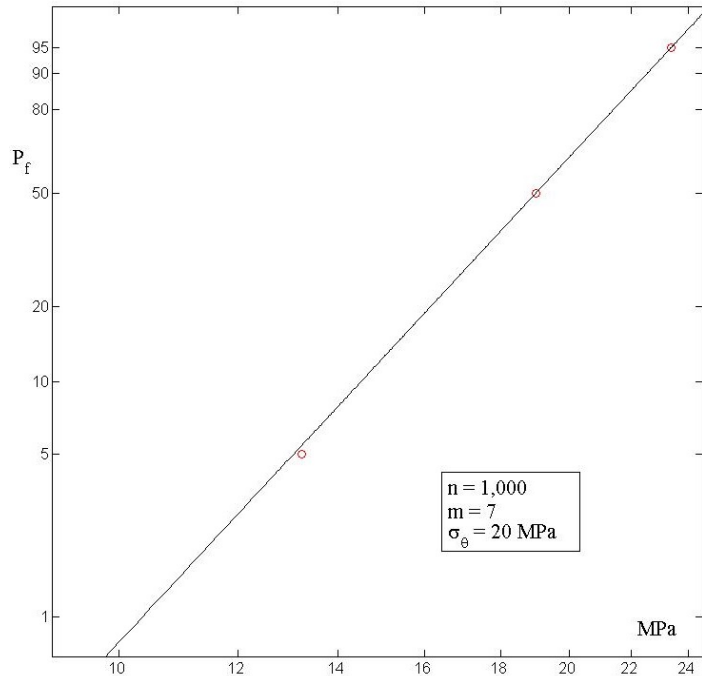


Figure 6.1.2 Estimates from Monte Carlo simulations ( $n=1,000$ ) at Low (5%), Medium (50%) and High (95%) Levels of Probability of Failure Compared to the Underlying Weibull Population Distribution ( $m = 7$  and  $\sigma_\theta = 20$  MPa)

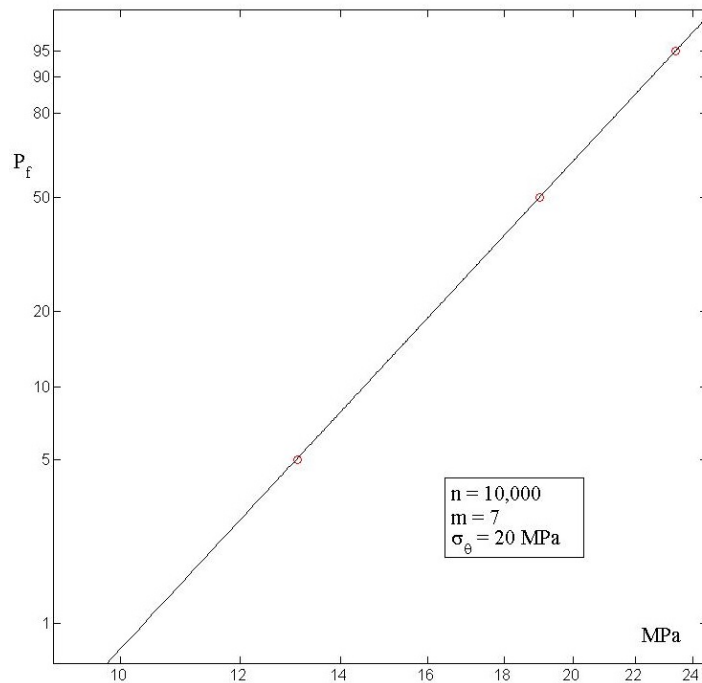
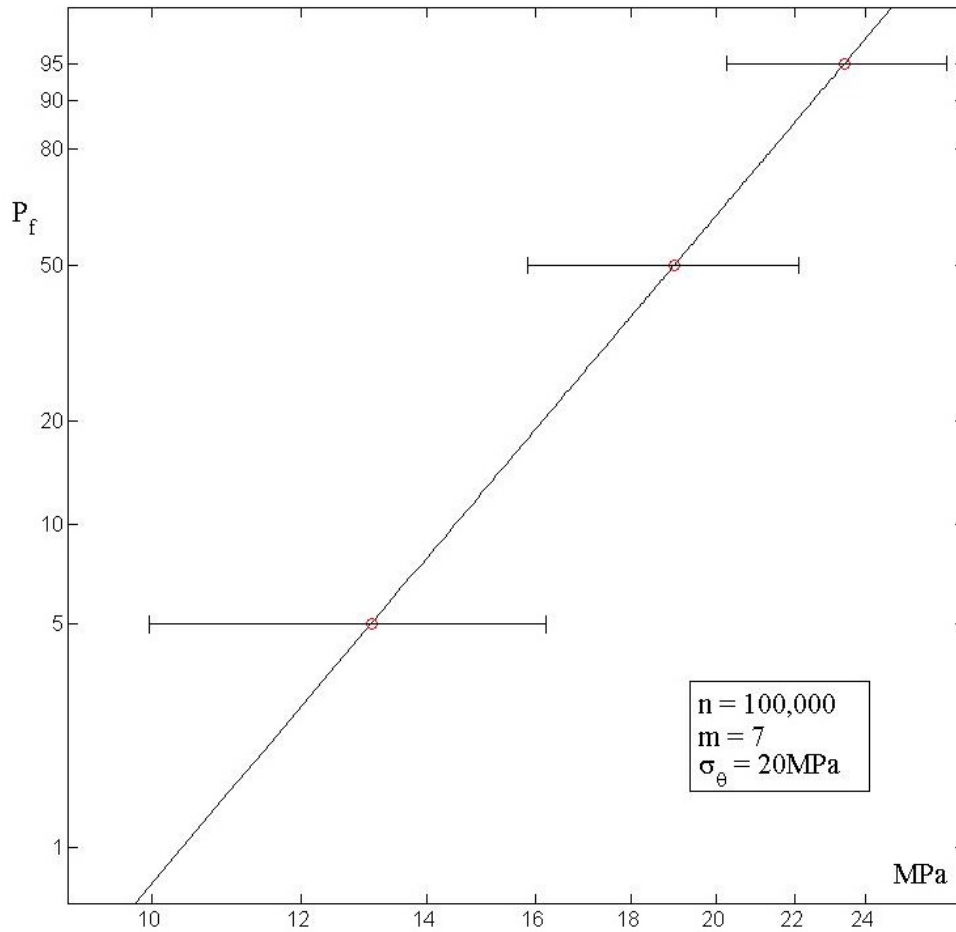


Figure 6.1.3 Estimates from Monte Carlo simulations ( $n=10,000$ ) at Low (5%), Medium (50%) and High (95%) Levels of Probability of Failure Compared to the Underlying Weibull Population Distribution ( $m = 7$  and  $\sigma_\theta = 20$  MPa)

The open circles in all four figures represent estimates of the probability of failure using conventional Monte Carlo simulation. The straight line in each figure represents the parent populations the sample strengths are being extracted from. Several observations can be made. First the estimate of the probability of failure at the 5% level is not good until the number of samples is increased to 10,000 (see figure 6.1.3). In addition, the estimate of the probability of failure is quite good for all sample sizes at the 95% probability of failure level. This second observation should not be considered meritorious for conventional Monte Carlo simulation since most engineering designs based on probabilistic methods will strive for the regions of low probability of failures. This loss of fidelity of the conventional Monte Carlo simulation approach in the low probability of failure regimes is a distinct disadvantage in using this numerical method to estimate the integral in equation 6.9.





*Figure 6.1.4 Estimates from Monte Carlo simulations ( $n=100,000$ ) at Low (5%), Medium (50%) and High (95%) Levels of Probability of Failure Compared to the Underlying Weibull Population Distribution ( $m = 7$  and  $\sigma_\theta = 20$  MPa)*

To a certain extent the loss of fidelity in the low probability of failure regimes can be rectified by increasing the number of simulations (see figure 6.1.4). However, depending on how low the required design failure rate is, this issue can still be a problem as evidenced by the probability of failure estimates presented in figure 6.1.5. Here values of probability of failure are estimated for uniaxial stress levels of *3.86 MPa*, *5.37 MPa* and *7.46 MPa* for the same population sampled in the previous four figures. These values of stress correspond to exact values of probability of failure in the parent

population (solid line) of 0.1%, 0.01% and 0.001%. In this figure 100,000 simulations were conducted and as Palko (1992) and Hu (1994) point out these estimates do not improve much when the number of simulations are increased even by several orders of magnitude.

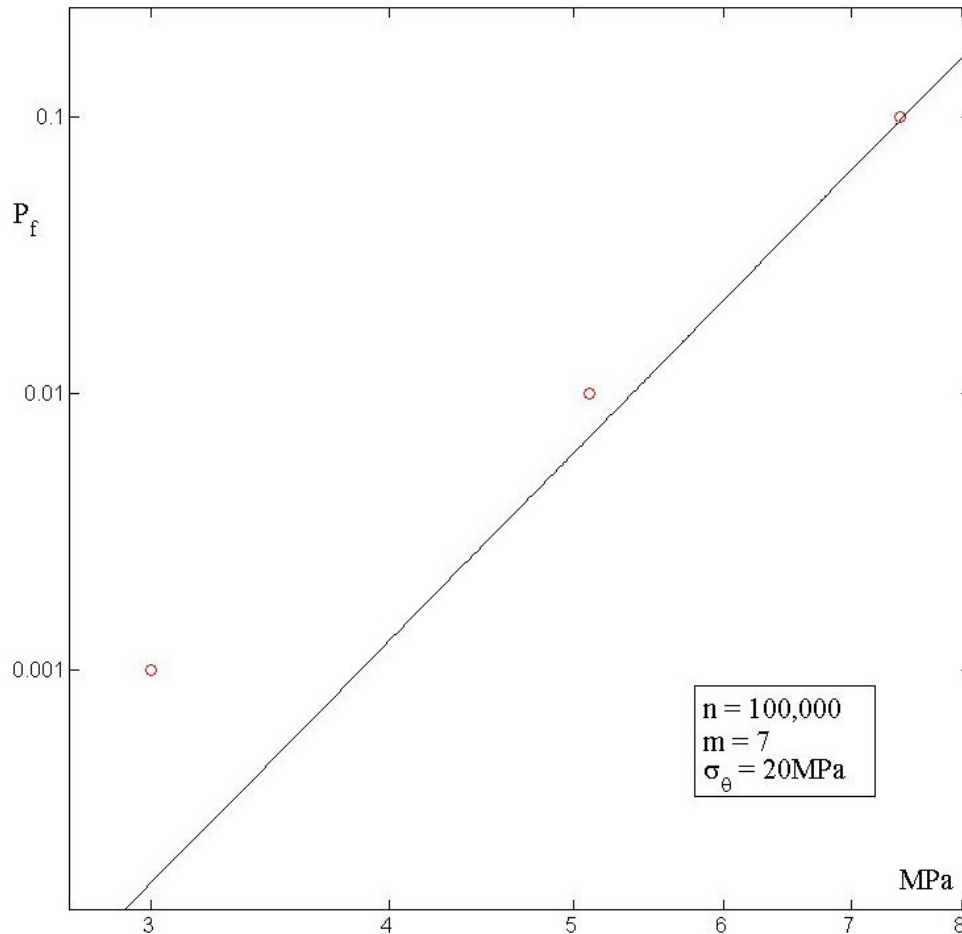


*Figure 6.1.5 Estimates from Monte Carlo simulations ( $n=100,000$ ) at Very Low (0.1%, 0.01% and 0.001%), Levels of Probability of Failure Compared to the Underlying Weibull Population Distribution ( $m = 7$  and  $\sigma_\theta = 20$  MPa)*

Fortunately there are numerical methods available to improve the computational fidelity of conventional Monte Carlo simulation in regions of low probability of failure.

One of the available methods is discussed in the next section.

## 6.2 The Concept of Importance Sampling Simulation

As noted above Monte Carlo simulation is computationally simple. To increase the accuracy of this numerical integration method the number of samples is simply increased. However, as Palko (1992) points out the method does not converge to correct answers in the low probability of failure regime even when utilizing a large number of simulations. As engineers we wish to design components with very low probabilities of failure. To work around the simulation difficulties at low probability of failure conventional Monte Carlo simulation can be modified using importance sampling. Using importance sampling techniques the design variable space is sampled only within the near vicinity of the most probable point (MPP – see Figure 6.2.1) point of failure. The location of the MPP is defined by the minimum distance from the origin of the design variable space (not the more familiar stress space) to the failure surface. In essence the MPP represents the value of the design random variable(s) at which failure is most likely to occur. This leads to the notion that more sampling of the parent population should take place in the most "important" region of the design variable space. The concept of the MPP is embedded in a technique known as fast probability integration (FPI). See Haldar and Mahadevan (2000) for a thorough discussion.

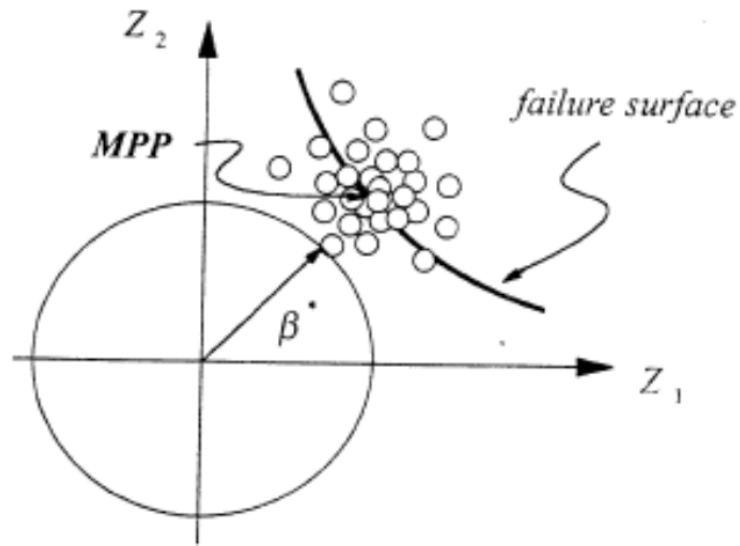


Figure 6.2.1 The Principal of the Importance Sampling

Importance sampling requires a general knowledge of the location of the MPP in the transformed variable space. This location is determined with FPI methods, so certain tools found in FPI methods are utilized here. First the transformed design variable space is constructed from a vector of “standard normal” random strength variables (see the figure above). A vector of standard normal random strength variables is defined as

$$Z_{\alpha} = \frac{(Y_{\alpha} - \mu_{f_{Y_{\alpha}}})}{\delta_{f_{Y_{\alpha}}}} \quad \alpha = 1, \dots, k \quad (6.2.1)$$

The vector of standard normal random strength variable,  $Z_{\alpha}$ , is directly dependent on the vector of parent random strength variables,  $Y_{\alpha}$ . Here  $\mu_{Y_{\alpha}}$  is the mean of the parent distribution and  $\delta_{Y_{\alpha}}$  is the standard deviation of the parent population. Assuming that each strength parameter is characterized by a two parameter Weibull distribution, and

with knowledge of the Weibull distribution parameters  $\sigma_\theta$  and  $m$  for each strength parameter, then the expression

$$\mu_{f_{y_\alpha}} = [(\sigma_\theta)_\alpha] \Gamma \left[ 1 + \frac{1}{(m)_\alpha} \right] \quad \alpha = 1, \dots, k \quad (6.2.2)$$

is used to compute the mean for each random strength variable (note that  $\Gamma$  is the gamma function). Note that vectors of distribution parameters, i.e.,  $m_\alpha$  and  $(\sigma_\theta)_\alpha$  are required, each pair corresponding to a particular strength random variable. The next expression

$$\delta_{f_{y_\alpha}} = [(\sigma_\theta)_\alpha]^2 \left\{ \Gamma \left( 1 + \frac{2}{m_\alpha} \right) - \left[ \Gamma \left( 1 + \frac{1}{m_\alpha} \right) \right]^2 \right\} \quad \alpha = 1, \dots, k \quad (6.2.3)$$

is used to calculate the standard deviation for each random strength variable. For completeness the following expression stipulates the probability density function for a vector of random strength variables characterized by a two parameter Weibull distribution

$$f_{Y_\alpha}(y_\alpha) = \frac{m_\alpha}{[\sigma_\theta]_\alpha} \left[ \frac{y_\alpha}{(\sigma_\theta)_\alpha} \right]^{m_\alpha - 1} \exp \left[ - \left[ \frac{y_\alpha}{(\sigma_\theta)_\alpha} \right]^{m_\alpha} \right] \quad \alpha = 1, \dots, k \quad (6.2.4)$$

The subscript  $\alpha$  is identified in various ways for each of the random strength variables adopted with a failure criterion, i.e., “ $T$ ”, “ $C$ ” and “ $BC$ ” ( $k=3$ ) for the isotropic version of the failure function. For the anisotropic version  $\alpha$  is identified with “ $YT$ ”, “ $YC$ ”, “ $TT$ ”, “ $TC$ ”, “ $BC$ ” and “ $MBC$ ” ( $k=6$ ). Assuming the strength random variables are statistically independent, then a joint probability density function can be formulated using the expression

$$f(y_\alpha) = \prod_{\alpha=1}^k f_{y_\alpha}(y_\alpha) \quad \alpha = 1, \dots, k \quad (6.2.5)$$

This notation is used momentarily.

If the limit state function is linearized and the design random variables can be transformed to standard normal variables then the reliability index  $\beta$  is used to locate the MPP – see Hu (1994), Wetherhold and Ucci (1994) as well as Haldar and Mahadevan (2000). However, determining the exact location of the MPP is not necessary to implement importance sampling – just a knowledge of the general vicinity of the MPP. An advantage of importance sampling relative to FPI methods is that importance sampling alleviates a potential non-conservative numerical error associated with FPI methods. The limit state function in this work is by no means a linear function in terms of the design random variables and when using FPI techniques the limit state function is approximated by a hyper-plane at the MPP. Wetherhold and Ucci (1994) point out that a planar approximation can yield non-conservative results depending on the curvature of the limit state function at the MPP. Since importance sampling does not depend on this curvature, it effectively avoids this potential non-conservative numerical error.

For importance sampling equation (6.1.4) is rearranged such that

$$P_f = \int_{\delta_f + \delta_f} I \frac{f(y_\alpha)}{k(y_\alpha)} k(y_\alpha) dy_\alpha \quad \alpha = 1, \dots, k \quad (6.2.6)$$

A new joint probability density function,  $k(y_\omega)$ , is introduced in the last expression. This function serves as a weighting function that forces the simulation process to sample in the

near vicinity of the MPP. This joint probability density function is formulated using the following expression

$$k(y_\alpha) = \prod_{\alpha=1}^n k_{Y_\alpha}(y_\alpha) \quad \alpha = 1, \dots, k \quad (6.2.7)$$

Although the procedure does not limit the type of probability distribution one can use for each individual random variable (the individual probability density function for each random variable is identified by  $k_{Y_\alpha}$ ) a standard normal distribution is assumed here for simplicity, i.e.,

$$\begin{aligned} k_{Y_\alpha} &= k_{Y_\alpha}(y_\alpha) \\ &= \left( \frac{1}{\delta_{k_{Y_\alpha}} \sqrt{2\pi}} \right) \exp \left[ -\frac{1}{2} \left( \frac{y_\alpha - \mu_{k_{Y_\alpha}}}{\delta_{k_{Y_\alpha}}} \right)^2 \right] \quad \alpha = 1, \dots, k \end{aligned} \quad (6.2.8)$$

An individual importance sampling function  $k_{Y_\alpha}$  should have the following properties:

1.  $k_{Y_\alpha} > 0$  whenever  $f(y_\alpha) \neq 0$ ;
2.  $k_{Y_\alpha}$  should be closely proportional to  $f(y_\alpha)$ , i.e., the importance sampling function should roughly have the same shape as the parent strength distribution; and
3. the importance sampling function should be selected such that values can be easily simulated from the function and the cumulative density function can be readily computed from the simulated value.

For demonstration purposes the standard normal distribution identified in equation (6.2.8)

was selected. This importance sampling function meets the three properties identified

above. Results for multiaxial simulations indicate that while the form of the function is appropriate, there is future efforts needed to better define how the variance (standard deviation) is computed. Note that

$$\mu_{k_{Y_\alpha}} \neq \mu_{f_{Y_\alpha}} \quad (6.2.9)$$

and

$$\delta_{k_{Y_\alpha}} \neq \delta_{f_{Y_\alpha}} \quad (6.2.10)$$

The mean associated with the standard normal probability density function  $k_{Y_\alpha}$  is given by the following expression

$$\mu_{k_{Y_\alpha}} = z_\alpha [\delta_{f(x)}] + \mu_{f(x)} \quad \alpha = 1, \dots, k \quad (6.2.11)$$

The parameters  $\mu_{f(x)}$  and  $\delta_{f(x)}$  are the mean and standard deviation associated with the actual probability distribution function that characterizes the random strength variable, i.e., the parent distribution  $f_X$ . Earlier the parent distribution for all the strength random variables was assumed to be a two parameter Weibull distribution and the parameters  $\mu_{f(x)}$  and  $\delta_{f(x)}$  are identified by equations 6.2.2 and 6.2.3. The standard deviation of the probability density function  $k_{Y_\alpha}$  is chosen in such a way that the sampling region is weighted towards the near vicinity of the MPP. Here an approach suggested by Melchers (1989) is adopted where

$$\delta_{k_{Y_\alpha}} = (1 \rightarrow 3) \left( \frac{\mu_{k_{Y_\alpha}}}{\mu_{f(x)}} \right) \delta_{f(x)} \quad \alpha = 1, \dots, k \quad (6.2.12)$$



As will be seen in the multiaxial simulations this approach for computing the standard deviation needs further optimization.

Given equation 6.2.5, the function  $k_{y_\alpha}$  serves as the parent probability density function for a transformed indicator function defined as

$$\hat{I} = I \frac{f(y_\alpha)}{k(y_\alpha)} \quad \alpha = 1, \dots, k \quad (6.2.13)$$

Equation (6.2.5) can be expressed as a Riemann sum, i.e.,

$$\begin{aligned} P_f &= E(I) \\ &= \lim_{n \rightarrow \infty} \left\{ \frac{1}{n} \sum_{j=1}^n I_j \left[ \frac{f(y_\alpha)}{k(y_\alpha)} \right] \right\} \\ &= \lim_{n \rightarrow \infty} \left\{ \frac{1}{n} \sum_{j=1}^n \hat{I}_j \right\} \end{aligned} \quad (6.2.14)$$

During a given simulation a separate random number is generated (the  $j^{\text{th}}$  random number) for each random strength variable and a realization for each of the random strength variables  $(Y_\alpha)_j$  is computed using the inverse of  $K_{y_\alpha}$  which is the cumulative distribution function corresponding to  $k_{y_\alpha}$ . These realizations are used to compute realizations of  $Z_\alpha$ , as well as individual values of  $k_{y_\alpha}$ ,  $f_{y_\alpha}$  and the limit state function  $g(y_\alpha)$ . The limit state function is dependent on the applied stress state, and the evaluation of  $g(y_\alpha)$  given the realization of the random variables  $(Y_\alpha)_j$  will once again yield a value of zero or one for the indicator function  $I$  in equation 6.2.11. Once the joint probability functions  $f(y_\alpha)$  and  $k(y_\alpha)$  are formulated the transformed indicator function is then computed from the same equation. This completes a simulation for the

$j^{th}$  iteration and the process is repeated  $n$  times. A mean is computed for the transformed indicator function after  $n$  iterations. This mean is an approximation of the probability of failure given the applied stress state and the statistical information associated with each strength random variable.

For a low probability of failure the main contribution to  $P_f$  will come from regions near the MPP. The reader is directed to Figure 3.7 in Hu (1994). This region will also correspond to the tail of the joint probability distribution function of the design strength random variables. Harbitz (1986) has shown that restricting the sampling domain in the design variable space to the tail of the joint probability distribution function produces a remarkable increase in efficiency in comparison to conventional Monte Carlo techniques. That efficiency is reproduced here.

Harbitz (1986) demonstrated that the number of simulations necessary to achieve the same order of accuracy obtained from conventional Monte Carlo methods is reduced by a factor of

$$\frac{1}{1 - \Gamma_{\alpha} \left[ (\beta^*)^2 \right]} \quad (6.2.15)$$

where  $\Gamma_{\alpha}$  is the chi-square distribution with  $\alpha$  degrees of freedom, and  $\beta^*$  is less than or equal to the actual the reliability index  $\beta$  for a given design problem. The degrees of freedom correspond to the number of design variables included in the limit state function. In essence, Harbitz (1986) reasoned that random design variables are being sampled from

a truncated distribution function. This corresponds to sampling from the actual probability distribution function, however the sampling domain is restricted to regions outside a sphere defined in the design variable space (see Figure 6.2.1). The center of the sphere is located at the origin of the transformed design variable space, and the radius of the sphere is equal to  $\beta^*$ . Proof of Harbitz (1986) argument follows from the interpretation of this geometrical concept. Elements of the FPI method is utilized to obtain approximate  $Z$  values in order to establish a general location of the MPP. For two random variables the location of the MPP is given by the expression

$$\beta = \left[ (z_1)^2 + (z_2)^2 \right]^{1/2} \quad (6.2.16)$$

where  $\beta$  is the reliability index. Three or more random variables would be a simple extension of this geometric concept.

The benefits of utilizing importance sampling can be seen in figure 6.2.2 and especially in figure 6.2.3. Figure 6.2.2 depicts the result from simple Monte Carlo simulation with 100 iterations (the open box) at uniaxial stress levels that correspond to the 5%, 50% and 95% levels of failure probability. Four points are depicted at the same levels of probability of failure. These points represent importance sampling with 100, 1,000, 10,000 and 100,000 iterations. The improvement in the low region of probability of failure, the region engineers wish to design in, is obvious with only 100 iterations.

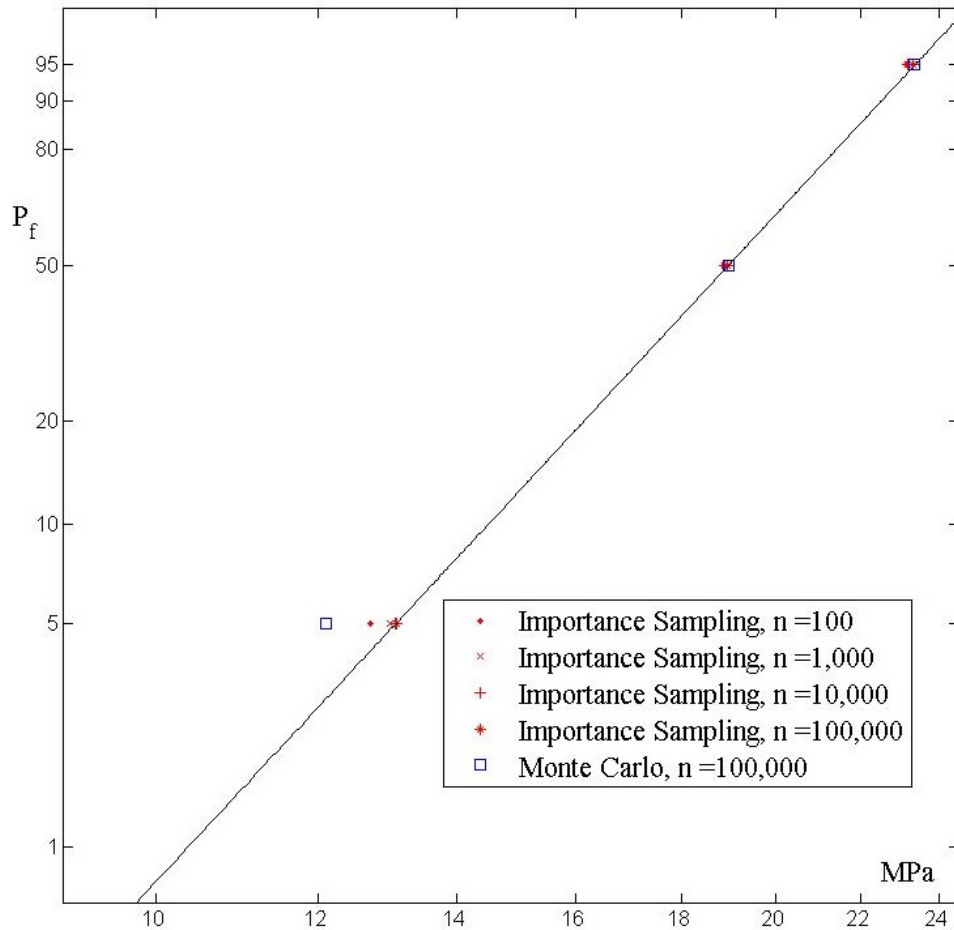


Figure 6.2.2 Reliability Estimates of Uniaxial Tensile Strengths Using Importance Sampling with 100 Simulations

Figure 6.2.3 depicts the results from simple Monte Carlo simulation with 100,000 iterations (the open box). The other four points at the 0.1%, 0.01% and 0.001% levels of probability of failure represent importance sampling with 100, 1,000, 10,000 and 100,000 iterations. The improvement in the low region of probability of failure is quite stark with only 100 iterations. At 100,000 iterations simple Monte Carlo simulation is well off the line representing the parent population while at 100 iterations importance sampling is nearly on the line at 0.001% probability of failure and on the line at the other

two probability of failure. In essence increasing the iterations above 100 the level does not greatly improve the prediction relative to the parent population. Here is the advantage of conducting Monte Carlo simulation with importance sampling – a numerical savings by incurred by dramatically decreasing the number of simulations required to produce high quality results.

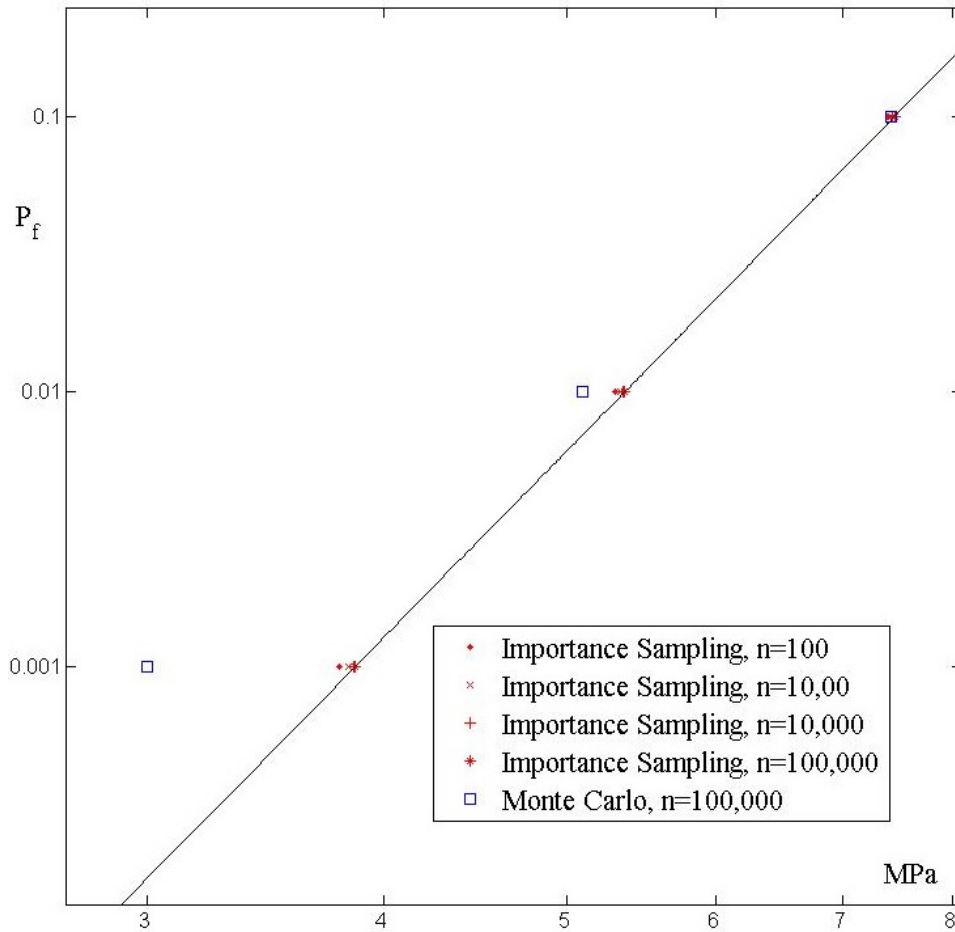


Figure 6.2.3 Reliability Estimates of Uniaxial Tensile Strengths Using Importance Sampling with 1,000 Simulations

### 6.3 Isotropic Limit State Function – Importance Sampling

The concept of importance sampling is first applied to the isotropic form of the limit state function. The tensile strength design variable ( $Y_T$ ), compressive strength design variable ( $Y_C$ ) and the biaxial compressive strength design variable ( $Y_{BC}$ ) are characterized by the two-parameter Weibull distributions. To begin the method the approximate location of the MPP must be determined. Methods to locate the MPP can be found in Haldar and Mahadevan (2000) as well as Hu (1994). The location of the MPP is determined through realizations of standard normal variables  $Z_T$ ,  $Z_C$  and  $Z_{BC}$ . With these realizations serving as the components of a vector, the MPP is located by this vector. The information regarding the MPP establishes the means for the importance sampling density functions  $k_{Y_T}$ ,  $k_{Y_C}$  and  $k_{Y_{BC}}$ . The importance sampling density functions facilitate obtaining samples in the near vicinity of the MPP through simulation. Once the means  $\mu_{k_{Y_T}}$ ,  $\mu_{k_{Y_C}}$  and  $\mu_{k_{Y_{BC}}}$  for the importance sampling density functions are computed using equation (6.2.11) then the values  $\delta_{k_{Y_T}} (\neq \delta_{f_{Y_T}})$ ,  $\delta_{k_{Y_C}} (\neq \delta_{f_{Y_C}})$  and  $\delta_{k_{Y_{BC}}} (\neq \delta_{f_{Y_{BC}}})$  are established using equation (6.2.12). These are the variances of the importance sampling density functions and not the variances of the random strength density functions. Use of equations (6.2.11) and (6.2.12) require the knowledge of the means from the parent Weibull strength distributions, i.e.,  $\mu_{f_{Y_T}}$ ,  $\mu_{f_{Y_C}}$  and  $\mu_{f_{Y_{BC}}}$  as well as the standard deviations of the parent Weibull strength distributions, i.e.,  $\delta_{f_{Y_T}}$ ,  $\delta_{f_{Y_C}}$  and  $\delta_{f_{Y_{BC}}}$ . These are assumed known.

Once the means and standard deviations are obtained for each importance sampling density function the next step requires three separate and distinct random numbers between zero and one. These random numbers serve as values for  $K_{Y_T}$  in the expression

$$K_{Y_T}(y_T) = \frac{1}{2} \left[ 1 + \operatorname{erf} \left( \frac{y_T - \mu_{k_{Y_T}}}{\delta_{k_{Y_T}} \sqrt{2}} \right) \right] \quad (6.3.1)$$

as well as  $K_{Y_C}$  in the expression

$$K_{Y_C}(y_C) = \frac{1}{2} \left[ 1 + \operatorname{erf} \left( \frac{y_C - \mu_{k_{Y_C}}}{\delta_{k_{Y_C}} \sqrt{2}} \right) \right] \quad (6.3.2)$$

and  $K_{Y_{BC}}$  in the expression

$$K_{Y_{BC}}(y_{BC}) = \frac{1}{2} \left[ 1 + \operatorname{erf} \left( \frac{y_{BC} - \mu_{k_{Y_{BC}}}}{\delta_{k_{Y_{BC}}} \sqrt{2}} \right) \right] \quad (6.3.3)$$

Here “*erf*” is the error function. The only unknowns in these expressions are the realizations of the random strength variables  $Y_T$ ,  $Y_C$  and  $Y_{BC}$ . The last three expressions are solved for these realizations.

Having realizations  $y_T$ ,  $y_C$  and  $y_{BC}$  along with means  $\mu_{k_{Y_T}}$ ,  $\mu_{k_{Y_C}}$  and  $\mu_{k_{Y_{BC}}}$  as well as variances  $\delta_{k_{Y_T}}$ ,  $\delta_{k_{Y_C}}$  and  $\delta_{k_{Y_{BC}}}$  then values of the importance sampling probability density function

$$k_{Y_T}(y_T) = \left( \frac{1}{\delta_{k_{Y_T}} \sqrt{2\pi}} \right) \exp \left[ -\frac{1}{2} \left( \frac{y_T - \mu_{k_{Y_T}}}{\delta_{k_{Y_T}}} \right)^2 \right] \quad (6.3.4)$$

the importance sampling probability density function

$$k_{Y_C}(y_C) = \left( \frac{1}{\delta_{k_{Y_C}} \sqrt{2\pi}} \right) \exp \left[ -\frac{1}{2} \left( \frac{y_C - \mu_{k_{Y_C}}}{\delta_{k_C}} \right)^2 \right] \quad (6.3.5)$$

and the Importance sampling probability density function

$$k_{Y_{BC}}(y_{BC}) = \left( \frac{1}{\delta_{k_{Y_{BC}}} \sqrt{2\pi}} \right) \exp \left[ -\frac{1}{2} \left( \frac{y_{BC} - \mu_{k_{Y_{BC}}}}{\delta_{k_{BC}}} \right)^2 \right] \quad (6.3.6)$$

can be computed. The value of the joint importance sampling probability function for the  $j^{th}$  simulation is then ascertained using

$$k_j(Y_T, Y_C, Y_{BC}) = [k_{Y_T}(y_T)]_j [k_{Y_C}(y_C)]_j [k_{Y_{BC}}(y_{BC})]_j \quad (6.3.6)$$

This joint importance probability sampling function is presumed centered over the MPP.

Realizations for the random strength variables  $Y_T$ ,  $Y_C$  and  $Y_{BC}$  along with Weibull parameter ( $m$ ,  $\sigma_\theta$ ) for each random strength variable are then used to evaluate the probability of density function

$$f_{Y_T}(y_T) = \frac{m_T}{[\sigma_\theta]_T} \left[ \frac{y_T}{(\sigma_\theta)_T} \right]^{m_T-1} \exp \left[ -\left[ \frac{y_T}{(\sigma_\theta)_T} \right]^{m_T} \right] \quad (6.3.7)$$

as well as

$$f_{Y_C}(y_C) = \frac{m_C}{[\sigma_\theta]_C} \left[ \frac{y_C}{(\sigma_\theta)_C} \right]^{m_C-1} \exp \left[ -\left[ \frac{y_C}{(\sigma_\theta)_C} \right]^{m_C} \right] \quad (6.3.8)$$

and

$$f_{Y_{BC}}(y_{BC}) = \frac{m_{BC}}{[\sigma_\theta]_{BC}} \left[ \frac{y_{BC}}{(\sigma_\theta)_{BC}} \right]^{m_{BC}-1} \exp \left[ -\left[ \frac{y_{BC}}{(\sigma_\theta)_{BC}} \right]^{m_{BC}} \right] \quad (6.3.9)$$

respectively. A numerical value for the joint probability density

$$f_j(Y_T, Y_C, Y_{BC}) = [f_{Y_T}(y_T)]_j [f_{Y_C}(y_C)]_j [f_{Y_{BC}}(y_{BC})]_j \quad (6.3.10)$$



can be computed.

Finally, a value for the limit state function is computed using equations (4.3.2), (4.3.10), (4.3.24) as well as (4.3.36) with the state of stress at the point in a component being evaluated and the realizations of the random strength variables. This allows the computation of the indicator function using equation (6.1.3). The quantities  $k_j(y_T, y_C, y_{BC})$ ,  $f_j(y_T, y_C, y_{BC})$  and  $I$  are inserted into equation (6.2.13) and the summation in equation (6.2.14) is performed for a sufficient number of iterations (i.e., large enough  $n$ ) such that the method converges to  $P_f$ .

The importance sampling process is put to use in the following manner. Projections of reliability surfaces are presented in a series of figures, i.e., Figures 6.3.1 through 6.3.4, for the isotropic formulation of the limit state function outlined in a previous section. The Weibull parameters ( $m$  and  $\sigma_\theta$ ) for each random strength design variable are

$$\begin{aligned} m_T &= 6.58 & m_C &= 12.29 & m_{BC} &= 13.99 \\ (\sigma_\theta)_T &= 17.05 \text{ MPa} & (\sigma_\theta)_C &= 54.39 \text{ MPa} & (\sigma_\theta)_{BC} &= 63.29 \text{ MPa} \end{aligned}$$

for isotropy. These values were extracted from the data from Burchell et al. (2007) assuming isotropy. Three surfaces depicted in the figures correspond to probabilities of failure of  $P_f = 5\%$ ,  $P_f = 50\%$ , and  $P_f = 95\%$ . These contours are determined numerically by probing the  $\sigma_{11} - \sigma_{22}$  stress space along rays emanating from the origin in an incremental fashion.

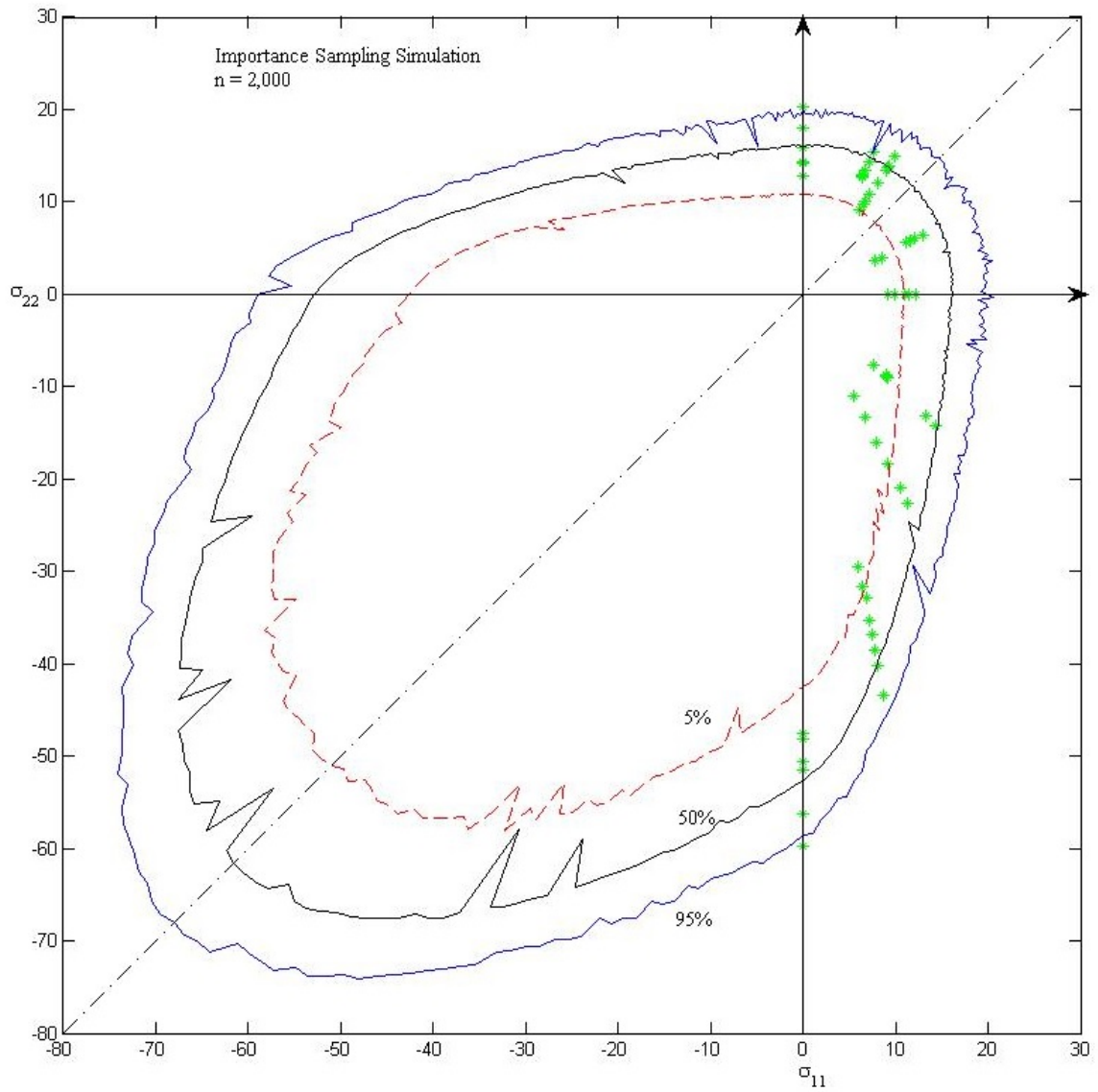


*Figure 6.3.1 Level Surfaces of Probability of Failure Obtained Using 2,000 Monte Carlo Simulations Modified with Importance Sampling Techniques for the Isotropic Version of the Failure Criterion. The Failure Data from Burchell et al. (2007) is Also Shown.*

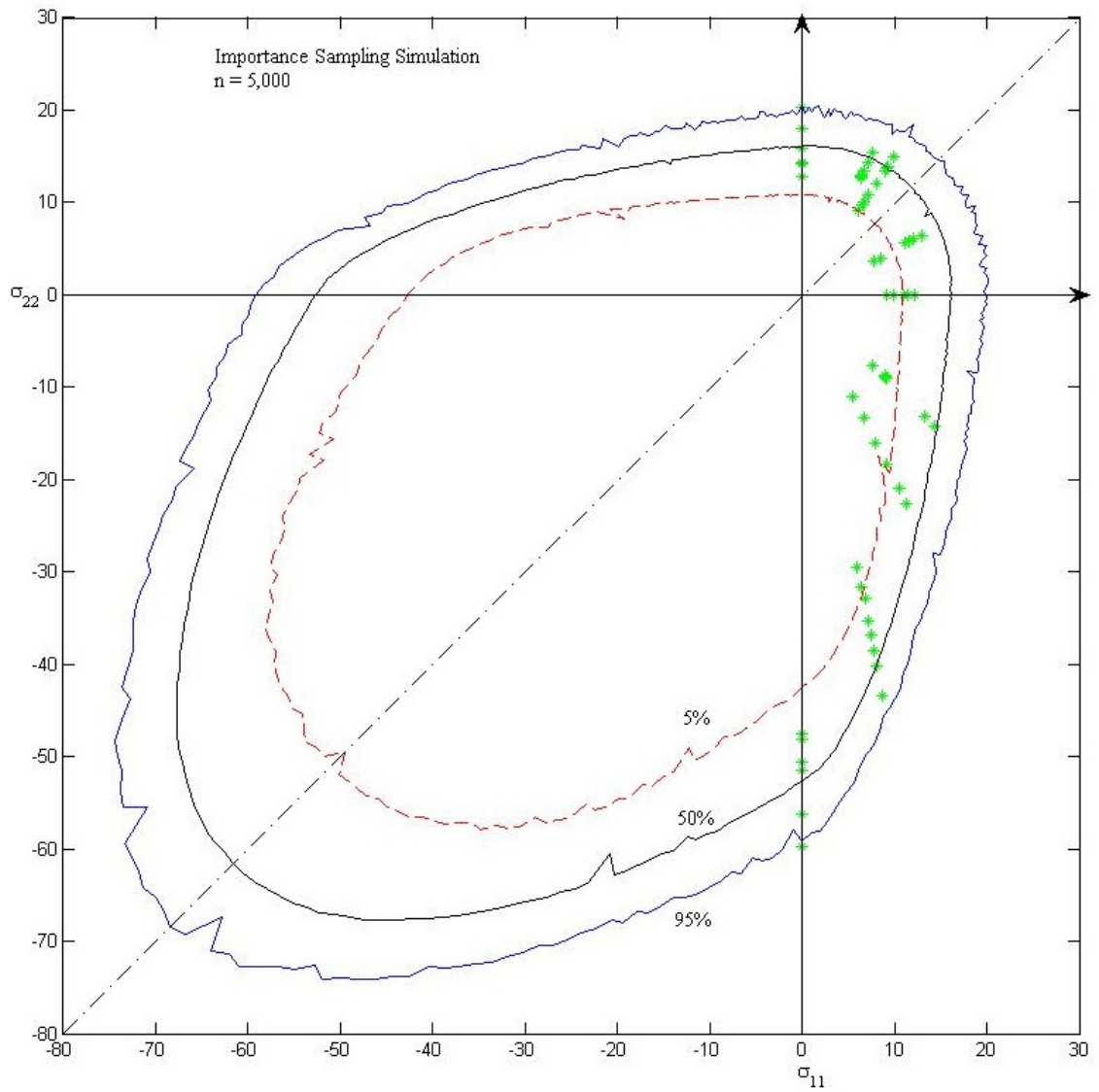


*Figure 6.3.2 Level Surfaces of Probability of Failure Obtained Using 5,000 Monte Carlo Simulations Modified with Importance Sampling Techniques for the Isotropic Version of the Failure Criterion. The Failure Data from Burchell et al. (2007) is Also Shown.*

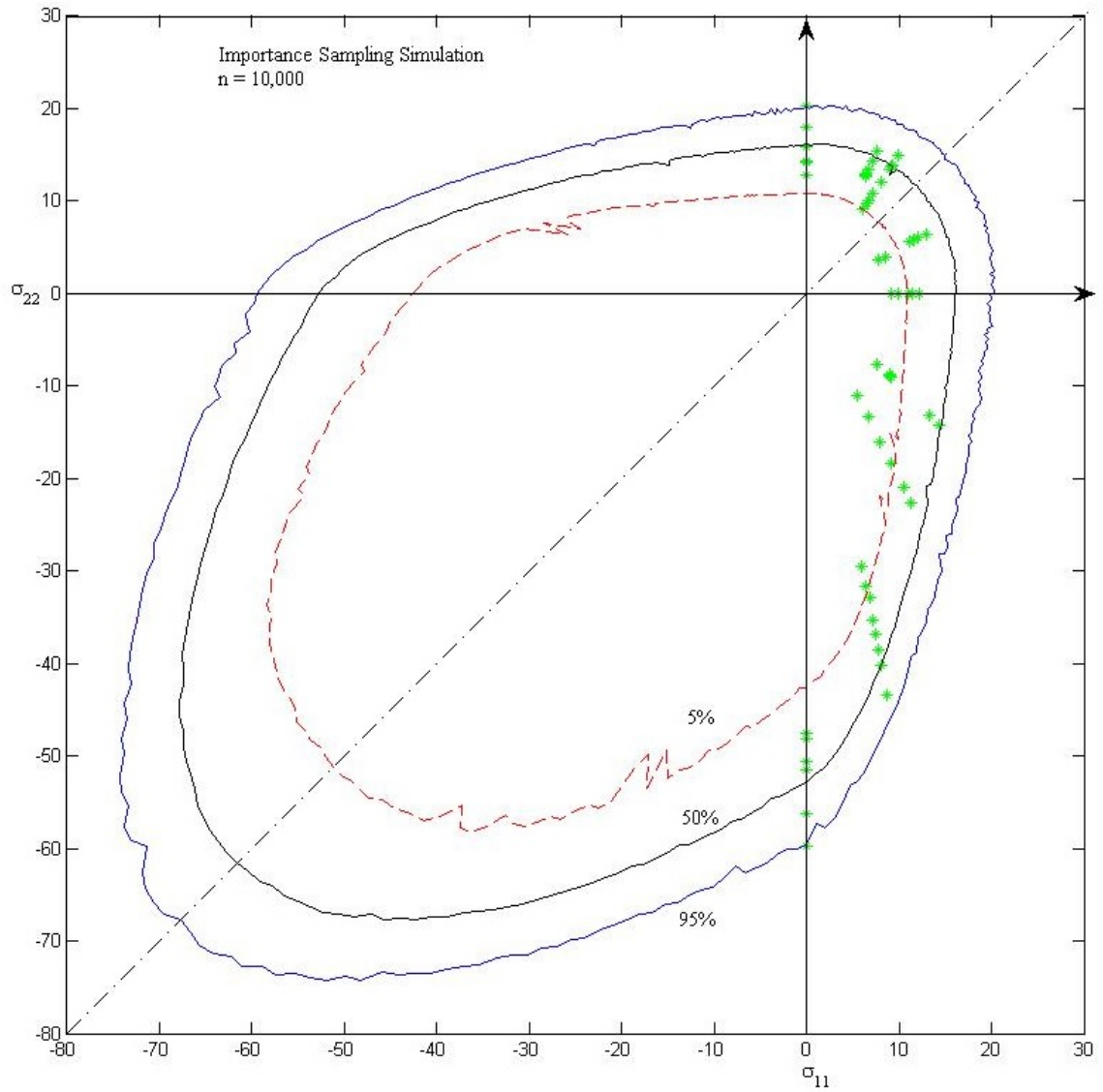


*Figure 6.3.3 Level Surfaces of Probability of Failure Obtained Using 10,000 Monte Carlo Simulations Modified with Importance Sampling Techniques for the Isotropic Version of the Failure Criterion. The Failure Data from Burchell et al. (2007) is Also Shown.*

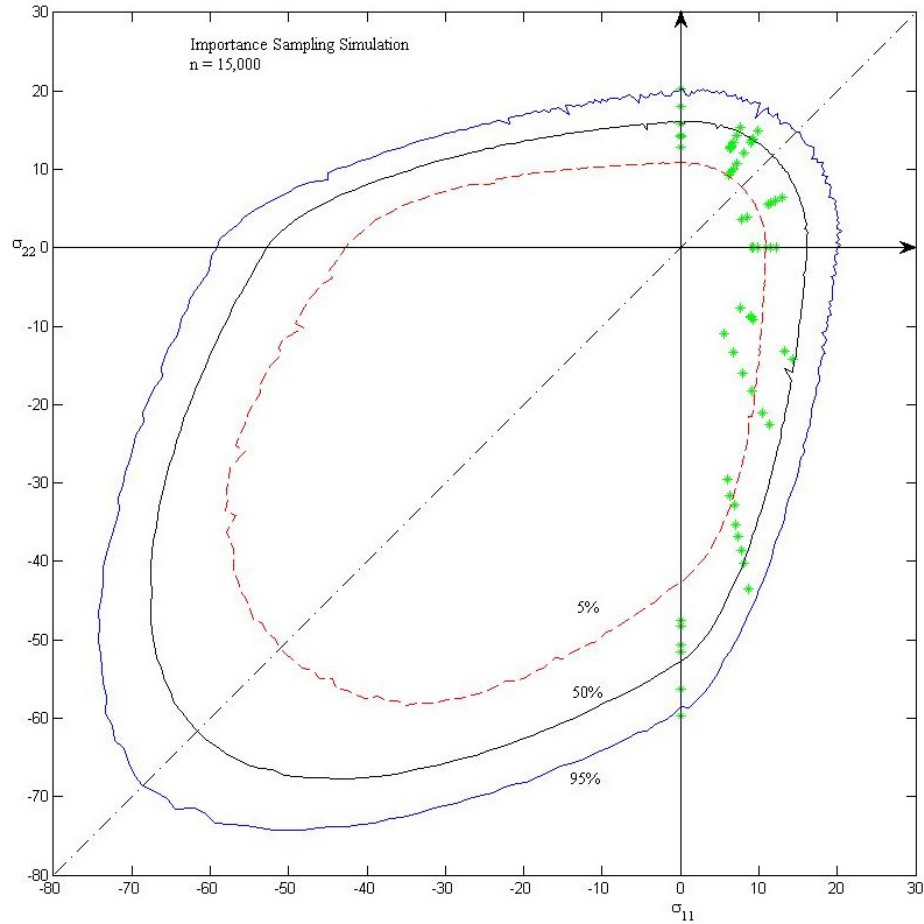


*Figure 6.3.4 Failure Probability Curves Obtained Using Monte Carlo Simulation Modified with Importance Sampling Techniques for the Isotropic Version of the Failure Criterion. The Failure Data from Burchell et al. (2007) is Also Shown.*

In the figures just presented the contours are symmetric with a line that bisects the first and third quadrant. This is due to isotropy. No such symmetry exists with respect to a line that bisects the second and third quadrant since the material strength behavior is different in tension and compression. Material anisotropy, in particular transverse isotropy, is explored in the next section. With each figure the number of simulations was increased from  $n = 2,000$  in Figure 6.3.1 to  $n = 15,000$  in Figure 6.3.4. The “noise”

or irregularities around the level surfaces of probability of failure decreases with each increase in the number of simulations.

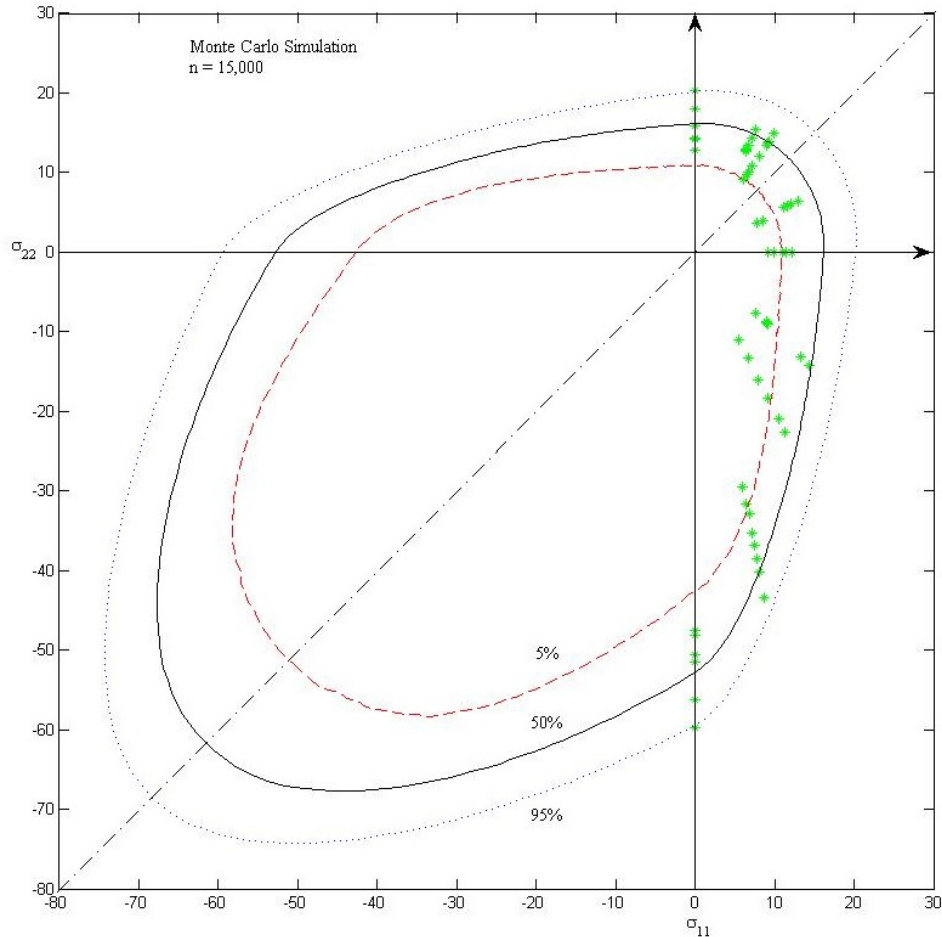


*Figure 6.3.5 Failure Probability Curves Obtained Using only Monte Carlo Simulation for the Isotropic Version of the Failure Criterion. The Failure Data from Burchell et al. (2007) is Also Shown.*

In Figure 6.3.5 the same level surfaces of probability of failure are established without the use of importance sampling, i.e., the curves were found using only Monte Carlo simulation. In this figure and Figure 6.3.4 note that 15,000 simulations were utilized to establish each point on the failure probability curves. The irregularities were smoothed out by increasing the number of simulations. Earlier it was indicated that

importance sampling is sensitive to the importance sampling function, i.e.,  $k_{Y_\alpha}$ . It is suspected that the irregularities in the probability of failure surfaces can also be smoothed out with a more optimal choice in the standard deviation used for  $k_{Y_\alpha}$ . Time did not permit conducting an optimization study for this parameter, and this effort is left for others to conduct. Methods suggested in Xue et al. (2013) would be an appropriate starting point. Once an optimization procedure has been established to compute a standard deviation for the importance sampling function representing each random strength variable it is anticipated that smooth curves can be obtained with fewer simulations. It is clearly evident that increasing the number of simulations improves the results obtained using importance sampling techniques. This is true for common Monte Carlo simulation techniques as well – up to a point. At very low probability failures it was clear (see Figure 6.2.3) that improving Monte Carlo simulation results was impractical by simply increasing the number of simulations. This indicates that importance sampling is the preferred method of computing equation (6.1.1) for typical designs where the probability of failure is quite low for economic and/or safety reasons.

#### 6.4 Anisotropic Limit State Functions – Importance Sampling

Next the concept of importance sampling is applied to the anisotropic form of the limit state function. The tensile strength design variable in the preferred material direction ( $Y_{YT}$ ), the compressive strength design variable in the preferred material

direction ( $Y_{YC}$ ), the equal biaxial compressive strength design variable in the plane of isotropy ( $Y_{BC}$ ), the tensile strength design variable in plane of isotropy ( $Y_{TT}$ ), the compressive strength design variable in plane of isotropy ( $Y_{TC}$ ), as well as the equal biaxial compressive strength design random variable with one stress component in the plane of isotropy ( $Y_{MBC}$ ) are characterized by the two-parameter Weibull distributions.

To begin the method the approximate location of the MPP must be determined. The location of the MPP is determined through the realizations  $z_{TT}$ ,  $z_{TC}$ ,  $z_{BC}$ ,  $z_{YT}$ ,  $z_{YC}$  and  $z_{MBC}$ . By equation (6.2.1) all six are realizations of standard normal variables. With these realizations serving as the components of a vector in the design variable space, the MPP is located by this vector. The information regarding the MPP establishes the means for the importance sampling density functions. Again, the importance sampling density functions facilitate obtaining samples in the near vicinity of the MPP during simulation. Once the means  $\mu_{k_{YTT}}$ ,  $\mu_{k_{YTC}}$ ,  $\mu_{k_{YBC}}$ ,  $\mu_{k_{YYT}}$ ,  $\mu_{k_{YYC}}$  and  $\mu_{k_{YMBC}}$  are computed using equation (6.2.11) then the values  $\delta_{k_{YTT}}$ ,  $\delta_{k_{YTC}}$ ,  $\delta_{k_{YBC}}$ ,  $\delta_{k_{YYT}}$ ,  $\delta_{k_{YYC}}$  and  $\delta_{k_{YMBC}}$  are established using equation (6.2.12). These last six parameters are the variances of the importance sampling density function. Use of equations (6.2.11) and (6.2.12) requires the knowledge of the means from the parent Weibull strength distributions, i.e.,  $\mu_{f_{YTT}}$ ,  $\mu_{f_{YTC}}$ ,  $\mu_{f_{YBC}}$ ,  $\mu_{f_{YYT}}$ ,  $\mu_{f_{YYC}}$  and  $\mu_{f_{YMBC}}$  as well as the standard deviations of the parent Weibull strength distributions, i.e.,  $\delta_{f_{YTT}}$ ,  $\delta_{f_{YTC}}$ ,  $\delta_{f_{YBC}}$ ,  $\delta_{f_{YYT}}$ ,  $\delta_{f_{YYC}}$  and  $\delta_{f_{YMBC}}$ .



Once the means and standard deviations are obtained for each importance sampling density function the next step requires six separate and distinct random numbers between zero and one. These will serve as values for  $K_{Y_{TT}}$  in the expression

$$K_{Y_{TT}} = \frac{1}{2} \left[ 1 + \operatorname{erf} \left( \frac{y_{TT} - \mu_{Y_{TT}}}{\sigma_{Y_{TT}} \sqrt{2}} \right) \right] \quad (6.4.1)$$

for  $K_{Y_{TC}}$  in the expression

$$K_{Y_{TC}} = \frac{1}{2} \left[ 1 + \operatorname{erf} \left( \frac{y_{TC} - \mu_{Y_{TC}}}{\sigma_{Y_{TC}} \sqrt{2}} \right) \right] \quad (6.4.2)$$

for  $K_{Y_{BC}}$  in the expression

$$K_{Y_{BC}} = \frac{1}{2} \left[ 1 + \operatorname{erf} \left( \frac{y_{BC} - \mu_{Y_{BC}}}{\sigma_{Y_{BC}} \sqrt{2}} \right) \right] \quad (6.4.3)$$

for  $K_{Y_{YT}}$  in the expression

$$K_{Y_{YT}} = \frac{1}{2} \left[ 1 + \operatorname{erf} \left( \frac{y_{YT} - \mu_{Y_{YT}}}{\sigma_{Y_{YT}} \sqrt{2}} \right) \right] \quad (6.4.5)$$

for  $K_{Y_{YC}}$  in the expression

$$K_{Y_{YC}} = \frac{1}{2} \left[ 1 + \operatorname{erf} \left( \frac{y_{YC} - \mu_{Y_{YC}}}{\sigma_{Y_{YC}} \sqrt{2}} \right) \right] \quad (6.4.6)$$

and for  $K_{Y_{MBC}}$  in the expression

$$K_{Y_{MBC}} = \frac{1}{2} \left[ 1 + \operatorname{erf} \left( \frac{y_{MBC} - \mu_{Y_{MBC}}}{\sigma_{Y_{MBC}} \sqrt{2}} \right) \right] \quad (6.4.7)$$

The only unknowns in these expressions are the realizations of the random strength variables  $Y_{TT}$ ,  $Y_{TC}$ ,  $Y_{BC}$ ,  $Y_{YT}$ ,  $Y_{YC}$  and  $Y_{MBC}$ . These realizations are obtained by inverting the last six expressions for these quantities.

Having realizations  $y_{TT}$ ,  $y_{TC}$ ,  $y_{BC}$ ,  $y_{YT}$ ,  $y_{YC}$  and  $y_{MBC}$  along with means

$\mu_{k_{y_{TT}}}$ ,  $\mu_{k_{y_{TC}}}$ ,  $\mu_{k_{y_{BC}}}$ ,  $\mu_{k_{y_{YT}}}$ ,  $\mu_{k_{y_{YC}}}$  and  $\mu_{k_{y_{MBC}}}$  as well as variances  $\delta_{k_{y_{TT}}}$ ,  $\delta_{k_{y_{TC}}}$ ,  $\delta_{k_{y_{BC}}}$ ,  $\delta_{k_{y_{YT}}}$ ,  $\delta_{k_{y_{YC}}}$  and  $\delta_{k_{y_{MBC}}}$  then values of the sampling probability density functions

$$k_{y_{TT}}(y_{TT}) = \left( \frac{1}{\delta_{k_{y_{TT}}} \sqrt{2\pi}} \right) \exp \left[ -\frac{1}{2} \left( \frac{y_{TT} - \mu_{k_{y_{TT}}}}{\delta_{k_{y_{TT}}}} \right)^2 \right] \quad (6.4.8)$$

$$k_{y_{TC}}(y_{TC}) = \left( \frac{1}{\delta_{k_{y_{TC}}} \sqrt{2\pi}} \right) \exp \left[ -\frac{1}{2} \left( \frac{y_{TC} - \mu_{k_{y_{TC}}}}{\delta_{k_{y_{TC}}}} \right)^2 \right] \quad (6.4.9)$$

$$k_{y_{BC}}(y_{BC}) = \left( \frac{1}{\delta_{k_{y_{BC}}} \sqrt{2\pi}} \right) \exp \left[ -\frac{1}{2} \left( \frac{y_{BC} - \mu_{k_{y_{BC}}}}{\delta_{k_{y_{BC}}}} \right)^2 \right] \quad (6.4.10)$$

$$k_{y_{YT}}(y_{YT}) = \left( \frac{1}{\delta_{k_{y_{YT}}} \sqrt{2\pi}} \right) \exp \left[ -\frac{1}{2} \left( \frac{y_{YT} - \mu_{k_{y_{YT}}}}{\delta_{k_{y_{YT}}}} \right)^2 \right] \quad (6.4.11)$$

$$k_{y_{YC}}(y_{YC}) = \left( \frac{1}{\delta_{k_{y_{YC}}} \sqrt{2\pi}} \right) \exp \left[ -\frac{1}{2} \left( \frac{y_{YC} - \mu_{k_{y_{YC}}}}{\delta_{k_{y_{YC}}}} \right)^2 \right] \quad (6.4.12)$$

as well as

$$k_{y_{MBC}}(y_{MBC}) = \left( \frac{1}{\delta_{k_{y_{MBC}}} \sqrt{2\pi}} \right) \exp \left[ -\frac{1}{2} \left( \frac{y_{MBC} - \mu_{k_{y_{MBC}}}}{\delta_{k_{y_{MBC}}}} \right)^2 \right] \quad (6.4.13)$$

can be computed. The value of the joint probability sampling function for the  $j^{th}$

simulation is then ascertained using

$$\begin{aligned} & k_j(Y_{TT}, Y_{TC}, Y_{BC}, Y_{YT}, Y_{YC}, Y_{MBC}) \\ &= [k_{y_{TT}}(y_{TT})]_j [k_{y_{TC}}(y_{TC})]_j [k_{y_{BC}}(y_{BC})]_j [k_{y_{YT}}(y_{YT})]_j [k_{y_{YC}}(y_{YC})]_j [k_{y_{MBC}}(y_{MBC})]_j \end{aligned} \quad (6.4.14)$$

This joint probability sampling function is centered over the MPP

Realizations for the random strength variables  $Y_{TT}$ ,  $Y_{TC}$ ,  $Y_{BC}$ ,  $Y_{YT}$ ,  $Y_{YC}$  and  $Y_{MBC}$  along with Weibull parameter ( $m$ ,  $\sigma_\theta$ ) for each random strength variable are then used to evaluate the probability of density function

$$f_{Y_{TT}}(y_{TT}) = \frac{m_{TT}}{(\sigma_\theta)_{TT}} \left[ \frac{y_{TT}}{(\sigma_\theta)_{TT}} \right]^{m_{TT}-1} \exp \left[ - \left[ \frac{y_{TT}}{(\sigma_\theta)_{TT}} \right]^{m_{TT}} \right] \quad (6.4.15)$$

$$f_{Y_{TC}}(y_{TC}) = \frac{m_{TC}}{(\sigma_\theta)_{TC}} \left[ \frac{y_{TC}}{(\sigma_\theta)_{TC}} \right]^{m_{TC}-1} \exp \left[ - \left[ \frac{y_{TC}}{(\sigma_\theta)_{TC}} \right]^{m_{TC}} \right] \quad (6.4.16)$$

$$f_{Y_{BC}}(y_{BC}) = \frac{m_{BC}}{(\sigma_\theta)_{BC}} \left[ \frac{y_{BC}}{(\sigma_\theta)_{BC}} \right]^{m_{BC}-1} \exp \left[ - \left[ \frac{y_{BC}}{(\sigma_\theta)_{BC}} \right]^{m_{BC}} \right] \quad (6.4.17)$$

$$f_{Y_{YT}}(y_{YT}) = \frac{m_{YT}}{(\sigma_\theta)_{YT}} \left[ \frac{y_{YT}}{(\sigma_\theta)_{YT}} \right]^{m_{YT}-1} \exp \left[ - \left[ \frac{y_{YT}}{(\sigma_\theta)_{YT}} \right]^{m_{YT}} \right] \quad (6.4.18)$$

$$f_{Y_{YC}}(y_{YC}) = \frac{m_{YC}}{(\sigma_\theta)_{YC}} \left[ \frac{y_{YC}}{(\sigma_\theta)_{YC}} \right]^{m_{YC}-1} \exp \left[ - \left[ \frac{y_{YC}}{(\sigma_\theta)_{YC}} \right]^{m_{YC}} \right] \quad (6.4.19)$$

and

$$f_{Y_{MBC}}(y_{MBC}) = \frac{m_{MBC}}{(\sigma_\theta)_{MBC}} \left[ \frac{y_{MBC}}{(\sigma_\theta)_{MBC}} \right]^{m_{MBC}-1} \exp \left[ - \left[ \frac{y_{MBC}}{(\sigma_\theta)_{MBC}} \right]^{m_{MBC}} \right] \quad (6.4.20)$$

respectively. A numerical value for the joint probability density

$$\begin{aligned} f_j(Y_{TT}, Y_{TC}, Y_{BC}, Y_{YT}, Y_{YC}, Y_{MBC}) \\ = [f_{Y_{TT}}(y_{TT})]_j [f_{Y_{TC}}(y_{TC})]_j [f_{Y_{BC}}(y_{BC})]_j \\ \cdot [f_{Y_{YT}}(y_{YT})]_j [f_{Y_{YC}}(y_{YC})]_j [f_{Y_{MBC}}(y_{MBC})]_j \end{aligned} \quad (6.4.21)$$

is computed.

Finally, a value for the limit state function is computed using equations (5.2.1), (5.2.13), (5.2.30) as well as (5.2.43) with the state of stress at the point in a component being evaluated and the realizations of the random strength variables. This allows the computation of the indicator function using equation (6.1.3). The quantities  $k_j(y_{TT}, y_{TC}, y_{BC}, y_{YT}, y_{YC}, y_{MBC})$ ,  $f_j(y_{TT}, y_{TC}, y_{BC}, y_{YT}, y_{YC}, y_{MBC})$  and  $I$  are inserted into equation (6.2.13) and the summation in equation (6.2.14) is performed for a sufficient number of iterations (i.e., large enough  $n$ ) such that the method converges appropriately to  $P_f$ .

Figure 6.4.1 depicts the reliability surfaces for the anisotropic version of the limit state function. Monte Carlo simulations with importance sampling were conducted in order to generate the surfaces in this figure. For anisotropy the Weibull distribution parameters for each random strength variable are listed in Table 6.4.1. Again three reliability surfaces are depicted in the figure that correspond to probabilities of failure of  $P_f = 5\%$ ,  $P_f = 50\%$ , and  $P_f = 95\%$ . The preferred direction of the material coincides with the  $\sigma_{11}$  axis. Thus there is a strengthening of the material along the  $\sigma_{11}$  – axis which is exhibited in the data from Burchell et al. (2007). The three curves bracket the data from Burchell et al. (2007) along both the tensile and compressive  $\sigma_{11}$  axes. This reliability model captures this strengthening in compression as it did with the isotropic model. The positions of the curve can be adjusted by information from the failure data along both the  $\sigma_{11}$  and  $\sigma_{22}$  axes – tensile information as well as compression information.

This gives an indication of the flexibility inherent in the model by the ability to accommodate for failure behavior in different material orientations.

There is “noise” present once again. It is quite evident in the third quadrant along the 95% failure probability curve. Again, it is anticipated that the irregularities can be smoothed out with a “better” importance sampling density function – that is, with optimized variances for the sampling functions identified above.

**Table 6.4.1 Anisotropic Weibull Parameters**

Tensile strength, preferred direction	$m_{YT} = 6.58$	$(\sigma_{\theta})_{YT} = 17.05 \text{ MPa}$
Compression strength, preferred direction	$m_{YC} = 12.19$	$(\sigma_{\theta})_{YC} = 54.39 \text{ MPa}$
Tensile strength, plane of isotropy	$m_{TT} = 10.12$	$(\sigma_{\theta})_{TT} = 11.01 \text{ MPa}$
Compression strength, plane of isotropy	$m_{TC} = 10.33$	$(\sigma_{\theta})_{TC} = 35.90 \text{ MPa}$
Equal biaxial compression both stress components in the plane of isotropy	$m_{BC} = 11.85$	$(\sigma_{\theta})_{BC} = 45.95 \text{ MPa}$
Equal biaxial compression, one stress component in the plane of isotropy	$m_{MBC} = 13.99$	$(\sigma_{\theta})_{MBC} = 63.29 \text{ MPa}$

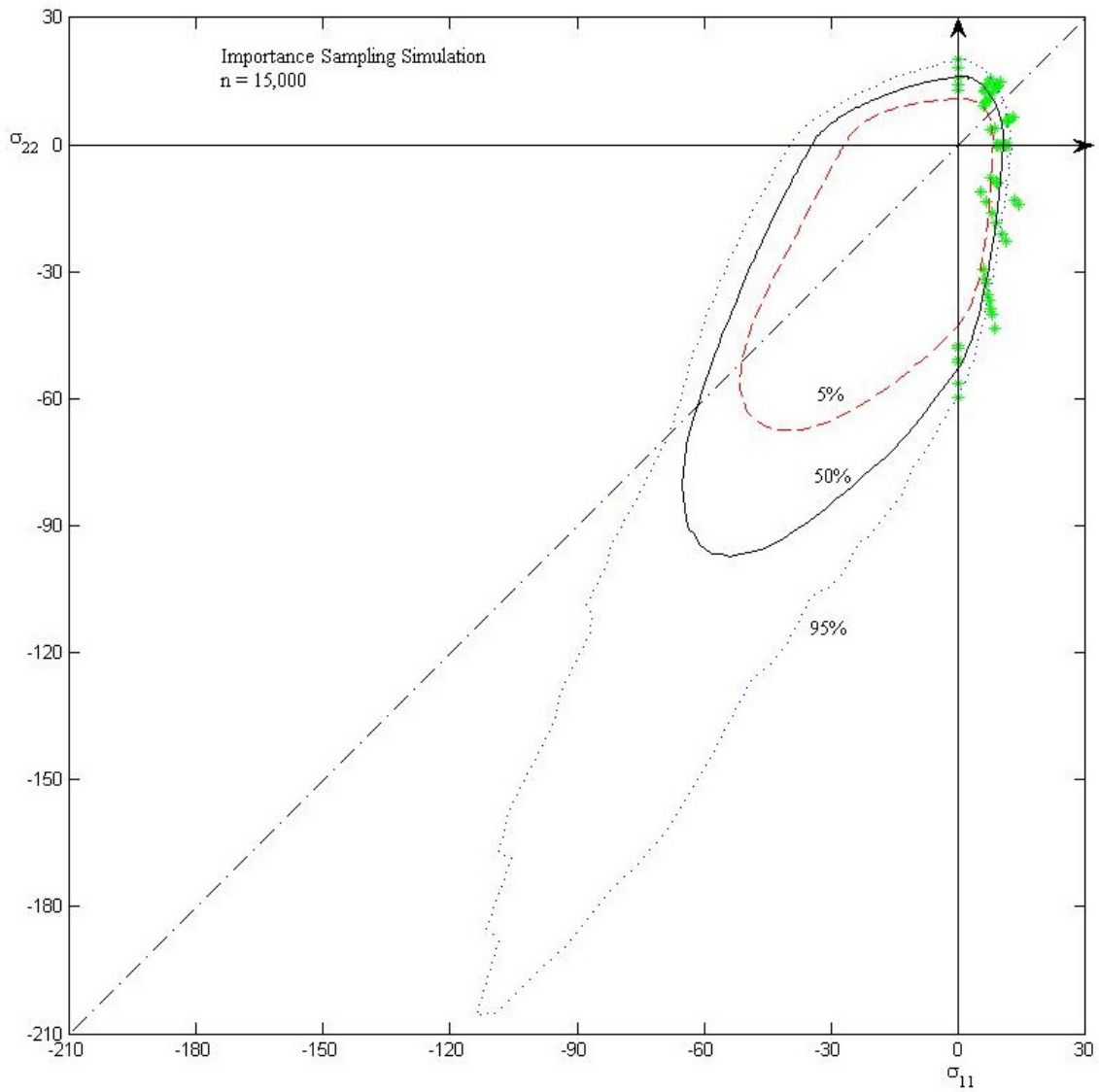


*Figure 6.4.1 The Failure Data from Burchell et al. (2007) with Probability of Failure Curves Obtained Using Monte Carlo Simulation Modified with Importance Sampling Techniques for the Anisotropic Version of the Failure Criterion.*

## **CHAPTER VII**

### **SUMMARY AND CONCLUSIONS**

This dissertation presents a multiaxial reliability model that captures the complex failure behavior of components fabricated from graphite. Of specific interest are graphite components that are deployed throughout the core of nuclear reactors. The failure behavior of graphite presents several unique challenges for the design engineer. First, bulk strength is different under tensile stress states in comparison to compressive stress states. In addition, depending on how the material is produced, graphite can exhibit isotropic or anisotropic failure behavior. The reliability models derived under this effort can account for either and the isotropic reliability model discussed earlier is a special case of the anisotropic model. At the present time anisotropic behavior is limited to stochastic failure that can be characterized as transversely isotropic. Other types of material symmetry, e.g., orthotropic failure behavior, can be accommodated using the stress invariant/integrity basis techniques utilized herein.

## 7.1 Comparison With the ASME Simplified Assessment Method

As part of the summary a brief comparison of the reliability models developed here is made with the stochastic methods advocated for in the *ASME Boiler and Pressure Vessel Code*. The design, integrity and functionality of graphite core components found in a nuclear reactor operating at elevated temperatures are controlled by a number of subsections of the “*ASME Boiler and Pressure Vessel Code Section III - Rules for Construction of Nuclear Facility Components - Division 5 - High Temperature Reactors*” (2010). Hereafter this document is simply referred to as the ASME Code, or the code. The ASME Code Article HHA 3200 entitled “*Design by Analysis – Graphite Core Components*” delineates a number of engineering issues. This particular section contains articles entitled “*Requirements for Acceptability*” (HHA 211), “*Detailed Requirements for Derivation of the Material Data Sheet – As-Manufactured Properties*” (HHA-II-3000), “*Basis for Determining Stresses*” (HHA 3213), “*Stress Analysis*” (HHA 3215), “*Calculation of Probability of Failure*” (HHA 3217), and “*Stress Limits for Graphite Core Component – Simplified Assessment*” (HHA 3220). All have specific relevance to this comparison made to work presented in this dissertation.

The acceptability of design under the ASME Code can be established by meeting the requirements of a simplified assessment. The simplified assessment is conservative and is outlined in HHA-3220 which points to the other sections of the code just mentioned. This particular code article outlines the fundamental elements of a static



load analysis. Designs that focus on fatigue and deformation are addressed elsewhere in the ASME Code. The static strength of graphite has been the research topic addressed throughout this dissertation and comparisons will be made based on this design issue. The simple assessment is a conservative design approach and as the code points out, not meeting this assessment does not disqualify a component design. Other more in-depth methods of analysis can be brought to bear. In addition, the comparison made here to the simplified assessment is with full knowledge that the ASME Code assumes isotropic material behavior. The code does not address anisotropic behavior and that it does not is briefly discussed at the end of this comparison,

The simplified assessment begins by requiring a detailed three dimensional stress analysis preferably conducted using finite element analysis. Regions of elevated stresses are identified, and an equivalent stress is computed in terms of the principal stresses in elevated stress regions. The equivalent stress is based on maximum distortional energy principles and the code adopts the following expression

$$\sigma_v = \left\{ (\bar{\sigma}_1)^2 + (\bar{\sigma}_2)^2 + (\bar{\sigma}_3)^2 - 2\nu [(\bar{\sigma}_1)(\bar{\sigma}_2) + (\bar{\sigma}_1)(\bar{\sigma}_3) + (\bar{\sigma}_2)(\bar{\sigma}_3)] \right\}^{\frac{1}{2}} \quad (7.1.1)$$

for the equivalent stress where

$$\bar{\sigma}_i = f\sigma_i \quad (7.1.2)$$

and

$$f = 1 \quad (7.1.3)$$

if the principal stress is tensile. If the principal stress is compressive then

$$f = \frac{1}{R_{tc}} \quad (7.1.4)$$

Here  $R_{tc}$  is the ratio of the mean compressive strength to the mean tensile strength. In addition,  $\nu$  is Poisson's ratio and for graphite this material constant is taken equal to 0.15.

The expression for the equivalent stress can be incorporated into a limit state function easily. That limit state function would be expressed as

$$g = 1 - \frac{\sigma_v}{\sigma_T} \quad (7.1.5)$$

where  $\sigma_T$  represents the tensile strength of the material. The tensile strength parameter is then treated as a random variable and reliability calculation proceed in a manner identical to the methods outlined in Chapter 6.

The code requires information regarding the mean strength of the compressive random variable in order to compute  $R_{tc}$  and subsequently the equivalent stress at any point. In statistics the mean value of a random variable is considered a location parameter for any density function whether the density function is a normal (Gaussian) density function or not. However, the code does not require, nor does it utilize any stochastic information relative to the scatter in compressive strength. The code considers the stochastic properties of the tensile random strength variable by using the Weibull characteristic strength (a location parameter) and the Weibull modulus (a

measure of scatter or variance). The ASME Code embraces the tensile strength as a random variable in a comprehensive manner but does not do the same with the compressive strength random variable. The ASME Code effectively ignores stochastic information relative to the compressive strength of the material by discarding the scatter quantified by the associated Weibull modulus. This is done with the thought that this simplifies design procedures.

The ASME limit state function in equation (7.1.5) is an isotropic failure criterion. It has been noted throughout that data from Burchell et al. (2007) represents anisotropic failure behavior. As will be seen momentarily, the data from Burchell et al. (2007) is convenient in facilitating a comparison between the reliability models derived here and the ASME based reliability models. As a work around the tensile and compressive mean strengths from the data found in Burchell et al. (2007) in the preferred direction can be used to compute a value for  $R_{tc}$ . With a value of the ratio of mean strengths and the Weibull parameters from tensile strength stress data one can map the probability of failure curve depicted in Figure 7.1.1 using equation (7.1.5). In this figure the 50% probability of failure curve is projected into the  $\sigma_{11} - \sigma_{22}$  stress space. The curve bisects the data from Burchell et al. (2007) along the  $\sigma_{11}$ -axis as it should. This stress axis coincides with the preferred (strong) direction of the material. The 50% probability of failure curve should be in close proximity with the mean values of the tensile and compressive strength data, and from the figure it is evident this happens.

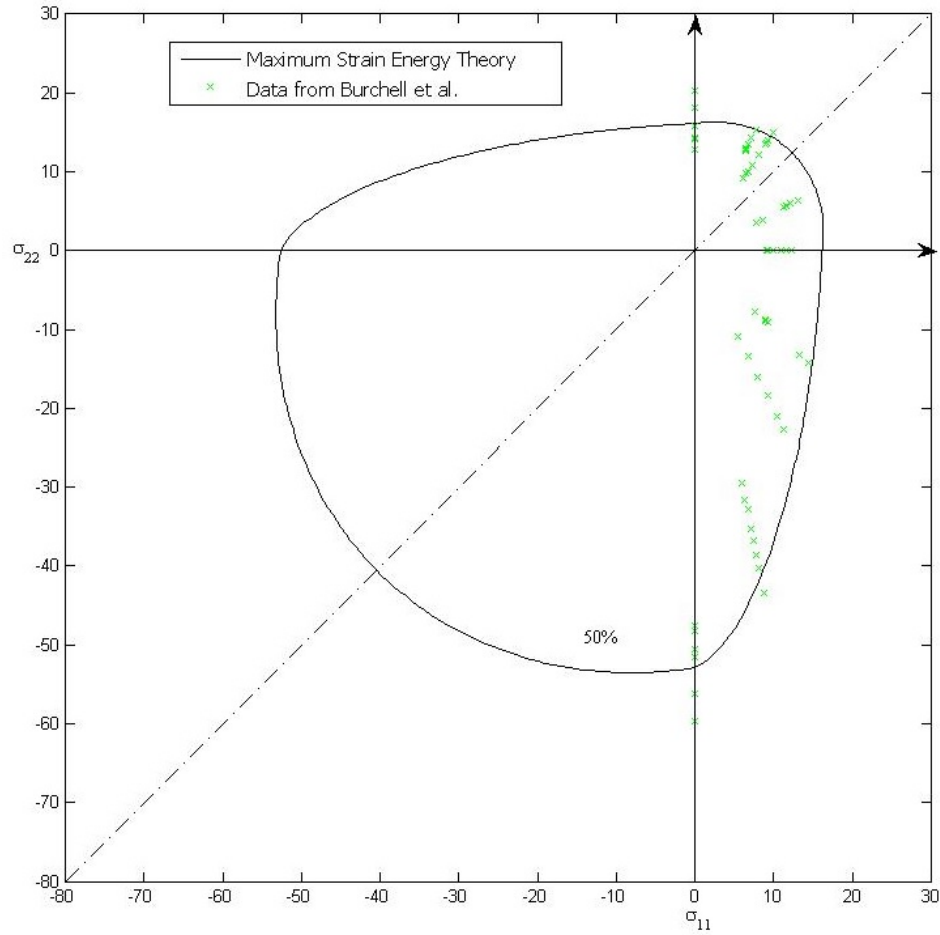


*Figure 7.1.1 ASME Maximum Distortional Energy Probability of Failure Curve (50%) with the Failure Data from Burchell et al. (2007).*

As a comparison, the isotropic reliability model derived here is also projected into a  $\sigma_{11} - \sigma_{22}$  stress space in Figure 7.1.2 along with the maximum distortional energy reliability model just presented. Both reliability curves are characterized using the data from Burchell et al. (2007) in the strong direction of the material. The 50% probability of failure curve generated by simulation was presented in the previous chapter. It is evident in this figure that the ASME maximum distortional energy reliability curve is more conservative than the isotropic reliability curve. This is starkly apparent in the

biaxial compression regions of the stress space. The isotropic reliability model is controlled by the biaxial strength parameter,  $\sigma_{BC}$ , along this stress path. Adjustment in the isotropic reliability model can be made along this stress path through this parameter indicating a degree of flexibility has been built into the model. No such flexibility exists in the ASME models along this stress path. Since failure data is unavailable for an equal biaxial stress load path because of the difficulty of attaining this state of stress in a test specimen, future efforts should include an optimization algorithm to determine the Weibull parameters for the biaxial compression strength random variable,  $\sigma_{BC}$ .

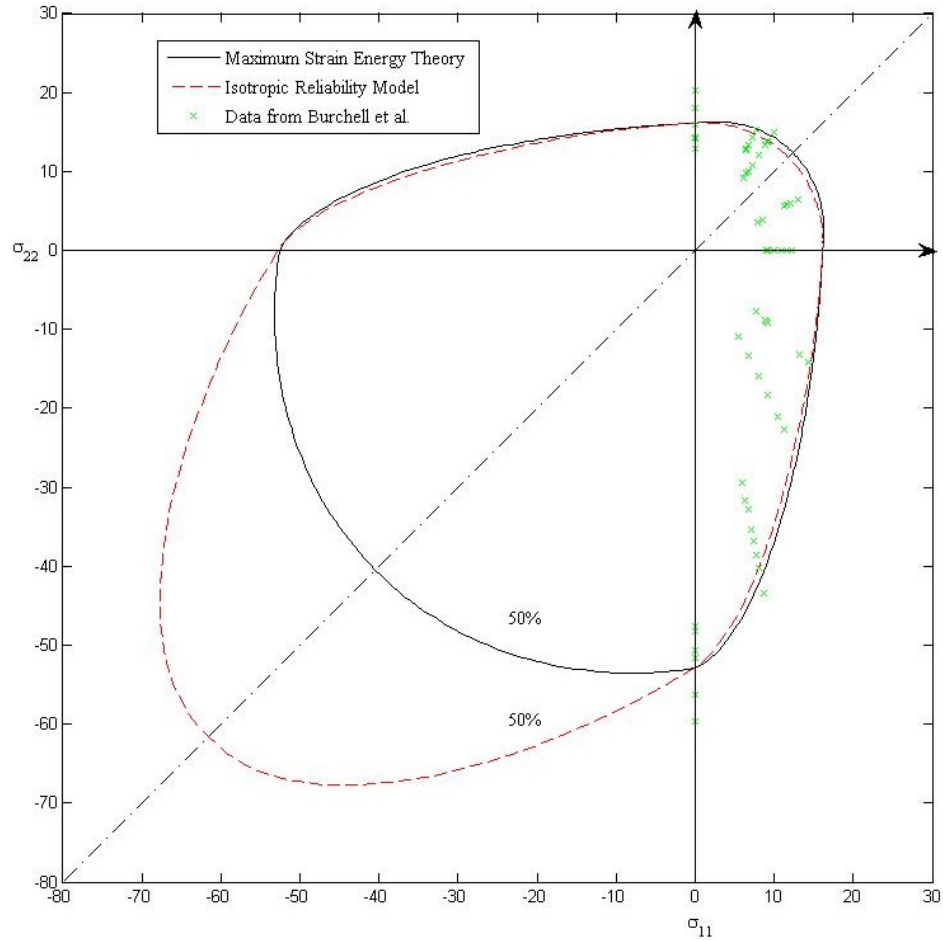


*Figure 7.1.2 Probability of Failure Curves (50%) from the Maximum Distortional Energy Reliability Model and the Isotropic Reliability Model. The Failure Data from Burchell et al. (2007) is shown.*

The ASME Code recognizes that the practice of assuming a fixed design margin, which is done for components fabricated from metal alloys, does not produce a uniform design reliability throughout a graphite reactor core. As mentioned, earlier the ASME Code treats the tensile strength of graphite as a random variable. The code assumes the tensile strength random variable is characterized by a two parameter Weibull distribution. This same assumption was made throughout this work for all random strength variables. In order to introduce a degree of conservatism in the ASME analysis the Weibull

parameters extracted from the tensile strength data are “knocked down.” The code calls for the use of Weibull parameters that correspond to the lower limit of the 95% confidence bound on the estimated parameters. At the time this dissertation was written the expression in the ASME code for the “knocked down” value of the Weibull characteristic strength at the lower bound of 95% confidence bound was incorrect. The correct relationship for the 95% lower bound on the Weibull characteristic strength is used here. The effects of the “knocked down” Weibull parameters called for in the ASME code are in evidence in Figure 7.1.3. As a result of using the “knocked down” Weibull parameters the ASME maximum distortional energy probability of failure curve shrinks isotropically. The stress states that correspond to the 50% failure probability using the “knocked down” Weibull parameters are smaller in magnitude relative to those in the previous figure. This imposes an unknown degree of conservatism on the design of graphite reactor core components. The 95% lower bound on Weibull parameter estimates does not correspond to a 95% lower bound on component reliability.

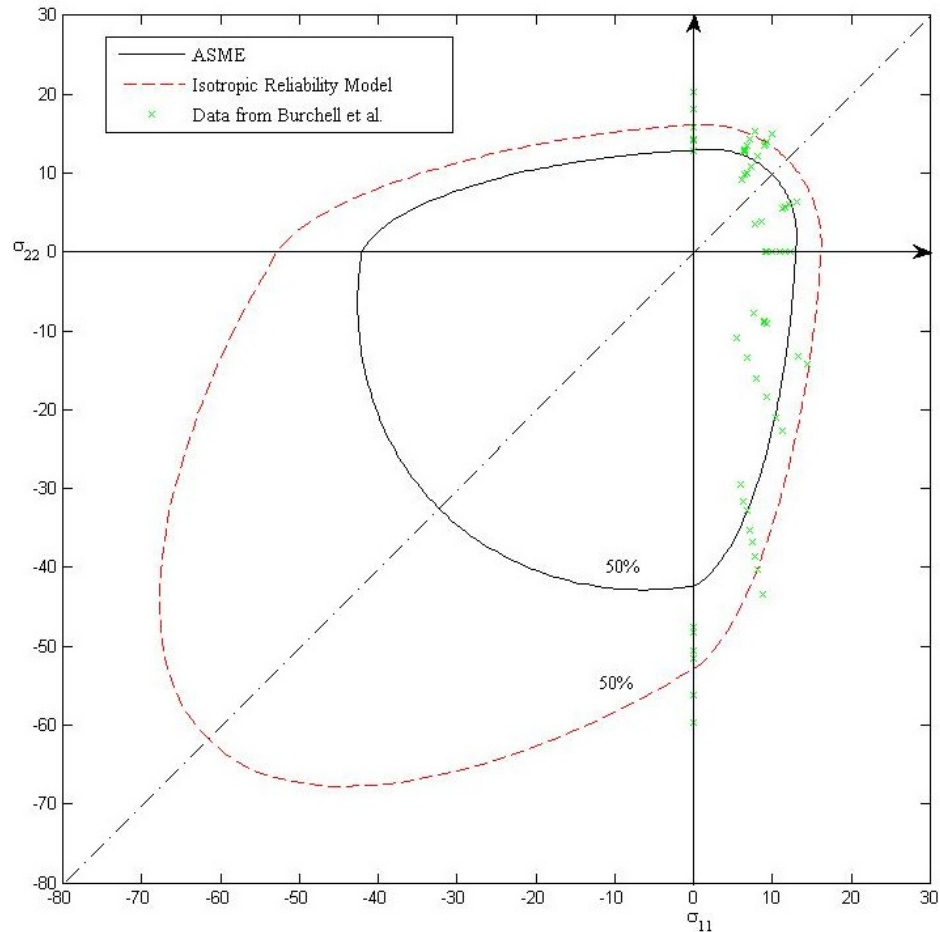


*Figure 7.1.3 Probability of Failure Curves (50%) Using the ASME Method with the Reduced Weibull Parameters and the Isotropic Reliability Model. The Failure Data from Burchell et al. (2007) is Included.*

In order to paint a comprehensive picture of the maximum distortional energy reliability model a nested set of reliability curves are presented in the next figure. Keep in mind that data from Burchell et al. (2007) along the tensile and compressive  $\sigma_{11}$ -axis is used as proscribed in the ASME code, i.e., “knocked down” Weibull parameters are used in Figure 7.1.4. The spacing between the curves is controlled by the Weibull modulus obtained from the tensile data. This aspect of the ASME approach should be interrogated in future efforts.



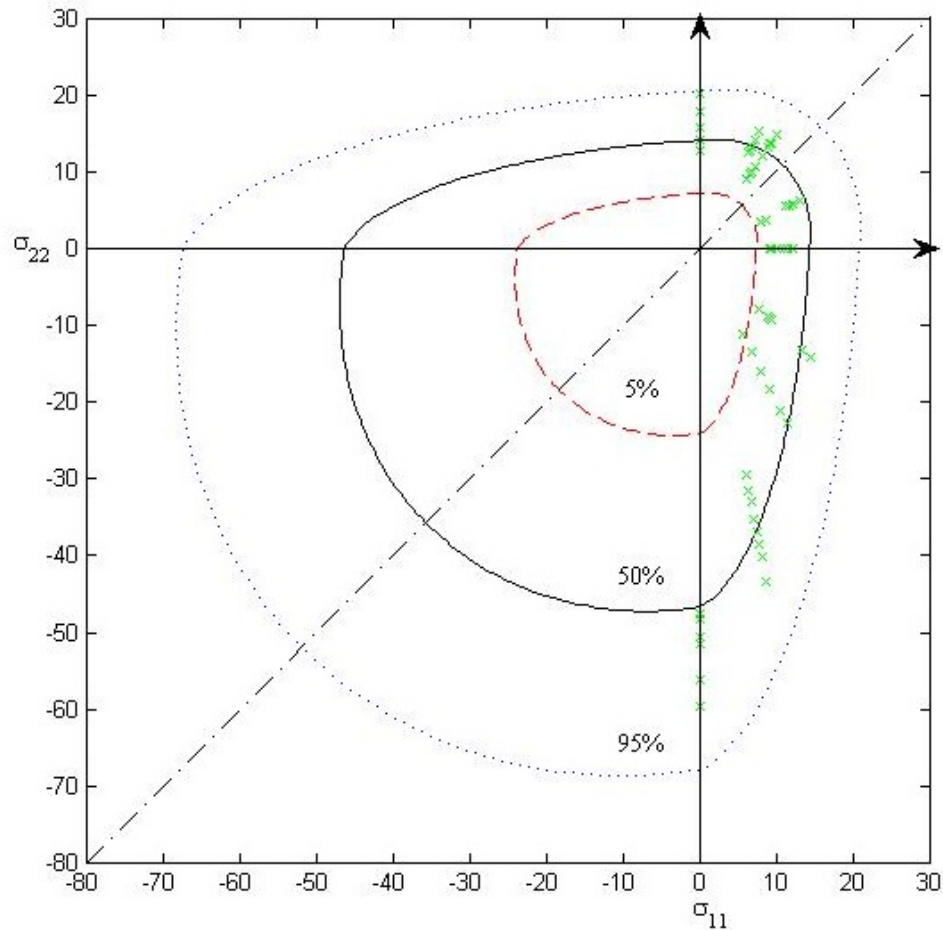


*Figure 7.1.4 Nested Reliability Surfaces Using ASME Code Methods to Determine Reliability. The Failure Data from Burchell et al. (2007) is Depicted.*

These curves correspond to failure probabilities of 5%, 50% and 95% and they should be compared to the reliability curves found in Figure 6.3.5. Note that the 95% probability of failure curve in Figure 7.1.4 is beyond the last compressive failure data point along the  $\sigma_{11}$ -axis. This seems to infer a bit of non-conservatism for compressive loads. The 95% probability of failure curve for the isotropic reliability model developed here is in close proximity to the largest compressive failure stress in Figure 6.3.5. This would indicate that the probability of failure curve in Figure 6.3.5 for the isotropic

reliability model developed here is more conservative, and this is born out in the next figure.

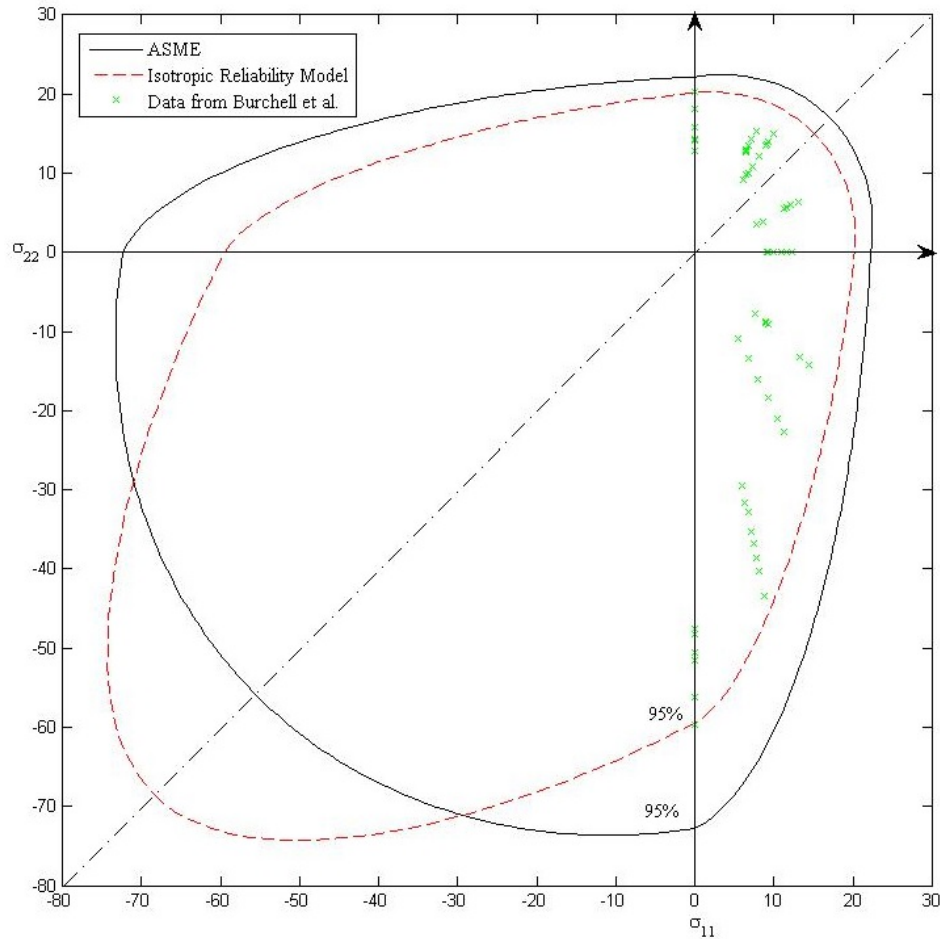


*Figure 7.1.5 Probability of Failure Curves (95%) Using the ASME Method with the Reduced Weibull Parameters and the Isotropic Reliability Model. The Failure Data from Burchell et al. (2007) is Included.*

A similar comparison is made in the next figure at the 5% probability of failure.

In Figure 7.1.6 the ASME reliability curve using the “knocked down” Weibull parameters is conservative at every stress state around the curve. This level of failure probability is more in line with the levels engineers would more than likely design to.

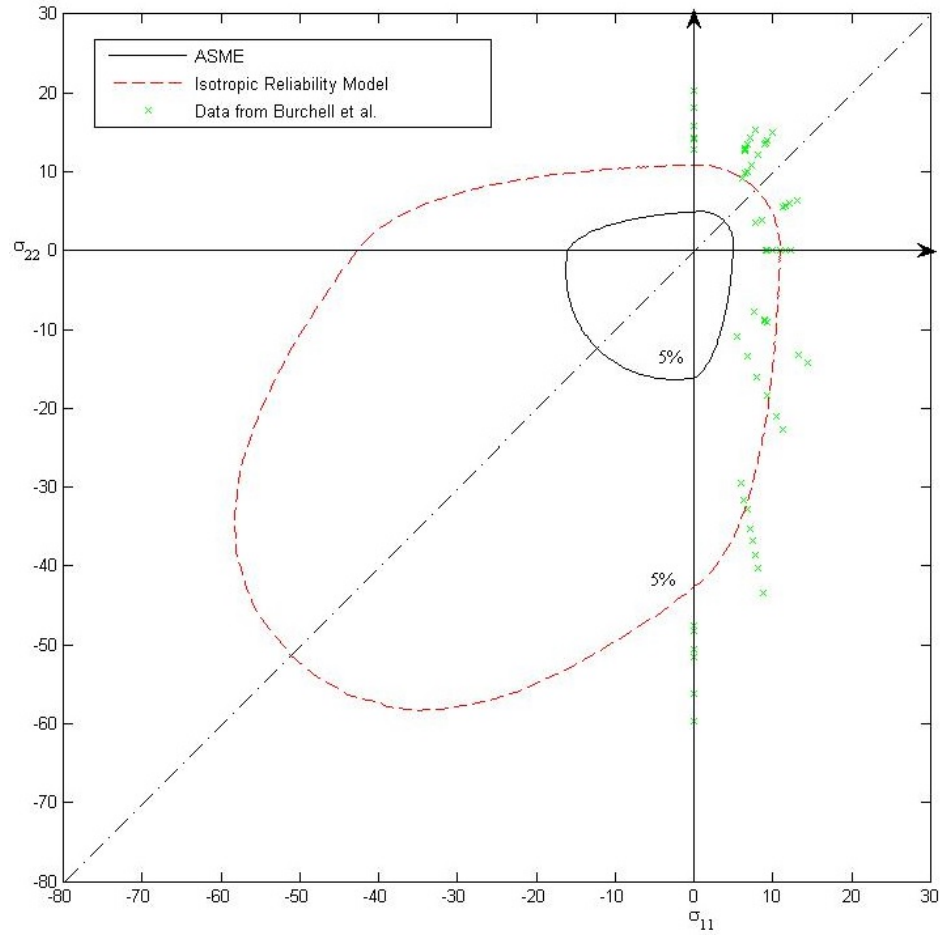


*Figure 7.1.6 Probability of Failure Curves (5%) Using the ASME Method with the Reduced Weibull Parameters and the Isotropic Reliability Model. The Failure Data from Burchell et al. (2007) is Included.*

Finally in Figures 7.1.5 and 7.1.6 the ASME reliability models are compared to the predictions from the anisotropic reliability model derived in this work. Again, all models are characterized using the data from Burchell et al. (2007). The first comparison of the anisotropic curve developed here is made with the ASME maximum distortional energy curve. Both curves appear in Figure 7.1.1 and both curves correspond to a failure probability of 50%

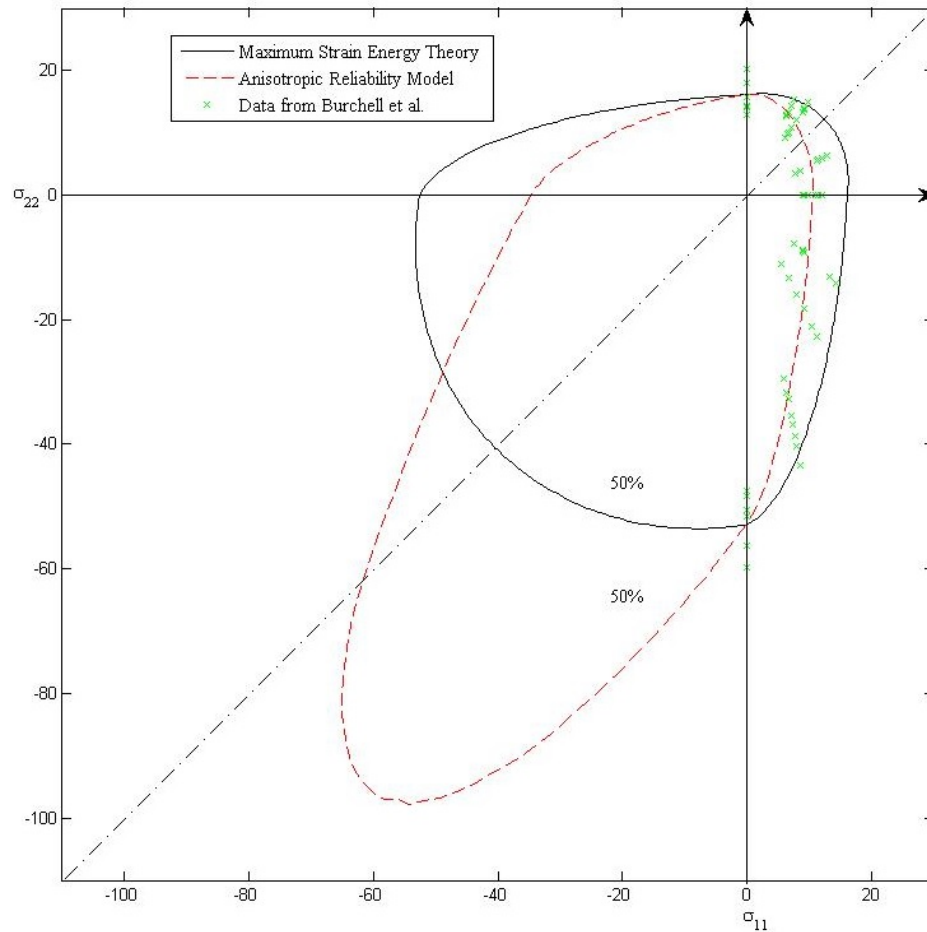


*Figure 7.1.7 Probability of Failure Curves (50%) from the ASME Maximum Distortional Energy Reliability Model and the Anisotropic Reliability Model. The Failure Data from Burchell et al. (2007) is Shown.*

In Figure 7.1.7 the anisotropic reliability model tracks the data from Burchell et al. (2007) better than the maximum distortional energy reliability model from the ASME code. This is not a surprise since it is evident at first glance at the data from Burchell et al. (2007) that the failure behavior of the H-451 graphite tested is anisotropic. In this figure the ASME code curve is no longer conservative for all stress states. In equal biaxial compression regions of the stress space the ASME code curve remains aggressively more conservative. However, stress states along the  $\sigma_{22}$  – axis, i.e., stress

states that corresponds to tensile and compressive strengths in the plane of isotropy, the ASME curve is no longer conservative. This reflects the fact that the anisotropic model allows for more information regarding the strengths of the material as well as by the fact that the ASME model is characterized with failure data oriented in the strong direction of the material, i.e., along the  $\sigma_{11}$ -axis. The fact that the ASME model does not track the  $s_{22}$  failure stresses well should not surprise. There is no provision in the ASME Code for anisotropic failure behavior. A conservative approach would be the utilization of the weak axis failure data, i.e., failure data in the plane of isotropy. At the present time that is not called for specifically in the ASME Code.

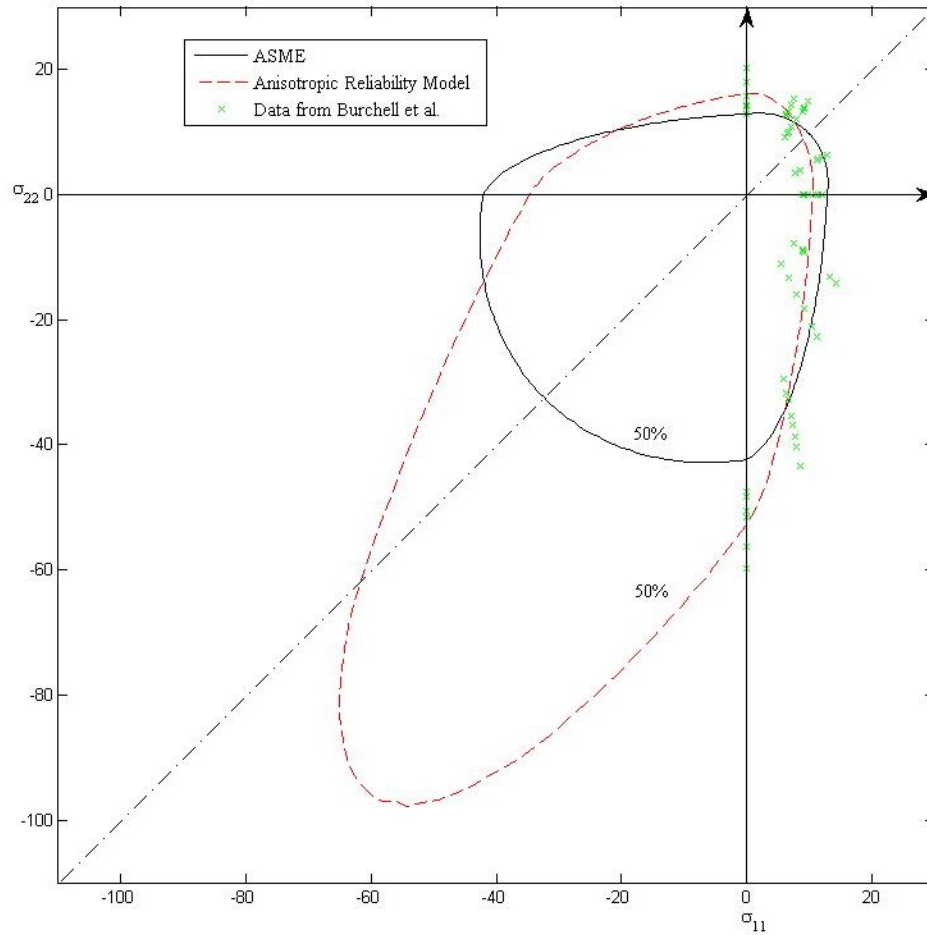


*Figure 7.1.8 Probability of Failure Curves (50%) Using the ASME Method with the Reduced Weibull Parameters and the Anisotropic Reliability Model. The Failure Data from Burchell et al. (2007) is Included.*

When the anisotropic model is compared to the ASME model with “knocked down” Weibull parameters the conservatism of the anisotropic model in the plane of isotropy is greatly diminished. When the comparison is made at the 5% probability of failure level the ASME model with the “knocked down” Weibull parameters is more conservative at any stress point on the reliability curve. This can be seen in Figure 7.1.9.

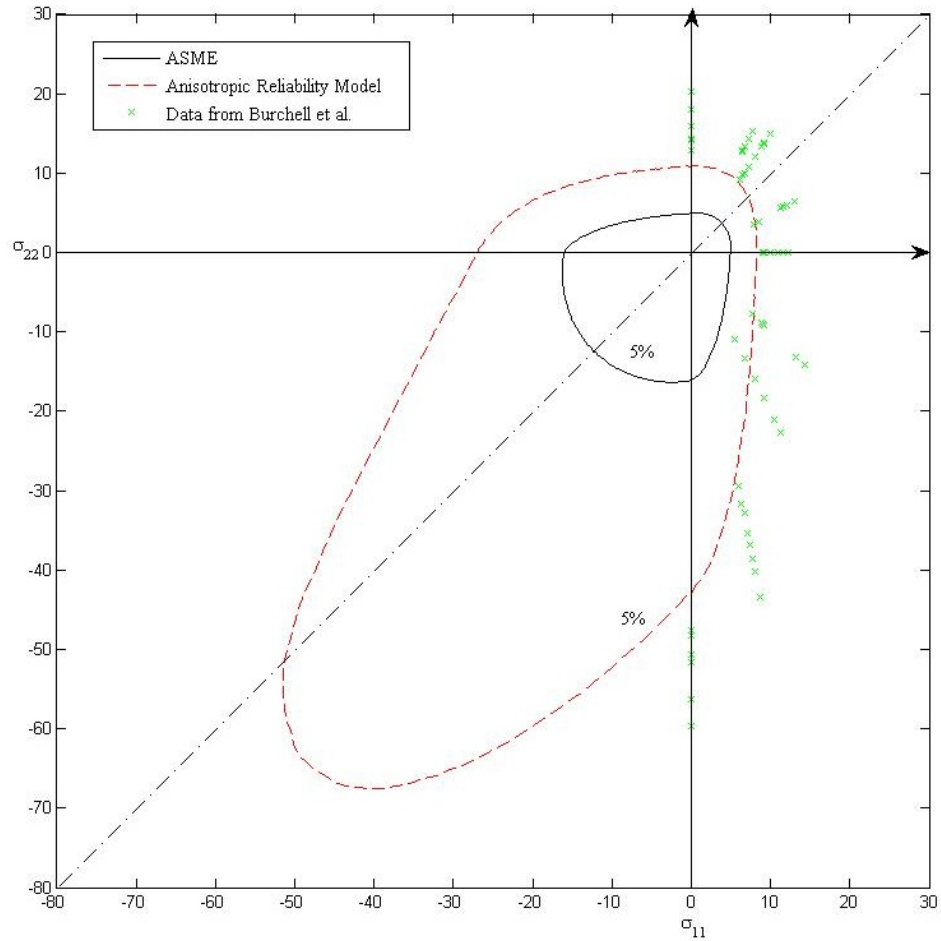


*Figure 7.1.9 Probability of Failure Curves (5%) Using the ASME Method with the Reduced Weibull Parameters and the Anisotropic Reliability Model. The Failure Data from Burchell et al. (2007) is Included.*

## 7.2 Theoretical Development - Summary

As noted throughout this dissertation the data from Burchell et al. (2007) demonstrates that certain grades of nuclear graphite exhibit anisotropic failure behavior. In general, anisotropy can be accounted for by introducing the concept of a vector representing the preferred material direction(s) to the reliability analysis. For the specific case of transverse anisotropy an integrity base was developed based on earlier

work of Green and Mkrtychian (1977). They developed their integrity basis in order to derive an isotropic constitutive model for non-linear elastic behavior. The non-linear stress-strain model accounted for different elastic deformation behavior in tension and compression by introducing a direction vector to the integrity basis that tracked the direction of the maximum principal stress. Their integrity basis was modified to account for a preferred direction in a material – that is, to account for material anisotropy exhibited in the failure behavior of nuclear graphite. This required a second vector in order to track material anisotropy. The second vector coincides with the preferred direction of the material, i.e., the “strong” direction of the material. Thus the integrity basis assembled here accounts for two directions – one associated with the stress state of the material and a second associated with material symmetry.

This integrity basis was constructed following the framework advocated for in Rivlin and Smith (1969) as well as Spencer (1971, 1984). This work focused on isotropic failure behavior first. A linear combination of the invariants identified by Green and Mkrtychian (1977) were used to formulate four separate isotropic failure functions for each region of the principal stress space defined by the relative magnitudes of the principal stresses. The linear combination of invariants serves as the limit state function for materials with different failure behavior in tension and compression. Constants associated with the linear combination were identified for each stress region in terms of simple mechanical test data. This identified the fundamental strength



parameters that were later treated as random variables in transitioning from deterministic models of limit state functions to reliability models. When the isotropic integrity basis adopted from the work of Green and Mkrtychian (1977) was extended to account for material anisotropy additional material strength parameters were identified. These additional strength parameters that were similarly treated as random strength variables for the anisotropic reliability model. Developing an isotropic failure criterion for graphite, transforming that failure criterion into a reliability model, and extending both to transverse isotropy represent the primary contribution to the body of knowledge made during this research project.

The transformation from a deterministic failure criterion to a reliability model was enabled numerically through the use of Monte Carlo simulations augmented with importance sampling. This makes the reliability model amenable for use in engineering design. States of stress in a graphite core component can be analyzed using finite element analysis and subsequently reliability evaluations can be conducted at each integration point of an element within the finite element mesh. This approach is advocated for at select points in a reactor component in the ASME Code. This is also the analytical structure utilized in the NASA CARES software algorithms (Gyekenyesi, 1986), but in a more comprehensive fashion.

### 7.3 Conclusions and Future Efforts

Research projects can raise more questions than are answered. This project took on that quality near the end. When the isotropic model was extended to capture transverse anisotropy failure behavior the model tracked failure behavior seen in the data from Burchell et al. (2007). The transversely isotropic model was characterized using data from Burchell et al. (2007) so the model should mimic the data used in characterizing the model, or the model is seriously flawed. Typically with analytical models one should characterize the model with data from one type of test specimen. The model should then be interrogated by asking the model to predict the behavior from a test specimen with a completely different specimen geometry and load configuration. The anisotropic reliability model can and should be characterized by the data from Burchell et al. (2007), which was done here. The model should then be used to predict failure probabilities say for an L-shaped bracket that is representative of reactor core components. The predictions from the model for the second test specimen geometry should be compared to the failure data from the L-shaped bracket geometry and conclusions regarding model performance can be drawn. This assumes the L-shaped brackets, or other type of test specimen with a complex stress distribution, is fabricated from the same material used to characterize the model.

This approach has been advocated in Department of Energy (DoE) research programs and internationally collaborative industry program with a focus on nuclear

grade graphite. To date this strategy has not been completely implemented for a particular material. Even if testing had taken place for the two types of test specimen the finite element analysis required to make this comparison is beyond the work scope here. This is another task for others to assess in the future.

Reliability calculations made using the models developed here required numerical methods for evaluation. The simplest approach, i.e., Monte Carlo simulation, was shown to be ineffective at low probabilities of failure. Too much error is present even at extremely large numbers of simulations. Yet low probabilities of failure is where an engineer wishes to operate a system of components. Importance sampling mitigated issues at low probability of failures, but the sense here is that the sampling density functions can and should be optimized somehow. Others following up on this research effort should look seriously into this issue.

With regards to failure analysis for material with material symmetries other than transversely isotropic, the extension of a phenomenological failure criterion was made here for transversely isotropic failure behavior. In the future other material symmetries, e.g., materials with orthotropic failure behavior, can be accommodated as well. Duffy and Manderscheid (1990b) as well as others have suggested an appropriate integrity basis for the orthotropic material symmetry. These should be studied in conjunction with the integrity basis outlined in the work of Green and Mkrtychian (1977).

Finally, the ASME design code is in need of a comprehensive software algorithm to aid design engineers in qualifying components. This algorithm must enable the design engineer to calculate the reliability of graphite core components as a system where the stress state at every point in the component contributes to a reduction of component reliability, not just a select number of locations of high stress. This admits the possibility of failure occurring at any point in a reactor component. Unfortunately, the size effect of graphite is somewhat enigmatic. As Nemeth and Bratton (2012) as well as others point out certain size effects in graphite materials is hard to characterize. With regard to system reliability materials can act as a weakest link system where failure at a point is catastrophic. Other materials can act as a series system where failure must take place at every point in the system for failure to occur. The suspicion here is that graphite acts like an “*r out of n*” system where failure of the system occurs after a finite number of failures have occurred throughout the component. This concept should be pursued in future efforts.

## REFERENCES

- ASME Boiler and Pressure Vessel Code, ASME, Section III, Division 5, 2010.
- Balzer, M.A., "Mechanical Behavior of Metals under Triaxial Stress: Apparatus and Experiments," *Ph.D. Dissertation*, University of Illinois at Urbana-Champaign, 1998.
- Batdorf, S.B. and Crose, J.G., "A Statistical Theory for the Fracture of Brittle Structure Subjected to Nonuniform Polyaxial Stress," *ASME Journal of Applied Mechanics*, Vol. 41, No. 2, pp. 459-464, 1974.
- Boehler, J.P. and Sawczuk, A., "On Yielding of Oriented Solids," *Acta Mechanica*, Vol. 27, pp. 185-204, 1977.
- Boehler, J.P., Kirillov, A.A. and Onat, E.T., "On the Polynomial Invariants of the Elasticity Tensor," *Journal of Elasticity*, Vol 34, pp. 97-110, 1994.
- Boehler, J.P., "Yielding and Failure of Transversely Isotropic Solids, Applications of Tensor Functions in Solid Mechanics," CISM Courses and Lectures No 292, Springer-Verlag, Berlin, pp. 3-140, 1987.
- Boresi, A.P. and Schmidt, R.J., Advanced Mechanics of Materials, 6<sup>th</sup> Edition, John Wiley and Sons, Inc., pp.117-129, 2003.
- Bridgman, P.W., "The Effect of Pressure on the Tensile Properties of Several Metals and Other Materials," *Journal of Applied Physics*, Vol. 24, No. 5, pp.560-570, 1953.
- Burchell, T., Yahr, T. and Battiste, R., "Modeling the Multiaxial Strength of H-451 Nuclear Grade Graphite," *Carbon*, Vol. 45, No. 13, pp. 2570-2583, 2007.
- Burchell, T.D. (editor), Carbon Materials for Advanced Technologies, Elsevier, 1999.
- Cazacu, O., Cristescu, N.D., Shao, J.F. and Henry, J.P., "A New Anisotropic Failure Criterion for Transversely Isotropic Solids," *Mechanics Cohesive-Frictional Material*, Vol. 3, pp. 89-103, 1998.
- Cazacu, O. and Cristescu, N.D., "A Paraboloid Failure Surface For Transversely Isotropic Materials," *Mechanics of Materials*, Vol. 31, No. 6, pp. 381-393, 1999.

Cooper, N.R., Margetson, J., and Humble, S., "Probability of Failure Calculations And Confidence Band Estimates For An Annular Brittle Disc Fracture Under Centrifugal Loading," *Journal of Strain Analysis for Engineering Design*, Vol. 21, No. 3, 121-126, 1986.

Cooper, N.R., "Probabilistic Failure Prediction of Rocket Motor Components," *Ph.D. Dissertation*, Royal Military College of Science, 1988.

Coulomb, C.A., "Essai sur une Application des Regles des Maximis et Minimis a Quelques Problemes de Statique Relatifs, a la Architecture," *Memoires de Mathematique et de Physique*, presentes a l'Academie Royales Des Sciences, Vol. 7, pp. 343-387, 1776.

Drucker, D.C. and Prager, W., "Soil Mechanics and Plastic Analysis For Limit Design," *Quarterly of Applied Mathematics*, Vol. 10, No. 2, pp. 157-165, 1952.

Duffy, S.F., "A Viscoplastic Constitutive Theory for Transversely Isotropic Metal Alloys," *Ph.D. Dissertation*, University of Akron, 1987.

Duffy, S.F. and Gyekenyesi, J.P., "Time Dependent Reliability Model Incorporating Continuum Damage Mechanics for High-Temperature Ceramics," *NASA Technical Memorandum 102046*, 1989.

Duffy, S.F. and Arnold, S.M., "Noninteractive Macroscopic Reliability Model for Whisker-Reinforced Ceramic Composites," *Journal of Composite Materials*, Vol. 24, No. 3, pp.235-344, 1990a.

Duffy, S.F. and Manderscheid, J.M., "Noninteractive Macroscopic Reliability Model for Ceramic Matrix Composites with Orthotropic Material Symmetry," *Journal of Engineering for Gas Turbines and Power*, Vol. 112, No. 4, pp. 507-511, 1990b.

Duffy, S.F., Chulya, A. and Gyekenyesi, J.P., "Structural Design Methodologies for Ceramic-Based Material Systems," *NASA Technical Memorandum 103097*, 1991.

Duffy, S.F., Wetherhold, R.C. and Jain, L.K., "Extension of a Noninteractive Reliability Model for Ceramic Matrix Composites," *Journal of Engineering for Gas Turbines and Power*, Vol. 115, No. 1, pp. 205-207, 1993.

Duffy, S.F., and Palko, J.L., "Analysis of Whisker Toughened CMC Structural Components Using an Interactive Reliability Model," *AIAA Journal*, Vol. 32, No. 5, pp. 1043-1048, 1994.

Duffy, S.F., Baker, E.H., and James, C., "Standard Practice for Reporting Uniaxial Strength Data And Estimating Weibull Distribution Parameters For Graphite," *ASTM Standard D 7846*, 2013.

Green, A.E. and Mkrtychian, J.Z., "Elastic Solids with Different Moduli in Tension and Compression," *Journal of Elasticity*, Vol. 7, No. 4, pp. 369-386, 1977.

Griffiths, A.A., "The Theory Of Rupture And Flow In Solids," *Philosophical Transactions of the Royal Society A: Mathematical, Physical and Engineering Sciences*, Vol. 221, pp. 163-198, 1921.

Gyekenyesi, J.P., "SCARE - A Post-Processor Program to MSC/NASTRAN for the Reliability Analysis of Ceramic Components," *ASME Journal of Engineering for Gas Turbines and Power*, Vol. 108, No. 3, 540-546, 1986.

Harbitz, A., "An Efficient Sampling Method for Probability of Failure Calculations," *Structural Safety*, Vol. 3, pp. 108-115, 1986.

Haldar, A. and Mahadevan, S., Reliability Assessment Using Stochastic Finite Element Analysis, John Wiley & Sons, 2000.

Hu, J., "Modeling Size Effects and Numerical Methods in Structural Reliability Analysis," *Masters Thesis*, Cleveland State University, 1994.

Kaufman, M. and Ferrante, J., "Statistical Model for Mechanical Failure," *NASA Technical Memorandum 107112*, 1996

Lamon, J., "Reliability Analysis of Ceramics Using the CERAM Computer Program," *ASME Paper No. 90-GT-98*, IGTI, 1990.

Li, Q.M., "Strain energy Density Failure Criterion," *International Journal of Solids and Structures*, Vol. 38, No. 38, pp. 6997-7013, 2001.

Melchers, R.E., "Importance Sampling in Structural Systems," *Structural Safety*, Vol. 6, pp. 3-10, 1989

Nova, R., and Zaninetti, A., "An Investigation Into the Tensile Behavior of a Schistose Rock," *International Journal of Rock Mechanics, Mining Sciences and Geomechanics*, Vol. 27, No. 4, pp. 231-242, 1990.

Palko, J.L., "An Interactive Reliability Model for Whisker- Toughened Ceramics," *Masters Thesis*, Cleveland State University, June 1992.

Paul, B., "Generalized Pyramidal Fracture and Yield Criteria," *International Journal of Solids and Structure*, Vol. 4, pp.175-196, 1968.

Romanoski, G.R. and Burchell, T.D., "Fracture in Graphite," in Carbon Materials for Advanced Technologies, Burchell, T.D. (editor), Elsevier, pp. 485-534, 1999.

Rivlin, R.S. and Smith, G.F., "Orthogonal Integrity Basis for N Symmetric Matrices," in Contributions to Mechanics, ed. D. Abir, Pergamon Press, Oxford, pp. 121-141, 1969.

Saito, S., "Role of Nuclear Energy to a Future Society of Shortage of Energy Resources and Global Warming," *Journal of Nuclear Materials*, Vol. 398, pp. 1-9, 2010.

Schleicher, F., "Der Spannungszustand an der Fließgrenze (Plastizitätsbedingung)," *Zeitschrift für Angewandte Mathematik und Mechanik*, Vol. 6, pp. 199- 216, 1926.

Spencer, A.J.M., "Theory of Invariants," in Continuum Physics, 1, ed. A.C. Eringen, Academic Press, London, pp. 259-353, 1971.

Spencer, A.J.M., "Continuum Theory of the Mechanics of Fibre-Reinforced Composites," Spring-Verlag, pp.1-32, 1984.

Sun, C.T., and S.E. Yamada. "Strength Distribution of a Unidirectional Fiber Composite," *Journal of Composite Materials*, Vol. 12.2, pp. 169-176, 1978.

Tabeddor, F., "A Survey of Constitutive Equations of Bimodulus Elastic Materials," in Mechanics of Bimodulus Materials, ed: C.W. Bert, *Proceedings of the American Society of Mechanical Engineering Winter Annual meeting*, AMD33, 2-5, 1979.

Tresca, H., "Mémoire sur L'écoulement des Corps Solides Soumis à de Fortes Pressions," *Comptes Rendus*, Academie de Science, Vol. 59, p. 754, 1864.



Tsai, S.W. and Wu, E.M., "A General Theory of Strength of Anisotropic Materials," *Journal of Composite Materials*, Vol. 5, pp. 58-80, 1971.

Theocaris, P.S., "The Elliptic Paraboloid Failure Criterion for Cellular Solids and Brittle Foams," *Acta Mechanica*, Vol. 89, pp. 93-121, 1991.

US DOE Nuclear Energy Research Advisory Committee and the Generation IV International Forum, "A Technology Roadmap for Generation IV Nuclear Energy Systems," GIF-002-00, December 2002.

Vijayakumar, K. and Ashoka, J.G., "A Bilinear Constitutive Model for Isotropic Bimodulus Materials," *ASME Journal of Engineering Materials and Technology*, Vol. 112, pp. 372-379, 1990.

Vijayakumar, K., and Rao, K.P., "Stress-Strain Relations for Composites with Different Stiffness in Tension and Compression," *Computational Mechanics*, Vol. 2, pp. 167-175, 1987.

von Mises, R., "Mechanik der Festen Korper im Plastisch Deformablen Zustand," *Göttinger Nachrichten*, pp. 582-592, 1913.

Weibull, W., "A Statistical Distribution Function of Wide Applicability," *Journal of Applied Mechanics*, Vol. 18, No. 3, pp. 293-297, 1951.

Weibull, W., *Ingeniors Vetenshaps Akadamein, Handlingar*, 151 (1939)

Wetherhold, R.C., "Statistics of Fracture of Composite Materials Under Multiaxial Loading," PhD Dissertation, University of Delaware, 1983.

Wetherhold, R.C. and Ucci, A.M., "Probability Techniques for Reliability Analyses of Composite Materials," *NASA CR-195294*, National Aeronautics and Space Administration, National Technical Information Service, 1994.

Willam, K.J. and Warnke, E.P., "Constitutive Models for the Triaxial Behavior of Concrete," in: *Proceedings of the International Association for Bridge and Structural Engineer Seminar on Structures Subjected to Triaxial Stresses (Bergamo, Italy)*, Vol. 19, pp. 1-31, 1974.

Xue, G.F., Dai, H.Z., and Zhang, H., “An Adaptive Importance Sampling Scheme for Efficient Reliability Analysis,” in *Safety, Reliability, Risk and Life-Cycle Performance of Structure & Infrastructures* – Deodatis, Ellingwood & Frangopo (Eds), Taylor & Francis Group, London, pp. 707- 713, 2013.